University of Witwatersrand

Doctoral Thesis

CLASSIFICATION AND MODELING OF POWER LINE NOISE USING MACHINE LEARNING TECHNIQUES

Author:
Ayokunle Damilola, Familua

A thesis submitted in fulfilment of the requirements for the degree of Doctor of Philosophy

in the

School of Electrical and Information Engineering
Faculty of Engineering and Built Environment

June 2017

Declaration

I, Ayokunle Damilola, Familua , declare that this thesis titled, "Classification and Modeling of Power Line Noise using Machine Learning Techniques" and the work presented in it are my own. I confirm that:

- This work was done wholly or mainly while in candidature for a research degree at this University.
- Where any part of this thesis has previously been submitted for a degree or any other qualification at this University or any other institution, this has been clearly stated.
- Where I have consulted the published work of others, this is always clearly attributed.
- Where I have quoted from the work of others, the source is always given. With the exception of such quotations, this thesis is entirely my own work.
- I have acknowledged all main sources of help.

Signed: _____

Date: _____

UNIVERSITY OF WITWATERSRAND

Abstract

Faculty of Engineering and Built Environment
School of Electrical and Information Engineering

Doctor of Philosophy

CLASSIFICATION AND MODELING OF POWER LINE NOISE USING MACHINE LEARNING TECHNIQUES

by Ayokunle Damilola, Familua

Supervisor: Prof. Ling Cheng

The realization of robust, reliable and efficient data transmission have been the theme of recent research, most importantly in real channel such as the noisy, fading prone power line communication (PLC) channel. The focus is to exploit old techniques or create new techniques capable of improving the transmission reliability and also increasing the transmission capacity of the real communication channels. Multi-carrier modulation scheme such as Orthogonal Frequency Division Multiplexing (OFDM) utilizing conventional single-carrier modulation is developed to facilitate a robust data transmission, increasing transmission capacity (efficient bandwidth usage) and further reducing design complexity in PLC systems.

On the contrary, the reliability of data transmission is subjected to several inhibiting factors as a result of the varying nature of the PLC channel. These inhibiting factors include noise, perturbation and disturbances. Contrary to the Additive White Gaussian noise (AWGN) model often assumed in several communication systems, this noise model fails to capture the attributes of noise encountered on the PLC channel. This is because periodic noise or random noise pulses injected by power electronic appliances on the network is a deviation from the AWGN. The nature of the noise is categorized as non-white non-Gaussian and unstable due to its impulsive attributes, thus, it is labeled as Non-additive White Gaussian Noise (NAWGN). These noise and disturbances results into long burst errors that corrupts signals being transmitted, thus, the PLC is labeled as a horrible or burst error channel.

The efficient and optimal performance of a conventional linear receiver in the white Gaussian noise environment can therefore be made to drastically degrade in this NAWGN environment. Therefore, transmission reliability in such environment can be greatly enhanced if we know and exploit the knowledge of the channel's statistical attributes, thus, the need for developing statistical channel model based on empirical data. In this thesis, attention is focused on developing a reconfigurable software defined un-coded single-carrier and multi-carrier PLC transceiver as a tool for realizing an optimized channel model for the narrowband PLC (NB-PLC) channel.

First, a novel reconfigurable software defined un-coded single-carrier and multi-carrier PLC transceiver is developed for real-time NB-PLC transmission. The transceivers can be adapted to implement different waveforms for several real-time scenarios and performance evaluation. Due to the varying noise parameters obtained from country to country as a result of the dependence of noise impairment on mains voltages, topology of power line, place and time, the developed transceivers is capable of facilitating constant measurement campaigns to capture these varying noise parameters before statistical and mathematically inclined channel models are derived.

Furthermore, the single-carrier (Binary Phase Shift Keying (BPSK), Differential BPSK (DBPSK), Quadrature Phase Shift Keying (QPSK) and Differential QPSK (DQPSK)) PLC transceiver system developed is used to facilitate a First-Order semi-hidden Fritchman Markov modeling (SHFMM) of the NB-PLC channel utilizing the efficient iterative Baum-Welch algorithm (BWA) for parameter estimation. The performance of each modulation scheme is evaluated in a mildly and heavily disturbed scenarios for both residential and laboratory site considered. The First-Order estimated error statistics of the realized First-Order SHFMM have been analytically validated in terms of performance metrics such as: log-likelihood ratio (LLR), error-free run distribution (EFRD), error probabilities, mean square error (MSE) and Chi-square (χ^2) test. The reliability of the model results is also confirmed by an excellent match between the empirically obtained error sequence and the SHFMM regenerated error sequence as shown by the error-free run distribution plot.

This thesis also reports a novel development of a low cost, low complexity Frequency-shift keying (FSK) - On-off keying (OOK) in-house hybrid PLC and VLC system. The functionality of this hybrid PLC-VLC transceiver system was ascertained at both residential and laboratory site at three different times of the day: morning, afternoon and evening. A First and Second-Order SHFMM of the hybrid system is realized. The error statistics of the realized First and Second-Order SHFMMs have been analytically validated in terms of LLR, EFRD, error probabilities, MSE and Chi-square (χ^2). The Second-Order SHFMMs have also been analytically validated to be superior to the First-Order SHFMMs although at the expense of added computational complexity. The reliability of both First and Second-Order

SHFMM results is confirmed by an excellent match between the empirical error sequences and SHFMM re-generated error sequences as shown by the EFRD plot.

In addition, the multi-carrier (QPSK-OFDM, Differential QPSK (DQPSK)-OFDM) and Differential 8-PSK (D8PSK)-OFDM) PLC transceiver system developed is used to facilitate a First and Second-Order modeling of the NB-PLC system using the SHFMM and BWA for parameter estimation. The performance of each OFDM modulation scheme in evaluated and compared taking into consideration the mildly and heavily disturbed noise scenarios for the two measurement sites considered. The estimated error statistics of the realized SHFMMs have been analytically validated in terms of LLR, EFRD, error probabilities, MSE and Chi-square (χ^2) test. The estimated Second-Order SHFMMs have been analytically validated to be outperform the First-Order SHFMMs although with added computational complexity. The reliability of the models is confirmed by an excellent match between the empirical data and SHFMM generated data as shown by the EFRD plot.

The statistical models obtained using Baum-Welch to adjust the parameters of the adopted SHFMM are often locally maximized. To solve this problem, a novel Metropolis-Hastings algorithm, a Bayesian inference approach based on Markov Chain Monte Carlo (MCMC) is developed to optimize the parameters of the adopted SHFMM. The algorithm is used to optimize the model results obtained from the single-carrier and multi-carrier PLC systems as well as that of the hybrid PLC-VLC system. Consequently, as deduced from the results, the models obtained utilizing the novel Metropolis-Hastings algorithm are more precise, near optimal model with parameter sets that are closer to the global maxima.

Generally, the model results obtained in this thesis are relevant in enhancing transmission reliability on the PLC channel through the use of the models to improve the adopted modulation schemes, create adaptive modulation techniques, develop and evaluate forward error correction (FEC) codes such as a concatenation of Reed-Solomon and Permutation codes and other robust codes suitable for exploiting and mitigating noise impairments encountered on the low voltage NB-PLC channel. Furthermore, the reconfigurable software defined NB-PLC transceiver test-bed developed can be utilized for future measurement campaign as well as adapted for multiple-input and multiple-output (MIMO) PLC applications.

This thesis is dedicated to the Almighty God,

the author of wisdom for giving me the grace

to complete this degree. I also dedicate this thesis

to my beautiful wife Mrs. Ifeoluwa

Familua and our daughter
Ikeoluwa Familua

Acknowledgements

I wish to express my profound gratitude to the following people for their contributions towards the successful completion of this PhD degree:

- My Lord and personal Savior, who has been my strength through thick and thin and has inspired me to the completion of this degree, I will forever be grateful Lord.
- My Supervisor, Prof. Ling Cheng for your guidance, supervision and rare thoroughness towards the fruitful completion of this PhD programme. Words can not articulate the profound impact your rare thoroughness, research style and professionalism had on me. I am most grateful for your thorough editing of this Thesis.
- Special thanks to my gift of love, my dear friend and wife Mrs. Ifeoluwa Deborah Familua and our daughter Ikeoluwa Elizabeth Familua. You are a comfort and joy to my heart always. Thanks for your support.
- My dear parents, Engr. and Mrs. Ajewole Joseph Familua, who instilled in me a desire for formal education and has been supportive morally and financially. I am forever indebted to you for the foundation you laid for me in life; To my parent-in-law Elder and Mrs. T.A. Obadare, thanks for your prayers and encouragement.
- My beloved brothers Dr. Franklin Oluwamayowa Familua, Mr. Victor Olanrewaju Familua, Mr. Oluwafemi Familua, Mr Taiwo and Kehinde Familua; and all my sister-in-laws for your moral and financial support. God bless you all.
- To the School of Electrical and Information Engineering, most especially, the Centre for Telecommunications Access and Services (CeTAS) for your financial support and sponsoring of my conference trips. I am not ungrateful.
- The University of Witwatersrand through the Financial Aids and Scholarships office for the award of Postgraduate Merit Award bursary all through this programme, thanks for your financial support.
- My colleagues in the School of Electrical and Information Engineering, most especially, past and present Telecommunications Research Group (TRG) members. I recognize your immense contributions.

Contents

List of Figures

List of Tables

Abbreviations

AC	**A**lternating **C**urrent
AMI	**A**dvance **M**etering **I**nfrastructure
AMR	**A**utomatic **M**eter **R**eading
ANSI	**A**merican **N**ational **S**tandards **I**nstitute
AWGN	**A**dditive **W**hite **G**aussian **N**oise
ASK	**A**mplitude **S**hift **K**eying
BAN	**B**uilding **A**rea **N**etwork
BB	**B**road **B**and
BER	**B**it **E**rror **R**ate
BN	**B**ackground **N**oise
BNC	**B**ayonet **N**ut **C**onnector
BPL	**B**roadband over **P**ower **L**ines
BPSK	**B**inary **P**hase **S**hift **K**eying
CENELEC	**C**omité **E**uropéen de **N**ormalization **É**lectrotechnique
CSMA	**C**arrier **S**ense **M**ultiple **A**ccess
DSM	**D**emand **S**ide **M**anagement
DSP	**D**igital **S**ignal **P**rocessing
DS-CDMA	**D**irect **S**equence **C**ode **D**ivision **M**ultiple **A**ccess
EMC	**E**lectro-**M**agnetic **C**ompatibility
FEC	**F**orward **E**rror **C**orrection
FFT	**F**ast **F**ourier **T**ransform
FSK	**F**requency **S**hift **K**eying
HD-PLC	**H**igh **D**efinition **P**ower **L**ine **C**ommunications
HDR	**H**igh **D**ata **R**ate
HF	**H**igh **F**requency
HMM	**H**idden **M**arkov **M**odel
IAT	**I**nter **A**rrival **T**ime
ICTSB	**I**nformation and **C**ommunications **T**echnologies **S**tandards **B**oard
IEC	The **I**nternational **E**lectro-technical **C**ommission

IF	**I**ntermediate **F**requency
IN	**I**mpulse **N**oise
IPTV	**I**nternet **P**rotocol **T**elevision
ISI	**I**nter- **S**ymbol **I**nterference
ISO	**I**nternational **O**rganization (for) **S**tandardization
ITU	**I**nternational **T**elecommunication **U**nion
LDR	**L**ow **D**ata **R**ate
LF	**L**ow **F**requency
LPTV	**L**inear and **P**eriodically **T**ime **V**arying
LonWorks	**L**ocal **O**peration **N**etwork
LV	**L**ow **V**oltage
MF	**M**edium **F**requency
MTL	**M**ulti-conductor **T**ransmission **L**ine
MV	**M**edium **V**oltage
NBN	**N**arrowband **N**oise
OFDM	**O**rthogonal **F**requency **D**ivision **M**ultiplexing
OPERA	**O**pen **P**lc **E**uropean **R**esearch **A**lliance
PC	**P**ersonal **C**omputer
P_E	**P**robability of **E**rror
PHY	**P**hysical **L**ayer
PLC	**P**ower **L**ine **C**ommunications
PLN	**P**ower **L**ine **N**etwork
PRIME	**P**owerline **R**elated **I**ntelligent **M**etering **E**volution
PSD	**P**ower **S**pectral **D**ensity
PSK	**P**hase **S**hift **K**eying
PSU	**P**ower **S**upply **U**nit
QPSK	**Q**uadrature **P**hase **S**hift **K**eying
RMS	**R**oot **M**ean **S**quare
SNR	**S**ignal to **N**oise **R**atio
SS	**S**pread **S**pectrum
SST	**S**pread **S**pectrum **T**echnique
UHF	**U**ltra **H**igh **F**requency
UPS	**U**ninterruptible **P**ower **S**upply

VLF **V**ery **L**ow **F**requency

List of Publications

Peer-reviewed Journals

1. **A. D. Familua** and L. Cheng, "A Semi-Hidden Fritchman Markov Modeling of Indoor CENELEC A Narrowband Power Line Noise based on Signal Level Measurements" *AEU - International Journal of Electronics And Communications*, vol. 74, 2017, pp. 21-30.

2. K. Ogunyanda, **A. D. Familua**, T. G. Swart, H. C. Ferreira, and L. Cheng, "Evaluation of mixed permutation codes in PLC channels using Hamming distance profile," *in Telecommunication Systems Journal,*, vol. 65, no 1, 2017, pp. 169-179.

3. **A. D. Familua** and L. Cheng, "First and Second-Order Semi-Hidden Fritchman Markov Models for a multi-carrier based Indoor Narrowband Power Line Communication System" - *Submitted to Physical Communication Journal -Elsevier, under review (2017).*

Peer-reviewed Conference Papers

1. **A. D. Familua**, A.R. Ndjiongue, K. Ogunyanda, L. Cheng , H.C. Ferreira and T.G. Swart, "A Semi-Hidden Markov Modeling of a Low Complexity FSK-OOK In-House PLC and VLC Integration," *in 2015 19th IEEE International Symposium on Power Line Communications and its Applications,* Austin, Texas, U.S.A Mar. 29-31, 2015, pp. 199-204.

2. K. M. Rabie, E. Alsusa, **A. D. Familua** and L. Cheng, "Constant Envelope OFDM Transmission Over Impulsive Noise Power-Line Communication Channels," *in* 19th *IEEE International Symposium on Power Line Communications and its Applications,* Austin, Texas, U.S.A, March 29-31, 2015, pp. 13-18. **(Best Student Paper Award)**

3. **A. D. Familua**, K. Ogunyanda, T.G. Swart, H.C. Ferreira, Rex Van Olst and L. Cheng, "Narrowband PLC Channel Modeling using USRP and PSK Modulations," *in* 18th *IEEE International Symposium on Power Line Communications and its Applications,* Glasgow, Scotland, U.K., March 30-April 2, 2014, pp. 156-161.

4. K. Ogunyanda, **A. D. Familua**, T.G. Swart, H.C. Ferreira and L. Cheng, "Permutation Coding with Differential Quinary Phase Shift Keying for Power Line Communication," *in* 5th *IEEE PES on Innovative Smart Grid Technologies (ISGT) Europe 2014,* Istanbul, Turkey, Oct. 12-15, 2014, pp. 1-6.

5. K. Ogunyanda, **A. D. Familua**, T. G. Swart, H. C. Ferreira, L. Cheng and T. Shongwe, "Evaluation and Implementation of Cyclic Permutation Coding for Power Line Communications," *in* 6th *International Conference On Adaptive Science and Technology (ICAST),* Ota, Nigeria, Oct. 29-31, 2014, pp. 1-7.

6. K. Ogunyanda, **A. D. Familua**, T. G. Swart, H. C. Ferreira and L. Cheng, "Adaptive Permutation Coded Differential OFDM System for Power Line Communications," *in* 6th *International Conference On Adaptive Science and Technology (ICAST),* Ota, Nigeria, Oct. 29-31, 2014, pp. 1-7.

7. **A. D. Familua** and L. Cheng, "Modeling of In-House CENELEC A-Band PLC Channel Using Fritchman Model and Baum-Welch Algorithm," *in* 17th *IEEE International Symposium on Power Line Communications and its Applications,* Johannesburg, South Africa, March 2013, pp.173-178.

8. **A. D. Familua**, A. O. Qatarey, P. A. Janse Van Rensburg and L. Cheng, "Error pattern/behavior of noise in in-house CENELEC A-band PLC channel," *in* 16th *IEEE International Symposium on Power Line Communications and its Applications,* Beijing, China, March 2012, pp. 114-119.

CHAPTER 1

Introduction

In recent times, the indoor low voltage power line has received significant research interest as an alternative medium of data transmission, mostly for smart home, home inter-networking and other data communication applications. Power line communication technology offers a cost effective means of data transmission especially in the home environment, as it utilizes the existing ubiquitous power line network (PLN). Therefore, saving cost of new cabling as existing power ports serve as transmit and receive ports (a plug and play scenario).

Data transmission on the PLC channel is subjected to power and frequency limitations communication engineers must adhere to as stipulated by the European regulatory body for narrowband PLC applications [1]. This is on account of the fact that PLNs were not originally conceptualized for its recent use for data communication, hence, the network acts as an antenna radiating some high frequency signals, thus interfering with other communication systems operating at such frequencies. Such standard includes the CENELEC standard [1] for narrowband PLC application in the 9 - 148.5 kHz spectrum and IEEE P1901.2 standard governing the use of narrowband spectrum below 500 kHz for smart grid applications [2]. The CENELEC standard defines the maximum allowable peak voltage at 9 kHz and 95 kHz (CENELEC A band) to be 5 V and 1 V respectively, while stipulating a maximum of 0.63 V for the 95-148.5 kHz (CENELEC B, C and D) frequency spectrum [1, 3, 4].

PLC technology generally operates in a hostile environment inherited from the PLN. This is as a result of the intrinsic attributes of the PLN itself and that of the power electronic appliances connected onto the network, hence, uncoordinated switching “on” and “off” of these appliances introduce noise harmonics (background, impulse and narrowband noise) as well as electromagnetic interference. Consequently, these noise impairments result into burst errors at the receiver, thus inhibiting reliable data transmission and leading to system performance degradation [5, 6]. Unlike the Additive White Gaussian noise (AWGN) model assumed for most communication systems, this noise model fails to capture the properties of noise encountered on the PLC channel. This is because periodic noise or random noise

pulses injected by power electronic appliances onto the network is a deviation from the AWGN model. These noise type are categorized as non-white, non-Gaussian and unstable due to its impulsive attributes, therefore, it is labeled as Non-additive White Gaussian Noise (NAWGN). The efficient and optimal performance of a conventional linear receiver in the white Gaussian noise environment can thus be made to drastically degrade in this NAWGN environment of the PLC channel. Therefore, communication performance in such non-Gaussian noise/impulsive channels could be greatly enhanced if we know and exploit the knowledge of the channels statistical attributes, hence, the need for an experimentally based statistical channel model.

Due to the varying noise parameters obtained from country to country, based on the fact that noise impairments are dependent on mains voltages, topology of power line, place and time, there is need for constant measurement campaigns before statistical mathematical models are derived.

Due to the noisy and unstable nature of the PLC channel, an ideal scenario would have been transmission of signals at high power or at selected frequencies devoid of noise, perturbation and interference associated with the NB-PLC channel. However, based on power and frequency restrictions enforced by regulatory bodies, it is vital to implement robust and flexible transceiver design based on these restrictions. The degradation in performance over NB-PLC systems is majorly caused by multipath-induced dispersion and impulse noise [7, 8]. Impulse noise (IN) poses as the most difficult noise impairment and the major cause of burst errors on the NB-PLC channel as a result of its high power spectral density (PSD) [6], though transient in nature, it could affect significant or all part of the frequency spectrum at a specific duration [9].

PLC-G3 and PRIME PLC standards [10–12] have established OFDM, a multi-carrier digital modulation system to be more robust against frequency disturbance, impulse noise and frequency selective fading when compared to M-ary frequency shift keying (M-FSK) modulation and other single carrier modulation systems [4, 13, 14]. This is due to attribute of the OFDM in spreading the noise energy over the available sub-carriers [15], hence, the choice of PLC-G3 standard in this thesis.

Therefore, efficient, flexible and reliable channel models are thus valuable to developing and

evaluating robust modulation schemes (preferably multi-carrier) and forward error correcting codes capable of exploiting or mitigating noise and fading on the low voltage NB-PLC channel. Graphical models such as semi-hidden Markov models (SHMMs) offer a powerful, universal framework for formulating statistical models of communication channel problems (such as noise, perturbation and interference). However, the formulation of SHMMs is only practicable if combined with efficient algorithms for learning and inference.

One of the classical models for channel modeling is based on Markov chains, where each state is linked to a peculiar channel status. Existing Markov chain models postulated the number of states, as well as their associated distribution which are based on the channel status (error-free state and error state) and other physical considerations such as the environment (rural or urban, residential or industrial sites etc.). Training algorithms are then used to adjust and estimate the SHMM parameters such as the state transition probability matrix and error distributions (error-free run distribution and error distribution) based on experimental measurement or simulations. Fritchman [16] have proposed a mathematically inclined graphical model based on SHMM for noise modeling in channels with fading and long burst errors (such as the PLC channel), and several investigations have been carried out to ascertain that this channel model have fitted the experimental measurement [17–19]. The major problems of this SHMMs is probability evaluation and learning or parameter estimation, which have been solved over the years by well-known Maximum likelihood estimation (MLE) or Expectation Maximization (EM) algorithm like the Baum-Welch algorithm employed in several literatures, [18], [20], [21]. Gradient method is another parameter estimation method as applied in [17] to digital mobile radio channels.

In this thesis, the development of a novel reconfigurable software-defined un-coded single carrier and multi-carrier (OFDM) transceiver systems for the NB-PLC channel transmission and modeling is undertaken. This implementation took into consideration flexibility of the transceiver systems for possible modulation upgrade and/or addition of forward error correction (FEC) scheme for the improvement of the overall system performance. This is achieved by making use of the universal software radio peripheral (USRP) for a reconfigurable software-based or advanced software programmable modulation. Figure 1.1 shows a typical architecture of a software-defined radio (SDR) and hardware defined radio system.

This figure illustrates communication elements that are implemented in the hardware and

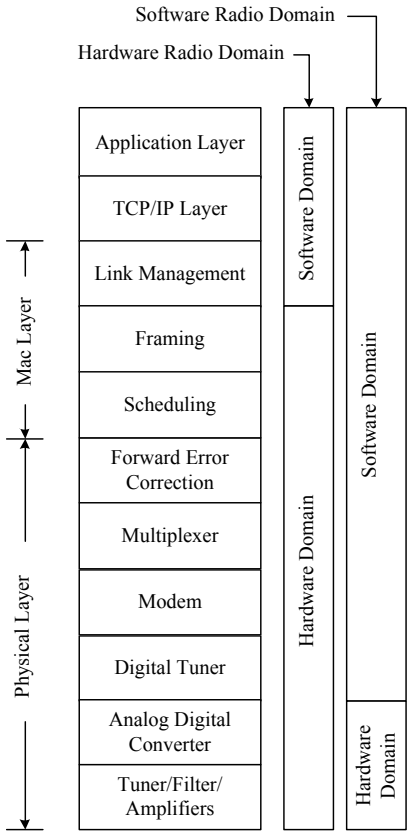

FIGURE 1.1: Basic software-defined radio vs. hardware-defined radio architecture.

software domain of the hardware and software-defined radios. The use of software-defined approach in this project is as a result of the advantages it offers such as: reconfigurability, interoperability, efficient use of resources under varying conditions, reduced obsolescence (future proofed) and lower cost, as most communication elements often implemented in hardware are now implemented in software realm.

Moreover, a First and Second-Order semi-hidden Fritchman model (SHFMM) is utilized to model the NB-PLC channel. Unlike simulation-based NB-PLC transmission often recorded in literature, empirical data (error sequences) are obtained based on real-time PLC transmission at the two measurement sites (residential and laboratory), taking into consideration the single-carrier and multi-carrier system, as well as the two distinct noise scenarios (mildly and heavily disturbed). Parameter estimation of the SHFMM model parameters is obtained using the First and Second-Order iterative BWA to train the model utilizing the empirical data as training data and assumed initial SHFMM parameters as the input. Precise statistical channel models that depict the NB-PLC channel is realized, validated and can be used to exploit and mitigate NB-PLC noise through robust modulation design, FEC design and

performance evaluation as the resulting models furnishes us with information about the error distribution on the NB-PLC channel.

A novel Metropolis-Hastings algorithm is also developed based on MCMC technique for Bayesian inference analysis and further utilized in optimizing model results obtained for both the single-carrier and multi-carrier systems. Resultant models obtained from the Metropolis-Hastings algorithm are near optimal model results with rich parameter sets guaranteed to be closer to the global maxima as opposed to locally maximized model results obtained based on BWA trained models.

Furthermore, this thesis also realizes a novel implementation of a low complexity Frequency-shift keying (FSK)-On-off keying (OOK) hybrid PLC and VLC transceiver system. The functionality and performance of the integrated PLC-VLC transceiver system is ascertained, empirical data (error sequences) are obtained based on real-time transmission at both in-house residential and laboratory site at three different times of the day. A First and Second-Order SHFMM is realized for the integrated system. Parameter estimation of the SHFMM model is obtained using the First and Second-Order iterative BWA to train the models utilizing the empirical data assumed and initial SHFMM parameters. The most probable parameter that depicts the empirical data are obtained and validated and further optimized for near optimal models using the Metropolis-Hastings algorithm.

1.1 Problem Statement/Motivation

The performance of several digital communication systems in the presence of AWGN has oftentimes been employed as a benchmark test in several studies over the years. On the contrary, NB-PLC channel is a principal example of a real channel where non-AWGN is predominant. In reality, the NB-PLC channel is a very harsh channel where the unusual mix of noise comprises, the permanent frequency disturbance and impulse noise, of which the major cause of burst error is the impulse noise.

There is a global consensus that OFDM, a digital multi-carrier modulation technique is the most appropriate for PLC channel in general. Furthermore, it should be noted that OFDM is also a modulation of choice in several other digital communication systems such as, wireless

communications network, digital television and audio broadcasting and 4G mobile communications. Thus, several inexpensive OFDM-based NB-PLC modem (hardware and chip sets) have become extensively accessible. Despite the availability of NB-PLC modems such as MAX2990, ST7590 and Cool Phoenix 2 (CPX2), the major problems of this on-board chip is, it lacks flexibility. This is peculiar to modems with application specific integrated circuits (ASICs), which are incapable of supporting multiple robust adaptive modulations and/or other robust FEC techniques. Assessment of new communication protocols may be expensive if these on-board ASICs are to be used for evaluation. Likewise, extensive alterations in the physical layer operation and transmit power of these modems is a difficult task as there is need for changes in the hardware architecture and hardware configuration respectively.

Due to the unstable nature of the PLC channel, constant measurement campaigns are needed from time to time before precise mathematical-based statistical model are obtained. This is due to varying noise parameters obtained from country to country, as a result of the dependence of noise impairments on mains voltages, topology of power line, place and time. Therefore, it is crucial to develop a flexible, reconfigurable, upgradable and reusable software-defined NB-PLC transceiver systems to cater for the demand of the ever-changing PLC channel at all time. This flexibility will help communication engineers to observe and ascertain the presumed robustness of adaptive modulation and FEC codes to exploit and mitigate noise on the unfriendly NB-PLC channel.

Obtaining globally maximized model parameters based on the use of BWA algorithms for training SHMM is a major challenge in the use of SHMM to model burst error channels like the NB-PLC channel. This is as a result of random initial parameters often chosen as input to the BWA algorithms. A solution to this problem is the use of Metropolis-Hastings algorithm, an MCMC technique based on Bayesian inference to optimize the model parameters and obtain near optimal models with rich parameter sets guaranteed to be close to the global maxima.

1.2 Research Questions

- Are reconfigurable software-defined NB-PLC transceiver system practically achievable to cater for the demands of the unstable and harsh NB-PLC channel to achieve improved data transmission without making architectural changes to the hardware?
- Are multi-carrier modulations (OFDM) more robust against the NB-PLC channel harshness than the single-carrier modulations on a real PLC channel in the presence of similar interference scenarios?
- Do SHMMs based on maximum likelihood estimation technique yield precise statistical channel models that are precise and statistically depicts measured data?
- Can we analytically validate that a Second-Order SHMM for the NB-PLC channel gives a better and more precise channel model than its First-Order counterpart?
- Can Metropolis-Hastings algorithm based on Markov Chain Monte Carlo technique for Bayesian inference aid the improvement of our MLE obtained models to obtain near-optimal, precise channel model with rich parameter sets guaranteed to be close to the global maxima?

This thesis is thus designed to answer these questions through a practical implementation of a reconfigurable software-defined un-coded single-carrier and multi-carrier (OFDM) NB-PLC transceiver systems for real-time NB-PLC transmission and channel modeling. The use of the universal software radio peripheral (USRP) originally intended for wireless radio frequency applications allows us to achieve a flexible, reconfigurable, upgradable and reusable NB-PLC transceiver system as majority of the digital signal processing (DSP) task is performed in the software domain. This includes adjustment in modulation technique; transmit power and frequency and other parameters. One important thing to note and that has been dealt with in details in this research, is that the use of the USRP requires adapting it for PLC transmission by designing a coupling circuit used to couple signals onto the channel.

1.3 Research Hypothesis

The key research hypothesis for our research in order to answer our research questions is highlighted as follows:

1. Practical measurement and experimentally based channel models offers a more precise channel model than simulation based modeling.

2. Semi-Hidden Markov model combined with efficient Baum-Welch algorithm gives a precise channel model that are statistically equivalent to the measured experimental data.

3. A Second-Order Semi-Hidden Markov model for the NB-PLC channel will outperform and give a more precise model than its First-Order counterpart.

4. Metropolis-Hastings algorithm, a Markov Chain Monte Carlo technique based on Bayesian inference approach will improve the SHMM parameter sets and guarantee the realization of parameters sets that are globally maximized for near optimal models.

1.4 Research Aim and Objectives

The development of robust, flexible and reconfigurable software-defined transceiver systems to achieve reliable transmission on burst error and fading affected non-AWGN channels is becoming paramount for communication engineers. Likewise, the realization of precise and near-optimal statistical channel models that depicts empirical data is also of vital importance. In this regard, this study is aimed at developing a reconfigurable software-defined un-coded single carrier and multi-carrier (OFDM) modulation transceiver systems for the evaluation of different modulation schemes (single and multi-carrier) on the in-house residential and laboratory NB-PLC channel, as well as realize precise channel models that depicts the NB-PLC channel based on maximum likelihood estimation technique and the Metropolis-Hastings MCMC Bayesian inference technique. To achieve the aim of this study, the following research objectives are emphasized.

1. To develop an efficient coupling circuit (a bandpass filter) based on differential mode and capacitive coupling recommended for low voltage power line transmission, as the coupling circuit plays an important role of coupling signals onto the PLC network as well as providing galvanic isolation between the power line and both transmit and receive USRP.

2. To develop a novel reconfigurable software-defined un-coded single carrier and multi-carrier (OFDM) modulation NB-PLC transceiver systems using USRPs, aimed at achieving a flexible, reconfigurable, upgradable and reusable NB-PLC transceiver system and test-bed for future channel measurements.

3. To develop a novel low complexity Frequency-shift keying (FSK)-On-off keying (OOK) hybrid PLC-VLC transceiver system test-bed and realize a statistical channel model for the hybrid system.

4. To carry out real-time transmission and obtain empirical data (error sequences) with test-beds in (2) and (3) in a residential and laboratory in-house site taking into consideration two distinct noise scenarios, "mildly disturbed" and "heavily disturbed" for modeling purposes.

5. To develop a First and Second-Order Baum-Welch algorithm based on maximum likelihood estimation technique for parameter estimation of the NB-PLC channel model and the hybrid PLC/VLC channel model. Channel models are then obtained using empirical data obtained in (4).

6. To validate and analyze models obtained in (5) using metrics such as: log-likelihood ratio, error-free run distribution, Chi-Squared test and Mean Square Error to ascertain the precision of the models.

7. To develop a novel Metropolis-Hastings algorithm based on Markov Chain Monte Carlo technique to improve the maximum likelihood estimated models obtained in (5) in order to obtain a near-optimal and precise channel models with rich parameter sets.

1.5 Research Approach

Having carefully analyzed the focal points and scope of this research, the following procedures were utilized in order to achieve the main objectives of the research spelt out in Section 1.4.

- **Literature and technical background review**: A concise but extensive technical review and technical background of related resources through consultation of published journals, conferences, books and websites is presented.

- **Hardware set-up and Software installation**: Here, set-up of the several hardware used in this research was done. The correct daughterboards low frequency transmitter (LFTX) and low frequency receiver (LFRX) appropriate for the narrowband PLC frequencies were installed on the two USRP hardware. The correct firmware and Field Programmable Gate Array (FPGA) images were also loaded onto the USRP. Matlab software was installed and the Matlab and Simulink communications systems toolbox support package for the USRPs (SDRU) were installed on the host transmitting and receiving PCs. Furthermore, a low complexity Frequency-shift keying (FSK)-On-off keying (OOK) hybrid PLC and VLC transceiver system is developed.

- **Configuration**: The transceiver (LFTX and LFRX USRP) were configured with Matlab to communicate with the host transmitter and receiver PCs together with the appropriate parameters in readiness for NB-PLC transmission.

- **Modification**: Since the USRP was originally conceptualized for radio frequency communication, an interface is needed to adapt it to the PLC channel, hence, a narrowband transmitting and receiving differential mode capacitive bandpass filter (coupling circuit) was designed and implemented to couple and decouple the signal to and from the PLC channel respectively in real-time.

- **Testing stage**: The implemented NB-PLC transceiver was used to transmit and receive on the PLC channel using the developed single-carrier and multi-carrier (OFDM) transceiver system. Proper coupling is ascertained and performance evaluation of the implemented single-carrier and OFDM transceiver scheme is done. The test-beds were employed at both residential and laboratory in-house site taking into consideration two distinct noise scenarios "mildly disturbed" and "heavily disturbed". Moreover, the implemented hybrid PLC-VLC system was also used to transmit and receive at different times of the day at both measurement sites.

- **Measurement stage**: Measurement and generation of empirical data for each modulation scheme was carried out at both measurement sites for the two distinct noise scenarios considered for modeling purposes.

- **Modeling and analysis**: After the implementation of the training algorithm (BWA algorithm) considered in this work, the empirical data obtained were utilized for channel modeling to obtain precise mathematically-inclined channel model using the

SHFMM and BWA algorithm. A Metropolis-Hastings algorithm, a MCMC technique based on Bayesian inference approach is used to improve the obtained modeling results for a near-optimal and precise channel models. Analysis of the obtained modeling results is then carried out.

1.6 Research Relevance and Application

Despite the availability of several inexpensive OFDM-based NB-PLC modems, these modems are built with application specific integrated circuits (ASICs) which reduces its flexibility in adapting to other scenarios different from that which it was configured. Hence, extensive alterations to meet the demand of the ever changing and varying NB-PLC channel will require hardware architectural changes. On the contrary, the developed flexible, reconfigurable, upgradable and reusable software-defined NB-PLC transceiver systems has the capability of been adapted to other modulation techniques and also allows the addition of FEC codes to mitigate noise on the harsh channel without the need for hardware changes or alteration. This test-bed can be used for constant measurement campaign required on the PLC channel and can also be adapted for Multiple-Input and Multiple-Output PLC (MIMO PLC) and hybrid PLC/VLC transceiver.

Moreover, the developed hybrid PLC-VLC system test-bed helps in realizing the underlying gain achievable by leveraging the existing ubiquitous PLN infrastructure to render connectivity, while exploiting the illumination system of power saving Light Emitting Diodes (LEDs) for wireless data transmission. The ubiquitous attribute of the two communication systems allows VLC to provide a good complementary wireless data transmission technology to the existing in-house PLC in a similar manner broad-band Ethernet connection enjoys the support of Wi-Fi.

Furthermore, the relevance of the realized precise and near-optimal statistical channel models are highlighted as follows:

(a) The realized precise near-optimal channel models can be used an effective link adaptation as well as efficient fading compensation on the NB-PLC channel.

(b) Channel measurement and modeling of the NB-PLC channel furnishes us with information about the severity of the burst errors that exist on the channel in real-time and from location to location considering different noise scenarios. It also allows us to know the impact of noise introduced by power electronics appliance on the high frequency signals transmitted on the channel, although this is not included in this study.

(c) The channel models give us statistical information about the channel impairments such as, error-free run distribution and error probability. The error-free run distribution (EFRD) denoted by $\Pr(0^m|1)$ implies the probability of m consecutive error-free transmissions that could possibly occur after transitioning from an error transmission. In other words, this gives how errors are distributed on the channel, which will help inform the choice of FEC code to use to exploit and mitigate noise impairments on the channel, as each FEC codes has its own error correcting capability.

(d) The above mentioned statistical information including: the state transition probabilities, EFRDs are useful in the design and evaluation of the performance of multi-carrier modulation schemes and FEC codes in order to optimize the performance of the NB-PLC transceiver system. Consequently, this reduces performance degradation and guarantees reliable communication on the harsh PLC channel.

(e) The evaluation above can then be used in optimizing and enhancing of the overall PLC transceiver system design to mitigate the unpleasant effect noise impairments have on high frequency signals transmission on the power line channel.

1.7 Research Contributions

This research contributes the following:

- Development of a novel reconfigurable software-defined PLC transceiver using USRP, a range of software defined radio. The developed system offers flexibility, interoperability, reconfigurability and the capability to be utilized to implement different waveforms for several real-time scenarios and performance analysis.

- Development of a novel low cost hybrid PLC/VLC to achieve a good complementary wireless data transmission technology in tandem with the existing In-House PLC in

a similar manner broad-band Ethernet connection enjoys the support of Wi-Fi. The realized hybrid system offers both illumination and data communication capabilities with the intent of upgrading to a more robust OFDM based hybrid PLC-VLC system as well as a software-defined hybrid PLC-VLC system.

- Development of a Second-Order SHFMM and analytical validation of the superiority of the Second-Order SHFMM over the First-Order SHFMM in modeling NB-PLC channel based on empirical data as opposed to simulation based modeling often reported in literatures.

- A novel development of a Metropolis-Hastings algorithm for SHFMM parameter optimization in order to obtain an optimized parameter set guaranteed to be near-optimal and globally maximized as opposed to locally maximized parameter sets obtained using only maximum likelihood estimation technique.

1.8 Thesis Organization

This thesis comprises of nine chapters. Chapter 1 gives an a brief introductory background of power line communication; problem statement/motivation; research questions; hypothesis; aims and objectives; research approach; research relevance and application; and lastly the thesis organization. From the findings of this research work, Chapters 5-6 are arranged as published and accepted peer-reviewed conference publications, while Chapter 7-8 are arranged as submitted for publication in a peer-reviewed journal publication. In conclusion, Chapter 9 summarizes the study with regards to modeling results and analysis of work presented in Chapters 5-8 of this thesis. Furthermore, research contributions are highlighted and recommendations for possible future research are stated. The synopsis of Chapter 2-8 are presented as follows.

In Chapter 2, background details and review of power line communications and visible light communications are presented. A concise but detailed literature on PLC channel characteristic, narrowband PLC historical overview, standards, PLC channel modeling and noise classification is well documented. Furthermore, single-carrier and multi-carrier modulations globally accepted as the modulation of choice for narrowband PLC applications is also presented.

In Chapter 3, a review of background details for Maximum Likelihood Estimation and Bayesian Inference Machine Learning algorithms for Semi-Hidden Fritchman Markov model parameter estimation is undertaken. Baum-Welch algorithm, the most popular expectation maximization or maximum likelihood estimation algorithm for parameterizing SHFMMs is discussed. In addition, Metropolis-Hastings algorithm, a Bayesian inference statistical algorithm based on Markov Chain Monte Carlo technique is presented as well as a literature review of its uniqueness in helping to realize near-optimal models with rich parameter sets.

In Chapter 4, detailed design and implementation of the coupling circuit, the reconfigurable software-defined un-coded single carrier and multi-carrier (OFDM) modulation NB-PLC transceiver systems using USRPs is well documented. Moreover, procedures for hardware set-up, configuration, modification and software installations are highlighted. This chapter also discusses an end-to-end modeling methodology and approach based on the use of BWA, an MLE algorithm utilized in realizing SHFMM for the developed systems.

In Chapter 5, the developed un-coded single carrier Binary Phase Shift Keying (BPSK), Differential BPSK (DBPSK), Quadrature Phase Shift Keying (QPSK) and Differential QPSK (DQPSK) narrowband PLC transceiver is used to carry out channel measurement, analysis and modeling of an in-house CENELEC A narrowband PLC channel. Fritchman model and the efficient Baum-Welch MLE algorithm is used to model the channel. Results obtained showed a statistical correlation between the measured error sequences (empirical data) and the model regenerated error sequence.

In Chapter 6, the focus is on the development of a low complexity Frequency-shift keying (FSK)-On-off keying (OOK) hybrid PLC and VLC transceiver system for in-house transmission. The ubiquitous nature of the PLC and VLC made it possible for VLC to offer a good complementary wireless data transmission technology to the existing In-House PLC in a similar manner broad-band Ethernet connection enjoys the support of Wi-Fi. Analysis and modeling of the overall system integration was undertaken. Precise channel models obtained for the hybrid system shows a correlation between the empirical data and model regenerated data.

In Chapter 7, measurements and modeling were carried out using the developed un-coded

multi-carrier (OFDM) modulation narrowband band PLC transceiver for two in-house measurements sites (residential and laboratory) taken into consideration two distinct noise scenarios: the mildly and the heavily disturbed. A First and Second-Order SHMM was undertaken and results obtained show a statistical correlation between measured and model generated data. Furthermore, results obtained ascertain the superiority of the Second-Order SHMM over its First-Order counterpart using Chi-Squared test and the mean squared error test as well as error-free run probability and the log-likelihood values.

In Chapter 8, Metropolis-Hastings algorithm based on MCMC technique was developed and used to improve the SHFMMs obtained for the systems in Chapters 5, 6, 7. The resulting models are more precise and near-optimal model with rich parameter sets guaranteed to be closer to the global maxima than model results obtained in Chapters 5, 6, 7. The near-optimal model chosen through the use of the Metropolis-Hastings (M-H) algorithm to optimize model results in Chapters 5, 6, 7 is presented in Appendix B.

Chapter 9 concludes the thesis. Summary of the thesis and key results are highlighted. Future research possibilities and recommendations are presented. This chapter is concluded by giving final remarks.

CHAPTER 2

Background Review: Power Line Communication, Visible Light Communication and PLC Digital Modulation

2.1 Introduction

Communication is broadly defined as the process of information transfer from a source to a sink via a medium identified as a channel. In communications, the physical medium or logical connection or pathway through which this information is conveyed is recognized as a communication channel. This pathway (communication channel) utilizes two major media types: cables (power line, co-axial cables, twisted pair, and optic fiber) and broadcast (visible light, infrared, free space, microwave, ionosphere, satellite, and radio). A typical communication system hence, consists of a transmitter, channel and receiver. The transmitter converts information into a signal carrying information that can be sent via the communication channel, while the communication channel then conveys the signal to the receiver. The receiver then takes the transmitted signal from the channel and converts it back into usable information. The receiver is tasked with making sure the recovered information from the noise impaired channel is error-free, hence, the reason for the deployment of digital modulation techniques as well as channel coding in digital communication systems. Figure 2.1 and Figure 2.2 show a typical communication system and a digital communication system and its components respectively. In a typical digital communication system, the transmitter majorly comprises of a source encoder, channel encoder and modulator, while the receiver components are source decoder, channel decoder and demodulator as shown in Figure 2.2.

The background or review related to the research project is presented in this Chapter. Detailed background of power line communication is presented. Modulation methods for PLC

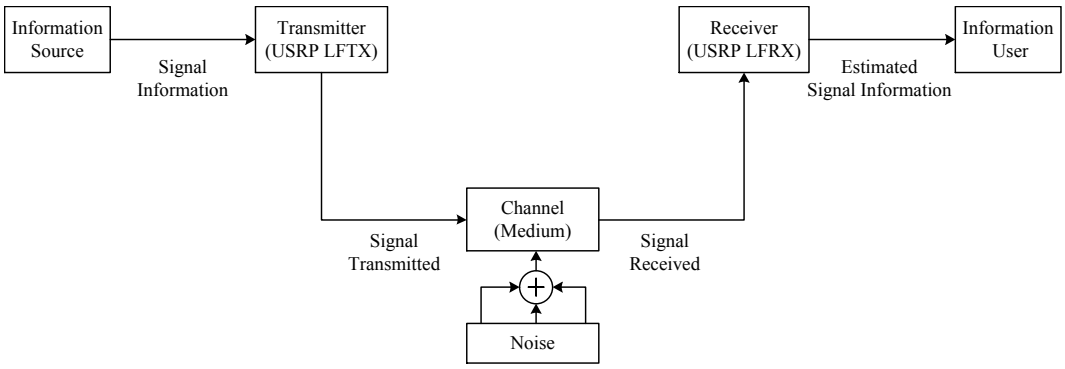

FIGURE 2.1: Basic components of a communication system.

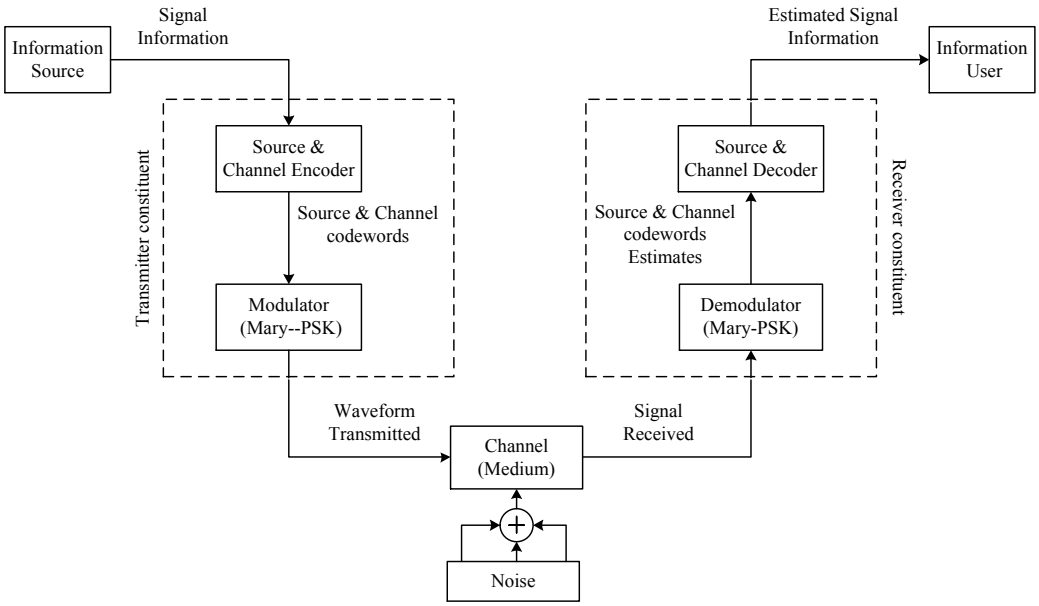

FIGURE 2.2: Digital communication systems block diagram.

transceiver system design is also detailed, as well as single-carrier modulation and orthogonal frequency division multiplexing system for narrowband PLC. This Chapter is concluded with a concise background and overview of visible light communications technology.

2.2 Power Line Communication

PLC technology is simply a communication technology that uses the ubiquitous power line network as a pathway for signal and data communication. Ever since the late 1990s, this technology has received increased research effort characterizing the PLC channels with the aim of developing cost-effective communication systems using the electrical power distribution line as a medium of data transmission.

Reliable power line communication systems for smart home, home inter-networking, smart grid and Internet protocol television (IPTV) are now readily available. Nevertheless, power lines were not originally conceptualized for communication purposes, hence, constitute a difficult (harsh and unstable) environment for information communication via old analog signaling or recent universal modern digital PLC systems [22]. Power line communication channel exhibits a low-pass behavior, frequency selective fading, and alternating current (AC) associated cyclic short and abrupt long-term imbalance or variations [22]. Furthermore, PLC channel noise has been classified based on temporal and spectral attributes. In [7, 23], one can identify narrowband noise (NBN), colored background noise (BN), periodic impulse noise (synchronous and asynchronous to AC mains frequency) and asynchronous impulsive noise as the dominant noise impairments on the PLC channel. These noise impairments are leading PLC researchers to label the channel as a horrible channel [24].

Aside from these, the fundamental concept of PLC entails the deployment of small-signal, high frequency technologies via power distribution networks and cables that were originally designed for power (electricity) distribution at low frequencies. Hence, the PLC equipment's communication ports are bound to fail should they be connected directly to the power line grid voltage. Therefore, PLC coupling circuits are crucial for transmitting and receiving on the power line while at the same time providing galvanic isolation and protection of PLC communication devices. PLC couplers are either designed as capacitive or inductive coupling and in either common or differential mode as will be discussed in Section 2.2.8.

2.2.1 PLC Frequency Bands Classification and Topologies

Power line communication technology uses the very-low frequency (VLF) up to the ultra-high frequency (UHF) of the International Telecommunications Union (ITU) stipulated frequency spectrum for power line application purposes as shown in Figure 2.3. The three main categories of power line technologies according to these frequency classifications are: Ultra-Narrowband, Narrowband and Broadband PLC technologies. As show in Figure 2.3, narrowband PLC operates in the frequency below 1.8 MHz (3-500 kHz to be specific), while the broadband PLC (BB-PLC) technologies operate at frequency above 1.8 MHz (1.8-100 MHz) [25]. Concise information on corresponding regulations for narrowband PLC frequency band is discussed in Section 2.2.2. Refer to [22] for corresponding regulations applicable to

Broadband PLC frequency bands. Besides, an overview of NB-PLC systems is discussed in Section 2.2.2.

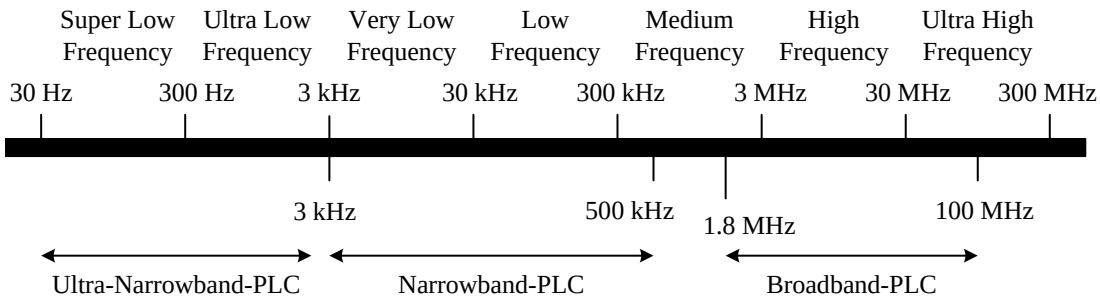

FIGURE 2.3: ITU frequency spectrum and its PLC usage.

Apart from the classification of PLC technologies into narrowband and broadband PLC, it has become common practice to categorize PLC technologies based on operational voltages of the PLN namely: the high voltage (HV) lines, medium voltage (MV) lines and low voltage (LV) line as discussed as follows [25–27].

- **HV Power lines**: The HV power lines with voltages ranging between 110-380 kV utilizes long overhead lines with small or no branches for nationwide power transmission, hence, making them suitable waveguides with lesser attenuation per line length compared to LV and MV power lines [22]. Nevertheless, their prospect for broadband communication applications has been limited till date due to time-varying HV electric arcing, corona-noise and besides, the feasibility and cost of transmitting and receiving signal on this line has been a drawback. However, some productive trials utilizing HV power lines are reported in [28–30].

- **MV Power lines**: These lines are in the 10-30 kV range and are linked with the HV power lines through primary transformer substations [22]. The MV power lines are either overhead or underground and are employed for the distribution of power between towns, cities and power-intensive industrial end-users [22]. These lines exhibit limited branches and are connected directly to intelligent electronic devices (IED) like capacitor banks, reclosers, phasor measurement units (PMU) and sectionalizers that only requires comparatively low data rates for monitoring and control which can be supplied by the narrowband PLC [22]. MV Power lines field trials and related studies are reported in [31–34].

- **LV Power lines**: The LV power lines are the most used topology for power line applications. Its voltage level ranges between 110-400 V and are interconnected to the MV power lines via secondary transformer substations. These lines are either directly or via LV bus bar cabinets linked to end-users premises. Note that relatively large territorial topology differences exist from country to country. In countries like US, a single house or few houses can be served by a small secondary transformer, however in Europe it is usually common to see up to 100 consumer premises being served by a secondary transformer substation. As reported in [35], notable differences also exist between building categories. Buildings are possibly grouped as high rise buildings, multiple-flat buildings with riser, isolated family houses, and multiple-flat buildings having communal meter room [22]. Their non-identical wiring topologies impact signal attenuation and disturbance between neighboring PLC networks [36]. Typically, the power grid is fed into the consumer premises via a house access point accompanied by an electricity meter and a fuse box also referred to as electrical distribution board (DB). Thence, the low voltage power lines are linked to several power points or sockets in all rooms in a star or tree topology fashion. An access network or systems often refers to PLC systems running from outside to the inside of the consumer premises while those operating inside are regarded as in-home systems. In summary, an access system or network makes data connection to a collection of consumers possible through overhead and/or underground power distribution network [24, 37–39], while the in-home network makes possible communication between different end-user devices within a consumer premises [24, 40–44].

2.2.2 NB-PLC Regulations

The power line network cables presently been used for communicating high frequency signals were not originally designed nor conceptualized for this purpose, therefore, conducted and radiated emissions often interfere with other communication systems like broadcast receivers operating in same frequency spectrum. Hence, both NB-PLC and BB-PLC electromagnetic compatibility (EMC) regulations exist to control interference on the network. The narrowband PLC regulations cater for the frequency spectrum within the 3-500 kHz range. Major narrowband PLC regulations are listed in Table 2.1 as follows.

Table 2.1: Narrowband PLC regulations

Country	Frequency Spectrum (kHz)	Regulatory Body
European Union (EU)	3-148.5	CENELEC
United States (US)	10-490	FCC
Japan	10-450	ARIB

Comité Européen de Normalization Électrotechnique (CENELEC) bands are a subset of all other NB-PLC bands and are the only bands accessible for use on a global scale. The CENELEC band is categorized into four different bands namely: CENELEC A in the range (9-95 kHz), CENELEC B in the range (95-125 kHz), CENELEC C in the range (125-140 kHz) and CENELEC D in the range (140-148.5 kHz) [1]. Apart from the specification of transmission limits and measurement routines, the CENELEC standard issued a directive on the use of CENELEC A band for electricity suppliers and their licensees, while bands B, C and D can be utilized by consumers. Furthermore, PLC devices or modems operating on the CENELEC C band must comply with the use of carrier sense medium access/collision avoidance (CSMA/CA) protocol. This protocol permits a maximal channel holding time of 1 second, a minimal of 125 milliseconds between channel usages by same device as well as a minimal of 85 milliseconds preceding the declaration of the channel as idle.

In US, efforts are underway [45] in the specification of 9-534 kHz spectrum for narrowband PLC purposes with the use of the stipulated CSMA/CA protocol conforming to CENELEC EN 50065-1 standard [1]. This is beneficial to equipment manufacturers as they would be able to effortlessly adapt their narrowband PLC products to European Union and United States market as well as lots of other market that adhere to these standards. Refer to [22] for detailed contemporary ITU and Institute of Electrical and Electronics Engineers (IEEE) narrowband PLC standards.

2.2.3 NB-PLC Specifications and Standards

NB-PLC technologies are operational in the very low frequency, low frequency and in a section of the medium frequency spectrum. NB-PLC bands comprise of the CENELEC bands (3-148.5 kHz), Chinese band (3-500 kHz), Japans Association of Radio Industries

and Businesses (ARIB) band (10-450 kHz) and the United States Federal Communications Commission (US-FCC) band (10-490 kHz). Apart from these classes of NB-PLC bands, the narrowband technology is further categorized as follows in terms of specification. Figure 2.4 shows an overview of NB-PLC specifications and standards.

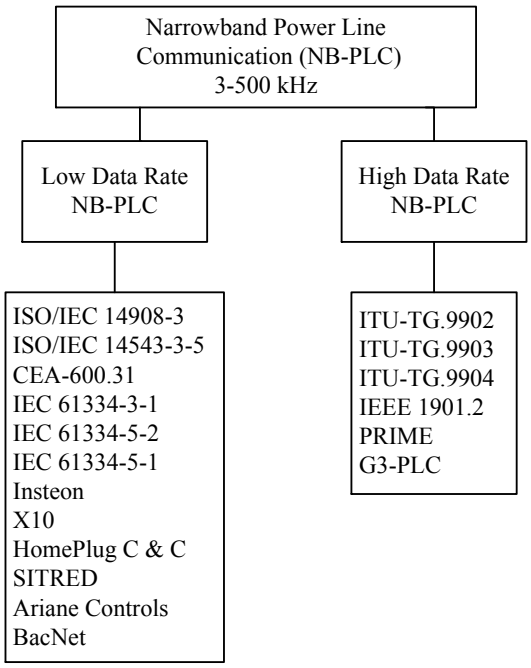

FIGURE 2.4: Overview of narrowband PLC specifications and standards.

Low data rate (LDR): The LDR specification refers to narrowband technologies that are able to achieve few kbits/sec of data rates and are commonly based on spread spectrum (SS) or single-carrier (SC) modulations. They are also described as power line carrier or distribution line carrier. Distinctive examples of NB-PLC LDR technologies are appliance complying with the following recommendations or standardization: ISO/IEC 14908-3 (local operating network (LonWorks)), IEC 61334-5 (Frequency Shift Keying (FSK) and spread-FSK), CEA-600.31 (Consumer Electronics Bus (CEBus)), ISO/IEC 14543-3-5 (Konnex Networks (KNX)) and IEC 61334-3-1. These recommendations are endorsed by two Standard Development Organizations (SDOs) namely: Organization for Standardization (ISO) and International Electro-technical Commission (IEC). Other examples of LDR NB-PLC technologies that are non-SDO based are: Building Automation and Control Network (BacNet), Ariane Control, Insteon, SITRED, HomePlug C & C and X10 [22].

High data rate (HDR): The HDR specification refers to multi-carrier narrowband technologies that are able to achieve data rates between tens of kbit/sec up to 500 kbit/sec. Current HDR NB-PLC technologies are OFDM-based and classic examples are those currently included in the ITU-Telecommunication Standard Sector (ITU-T) approved NB-PLC recommendations: ITU-T G.9902, ITU-T G.9903 and ITU-T G.9904 [46–48] as well as the ongoing IEEE 1901.2 project [2]. Non-SDO based HDR NB-PLC examples are the G3-PLC and Power line-Related Intelligent Metering Evolution (PRIME) which are industry specifications recently turned ITU-T recommendations G.9903 and G.9904 respectively [22].

2.2.4 PLC Channel Characteristics Overview

Reliable communication on the NB-PLC channel is vital in home automation, home internetworking and smart grid's value added services such as: remote diagnostics, distribution automation, load control and advanced meter reading [5, 22, 25]. The use of NB-PLC frequency spectrum up to 500 kHz is growing popular and is often utilized within Smart Grids as a result of its comparatively vast coverage. Regrettably, the NB-PLC channel exhibits extremely dynamic irreproducible and unpredictable attributes and is well known to subject high frequency communication signals to harsh or hostile channel conditions thus making data transmission at low speed absolutely challenging.

The PLC channel and noise conditions is heavily dependent on the scenarios defined in Section 2.2.1. Typically, the NB-PLC frequencies is characterized by complex noise scenarios, a low-pass behavior, low access impedance, alternating current-related cyclic short-term and abrupt long-term variations, frequency-selective multi-path fading, frequency-selective attenuation and time-selective and frequency-selective interferences [5, 25, 27, 49–51]. Frequency-selective attenuation also referred to as coupling loss is induced by impedance mismatch [52]. The frequency-selective multi-path fading is induced by non-uniformity of the power line network parts where cabling and coupled loads having dissimilar impedances produces signal reflections and consequently in-phase and out-of-phase combinations of the arriving signal components [22]. The equivalent transfer function could without much difficulty be derived as infinite impulse response filter as in [53]. One significant parameter that captures the feature of the frequency-selectivity that exist on PLC channel is the root mean square (rms) delay spread (DS). For instance, in the design of OFDM systems, delivering good

system performance requires that the guard interval be 2 to 3 times the root mean square delay spread [54].

Aside fading, the in-home PLC channel do exhibit time variation as a result of end-user appliances (loads) and/or line sections being connected or disconnected [55]. Furthermore, through the synchronization of channel measurements with the power line alternating current mains cycle, authors in [56, 57], showed that the in-home PLC channel varies in a cyclostationary fashion [22].

Till now, the PLC channel's low-pass behavior has not been studied. This low-pass behavior is as a result of di-electric losses that occur in the insulation between cable conductors and is more pronounced in outdoor underground long cable segments. Several differing cable types and differing length have been studied and their transfer function measurements detailed in [38, 58].

2.2.5 PLC Channel Modeling Overview

The characterization and modeling of the PLC channel have been a topic of constant research in recent times. Characterization of the PLC channel based on channel measurements is essential as it facilitates the derivation, validation and fine-tuning of PLC channel models, while the models themselves oftentimes furnishes communication engineers with valuable knowledge and insight thus stimulating more innovative PLC channel characterization.

Generally, PLC channel models are categorized into physical and parametric modeling approach, also referred to as *bottom-up* and *top-down* approach respectively [24]. The bottom-up physical modeling approach gives a description of the electrical attributes of the power line, for instance, through cable type specification (line parameters), the length of cable and location of branches [59–63], while the top-down parametric modeling approach focuses on a higher level of abstraction far from physical reality in describing the channel, for instance, through the channel's transfer function or impulse response [38, 64, 65].

Furthermore, each modeling classification specified above is further subdivided into stochastic and deterministic modeling. Deterministic modeling approach is based on describing one or a small set of particular reproducible PLC channel realization, while stochastic modeling

approach is concentrated at reflecting a wider range of PLC channel realization based on their probability of occurrence [22]. These classifications of PLC modeling approach is shown in Figure 2.5 and each further discussed as follows.

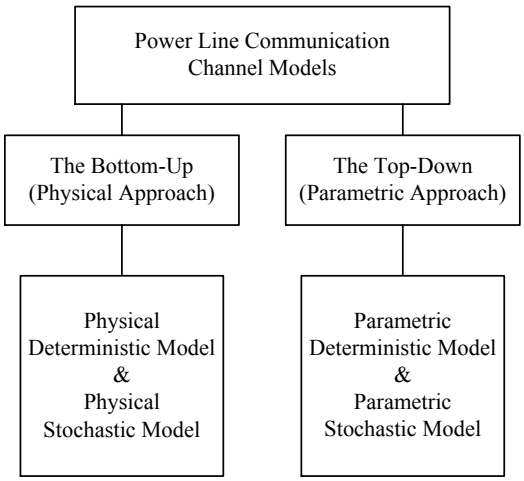

FIGURE 2.5: Classification of PLC channel modeling approach.

Physical-deterministic modeling: This modeling approach details the electrical attributes of the power line through cabling parameters specification, length of cable, location of branches and so forth [60–63, 66]. Majority of physical models are established on the representation of power line elements and their connected loads in their S-parameters or ABCD format [67] and are eventually interconnected to create the power line channel's frequency response [22, 60–63, 66, 68–70]. As an alternative, Berger and Moreno in [53, 71] proposed representing power line elements and connected loads as infinite impulse response (IIR) filters, a novel and intuitive viewpoint considering the fact that communication signals are transmitted on the PLC channel in electromagnetic waves form and might ricochet (bounce) an innumerable number of times between neighboring power line discontinuities. This type of physical modeling is specially and effectively fit for representing and testing deterministic power line conditions. It is also been labeled *bottom up* approach as they begin with an exact description of the electrical power line network being considered so as to attain a universal behavior of the communication channel. For a network (electrical) under consideration, this modeling approach can give a channel transfer function (CTF) model extremely close to the real or actual measurement. The disadvantage of this modeling approach is its requirement for a substantial number of input data and computational pool particularly should one desire to deduce channel statistics for quite a large amount of dissimilar network topologies.

Physical-stochastic modeling: This modeling type is a combination of the physical-deterministic modeling approach with stochastic components. In [72, 73], Tonello and Versolatto proposed a *statistical bottom-up* PLC channel modeling approach, where the channel transfer function is determined from the precise network topology through the use of a deterministic algorithm. The stochastic attribute of the model originates from random creation of practical electrical network topologies, founded on certain rules that are obtained from observed wiring practices, a technique also proposed in [53]. The physical-stochastic modeling approach inherits the advantages the deterministic approach has to offer in terms of accuracy with regards to physical transmission phenomena, with the possibility of randomly generating representative channel actualizations. Communication system engineers usually perform digital simulations of the overall system, thus allowing evaluation of the behavior and efficiency of differing digital signal processing algorithms. A physical-stochastic channel model is therefore anticipated to replicate key effects of the communication channel by producing a fairly large number of arbitrary channel actualizations that are statistical representation of real-life observations [22].

Parametric-deterministic modeling: This modeling category is probably the most frequently utilized but it is generally not labeled as parametric-deterministic model. Here, parametric-deterministic refers to a database of measured parameters for example the channel transfer function, where measurement results played-back could be utilized in PLC system simulations and performance analysis. The benefit is that the precise parameters based on observed actual scenarios are utilized devoid of the risk of generating impracticable channels due to inaccuracies in modeling. The drawback is that in order to get significant results generally, a large as well as diverse database is required [22].

Parametric-stochastic modeling: This modeling approach utilizes an advanced level of abstraction and also gives a description of the channel, for instance, by its impulse response features as reported in [58, 74, 75]. Analysis of gathered measurement data permits one to mathematically express and as well define a model. The mathematically expressed model is not essentially associated to the physical phenomena that occur while transmitting signals in electromagnetic form, but it is designed to reliably replicate the key features of the channel being considered. The parameters of the model are statistically defined, hence, allowing generation of diverse random realizations of the channel's impulse response or channel transfer

function that possesses similar statistics as the experimentally measured data. This modeling approach is occasionally labeled as a *top-down* approach, because it firstly takes into consideration the global statistics of the communication channel so as to define in-depth specifics of the channel structure. This modeling method usually delivers practicable results, but its drawback is that in order to produce the model, fairly large experimental data is required. In [38], an early instance of a statistical channel model was presented by Zimmermann and Dostert, where a general channel transfer function is defined conditioned on physical studies of the communication signal via simple electrical network topologies. The parameters of the model were then gotten through fitting of the mathematical model to several experimental measurements acquired on the broadband PLC channel in the 0-20 MHz spectrum. More recent statistical channel modeling results using this strategy can be found in [18, 19, 76, 77].

Figure 2.6 shows a juxtaposition of the four PLC channel modeling possibilities discussed, it important to note that each approach possess its own advantages and disadvantages for specific applications, hence, before making a decision on a choice of channel model one must ask what the channel model is meant to do or achieve? [22].

Some desirable attributes of a channel model are for instance highlighted as follows [22].

1. Identify the effect of the time-variant channel on the quality of the received signal in channel and system simulations as well as in algorithm testing, for instance, on SNR estimation, Multiple-input multiple-output (MIMO) schemes, tracking of channel filter.

2. Modeling of the correlation (in other words statistical relation) that exists between temporal and spatial channel variations as well as noise variations.

3. Reinforce the research of multi-user (in other words multi-point) power line communication systems.

4. Potential of extending to several other communication scenarios just by addition of a small set of measurement scenarios.

5. Description of modal coupling useful in designing of Multiple-Input Multiple-Output coupling circuits.

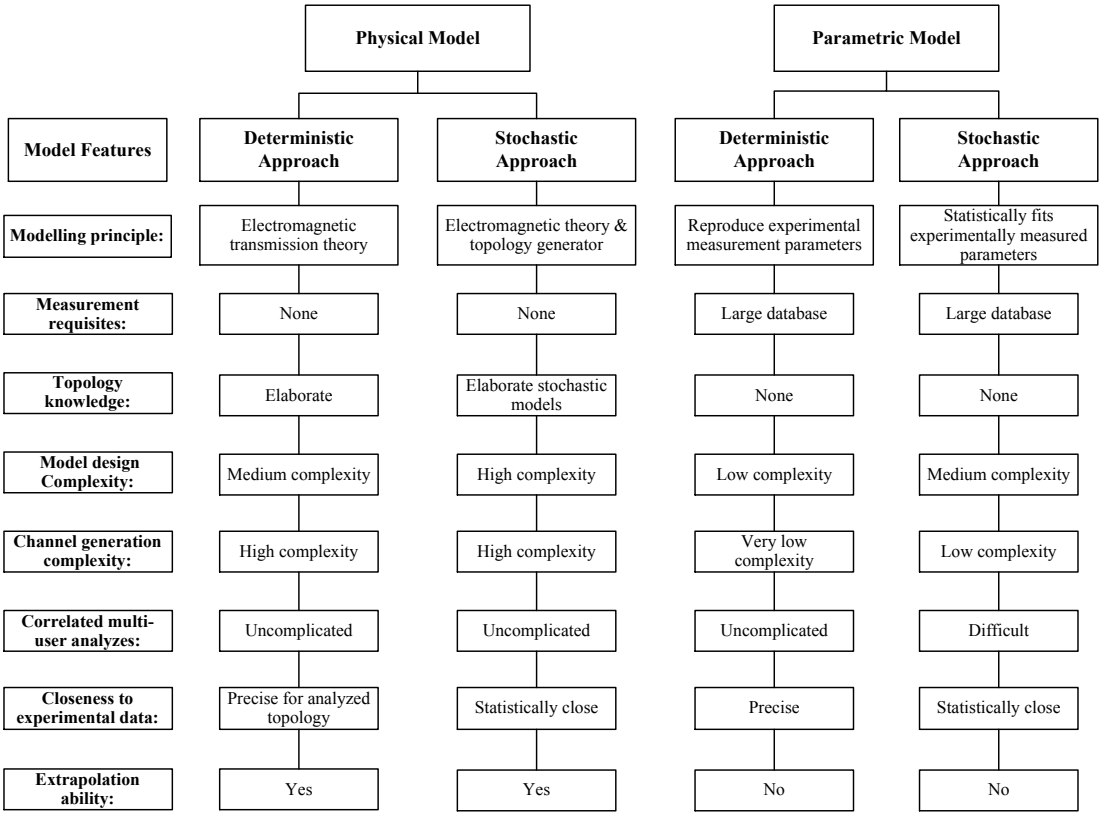

FIGURE 2.6: Juxtaposition of modeling approaches for PLC channel.

6. It must facilitate the design and improvement of PLC modem's analog front end (AFE).

The physical bottom-up or parametric top-down modeling approach can be used to realize goals (1-3) and (5) with more or less effort. Nevertheless, goals (4) and (6) are difficult to actualize with the parametric modeling option. Generally, adjusting the model parameters of parametric models requires large range of experimental measurement. On the other hand, physical models permit knowledge deployment, for instance, on the physical dimensioning of a novel scenario, to fine-tune physical model parameter. Subsequently, just a reduced set of experimental measurement is required for rough validation purposes. Considering related issues with regards to digital signal processing for MIMO-PLC systems, the use of a parametric model offers certain advantages, as its deployment could be more easily achieved and since similar studies exist in the wireless domain [78], parameters like spatial correlation is comfortably understood. Nevertheless, considering the real-world implementation of say for instance MIMO coupling circuits or the adjustment of analog front ends (AFEs), a physical model because of its significant closeness to the reality of electronic components may be

more suitable and practicable. Based on these illustrations, it is evident that selection of a channel model must be dependent on case-by-case basis [22].

2.2.6 PLC Noise Characteristics Overview

It is important to know that the noise that exists on the PLC channel is a deviation from the AWGN scenario often assumed for other communication channels. On the in-home PLN, observed noise has been conventionally categorized into various classes, based on their source, their level and their time domain signature [79]. PLC channel noise can be classified based on both temporal and spectral attributes. According to [7, 58], one can differentiate narrowband noise (NBN), asynchronous periodic impulse noise, synchronous periodic impulse noise, aperiodic impulse noise and colored background noise (BN) as the major power line noise types as shown in Figure 2.7.

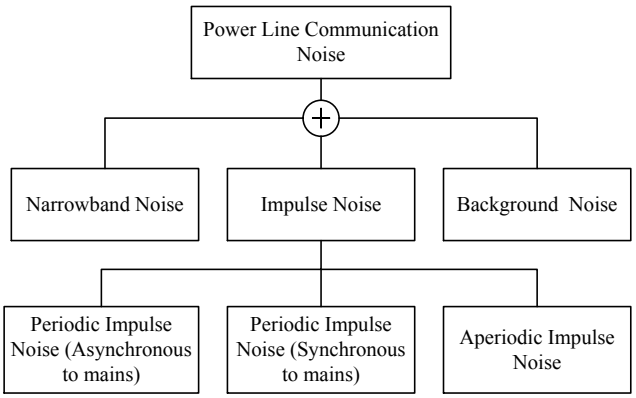

FIGURE 2.7: Power line communication noise classification.

The first noise category, the ***Narrowband noise (NBN)*** typically consists of noise ingress from external noise sources like short-wave (SW) and frequency-modulation (FM) broadcasting radio bands. Other sources of this kind of ingress noise include leakages from close range electrical and industrial consumer appliances or equipment. This noise type normally produces strong interference over a very long duration as long as the interferer is active on the network and it is confined to a narrow portion of the frequency spectrum.

The Second noise class is the ***Impulse noise (IN)*** emanating from the power electronic appliances connected and powered by the AC mains grid. Consumer appliances such as light dimmers, fluorescent lamps and switched mode power supplies are major sources of impulse

noise. Unlike NBN, this noise type is characterized by short duration (transient in nature- a few microseconds), and relatively high amplitude (level) often in the order of tens of milli-Volts (mV). As a result of the periodic attribute of the mains, impulse noise sources can produce impulses in a synchronous manner with the mains period. In such cases, the impulse noise is labeled as ***periodic-impulse noise synchronous to the mains frequency*** with a repetition rate depending on the AC mains frequency (multiples of 50/60 Hz). Other impulse noise sources produce impulses at higher repetition rate (50-200 kHz) and hence are categorized as ***periodic impulse noise asynchronous to the mains frequency***. Lastly, sporadic strong impulses with no periodicity with the mains or itself are also observed on the power line. This noise class is referred to as ***aperiodic impulse noise***.

In [80], dissimilar attributes of the IN have been statistically studied based on experimental measurement data. Similarly, an extensive PLC impulse noise model has been suggested in [79], where a statistical characterization of the pulses based on amplitude, repetition rate and duration are first carried out, while a Markov chain is utilized to model the global noise situation.

Lastly, noise sources producing a low interference level form the third category of power line noise referred to as ***Background Noise (BN)*** and is commonly colored as a result of a stronger power spectral density (PSD) at lower frequencies. Esmailian et al. in [42] modeled the BN PSD with decreasing power as a function of frequency [22]. Based on large measurement campaign in the medium voltage, low voltage-access and low voltage in-home scenarios, Meier et al. presented a statistical approach to average colored BN modeling. A major finding is that the mean noise power decreases exponentially with frequency. In a different manner, neural network method was deployed to generate a model for single input single output (SISO) PLC BN in [81].

A crucial characteristic of all the major power line noise discussed is their time-dependency. This is as a result of the un-coordinated use of the power electronics (noise sources) on the network, hence, the attributes of the noise observed at a given power outlet often significantly changes over time. For example, human activity increases in the in-home environment after work hours leading to a stronger contribution of power electronic appliances to the noise observed on the channel. It is less evident that power line noise possesses cyclostationary

structure, with a period associated to the mains signal. This is largely as a result of periodically changing impedance at the load termination point on the network dependent on the mains cycle. A detailed investigation of SISO PLC noise time variation is carried out in [82].

2.2.7 PLC Noise Classification

The noise class encountered on the PLC channel have been labeled as NAWGN as several power electronics appliances on the network, particularly those having switching circuits inject periodic or random noise pulses onto the channel. The resulting noise is a deviation from the AWGN model, consequently, leading to labeling of the channel as a long burst error or horrible channel [24, 52]. As documented in several literatures, PLC noise have been categorized into three major types namely: background noise, narrowband noise and impulse noise as shown in Figure 2.7 [5, 24, 52, 83–85].

As presented in [86], the combination of Multiple frequency-shift keying (MFSK) modulation with permutation code is done by mapping of each symbol from an alphabet of magnitude M onto a distinct frequency of M dissimilar available frequencies, hence we obtain a binary decision matrix $M \times M$. For a permutation codeword 1234, where $M = 4$, the decision matrix denoted as $Y_{noisefree}$ is shown as follows in (2.1), where the row indices represents the frequency location of the information, while the column indices represents every discrete time instance.

The decision matrix $Y_{noisefree}$ is noise-free, but will be used to describe the impact of the different types of NB-PLC noise henceforth. The major PLC noise types are thus discussed as follows.

$$Y_{noisefree} = \begin{array}{c} \\ f_1 \\ f_2 \\ f_3 \\ f_4 \end{array} \begin{array}{c} \begin{array}{cccc} t_1 & t_2 & t_3 & t_4 \end{array} \\ \begin{bmatrix} 1 & 0 & 0 & 0 \\ 0 & 1 & 0 & 0 \\ 0 & 0 & 1 & 0 \\ 0 & 0 & 0 & 1 \end{bmatrix} \end{array} \tag{2.1}$$

The colored background noise: Background noise (BN) possesses comparatively low power spectral density (PSD) resulting from the sum of various low power noise sources connected onto the channel. It is frequently identified by a constant envelope occurring over

a prolonged duration [5]. This noise type includes flickering noise, thermal noise emanating from receivers' front end amplifier. This noise type also emerges from universal motors often found in but not limited to end user gadgets such as fans, drilling tools and dryers. BN is also identified due to it's non-white attribute, hence it possesses a frequency-dependent PSD and is always present on the NB-PLC channel. The PSD of this noise type decays as frequency increases, possessing a slope varying between 20-25 dB/decade in an indoor low voltage NB-PLC environment [5], [87] and is principally present in narrowband frequencies than in broadband frequencies [87]. In (2.2), two received decision matrices corrupted by background noise is shown. $Y_{background1}(2,2)$ is corrupted through the random substitution of 1 with 0 (deletion error), while $Y_{background2}(4,3)$ is corrupted by the replacement of 0 with 1 (insertion error).

$$Y_{background1} = \begin{array}{c} \\ f_1 \\ f_2 \\ f_3 \\ f_4 \end{array} \begin{array}{c} \begin{array}{cccc} t_1 & t_2 & t_3 & t_4 \end{array} \\ \begin{bmatrix} 1 & 0 & 0 & 0 \\ 0 & \underline{0} & 0 & 0 \\ 0 & 0 & 1 & 0 \\ 0 & 0 & 0 & 1 \end{bmatrix} \end{array}, \quad Y_{background2} = \begin{array}{c} \\ f_1 \\ f_2 \\ f_3 \\ f_4 \end{array} \begin{array}{c} \begin{array}{cccc} t_1 & t_2 & t_3 & t_4 \end{array} \\ \begin{bmatrix} 1 & 0 & 0 & 0 \\ 0 & 1 & 0 & 0 \\ 0 & 0 & 1 & 0 \\ 0 & 0 & \underline{1} & 1 \end{bmatrix} \end{array} \tag{2.2}$$

The narrowband noise: Narrowband noise (NBN) is typically limited to a certain frequency slot dependent on its source. It emanates primarily from signals (sinusoidal) having modulated amplitude and are radiated or conducted from both internal and external appliances onto the network, hence the power line acting as an antenna. In literatures, this noise have been found to originate from the horizontal retrace frequency of televisions [5]. Other NBN origins are spurious electromagnetic disturbances emanating from end user gadgets with built-in transmitters and receivers [5], [87]. In (2.3), $Y_{narrowband1}$ and $Y_{narrowband2}$ show two received decision matrices corrupted by narrowband noise at the f_4 and f_2 respectively, with the noise impairment lasting for a number of continuous frames as shown.

$$Y_{narrowband1} = \begin{array}{c} \\ f_1 \\ f_2 \\ f_3 \\ f_4 \end{array} \begin{array}{c} \begin{array}{cccc} t_1 & t_2 & t_3 & t_4 \end{array} \\ \begin{bmatrix} 1 & 0 & 0 & 0 \\ 0 & 1 & 0 & 0 \\ 0 & 0 & 1 & 0 \\ \underline{1} & \underline{1} & \underline{1} & \underline{1} \end{bmatrix} \end{array}, \quad Y_{narrowband2} = \begin{array}{c} \\ f_1 \\ f_2 \\ f_3 \\ f_4 \end{array} \begin{array}{c} \begin{array}{cccc} t_1 & t_2 & t_3 & t_4 \end{array} \\ \begin{bmatrix} 1 & 0 & 0 & 0 \\ \underline{1} & \underline{1} & \underline{1} & \underline{1} \\ 0 & 0 & 1 & 0 \\ 0 & 0 & 0 & 1 \end{bmatrix} \end{array} \tag{2.3}$$

The Impulse noise: Impulse noise (IN) is transient in nature and it has been described to be the principal cause of burst errors on the PLC channel. Unlike NBN, impulse noise covers a wider part of the spectrum in use. It possesses a high PSD and is distinguished by its inter-arrival time, duration and amplitude. It is significant to clarify that on a low voltage NB-PLC channel, two main classification of impulse noise exist: the *"Periodic impulse noise"* and *"Aperiodic impulse noise"* [5, 85, 87].

1. ***Aperiodic impulse noise***: also regarded as *asynchronous impulsive noise* originates from arbitrary emission events or isolated activities at both homes and industrial sites. Classic aperiodic impulse noise emanates from switching transient such as: on and off switching, plugging and unplugging of appliances and co-existence issues that often occur due to uncoordinated PLC transmissions. This impulse noise type is predominant in the high frequency band ranging from several hundred kHz to 20 MHz [7], [88]. The duration of the impulses lies mostly in the range of 10-100 μs. The PSD of this noise type is especially concentrated at frequency range below 1 MHz as a result of noise oscillations. It has been established as the noise with the highest power compared to other noise and disturbances as the noise PSD can be 50 dB greater than the background noise or even more [79].

2. ***Periodic impulse noise*** also referred to as *"Cyclostationary impulsive noise"* is sub-divided into two: *Periodic synchronous impulse noise* and *Periodic asynchronous impulsive noise* as discussed as follows:

   (a) *Periodic synchronous impulse noise*: This impulse noise waveform exhibits a train of impulses synchronous to the low voltage AC mains 50/60 Hz frequency. It is comprised of a series of impulses that are isolated, with fairly large amplitude and duration. They originate from non-linear power electronic gadgets like; silicon controlled rectifier operations in power supplies, thyristors operation in light dimmer, laptops, desktop computers, LCD monitors and from a brush motor commutating effects [83, 84, 89].

   (b) *Periodic asynchronous impulse noise*: This noise type is characterized by periodic noise impulses or trains of impulses which occurs with a frequency and repetition rates independent of mains frequency [89], [90]. It has repetition rates between 50-200 kHz and is majorly injected by transient operations such as switching of

relays that occurs in switch mode power supplies connected to the network [5], [89]. The noise impulses typically possess much shorter durations and much lower amplitudes than those of the periodic synchronous impulse noise [89], [91]. According to [79], [83, 84], the duration of this noise type is usually less than 1.5 μs and on certain occasions up to 10 μs. In (2.4), $Y_{impulse1}$ and $Y_{impulse2}$ show two received decision matrices corrupted by impulse noise dominating all frequencies at time instant t_1 and t_3 respectively.

$$Y_{impulse1} = \begin{array}{c} \\ f_1 \\ f_2 \\ f_3 \\ f_4 \end{array} \begin{array}{c} \begin{array}{cccc} t_1 & t_2 & t_3 & t_4 \end{array} \\ \begin{bmatrix} \underline{1} & 0 & 0 & 0 \\ \underline{1} & 1 & 0 & 0 \\ \underline{1} & 0 & 1 & 0 \\ \underline{1} & 0 & 0 & 1 \end{bmatrix} \end{array}, \quad Y_{impulse2} = \begin{array}{c} \\ f_1 \\ f_2 \\ f_3 \\ f_4 \end{array} \begin{array}{c} \begin{array}{cccc} t_1 & t_2 & t_3 & t_4 \end{array} \\ \begin{bmatrix} 1 & 0 & \underline{1} & 0 \\ 0 & 1 & \underline{1} & 0 \\ 0 & 0 & \underline{1} & 0 \\ 0 & 0 & \underline{1} & 1 \end{bmatrix} \end{array} \tag{2.4}$$

As aperiodic impulse noise is predominant on broadband power lines, recent indoor and outdoor noise measurements on both low-voltage and medium-voltage PLNs established that "cyclostationary noise (both periodic synchronous and asynchronous to mains frequency impulse noise)" are the prevailing noise impairment present on the 3-500 kHz NB-PLC spectrum [92–94]. This kind of noise possesses long noise bursts with periodically varying statistics and whose period is the same as half the AC main's cycle. In PLC systems, a typical periodic synchronous impulse noise is composed of noise bursts having high power which spans from 10% - 30% of the period [94], which is oftentimes a lot prolonged than the standardized duration of a typical OFDM symbol [88] and amounts to 833μs-2.5 ms in the US FCC band [94, 95]. A single cyclostationary noise burst could posssibly lead to corruption of multiple successive OFDM symbols. For instance, for a PLC-G3 standard functioning in the 3-95 kHz CENELEC A band [92], the OFDM symbol duration is 695μs, hence, cyclostationary noise burst that lasts 30% of a period is bound to corrupt up to four successive OFDM symbols [95]. During certain period of the bursts, the noise power at particular frequency bands could rise to 30-50dB greater than in the remaining period [94], [95].

In (2.5), $Y_{fading1}$ and $Y_{fading2}$ show two received decision matrices corrupted by frequency selective fading, with the fading occurring at the f_1 and f_3 respectively.

$$Y_{fading1} = \begin{array}{c} \\ f_1 \\ f_2 \\ f_3 \\ f_4 \end{array} \begin{array}{c} \begin{array}{cccc} t_1 & t_2 & t_3 & t_4 \end{array} \\ \begin{bmatrix} \underline{0} & \underline{0} & \underline{0} & \underline{0} \\ 0 & 1 & 0 & 0 \\ 0 & 0 & 1 & 0 \\ 0 & 0 & 0 & 1 \end{bmatrix} \end{array}, \quad Y_{fading1} = \begin{array}{c} \\ f_1 \\ f_2 \\ f_3 \\ f_4 \end{array} \begin{array}{c} \begin{array}{cccc} t_1 & t_2 & t_3 & t_4 \end{array} \\ \begin{bmatrix} 1 & 0 & 0 & 0 \\ 0 & 1 & 0 & 0 \\ \underline{0} & \underline{0} & \underline{0} & \underline{0} \\ 0 & 0 & 0 & 1 \end{bmatrix} \end{array} \tag{2.5}$$

2.2.8 NB-PLC Coupling Circuit

The coupling circuit is an inevitable part of the NB-PLC transceiver system. Apart from providing galvanic isolation and preventing excessive voltage from damaging the sensitive transceiver equipment, this interface must also be able to adapt to the varying impedance on the channel in order to overcome insertion and coupling losses at the coupling point [96]. It is also important for this piece of circuitry to adhere to standards and regulation stipulated by PLC communication regulatory bodies. A coupling circuit is designed as a bandpass filter with the primary aim of injecting communication signals onto the power line network. While it blocks and filters the power grid AC mains power waveform, it allows high frequency communication signal pass onto the network [96–98].

When choosing a coupling method, one usually has to choose between *capacitive* and *inductive* couplers. Inductive coupling guarantees a balance between the lines while capacitive coupling generally introduces asymmetries as a result of the manufacturing tolerances of the passive electronic components used for its implementation [22]. Aside symmetry, the communication signal bandwidth and the dimensioning in order to protect transceiver equipment from excessive voltage from the AC mains are decisive coupling attributes. Additionally, the observed channel attributes are not independent of the coupler employed to inject and decouple signals from the power line.

As stated by *Biot-Savart law*, the chief origin of radiated emission is the common-mode current denoted as I_{CM}. Hence, in order to circumvent radiated emission, conventional PLC modem designers target the injection of communication signal in the most possible symmetric way. Consequently, small-scale radiated emission is observed as 180° out-of-phase electric fields produced neutralize or cancel out each other. This suitable symmetrical mode of signal propagation is referred to as *differential-mode (DM)* coupling with an accompanying signal

voltage denoted as U_{DM}. Thus, the reason for the stipulated use of a *capacitive-differential mode* coupling circuit for low voltage PLC applications [22]. Refer to Section 4.2 for the development of the coupling circuit utilized in this project.

2.3 Modulation Methods for PLC Transceiver System

To propagate a signal over a PLC channel, it is essential that the signal be modulated onto a carrier frequency for two major purposes. First, attenuation is considerably reduced when baseband signals are modulated onto higher-frequency carriers. Second, for effective use of the available frequency spectrums PLC channel offers, there is need to multiplex as many channels as practically feasible in the same PLC channel [99]. This implies the frequency division multiplexing (FDM) of multiple frequencies over the same PLC channel.

Several methods have been suggested and analyzed in the pursuit of the most suitable modulation scheme for PLC applications. In selecting a modulation technique, it is imperative to consider the attributes of the power line channel such as: time-variation and frequency-selectivity, impulsive noise and other noise and interference types, as well as transmit power limitation due to regulatory constraints [24].

The transmission techniques commonly utilized for PLC technologies are single-carrier (amplitude-shift keying (ASK), frequency shift keying (FSK) and phase shift keying (PSK)), spread spectrum (SS) and multi-carrier OFDM techniques. Figure 2.8 shows a typical representation of a single-carrier, spread spectrum and multi-carrier transmission and modulation technique. The simplest of these techniques is FSK, achieved by the modulation of multiple signals with frequency separated carriers. The simplicity of this scheme is due to channel response variation and the manner the system behaves, however, its downside is its intrinsic limitations in PLC applications operating beyond the 1 megabits per second (Mbps) rates [99].

The trait of spread spectrum as a modulation scheme implies that modulated signals are almost practically safe from any form of interference. SS permits signal transmission beyond the 1 Mbps rates over the PLC channel. Two variants of this technique are Frequency Hopping Spread Spectrum (FHSS) and Direct Sequence Spread Spectrum (DSSS). In the former, user transmitted signal randomly changes frequency from time to time, hence, the

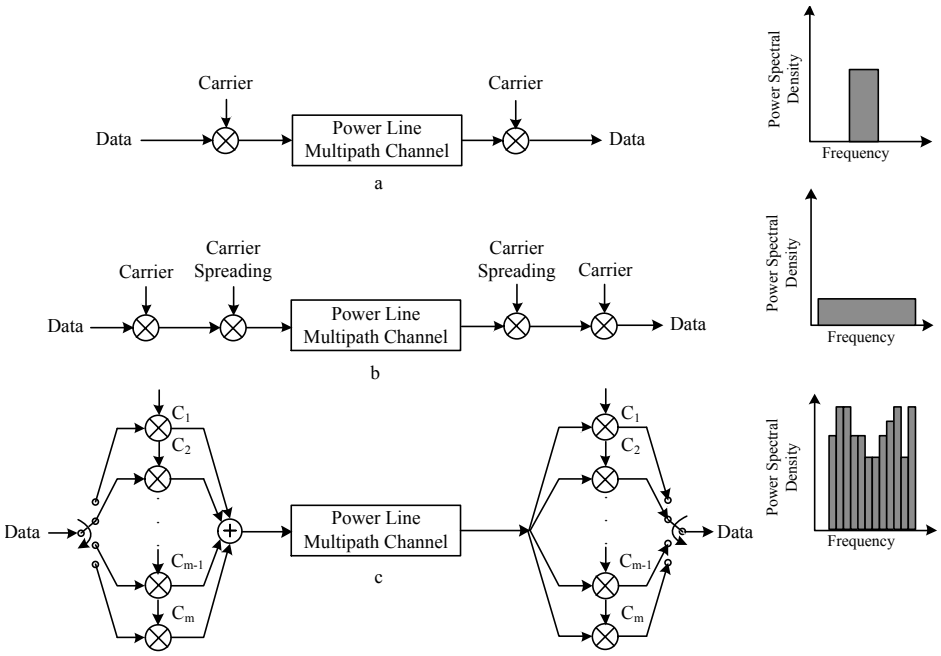

FIGURE 2.8: Power line communication transmission techniques. (a: single-carrier, b: spread spectrum and c: multi-carrier (OFDM))

transmitted signals cannot be easily intercepted or tracked due to changing frequency. In the latter, the user does not change frequency but changes the pseudo-random code, with this code having the attribute of not repeating itself. The code is unique, hence, implying that users encrypt their signal using this code, with the code changing from time to time. DSSS offers a great technique as well as provides maximum security but its a bit difficult to implement, while FHSS is easily implementable but has lesser security compared to DSSS. A viable solution is needed to solve the main synchronization drawback of SS [100].

Another PLC transmission technique is OFDM, where the entire bandwidth is sub-divided into N parallel sub-channels, while bits are allocated to sub-channels in direct proportion to the sub-channel signal-to-noise ratio (SNR). OFDM offers a distinct advantage of being robust in the presence of multi-path fading, and its effective and efficient utilization of the limited frequency spectrum.

The eventual choice of a modulation scheme is dependent upon the PLC application and channel environment. A suitable PLC modulation should offer adequate robustness against PLC channel impairments such as impulse noise the major cause of burst errors and should be capable of mitigating severe inter-symbol interference (ISI) resulting from greater delay

spread of the PLC channel. Section 2.4 and Section 2.5 give a concise description of single-carrier digital modulations and multi-carrier OFDM techniques respectively.

2.4 Single-Carrier Modulation for Narrowband PLC

The three major categories of digital modulation techniques (ASK, FSK and PSK) often used in transmitting digitally represented data in communication systems is discussed as follows.

2.4.1 Amplitude Shift Keying (ASK)

Shift keying refers to a process whereby digital bits commonly used to represent digital data are represented in analog format. Amplitude shift keying is a class of amplitude modulation that is realized through variation of the amplitude of a sinusoidal carrier signal in order to reflect the amplitude levels in the digital information or signal. In a typical ASK system, a binary symbol 1 is depicted by the transmission of a fixed amplitude carrier signal and frequency for a bit period denoted as T seconds. In essence, if a binary "1" is the value of the signal to be transmitted the carrier signal is transmitted with amplitude 10, while for "0", a carrier signal with amplitude 5 is transmitted.

All digital modulation techniques utilize finite distinct signals in representing digital data. ASK employs finite amount of amplitudes, each allocated a distinct arrangement of binary digits. Generally, every of the amplitude normally encodes the same number of bits. Each bit arrangement gives rise to a symbol that is depicted by the specific amplitude. The demodulator often designed precisely for the same symbol-set utilized by the modulator then determines the received signal's amplitude and thus mapping it back to the represented symbol, hence, a recovery of the original transmitted data without changing the phase and frequency of the carrier wave. Figure 2.9 is a typical representation of an ASK scheme, the upper diagram shows particular digital bits in binary format before encoding, while the lower figure shows the corresponding ASK modulated waveform representing the digital bits.

ASK is a linear, low-complexity, low-power, low-cost and limited data rate technique but its major disadvantages are its sensitivity to distortions, atmospheric noise and amplitude

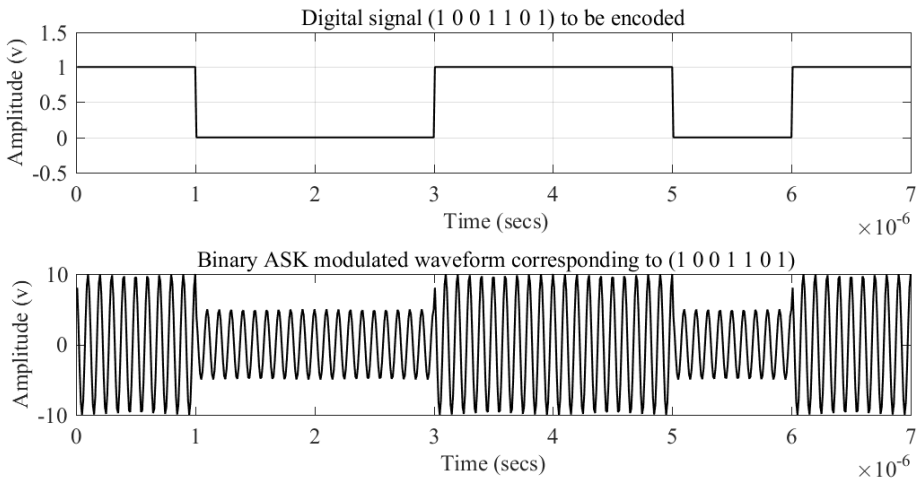

FIGURE 2.9: Waveform representation of a typical ASK technique.

attenuation resulting from non-linearity in components used in several communication equipment. Consequently, regardless of the simplicity in its implementation, it still not suitable for a robust NB-PLC communication as a result of non-linear PLC equipment used on the network.

2.4.2 Frequency Shift Keying (FSK)

Frequency shift keying is a class of frequency modulation technique in which transmission of digital information is achieved through discrete changes in frequency of a carrier signal. In essence, the digital data stream varies the frequency of the carrier signal. The simplest type of FSK technique is the binary FSK (B-FSK). This form of FSK utilizes a pair of discrete frequencies in the transmission of binary information “0s” and “1s”, with the “1” being labeled as the mark frequency while “0” is referred to as the space frequency. Figure 2.10 shows a typical waveform representation of a particular digital signal bits modulated with FSK technique.

Other forms of FSK include continuous-phase frequency-shift keying (CP-FSK), Gaussian frequency-shift keying (G-FSK) and multiple frequency-shift keying (MFSK). FSK like ASK is also easy to implement and possess better noise immunity when compare to ASK, hence there is high probability of error-free reception. Its major drawback is high bandwidth requirement, hence, it is extensively used in low speed applications because an increase in speed results in a corresponding increase in bit rate.

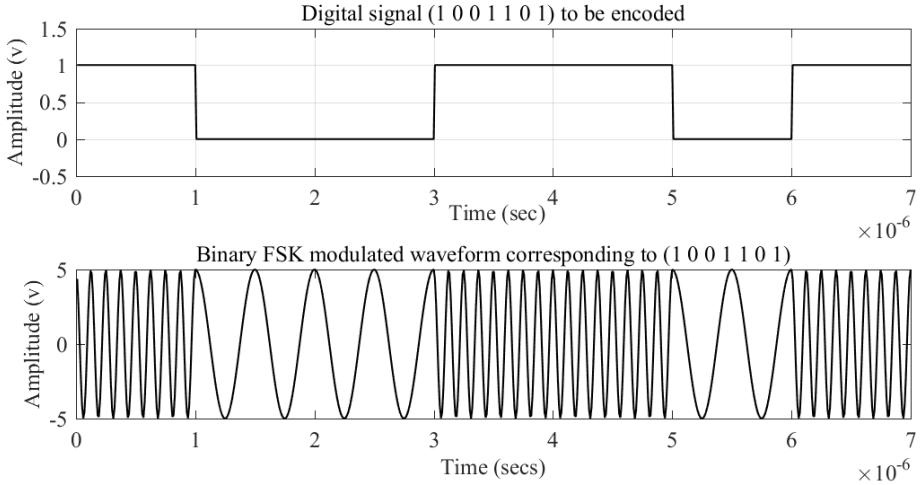

FIGURE 2.10: Waveform representation of a typical FSK technique.

2.4.3 Phase Shift Keying (PSK)

Phase-shift keying (PSK) techniques are a class of single carrier digital modulation techniques achieved through the encoding of digital data bits into an analog format. This is generally realized by changing (modulating) the phase of a sinusoidal carrier wave (reference signal). In PSK modulation, finite number of phases is utilized, with each phase assigned a distinct configuration of binary digits. Generally, each phase is encoded with an equivalent number of bits. Each bits configuration produces the symbol that is a representation of a specific phase. The PSK demodulator made precisely for a set of symbol utilized by the PSK modulator carries out a mapping of the phase of the received signal to the represented symbol, hence, a recovery of the original data. This normally needs the receiver to be capable of comparing the phase of the received signal to a carrier signal (reference signal), hence such a system is referred to as being *coherent*, thus we have a class of PSK called coherent PSK (CPSK).

On the contrary, another class of PSK technique exist where the demodulator decides the received signal phase change rather than it been decided by the phase (relative to a reference signal) itself. Due to the dependence of this scheme on the difference between sequential phases, it is referred to as differential phase-shift keying (DPSK). DPSK schemes are considerably easier and cheaper to implement when compared to the normal PSK (CPSK) since the demodulator is not required to have a replica of the reference signal at the receiver before it can determine the precise phase of the received signal. Consequently, DPSK schemes

are referred to as *non-coherent* PSK techniques. In DPSK modulation schemes, the input binary sequence is initially differentially encoded before being finally modulated by a single-carrier PSK modulator. In terms of performance coherent schemes outperforms non-coherent schemes.

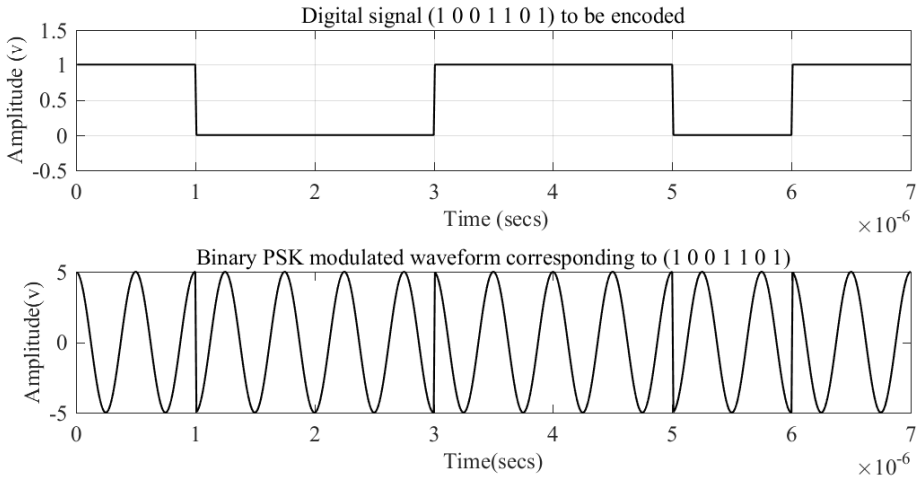

FIGURE 2.11: Waveform representation of a typical PSK technique.

Figure 2.11 shows a typical representation of a Binary PSK modulation scheme with the topmost figure showing the digital input signal to be encoded, while the lower figure is a representation of a BPSK modulated waveform of the digital input signal.

Binary phase shift keying (BPSK) also often referred to as 2PSK is the simplest class of the PSK family. It maps just one bit of data to the carrier, utilizing two possible phases-bit 0 (representing 0 radian) and bit 1 (representing π radians). It employs two phases that are 180° separated and it does not specially matter the position of the constellation points. Figure 2.12 shows the BPSK constellation at 0° and 180° on the in-phase or real axis.

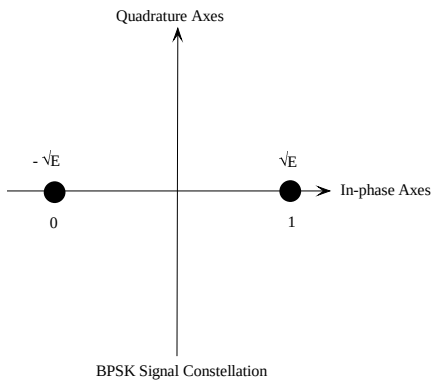

FIGURE 2.12: A typical BPSK constellation diagram.

BPSK is the most robust of the PSK family as it requires the highest level of distortion or noise for an incorrect decision to be achieved at the demodulator. It is however capable of modulating at 1 bit per symbol as seen in Figure 2.12, hence, it is inappropriate for high data rate applications. In a case of the introduction of arbitrary phase-shift by the communication channel, the demodulator is incapable of distinguishing the constellation, hence, the data is oftentimes differentially encoded before modulating.

Quadrature phase-shift keying (QPSK) also referred to as 4-PSK and functionally equivalent to 4-QAM is another class of the PSK family. QPSK utilizes four constellation points which are equi-spaced in Figure 2.13 around a circle. In this PSK technique, mapping or encoding of two bits/symbol using four equidistant phases ($\frac{\pi}{4}$, $\frac{3\pi}{4}$, $\frac{5\pi}{4}$ and $\frac{7\pi}{4}$) is realized.

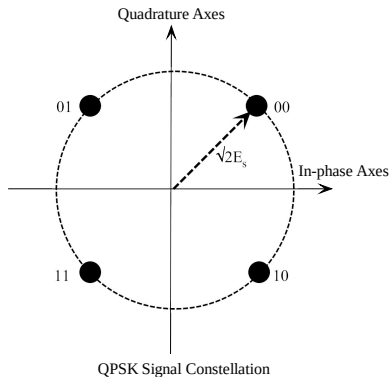

FIGURE 2.13: A typical QPSK and 8PSK constellation diagram.

Analytic mathematics demonstrates that QPSK is dually employed in order to double data rates compared with BPSK systems while the same bandwidth of the signal is maintained, or employed in maintaining BPSK data rate while halving the bandwidth required. In the later scenario, the bit error rate (BER) of QPSK is precisely equivalent to BPSK's BER. Due to the stipulation of maximum allowable bandwidth by communication bodies, QPSK has an advantage over BPSK in that it is able to transmit twice the data-rate in a specified bandwidth at the same BER compared to BPSK. The only penalty is that QPSK transmitters and receiver implementation are rather more complex than the BPSK ones, however, the penalty in terms of cost in the advent of modern electronics technologies is moderate. If coherent transmission is guaranteed, PSK is mostly preferred over FSK and vice versa. Due to phase ambiguity issues at the receiver, QPSK is often differentially encoded [101].

Eight Phase Shift Keying (8PSK) is another class of the PSK family. 8PSK refers to a PSK scheme that utilizes eight equi-spaced constellation points or states as shown in

Figure 2.14. In 8PSK modulation implementation, mapping of three bits/symbol using eight equidistant phases is achieved. QPSK is more tolerant to channel degradation than 8PSK, but 8PSK offers more data capacity.

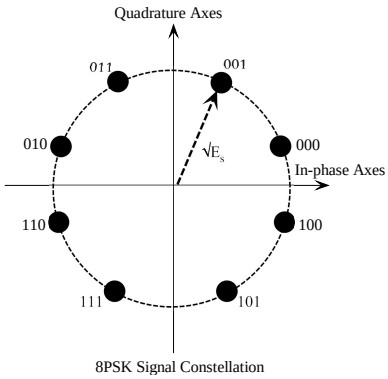

FIGURE 2.14: A typical 8PSK constellation diagram.

Summarily, BPSK, QPSK and 8PSK are special cases of Mary-PSK with M the number of constellation point equals 2, 4 and 8 respectively, while N the number of bits a symbol is mapped to and is 1, 2 and 3 for BPSK, QPSK and 8PSK respectively.

It should be noted that the single-carrier PSK modulations are more robust than each other, due to differing symbol energy and Euclidean distance on the constellation diagram. Hence, they perform better than each other in the presence of similar interferers, as the PSK modulation with the most superior spatial proximity and angular separation or Euclidean distance on the constellation diagram representation graph offers better robustness [102].

2.5 Orthogonal Frequency Division Multiplexing System

The Orthogonal Frequency Division Multiplexing (OFDM) technique was first invented in [103] in the year 1966. The work in [103] described a principle where information are conveyed through a linear band limited orthogonal channel assuming no ISI and Inter Carrier Interference (ICI). In 1967, [104] gives the performance analysis of parallel data transmission in a number of overlapping channels. Relevant contributions in literature to support the use of OFDM technique in its early stage includes reference [105, 106], among others. OFDM technique was first proposed in [107] as a viable solution to wireless communication in 1985. OFDM is now widely accepted and its principle has been deployed in many wireless and power line communication applications and standards. In fact, many researchers

see OFDM as a tenable solution for highspeed PLC applications and future generation mobile wireless applications most especially in the Fourth Generation (4G) mobile systems.

The OFDM is a frequency division multiplexing technology deployed as a multi-carrier modulation scheme. OFDM systems uses multiple orthogonal sub-carriers to convey message over a communication channel [108]. It offers a couple of advantages which include its effective and efficient use of the limited spectrum resource, simple implementation using Inverse Fast Fourier Transform (IFFT) and Fast Fourier Transform (FFT), its robustness against multi-path fading which is the main contributor of ISI and co-channel interference. Also, in time-varying frequency-selective fading channels such as PLC channel, OFDM systems perform efficiently in comparison with single carrier systems because it converts the frequency-selective fading properties of the channel into a number of parallel flat fading sub-channels [109, 110].

2.5.1 Principles of OFDM

The operational principle of an OFDM transceiver system is centered around the muxing and demuxing of sub-carriers at the respective transmitter and receiver stages. The fundamental components or process in the use of OFDM are the Inverse Discrete Fourier Transform (IDFT) and Discrete Fourier Transform (DFT), practically realized through the use of Inverse Fast Fourier Transform (IFFT) and Fast Fourier Transform (FFT) respectively. A typical OFDM transceiver system is shown in Figure 2.15. The OFDM system uses the conventional M-PSK and M-DPSK single-carrier modulators for its signal mapping.

In the absence of FEC codes, the serial input data is mapped to the M-PSK or M-DPSK constellation symbol in the frequency domain dependent on the bit rate of interest. Although not shown, at this stage pilot symbols, preambles and paddings are inserted as this insertions are needed at the receiver for proper synchronization in order to avoid both ISI and ICI. The resultant set of complex baseband symbols is then de-multiplexed by passing it through the serial-parallel converter, which splits the complex baseband symbols into parallel streams. The inverse fast Fourier transform (IFFT) block converts the frequency domain OFDM symbols to the time domain so as to be able to transmit the signal on the PLC channel. The transformed time domain OFDM symbol is multiplexed by feeding it through

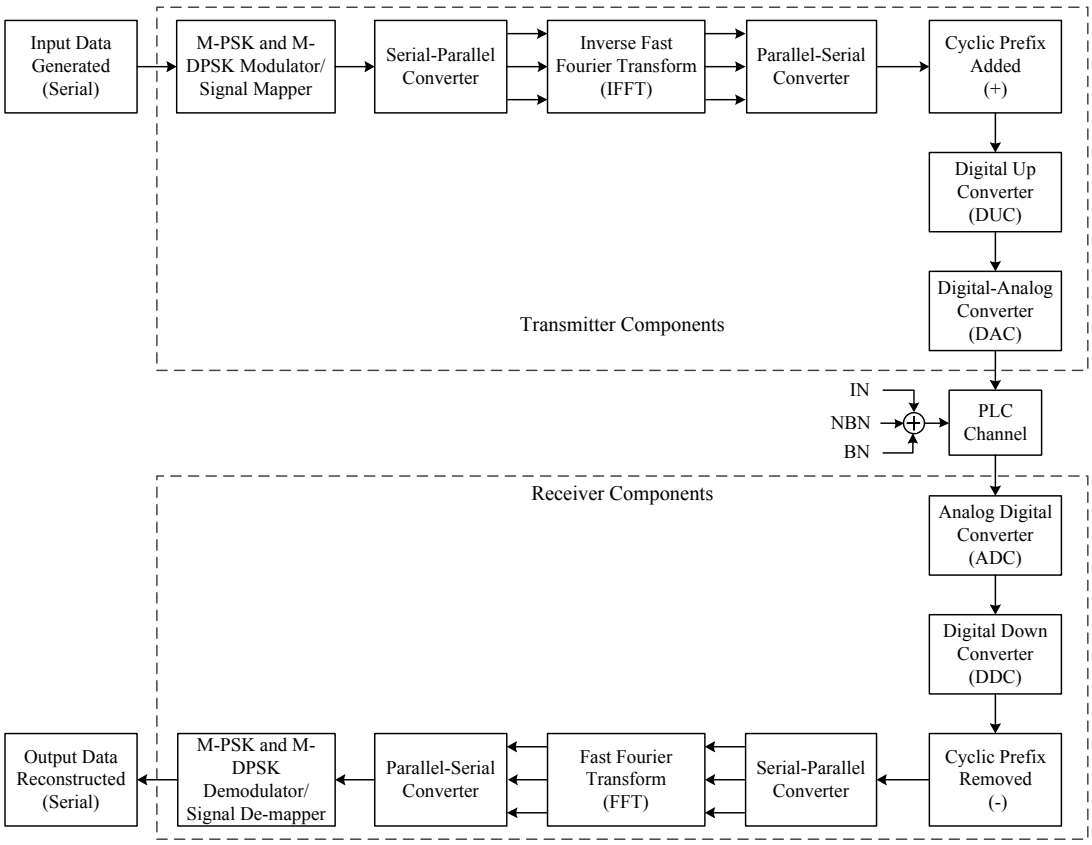

FIGURE 2.15: Typical block diagram of OFDM transceiver system.

the parallel-serial converter, after which cyclic prefix is added to the resultant serial data stream to combat ISI. The cyclic prefix is included to the time domain OFDM signal by adding typically 10% - 25% of the symbols at the end of time domain OFDM signal to the beginning of the signal.

The serial time domain signal is then fed into the digital up-converter (DUC) block, where it is digitally up-converted from a complex digital baseband signal to a real passband signal based on specified center frequency in preparation for transmission. The resultant passband signal is then fed through the digital to analog converter (DAC) in order to convert the digital signal into analog form. The analog signal is now transmitted over the time-varying frequency-selective PLC channel.

The reverse task is performed at the receiver, where the received time domain OFDM signal is first converted to analog signal by the analog to digital converter (ADC), before the passband signal is digitally down converted by the digital down converter (DDC). The cyclic prefix are subsequently removed from the received time domain OFDM signal. The time domain OFDM

signal is passed through the serial-parallel converter block before it is transformed to the frequency domain in the FFT block and subsequently converted to serial data streams by the parallel to serial converter. After the parallel to serial conversion, usually channel estimation is carried out in order to compensate for the varying properties of the channel before the closing steps of signal demodulation and reconstruction are performed to reconstruct the transmitted data.

2.5.2 Challenges in OFDM System

In spite of the numerous advantages and ease that comes with the use of OFDM systems in different digital communication applications, OFDM system has a couple of disadvantages. Common of these disadvantages is the high Peak-to-Average Power Ratio (PAPR) that OFDM signals exhibit compared to single carrier system because OFDM signal is a combination of many sub-carriers in the time domain [111, 112]. High PAPR occur when the different sub-carriers are out of phase with each other. This causes different problems in OFDM systems, more significantly at the transmitting end. One of the problems caused by high PAPR is that it makes the DAC at the transmitter end to be intricate while also reducing the efficiency of the power amplifier [110]. Another challenge with the use of OFDM system is the time and frequency synchronization errors which result in ISI and ICI that eventually degrade the performance of the overall OFDM system [113, 114]. Other challenges related with the use of OFDM system includes: channel estimation and equalization, co-channel interference, etc. This thesis will however focus on NB-PLC modeling using OFDM transceiver systems.

2.6 Visible Light Communications

White light-emitting diodes (LED) are gradually taking over a great deal of our everyday life. An attractive aspect of these LED devices is the fact that apart from its original use for lighting purposes, it can also be used for data communication purposes. Data transmission at high speed is fast becoming part of what is playing a major role in our day-to-day life in this modern century. Availability of multimedia data/information is envisioned to be within our reach at different places at any given time. A key element in the realization and achievement

of this feat is the wireless access networks (WANs). Nevertheless, there is scarcity of frequency in the radio frequency spectrum where practicable spatial coverage could be achieved, hence it poses a limiting factor. Consequently, other wireless communication means needed to be explored. Visible light communication (VLC) utilizing solid-state visible light sources such as white LEDs offers a possible alternative with the following advantages [115].

1. White Light-emitting diodes (LED) are gradually taking over and replacing high power/energy consuming incandescent light bulbs in homes and offices and also street lighting systems. They also find applications in trains, cars, and aeroplanes where they are used as back-lights and/or front-lights as the case may be.
2. Unlimited bandwidth availability.
3. Possible integration with existing power line network.
4. Visible light transmitters and receivers are inexpensive.
5. Free from external intruders and eavesdroppers as the light-waves are only concentrated in a particular region and can not penetrate opaque objects.
6. Radiations from the visible light sources are health hazard free and therefore pose no harm in its introduction to homes and hospital. Moreover, it is also free from radio frequency interference, as a result, its use in airplane is safe.

Infrared wireless communication is another alternative for data transmission in the wireless environment. This means of data communication offers application in indoor WLANs (wireless local area networks), and has been investigated in several literatures such as Kahn et al. [116], Park and Barry [117], Moreira et al. [118], Carruthers and Kahn [119], and Kahn and Barry [120]. In a qualitative manner, visible light sources and infrared signals display homogeneous propagation or radiation pattern due to their nearly close wavelengths. Consequently, white light emitting diodes have attracted a lot of research interest and attention as a viable alternative means of data communications [121–123]. Apart from the fact that white light emitting diodes offers a low energy consuming, extremely bright and a long lifespan device for illumination, it also offers a unique characteristics of being used to achieve high data rate in high speed wireless data communication. It is equally important to note also that white LEDs do not suffer from transmit power restriction due to health regulations as

we have in infrared wireless transmission. Visible light communication is thus defined as a short-range OWC (optical wireless communication) employing visible light source (e.g White LEDs) for both illumination and high speed wireless data transmission purposes [124].

Integration of broadband power line communication (PLC) and visible light communication (VLC) has received a boost with the advent of (IEEE 1901 [125], ITUT G.9960/61) and IEEE 802.15.7 [126] standardization for PLC and VLC respectively. In specific, there is an underlying gain that could be realized if we leverage the existing ubiquitous power line network infrastructure to render connectivity while we exploit the illumination system of power-saving LEDs for wireless data communication (downlink). The ubiquitous nature of these two systems makes us believe that VLC can offer a good complementary wireless data transmission technology to the existing in-house PLC in a similar manner broad-band Ethernet connections enjoys the support of Wi-Fi [127].

A comprehensive literature on VLC systems, its underlying fundamentals and its integration with PLC systems can be found in the following literatures: [115], [121–124], [127], [128]. A novel development and modeling of a low complexity FSK-OOK in-house hybrid PLC and VLC system is thus reported in Chapter 6.

CHAPTER 3

Background Techniques: Machine Learning based on Maximum Likelihood Estimation and Bayesian Inference Algorithms

The fundamental concern of advanced statistical inference and reasoning is based on estimation [129]. The choice of techniques utilized is dependent essentially on the inferential paradigm the user is philosophically devoted to. The predominant focal point of frequentist inference otherwise known as classical inference has been the study of estimators which satisfies constraints that results to tractable analytic solutions. Furthermore, these frequentist inferences were commonly established on asymptotic attributes of these estimators. Modern techniques were developed due to the advent of advanced computer engineering technologies, leading to relaxed constraints which further facilitated a better understanding of the exact attributes of these techniques. The advent of these new techniques has created novel opportunities for practically analyzing data. Statistical inferences for parameter estimation are based on two major approaches: Frequentist inference and Bayesian inference [130].

The frequentist approach is targeted at the evaluation of statistical procedures that are conditional on some class of postulated probability models. In this approach, the parameter estimate are imputed while properties are derived based on a lot of potential outcomes. In contrast, Bayesian inference approach is a method used for summarization of uncertainty and arriving at predictions employing probability assertions dependent on observed data and an assumed model. The Bayesian approach allows for the following: assumption of informative prior for the parameters; integration of uncertainty about the parameters, and probability assertions made are dependent on observed data.

In this work, both statistical approaches will be considered. For the frequentist approach, the iterative Baum-Welch algorithm is adopted for the maximum likelihood estimation of the SHFMM parameters for NB-PLC channel modeling, while a Metropolis-Hastings algorithm based on Markov Chain Monte Carlo (MCMC) technique [129], [131], [132] is used for the

Bayesian inference approach. Both statistical inference approaches make use of probability distribution in the description of random outcome behavior, but differ in their approach of treating unknown parameters' uncertainty.

In the frequentist inference approach, a random event's probability is seen as a long-run fraction of the number of times such event would occur, over significant trial times. Probabilities are only assigned to random quantities, i.e. the potential data values, which are assumed to be random in the frequentist method [133]. On the other hand, parameters are not described using probability distributions, because parameters are assumed to be fixed and not random as we have in the Bayesian approach. When an estimate is being quantified for uncertainty, the questions that comes to a frequentist mind are; Based on identical conditions, what other likely data sets may we have generated? Under varying data set, in our parameter estimate what degree of variation would be observed? For any given data set, how close or far away is our parameter estimate from the true parameter? " [133]. This method disregards any known external information or prior that concerns the value of the parameter. The major disadvantage of this method is based on the fact that it does not give a prescription of the best estimator, hence, *we can have more than one solution for any statistical problem and therefore can not ascertain which one is best* [130].

In this Chapter, a concise discussion of discrete channel models is first presented. Furthermore, basic definitions, notations and structure of the conventional Hidden Markov model (HMM), followed by the adopted Semi-Hidden Markov model (SHMM), highlighting the motivation behind the choice of this class of HMM over the conventional HMM. In subsequent sections, two machine-learning techniques for training the adopted SHFMM and optimizing the model parameters are discussed namely: the iterative Baum-Welch algorithm a frequentist inference statistical approach based on maximum likelihood estimation optimization criterion, and the Metropolis-Hastings algorithm a Bayesian statistical inference approach based on Markov Chain Monte Carlo technique.

3.1 Discrete Channel Model

The fundamental model of a communication system, usually comprises of a data source (discrete), a source and channel encoder for error control purposes, a modulator and transmitter,

a channel, a demodulator and receiver, a source and channel decoder and an output data destination as illustrated in Figure 3.1 [21].

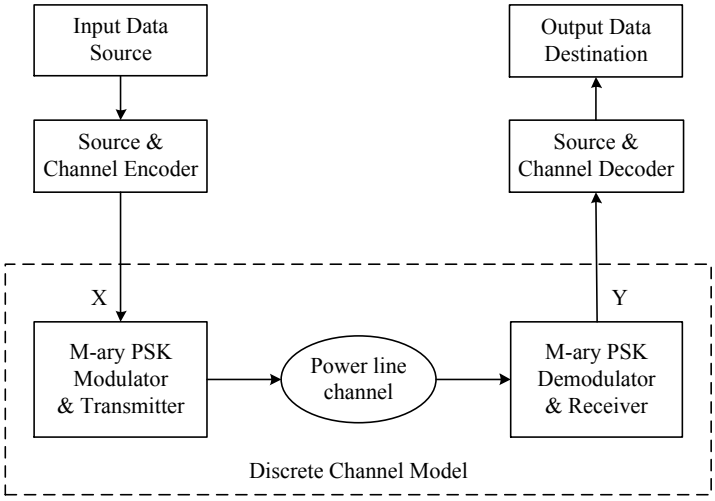

FIGURE 3.1: Constituents of discrete channel model for communication systems.

The term *Finite State Channel Model (FSCM)* or *Discrete channel model (DCM)* refers to the communication system elements that lie between points X and Y. The input sequence at X is a vector of discrete symbols, while at point Y, the output sequence is supposed to be a similar vector of discrete symbols in the absence of noise impairments often caused by imperfections in system elements present between point X and Y [21].

DCMs depict the error generation mechanism in a probabilistic manner. Two categories of DCM exist: discrete channel models without memory often referred to as "memoryless" channel models and discrete channel models with memory referred to as "memory" channel models.

Memoryless channel models are applicable to channels such as, AWGN channels without fading or inter-symbol interference (ISI), having no temporal correlation (uncorrelated) in their transition mechanism. This implies a channel whose input-to-output changeover probabilities for its nth channel input symbol is independent of any other input symbol.

Memory channel models, on the other hand are applicable in scenarios where the input-to-output symbols are temporally correlated. This implies that the nth symbol error probability is dependent on the occurrence or non-occurrence of error in the previous symbol transmission. The occurrence of frequency-selective fading and high impulsive noise in PLC channels

are typical scenarios of a channel with correlated errors, with such errors occurring in long bursts and such channels referred to as memory or burst error channel.

DCMs are vital in the analysis of transmission error occurrences on real channels. It is more appropriate to exploit samples of error sequences obtained from measurement rather than searching for an analytical depiction of the physical phenomenon that produced the errors [134].

In PLC channels and several other real communication channels, errors occur in sequence due to the fact that they are not independent, hence, reflecting the phenomenon referred to as channel memory, otherwise implying a statistical dependence in occurrence of errors [134]. Therefore, the use of simple model, referred to as Binary Symmetric Channel (BSC) to characterize channel errors does not depict reality in most digital communication channels, as channel memory is not taken into consideration [134]. The characterization of the behavior of digital transmission in memory channels, as well as modeling of such channels have been achieved with several DCMs for different communication channels [135–142]. In the following sections, HMM and SHFMM a class of DCM with memory is discussed in tandem with the suitable model training algorithms.

3.2 Hidden Markov Models

Hidden Markov Models (HMMs) are extensively utilized statistical models as a result of the existence of many reliable and efficient algorithms. This class of models are finite or determinate stochastic automates that are learnable and comprises two stochastic processes [143]. A Markov chain (discrete in time) characterized by finite set of states and state transition probabilities form the first stochastic process. The states of the Markov chain are "hidden", as they are not externally visible, implying an unobservable state sequence. The second stochastic process yields emissions that are observable at each time instant, based on a probability distribution that is state-dependent. Note, that the term "hidden" when defining a HMM do not refer to the parameters of the model but the states of the Markov chain. In subsequent sections, we will concisely discuss basic HMM notations, its structural architecture, suitable parameter estimation algorithm and the class of HMM adopted in this project.

3.2.1 Hidden Markov Model Basic Notations

Hidden Markov models has been defined as a finite doubly stochastic automates that are learnable. Each HMM is clearly defined by set of states, corresponding state probabilities, state transition probabilities, state emission probabilities and state initial probabilities. To completely define a HMM, the following major notations have to be specified [144], [145]:

1. N: denotes the number of states in a given model.
2. M: denotes the number of distinct observed symbol per state $V = v_1, \ldots, v_M$. For a non-continuous observation M is finite and vice versa.
3. A: denotes the state transitional probability distribution. $A = a_{ij}$, where a_{ij} is the transitional probability between state S_i at time t to S_j at time $t+1$. The state transitional probability distribution A is a stochastic $N \times N$ matrix that defines the transition or connection structure of the HMM. Note that the transitional probabilities a_{ij} ought to satisfy the following conventional stochastic constraints: $a_{ij} \geq 0, \;\; 1 \leq i, j \leq N$ and $\sum_{j=1}^{N} a_{ij} = 1, \;\; 1 \leq i \leq N$.
4. B: denotes the observation or error symbol (input-to-output transition) probability distribution in each state $B = b_i(o_k)$, where $b_i(o_k)$ depicts the probability that the observed symbol o_k is emitted in state i (S_i).
5. π: denotes the state prior probability or initial state distribution vector $\Pi = \pi_i$, where π_i denotes the probability that the model is in state i (S_i) at time $t = 0$.

Therefore, an HMM is distinctly defined by the compact notation stated as follows in Equation (3.1), indicating a complete parameter set for a discrete HMM.

$$\Gamma = (A, B, \pi) \tag{3.1}$$

3.2.2 Hidden Markov Model Architecture

Application of HMMs in order to solve real engineering problems requires a clear definition of statistical rules. Furthermore, stochastic modeling of HMM automate involve two stages. The

first stage is defining the model architecture, while the second stage involves selection of an appropriate, reliable and efficient operational algorithm.

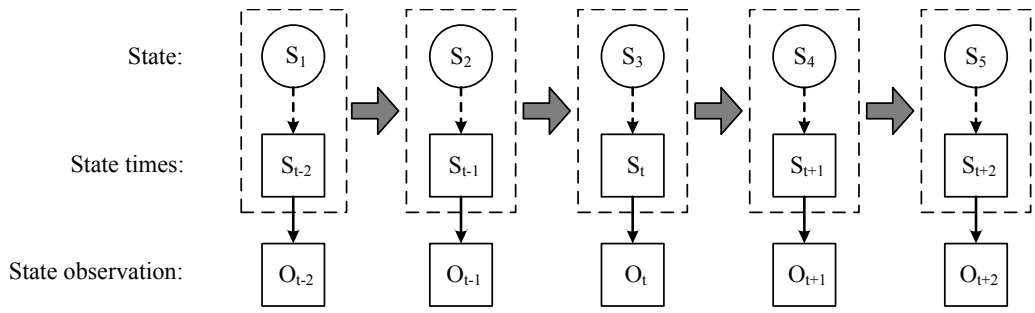

FIGURE 3.2: Generalized architecture of First-Order hidden Markov model.

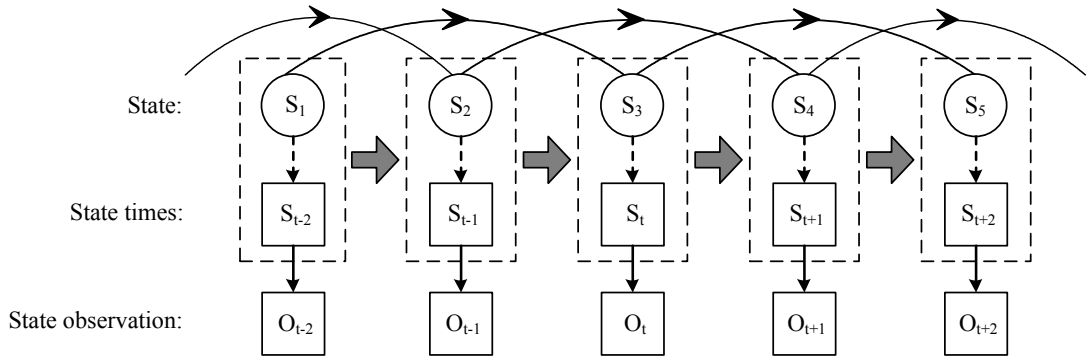

FIGURE 3.3: Generalized architecture of Second-Order hidden Markov model.

Figure 3.2 and Figure 3.3 show a generalized architecture of First and Second-Order hidden Markov model respectively. Note that five states are assumed for simplicity of illustration, otherwise, each shape symbolizes a random variable that can adopt any of a number of finite integer values. The random variable s_t at state S_3 denotes the hidden state at time instant t. The random variable O_t is the emitted observation in state S_3 at time instant t.

First-Order Markov model: In Figure 3.2, the law of conditional probability for HMM states that for variable s_t at time t, knowing the values of the hidden variable at all times is dependent only on the value of hidden variable s_{t-1} at time instant $t-1$. For the second stochastic process, the value of emitted variable O_t is dependent solely on the value of the hidden variable s_t at time instant t. In essence, a *First-order Markov chain model* is one for which the probability of transitioning to a particular state at a particular time instant is solely dependent on previous transition made and is mathematically expressed as follows in Equation (3.2).

$$\Pr[s_t|s_{t-1}, s_{t-2}, \ldots] = \Pr[s_t|s_{t-1}] \tag{3.2}$$

The conditional probability of the First-order Markov model shown in Figure 3.2 takes the form $a_{ij} = \Pr[s_t = S_3 | s_{t-1} = S_2]$, which states that the probability of transitioning to state S_3 at time s_t is dependent on previous transition to state S_2 at time s_{t-1}. The First-Order transitional probability matrix for an N-state HMM is a stochastic $N \times N$ matrix whose rows sum up to 1 ($\sum_{j=1}^{N} a_{ij} = 1$).

Second-Order Markov model: In Figure 3.3, the law of conditional probability for HMM states that for variable s_t at time t, knowing the values of the hidden variable at all times is dependent on the values of hidden variables s_{t-1} and s_{t-2} at time instants $t-1$ and $t-2$ respectively and is expressed in mathematical form in Equation (3.3) as follows

$$\Pr[s_t | s_{t-1}, s_{t-2}, \ldots] = \Pr[s_t | s_{t-1}, s_{t-2}] \tag{3.3}$$

The conditional probability of the Second-order Markov model shown in Figure 3.3 is mathematically written as $a_{ijk} = \Pr[s_t = S_3 | s_{t-1} = S_2, s_{t-2} = S_1]$, which implies that the probability of transitioning to state S_3 at time S_t is dependent on two previous transitions to state S_2 and S_1 at time instants $t-1$ and $t-2$ respectively. The Second-Order transitional probability matrix for an N-state HMM is a stochastic $N \times N \times N$ matrix.

3.2.3 HMM Problems

The task of any functional learning algorithm is to obtain the best or most probable set of model parameters (state transition probabilities and emission probabilities for HMM). Before we give a concise description of the choice of algorithm employed for the adopted HMM utilized in this project, we first reiterate three well-known basic HMM problems [21], [145].

1. **The Evaluation Problem**: What is the probability that a giving observation sequence denoted by $O = o_1, o_2, \ldots, o_T$ are produced by the model $Pr\ (O|\Gamma)$, given the HMM parameters $\Gamma = (A, B, \pi)$?

2. **The Decoding Problem**: What is the most probable sequence in the given model $\Gamma = (A, B, \pi)$ that generated the specified observation sequence $O = o_1, o_2, \ldots, o_T$?

3. **The Learning Problem**: How can we adjust the model parameters (A, B, π) so as to maximize $\Pr(O|\Gamma)$, given the model Γ and observation sequence $O = o_1, o_2, \ldots, o_T$?

In this project, we focus solely on the learning problem, as the aim is to obtain the most likely SHFMM parameter sets that best depict the observed sequence (training set) using appropriate and efficient algorithm. In essence, we focus on adjusting the SHFMM parameters in such a way that the training set is depicted by the model in the best way possible for the proposed application. In the learning process, the "quantity" that ought to be optimized differ based on the application. In literature, several optimization criteria exist for learning process, but the two most popular optimization criteria for learning problems are: the *Maximum Mutual Information (MMI)* and, the *Maximum Likelihood (ML)*.

Before a concise discussion of the well-known ML criterion optimization solution used to optimize the parameters of the class of SHFMM adopted in this research, a generalized N-State HMM for modeling discrete communication channel is first presented. Afterwards, a sample 3-State HMM is illustrated. Furthermore, the proposed Semi-Hidden Fritchman Markov model adapted for the NB-PLC channel modeling is discussed.

3.2.4 Generalized *N*-state and *3*-state Hidden Markov Model

Consider a discrete communication channel represented by an N-state HMM as shown in Figure 3.4. A number of parameters clearly defines this model. Let S denote the set of finite

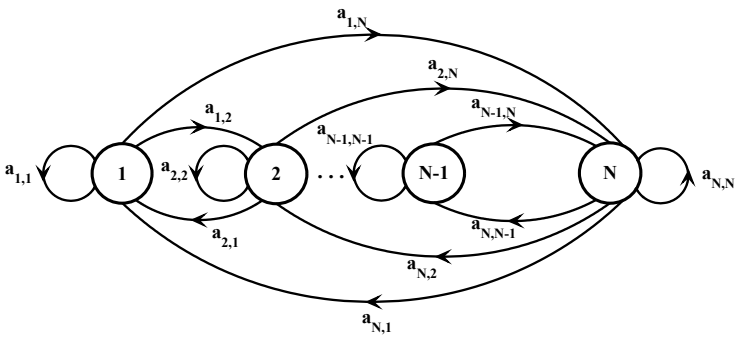

FIGURE 3.4: A generalized N-state hidden Markov model.

states as shown in Equation (3.4), while s_t denotes the state at discrete time t. Therefore, s_t spans over the set of finite state S.

$$S = \{1, 2, \ldots, N\} \tag{3.4}$$

Let $\Pi_{t,i}$ be a probability of interest, representing the probability that the model will be in state S_i at time instant s_t and is mathematically denoted in Equation (3.5) as follows.

$$\Pi_{t,i} = \Pr[s_t = S_i], \quad 1 \leq i \leq N \tag{3.5}$$

The initial state probability matrix is thus written as follows.

$$\Pi = [\pi_1 \ \pi_2 \ , \ldots, \pi_N]. \tag{3.6}$$

The state transition probabilities denoted by a_{ij}, refers to the probability of transitioning from state S_i at time instant s_t ($s_t = S_i$) to state S_j at time instant s_{t+1} ($s_{t+1} = S_j$). This state transitions usually occurs in a discrete time increment equivalent to a bit or symbol duration, and is represented in equation form as follows.

$$a_{i,j} = \Pr[s_{t+1} = S_j | s_t = S_i], \quad 1 \leq i, j \leq N \tag{3.7}$$

Modeling of communication channel's analog part normally requires assuming stationarity, thus, it is standard practice that stationarity is also assumed for the Markov modeling of discrete channels. Stationarity connotes the fact that the model parameters, that is, the initial state probabilities $\Pi_{t,i}$, the state transition probabilities $a_{i,j}$, and error symbol probabilities $b_i(o_k)$ are independent of t.

The state transition matrix denoted by A is thus written in Equation (3.8) as follows. Note that as shown in Figure 3.4, the Markov chains are fully connected, that is, transitions are allowed between all the states of the model with no restriction in state transition.

$$A = \begin{bmatrix} a_{1,1} & a_{1,2} & \cdots & a_{1,i} & \cdots & a_{1,N} \\ a_{2,1} & a_{2,2} & \cdots & a_{2,i} & \cdots & a_{2,N} \\ \vdots & \vdots & \ddots & \vdots & \ddots & \vdots \\ a_{N,1} & a_{N,2} & \cdots & a_{N,i} & \cdots & a_{N,N} \end{bmatrix} \tag{3.8}$$

Lastly, is the error symbol or output symbol probabilities (the input-to-output transition), otherwise referred to as the observation sequence. The observation sequence O for an M-ary constellation is represented as follows.

$$O = \{o_1, o_2, \ldots, o_M\} \tag{3.9}$$

For a binary scenario, $O = \{0, 1\}$, where "0" refers to a no transmission error and "1" denotes a transmission error. The probability that the observed symbol o_k is emitted in state S_i of the model is denoted by $b_i(o_k)$ and expressed as follows [21].

$$b_i(o_k) = \Pr[o_k | s_t = S_i] \tag{3.10}$$

The parameters $b_i(o_k)$ are written in a two rows by N columns matrix form for a binary hard decision case, N being the number of states in the Markov model. Note that transmission error occurs in any of the N states, hence, the error producing or symbol probabilities denoted by B is written in matrix as follows [21].

$$B = \begin{bmatrix} b_{1,1} & b_{1,2} & \cdots & b_{1,i} & \cdots & b_{1,N} \\ b_{2,1} & b_{2,2} & \cdots & b_{2,i} & \cdots & b_{2,N} \end{bmatrix} \tag{3.11}$$

where $b_{1,i}$ represents the probability of no transmission error (correct decision) provided the model is in state S_i, and $b_{2,i}$ denotes the probability of a transmission error (incorrect decision) provided the model is in state S_i. For a binary soft decision or non-binary cases, note that the error producing matrix denoted by B will possess more than two rows [21].

These defined parameters describe a finite state-space discrete-time Markov process functioning at a state transition rate equivalent to the bit or symbol rate of the communication system, with the process output consisting of two sequences: state sequence s_t, and error symbol sequence O_t, t being the discrete time index ranging over integer set $\{0, 1, 2, 3, \ldots\}$. Typically, only the channel's input and output and thus the error sequence are observable. On the contrary, the state sequence is not visible nor can it be observed externally, hence, the term "Hidden" and thus, the Markov model referred to as a hidden Markov model. Figure 3.5 illustrates a three state hidden Markov model having fully connected states, with transmission errors assumed to occur in any of the three states.

The corresponding model parameters: the state transition probabilities, the error symbol probabilities and the initial state probabilities are illustrated in matrix form in Equations (3.12), (3.13) and (3.14) respectively. As earlier stated, the transitional probabilities a_{ij} ought to satisfy the following conventional stochastic constraints: $a_{ij} \geq 0,\ 1 \leq i, j \leq N$ and

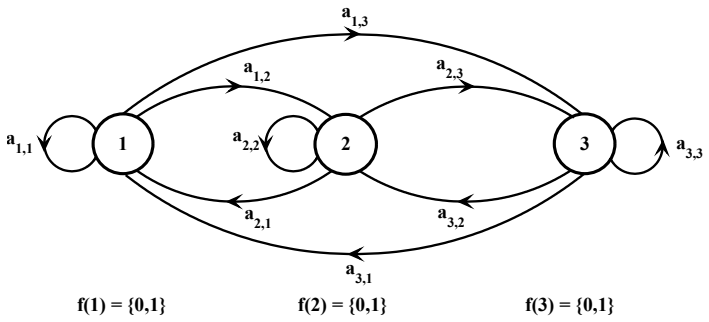

FIGURE 3.5: A 3-state hidden Markov model.

$\sum_{j=1}^{N} a_{ij} = 1, \;\; 1 \leq i \leq N.$

$$A = \begin{bmatrix} a_{1,1} & a_{1,2} & a_{1,3} \\ a_{2,1} & a_{2,2} & a_{2,3} \\ a_{3,1} & a_{3,2} & a_{3,3} \end{bmatrix}. \tag{3.12}$$

Consequently, all elements of the state transition matrix are greater than zero since all the states are fully connected and each of the rows must sum up to one to meet the aforementioned stochastic constraints.

$$B = \begin{bmatrix} b_{1,1} & b_{1,2} & b_{1,3} \\ b_{2,1} & b_{2,2} & b_{2,3} \end{bmatrix}. \tag{3.13}$$

The first row of the error symbol probability matrix in Equation (3.13) denotes the probability of correct decision (that is no transmission error), while the second row denotes the probability of an incorrect decision (transmission error). Furthermore, columns one, two and three denote state one, state two and state three respectively with each column summing up to one.

$$\Pi = [\pi_1 \; \pi_2 \; \pi_3]. \tag{3.14}$$

Lastly, the prior probability of being in any of the three states in Equation (3.14) must sum up to one.

3.3 Semi-Hidden Fritchman Markov Model

The resultant effect of the channel impairments often encountered in non-AWGN channels, such as the PLC channel is distortion in transmission, such that errors produced are grouped in bursts or clusters. Memory is thus introduced into the error process, as a result of the statistical dependence in error occurrence. An adequate understanding of how the channel

behaves in memory channels like the PLC channel is thus needed to achieve high reliability in data transmission. The generative or reproductive approach for modeling memory channels adopted in this work, is through the use of stochastic sequential machines referred to as semi-hidden Markov models, suitably parameterized utilizing experimentally measured data, capable of producing error sequences that are similar to distinct error sequences generated by a real PLC channel.

The goal of channel modeling in communication systems like the PLC system is the realization of simple and analytical models capable of accurately reflecting the essential statistical description of the real error generating process. Fritchman model [16], a semi-hidden Markov model, thus the name semi-hidden Fritchman Markov model (SHFMM) chronicles the statistical error distribution caused by noise impairments. This model helps realize a mathematically inclined statistical channel model that helps understand the statistical distribution of error on the PLC channel, and thus facilitate the use of such statistics to evaluate forward error correcting codes and also optimize system design based on evaluations, thus improving the overall system performance.

3.3.1 Semi-Hidden Fritchman Markov Model Basics

Fritchman [16], characterized binary communication channel utilizing functions of finite-state Markov chain. He proposed the grouping of an N-state model into two major partitions namely an error-free state (good state) and an error state (bad state). A good state is synonymous to an error-free or noise-free transmission (correct bit), while a bad state depicts an occurrence of transmission error (incorrect bit). In [87], [146], and several other literatures about signal propagation in PLC channel, a quite reasonable assumption is made that the *traditional* or *ordinary* Markov is capable of modeling the PLC channel. However, PLC channel is quite unlike the ordinary digital channels as impulsive noise is quite common, and with high occurrence often encountered. Thus, to correctly depict the unusual nature of the PLC channel, the semi-hidden Markov model also referred to as partitioned Markov chain model seems a more suitable candidate. Figure 3.6 shows the generalized architecture of an N-state semi-hidden Fritchman Markov model having a single error state as adopted in this work.

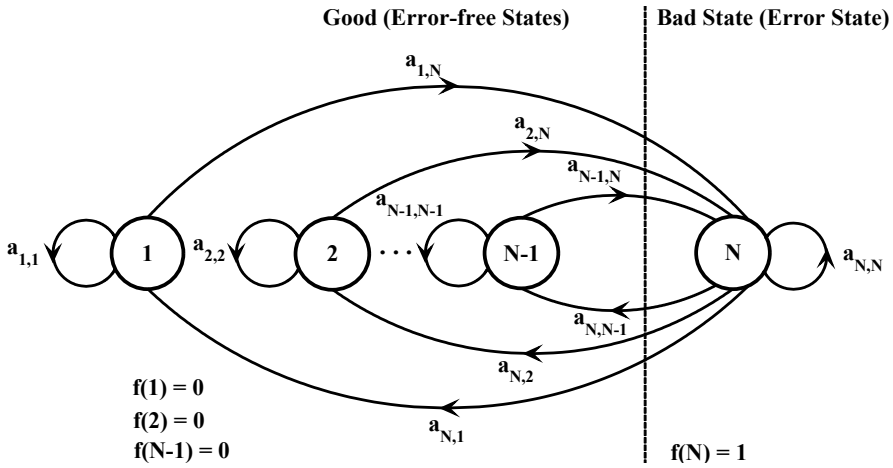

FIGURE 3.6: A generalized semi-hidden Fritchman model (one-error state).

As depicted in Figure 3.6 the partitioned Fritchman Markov chain classifies the information transmission mechanism into two distinct state categories. State N typifies an error state where incorrect decisions emanate, while the $N-1$ states refer to the error-free state where correct decisions are produced. State crossover occur synchronously with symbol transmission. In Figure 3.6, $f(1), f(2)$ and $f(N-1) = 0$ depicts the correct decision synonymous with the error-free state, while $f(N) = 1$ typifies an incorrect decision synonymous with the single error state. Although two major states exist in the application of the SHFMM in modeling communication problems, the key state is the error state, as it shows the existence of impulse noise and long error burst encountered on the channel and produced in the error state.

The essential feature of the adopted single error state SHFMM as depicted in Figure 3.6 is that self-transition is permissible, while state crossover are not permitted between states of the same group, hence, transitions are made between the good to bad state and vice versa and not between two good states in the same partition. Consequently, the state crossover probabilities A are written in matrix form as follows.

$$A = \begin{bmatrix} a_{1,1} & 0 & \cdots & \cdots & a_{1,N} \\ 0 & a_{2,2} & \cdots & \cdots & a_{2,N} \\ \vdots & \vdots & \vdots & \ddots & \vdots \\ a_{N,1} & a_{N,2} & \cdots & a_{N,N-1} & a_{N,N} \end{bmatrix} \tag{3.15}$$

Based on crossover restriction between states of the same group adopted in Figure 3.6, the error symbol probability denoted by B is written in matrix form as follows.

$$B = \begin{bmatrix} 1 & 1 & \cdots & b_{1,i} & \cdots & b_{1,N} \\ 0 & 0 & \cdots & b_{2,i} & \cdots & b_{2,N} \end{bmatrix}. \tag{3.16}$$

The initial state probability denoting the probability of being in any of the N states is written as follows.

$$\Pi = [\pi_1 \ \pi_2 \ , \ldots, \pi_N]. \tag{3.17}$$

A stochastic process like the Fritchman Markov chain can be parameterized through empirical estimation of the transition probabilities between discrete states in the observed system [147]. In the following Section 3.3.2 and Section 3.3.3, the architecture and parameters of the First and Second-Order SHFMM adopted for the modeling of the in-house NB-PLC channel in this work is presented, while Section 3.4.2 and Section 3.4.3 discusses the corresponding iterative Baum-Welch algorithm for parameter estimation of the SHFMM based on training data obtained experimentally from the real in-house NB-PLC channel.

3.3.2 First-Order Semi-Hidden Fritchman Markov Model

Based on the law of conditional probability for First-Order HMM, the probability of crossover to any state at time t is dependent on solely the previous transition made at time $t-1$. Applying this law to the partitioned SHFMM we have a First-Order SHFMM. Figure 3.7 shows the First-Order SHFMM with single error state adopted in this work.

The adopted SHFMM shown in Figure 3.7 has three states and the corresponding First-Order state crossover probabilities denoted by A_1 is a 3×3 matrix written as follows.

$$\mathbf{A_1} = \begin{bmatrix} a_{1,1} & 0 & a_{1,3} \\ 0 & a_{2,2} & a_{2,3} \\ a_{3,1} & a_{3,2} & a_{3,3} \end{bmatrix} = \begin{bmatrix} a_{11} & 0 & a_{13} \\ 0 & a_{22} & a_{23} \\ a_{31} & a_{32} & a_{33} \end{bmatrix} \tag{3.18}$$

As depicted in Equation (3.18) elements $a_{1,2}$ and $a_{2,1}$ are zeros due to the uniqueness of the chosen SHFMM (impermissible crossover between state one and two). It is also important

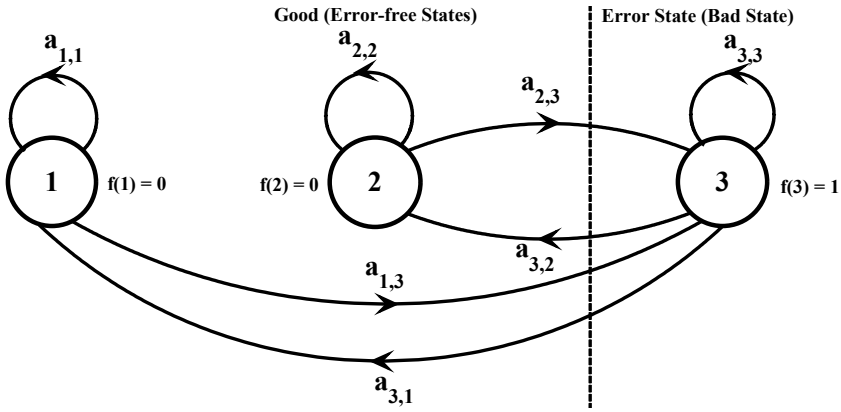

FIGURE 3.7: Adopted First-Order SHFMM with single error state.

to note that elements of A_1 are randomly and uniquely chosen for this application such that probability of crossover to an error-free state denoted by the matrix elements $a_{1,1}$, $a_{2,2}$, $a_{3,1}$ and $a_{3,2}$ is high, while the crossover probability to an error state denoted by the matrix elements $a_{1,3}$, $a_{2,3}$ and $a_{3,3}$ is low in order to depict the observed data. The error symbol probability B is a 2×3 binary matrix and the prior probability of being in any of the three states denoted by Π, a 1×3 is written as follows.

$$B = \begin{bmatrix} 1 & 1 & 0 \\ 0 & 0 & 1 \end{bmatrix}. \tag{3.19}$$

$$\Pi = [\pi_1 \ \pi_2 \ \pi_3]. \tag{3.20}$$

3.3.3 Second-Order Semi-Hidden Fritchman Markov Model

Based on the law of conditional probability for Second-Order HMM, the probability of crossover to any state at time t is dependent on two previous transitions at time $t-1$ and $t-2$. Applying this law to the partitioned SHFMM we have a Second-Order SHFMM. Figure 3.8 shows the adopted Second-Order SHFMM with single error state.

The Second-Order state crossover probabilities denoted by A_2 is written in matrix form as follows.

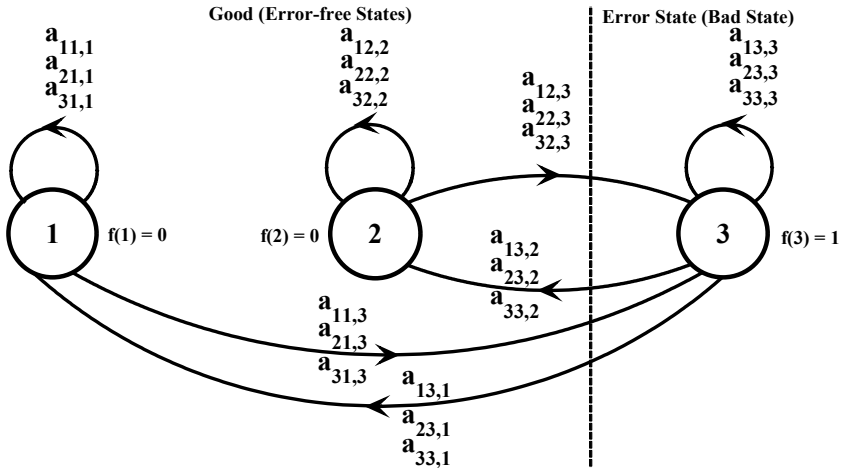

FIGURE 3.8: Adopted Second-Order SHFMM with single error state.

$$\mathbf{A_2} = \begin{bmatrix} a_{11,1} & 0 & a_{11,3} \\ 0 & a_{12,2} & a_{12,3} \\ a_{13,1} & a_{13,2} & a_{13,3} \\ a_{21,1} & 0 & a_{21,3} \\ 0 & a_{22,2} & a_{22,3} \\ a_{23,1} & a_{23,2} & a_{23,3} \\ a_{31,1} & 0 & a_{31,3} \\ 0 & a_{32,2} & a_{32,3} \\ a_{33,1} & a_{33,2} & a_{33,3} \end{bmatrix} = \begin{bmatrix} a_{111} & 0 & a_{113} \\ 0 & a_{122} & a_{123} \\ a_{131} & a_{132} & a_{133} \\ a_{211} & 0 & a_{213} \\ 0 & a_{222} & a_{223} \\ a_{231} & a_{232} & a_{233} \\ a_{311} & 0 & a_{313} \\ 0 & a_{322} & a_{323} \\ a_{331} & a_{332} & a_{333} \end{bmatrix} \tag{3.21}$$

As depicted in Equation (3.21) elements $a_{11,2}$, $a_{12,1}$, $a_{21,2}$, $a_{22,1}$, $a_{31,2}$ and $a_{32,1}$ are zeros due to impermissible crossover between state one and two. It is also important to note that elements of A_2 are randomly and uniquely chosen for this application such that probability of crossover to an error-free state denoted by the matrix elements $a_{11,1}$, $a_{12,2}$, $a_{13,1}$, $a_{13,2}$, $a_{21,1}$, $a_{22,2}$, $a_{23,1}$, $a_{23,2}$, $a_{31,1}$, $a_{32,2}$, $a_{33,1}$, $a_{33,2}$ is high, while the crossover probability to an error state denoted by the matrix elements $a_{11,3}$, $a_{12,3}$, $a_{13,3}$, $a_{21,3}$, $a_{22,3}$, $a_{23,3}$, $a_{31,3}$, $a_{32,3}$ and $a_{33,3}$ is low in order to depict the observed data. The error symbol probability B and the prior probability of being in any of the three states denoted by Π is written as follows.

$$B = \begin{bmatrix} 1 & 1 & 0 \\ 0 & 0 & 1 \end{bmatrix}. \tag{3.22}$$

$$\Pi = [\pi_1 \ \pi_2 \ \pi_3]. \tag{3.23}$$

It is important to note that, the choice of the distinct partitioned SHFMM adopted in this work as opposed to the fully connected HMM is because of the major drawback of local maxima associated with fully connected HMM. Note, this model is semi-hidden because if there is an occurrence of an error, we know it is generated from the single error state, otherwise, should there be no error occurrence, we cannot identify the state.

3.4 Machine Learning Based on Maximum Likelihood Estimation Algorithm

Given a specified model such as the adopted SHFMM with its parameters, and empirical data from real NB-PLC channel, evaluation of its goodness of fit is required to ascertain how well the model parameter fits the empirical data. The goodness of fit is evaluated through determining the model parameter values that best fit or depict the empirical data, a process called *parameter estimation* [148]. The *maximum likelihood estimation* (MLE) and the *least squares estimation* (LSE) are the two universal parameter estimation approaches commonly used [148]. The former is discussed as adopted in the parameter estimation task for the SHFMM adopted in this project.

The MLE is a typical approach in estimation of parameter and inference in statistical modeling analysis. Its use in parameter estimation of SHMM has been linked to the following optimal attributes [148].

- **Sufficient**: the MLE estimator contains comprehensive information about the parameter of interest.
- **Consistent**: for sufficiently large empirical data samples, true parameter value that produced the empirical data is obtained asymptotically.
- **Efficient**: estimated parameter achieved asymptotically is of the lowest possible variance.
- **Parameterization invariance**: the same maximum likelihood estimation solution is gotten independent of the parameters utilized.

On the contrary, the above cannot be said of LSE as statisticians do not view the LSE method as an all-purpose approach for parameter estimation, but as a method mainly for linear regression models. The MLE of SHMM parameters can be achieved either by *direct numerical maximization* (DNM) with algorithm such as Newton-type minimization algorithm or the *expectation maximization* (EM) algorithm with the widely used iterative Baum-Welch algorithm. DNM of the likelihood utilizing Newton-type minimization algorithms has been found to converge quicker that EM algorithms, particularly in the neighbourhood of a maximum, although in order to converge at all, accurate initial model parameter values are required compared to EM.

Given the SHFMM with parameter Γ_m, denoting the full parameters of the SHFMM, our aim is to maximize the probability of an empirical data (observed sequence O - obtained from real NB-PLC channel) associated with a given class m and corresponding to the model parameters denoted by Γ_m. In other words, given the empirical data and model of interest (the SHFMM), we aim at obtaining the most probable parameter set that produced the empirical data. The likelihood can be mathematically expressed as follows.

$$L = \Pr(O^m|\Gamma_m) \tag{3.24}$$

Since only one class of m is considered at a time say for example an empirical data gotten for a particular modulation scheme, we drop the subscript and superscript m in Equation (3.24) and rewrite the maximum likelihood formula as follows.

$$L = \Pr(O|\Gamma) \tag{3.25}$$

Analytically solving for the SHFMM parameters $\Gamma = (A, B, \Pi)$ that maximizes L is impossible, rather a known option is the use of the iterative *Baum-Welch algorithm* (BWA) or the *gradient based method* (GBM) to obtain local maxima close to the global maxima by carefully selecting suitable model parameters.

3.4.1 Baum-Welch algorithm

Baum-Welch algorithm (BWA) [20, 21] is a MLE algorithm, which is a distinct case of the EM algorithm for SHMM. The algorithm is an unsupervised learning algorithm that uses an iterative procedure in optimizing the parameters of the SHFMM given empirical data obtained from the NB-PLC channel. The BWA is capable of computing maximum likelihood estimates as well as posterior mode estimates for the crossover/transition and emission probabilities of a SHFMM utilizing the empirical data as the training data set.

The BWA is designed to converge to the maximum likelihood estimator of the SHFMM $\Gamma = (A, B, \Pi)$ that maximizes $\Pr(O|\Gamma)$, where O is the empirical data or the error sequence obtained through experimental measurement on the NB-PLC channel. Henceforth, O is replaced with $\bar{E}$ for the purpose of defining the First and Second-Order Baum-Welch algorithm for optimizing the First and Second-Order SHFMM parameters in this project. Hence, $\Pr(O|\Gamma)$ becomes $\Pr(\bar{E}|\Gamma)$, and $O = o_1, o_2, o_3, \ldots, o_T$ becomes $\bar{E} = e_1, e_2, e_3, \ldots, e_T$, where T is the length of the empirical error sequence.

3.4.2 First-Order Baum-Welch algorithm

In [149], we showed an elaborate derivation and implementation of First-Order Baum-Welch algorithm formulas for First-Order SHFMM. Consequently, a summarized version of how the First-order Baum-Welch algorithm is utilized in obtaining the most probable First-Order SHFMM parameter set that produced the empirical error sequence is summarized and shown in pictorial form. An elaborate mathematical representation and implementation can be found in [21] and in Appendix A of [149] credited to the author of this thesis. Figure 3.9 show the flowchart of the First-Order iterative Baum-Welch algorithm used to optimize the First-Order SHFMM parameters that maximizes $\Pr(\bar{E}|\Gamma)$.

In order to maximize the likelihood function $\Pr(\bar{E}|\Gamma)$, the following BWA learning process are carried out as shown in Figure 3.9. Given the empirical training error sequence $\bar{E}$, first, an initial model $\Gamma_1^0 = (A_1^0, B^0, \Pi^0)$ is assumed and a computation of the forward path probability vector "α" and second the backward path probability vector "β" utilizing the forward backward algorithm [21] is carried out. Furthermore, two intermediate variables "ξ"

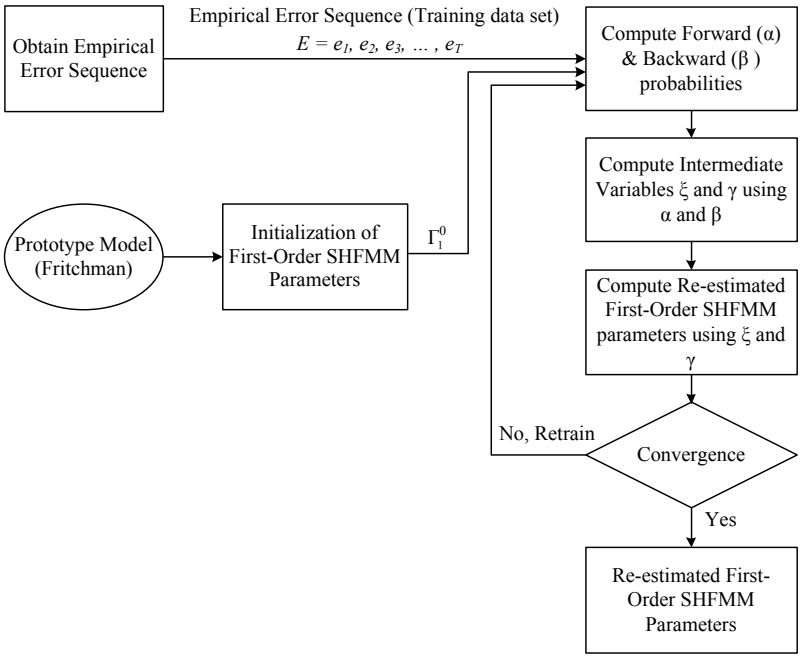

FIGURE 3.9: Flowchart of a First-Order iterative Baum-Welch algorithm.

and "γ" are computed and later used for parameter re-estimation. Lastly, the First-Order re-estimation formula used in updating the SHFMM parameters $\hat{a}_{ij}, \hat{b}_j(e_k)$ and $\hat{\Pi}$ utilizing 'α", "β", "ξ" and "γ" as illustrated in [149]

3.4.3 Second-Order Baum-Welch algorithm

In this Section, an implementation of the Second-Order Baum-Welch algorithm utilized in obtaining the most probable Second-Order SHFMM parameter set that produced the empirical error sequence is discussed. Figure 3.10 shows the flowchart of the Second-Order iterative Baum-Welch algorithm used to optimize the Second-Order SHFMM parameters that maximizes $\Pr(\bar{E}|\Gamma)$. For detailed mathematical derivation of the Second-Order Baum-Welch algorithm training steps for an error sequence of length $T = 5$, refer to Appendix A.

The training procedures are highlighted as follows given the empirical error sequence $\bar{E}$ and the model of interest, the SHFMM [150].

1. Initialize the Second-Order SHFMM parameter $\Gamma_2^0 = (A_2^0, B^0, \Pi^0)$: Π_i^0, a_{ij}^0, a_{ijk}^0 and ${b_k}^0(l)$, for $1 \leq i, \quad j, k \leq N, \quad 1 \leq l \leq M$.

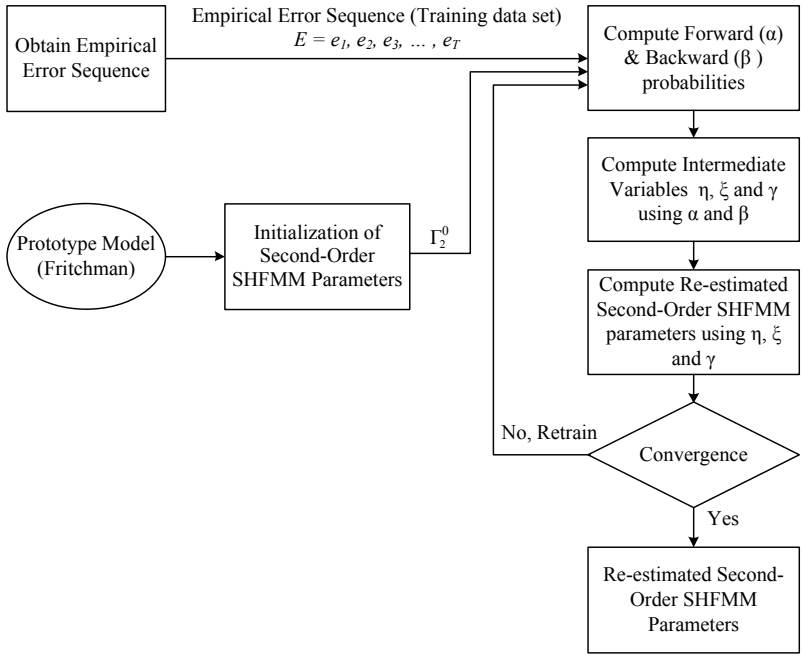

FIGURE 3.10: Flowchart of a Second-Order iterative Baum-Welch algorithm.

2. Computation of the forward path α and backward path β probability vector using the initialized model as input and the empirical error sequence $\bar{E}$ as training data.

3. Computation of the re-estimation formulas: $\eta_t(i,j,k)$, $\xi_t(i,j)$ and $\gamma_t(i)$, for $1 \leq i, \quad j,k \leq N, \quad 2 \leq t \leq T-1$ using the computed forward and backward probabilities.

4. Computation of the new re-estimated parameters: $\hat{\Pi}_i$, $\hat{a}_{ij}$, $\hat{a}_{ijk}$ and $\hat{b_k}(l)$ for $1 \leq i, \quad j,k \leq N, \quad 1 \leq l \leq M$ utilizing the parameter re-estimation formulas.

5. Reiteration of steps 2-4 with the re-estimated parameters until the desired level of convergence is reached, that is, $\Pi_i = \hat{\Pi}_i$, $a_{ij} = \hat{a}_{ij}$, $a_{ijk} = \hat{a}_{ijk}$ and $b_k(l) = \hat{b_k}(l)$ for $1 \leq i, \quad j,k \leq N, \quad 1 \leq l \leq M$.

Let the observation symbol sequence be denoted by $\bar{E} = e_1, e_2, e_3, \ldots, e_T$, where the observation symbol at discrete time t is denoted by e_t. Let $S = S_1, S_2, S_3, \ldots, S_T$ represent the state sequence and the state sequence at time t denoted by $s_t \in S$. Hence, for an observation sequence $\bar{E}$ and a given model Γ_2, $\Pr(\bar{E}|\Gamma_2)$, the observation probability evaluation problem can be worked out as orderly discussed as follows [150].

Forward probability function: The forward probability function denoted as $\alpha_t(j,k)$, determines the probability of the partial observation sequence $e_1, e_2, e_3, \ldots, e_t$ for transition

from $(S_j \rightarrow S_k)$ at times $t-1$ and t, given the model Γ_2 and is mathematically represented as follows for $2 \leq t \leq T-1$ and $1 \leq j,k \leq N$, where N depicts number of states and T, the error sequence length [150]:

$$\alpha_t(j,k) = \Pr(e_1, e_2, e_3, \ldots, e_t,\ s_{t-1} = S_j, s_t = S_k|\Gamma_2) \tag{3.26}$$

Note that just like in First-Order Baum-Welch, for Second-order, $\alpha_t(j,k)$ in Equation (3.27) is normally computed from $\alpha_t(i,j)$ based on two transitions $(S_i \rightarrow S_j)$ and $(S_j \rightarrow S_k)$ which represents transition between states i, j and k $(S_i \rightarrow S_j \rightarrow S_k)$.

$$\alpha_{t+1}(j,k) = \left[\sum_{i=1}^{N} \alpha_t(i,j) a_{ijk}\right] b_k(e_{t+1}) \tag{3.27}$$

Note also, that the entire observation sequence's probability is determined as shown in Equation (3.28);

$$\Pr(e_1, e_2, e_3, \ldots, e_T|\Gamma_2) = \sum_{i=1}^{N} \alpha_T(i,N) \tag{3.28}$$

Backward probability function: Similarly, the backward probability function denoted as $\beta_t(i,j)$, is specified as the probability of the partial observation sequence $e_1, e_2, e_3, \ldots, e_t$ for transition from state $(S_i \rightarrow S_j)$ between time instants $t-1$ and t, with Γ_2 specified and is depicted as follows in Equation (3.29) for $2 \leq t \leq T-1$ and $1 \leq i,j \leq N$ [150].

$$\beta_t(i,j) = \sum_{k=1}^{N} a_{ijk} b_k(e_{t+1}) \beta_{t+1}(j,k) \tag{3.29}$$

Parameter Re-estimation Variables: Just as in First-Order Baum-Welch, three intermediate variables are computed from the forward and backward probability function in order to re-estimate the Second-Order SHFMM parameters. We compute $\eta_t(i,j,k)$ which depicts the transition probabilities between states S_i, S_j and S_k $(S_i \rightarrow S_j \rightarrow S_k)$ at times t-1, t and t+1 respectively, given the model Γ_2 and training sequence $\bar{E}$ as depicted in Equations (3.30) and (3.31) for $2 \leq t \leq T-1$ [150]:

$$\eta_t(i,j,k) = \frac{\alpha_t(i,j) a_{ijk} b_k(e_{t+1}) \beta_{t+1}(j,k)}{Pr(\bar{E}|\Gamma_2)} \tag{3.30}$$

$$\eta_{t+1}(i,j,k) = \frac{\alpha_{t+1}(i,j) a_{ijk} b_k(e_{t+2}) \beta_{t+2}(j,k)}{Pr(\bar{E}|\Gamma_2)} \tag{3.31}$$

Similarly, we compute $\xi_t(i,j)$ defined as the probability of transitioning between state S_i at time instant t and state S_j at time instant t+1 with the model Γ_2 specified and the training sequence $\bar{E}$ as shown in Equation (3.32). While on the other hand, $\gamma_t(i)$ is defined as the probability of transitioning to state S_i at time instant t, with Γ_2 and the training sequence $\bar{E}$ specified as shown in Equations (3.33) [150].

$$\xi_t(i,j) = \sum_{k=1}^{N} \eta_{t+1}(i,j,k) = \sum_{k=1}^{N} \left[\frac{\alpha_{t+1}(i,j) a_{ijk} b_k(e_{t+2}) \beta_{t+2}(j,k)}{Pr(\bar{E}|\Gamma_2)} \right] \tag{3.32}$$

$$\gamma_t(i) = \sum_{j=1}^{N} \xi_t(i,j) = \sum_{j=1}^{N} \sum_{k=1}^{N} \left[\frac{\alpha_{t+1}(i,j) a_{ijk} b_k(e_{t+2}) \beta_{t+2}(j,k)}{Pr(\bar{E}|\Gamma_2)} \right] \tag{3.33}$$

Parameter Re-estimation Formulas: The Second-order re-estimated parameter set are then computed using the following re-estimation formulas computed using the three intermediate variables derived earlier. The re-estimated First-Order state transition/crossover probabilities is computed as follows [150].

$$\hat{a}_{ij} = A_1 = \frac{\xi_1(i,j)}{\gamma_1(i)} \tag{3.34}$$

The computation of the re-estimated Second-Order state transition/crossover probabilities is carried out by the equation shown as follows [150].

$$\hat{a}_{ijk} = A_2 = \frac{\sum_{t=1}^{T-3} \eta_{t+1}(i,j,k)}{\sum_{t=1}^{T-3} \xi_t(i,j)} \tag{3.35}$$

The re-estimated output symbol probability matrix is computed using the equation shown as follow [150].

$$\hat{b_k}(l) = \frac{\sum_{t=1, e_t=V_l}^{T} \gamma_t(k)}{\sum_{t=1}^{T} \gamma_t(k)} \tag{3.36}$$

The re-estimated initial state probability is computed as follows [150].

$$\hat{\Pi}_i = \frac{\gamma_1(i)}{\sum_{i=1}^{N} \gamma_1(i)} \tag{3.37}$$

The SHFMM re-estimated parameters obtained through training is then used to generate an error sequence with equal length as the original empirical error sequence. The error-free run distribution (EFRD) denoted by $\Pr(0^m|1)$ is then computed for both the original empirical error sequence and the SHFMM generated error sequence. A plot of $\Pr(0^m|1)$ for both the original empirical error sequence and the SHFMM generated error sequence is realized and then compared to assess the fitness of the model. It is important to note that the SHFMM will not replicate the original empirical error sequence but will however reproduce a statistical equivalent of it [21].

The forward path probability vector "α" and the backward path probability vectors "β" tend to zero exponentially given large empirical data size as multiplication of many probabilities often leads to numerical underflow problem [21]. This problem of numerical stability in the use of the adopted Baum-Welch algorithms is solved through the use of log transformation and proper scaling of "α" and "β". The scaling constant C_t is then defined as follows [21].

$$C_t = \sum_{i=1}^{N} \alpha_t(i) \tag{3.38}$$

The scaled value of the forward path probability vector is denoted by "$\bar{\alpha}_t(j)$" and written as follows.

$$\bar{\alpha}_t(j) = \frac{\alpha_t(j)}{C_t} \tag{3.39}$$

This implies that $\sum_{i=1}^{N} \bar{\alpha}_t(i) = 1$. Furthermore, the scaled value of the backward path probability vector is denoted by "$\bar{\beta}_t(i)$" and initialized with $\bar{\beta}_T = \frac{1}{C_T}$, where 1 indicates the column vector containing all 1's and is mathematically written as follows.

$$\bar{\beta}_t(i) = \frac{\beta_t(i)}{C_t} \tag{3.40}$$

The number of iterations required for the desired level of convergence can be obtained by running the algorithm until either the variation in the value of $\Pr(\bar{E}|\Gamma_2)$ becomes very small or no changes in value occurs. The value of $\Pr(\bar{E}|\Gamma_2)$ is mathematically computed using the scaling constant C_t in Equation (3.38) as follows.

$$\Pr\ [\bar{E}|\Gamma_2] = \prod_{t=1}^{T} C_t \tag{3.41}$$

For large empirical error sequences, this probability is extremely small, hence to prevent numerical underflow it is expressed in logarithmic form as follows and referred to as *log-likelihood ratio* often denoted by L.

$$L = \log_{10} Pr\ [\bar{E}|\Gamma_2] = \sum_{t=1}^{T} \log_{10} C_t \tag{3.42}$$

Note, that the computation of the recursive forward probability function (α) and backward probability function (β) require the order of N^2T operations for the First-Order Baum-Welch compared to the order of (N^3T) operations for the Second-Order Baum-Welch parameter estimation algorithm. Hence, there is a trade-off in terms of computational complexity, as the Second-Order model is more computationally intensive than its First-Order counterpart, although the Second-Order model gives a better model than the First-Order.

3.5 Machine Learning Based on Bayesian Inference Algorithm

3.5.1 Introduction

In the Bayesian inference approach, probability is seen as a measure of uncertainty, and how degrees of belief are quantified [133]. This methodology is mainly employed in a logically coherent manner for the modification of uncertainty, such that we end up with a rational degree of belief and not just degree of belief simply based on personal opinion. In this method of inference, we assign an initial prior probability distribution to each and every unknown parameter. This does not imply that the parameter randomly varies, but just an indication that they are unknown, with the probability distribution used to model belief about the parameter's true value. Based on observed data, we employ Bayes' theorem to update our prior belief as it concern the unknown parameter. The statement of final inference then utilizes the parameter's posterior distribution in the quantification of the parameter's final uncertainty. This is conditionally based on data observed [133].

3.5.2 Metropolis-Hastings algorithm

In this section, a presentation and discussion of one of the methods for generating Markov chain used in MCMC known as Metropolis-Hastings (M-H) will be carried out. The characterization of this MCMC algorithm resulted from the work of Metropolis et al. [151] and Hastings [152]. Other papers by authors who have contributed to the Metropolis-Hastings algorithm MCMC method includes Barker [153] and [154].

Let's assume a case that we desire to sample from a given posterior distribution $P(\theta|y)$, but the following conditions hold for the posterior distribution in question.

1. The given posterior distribution is dissimilar to any known distribution, i.e. conjugacy does not exist.
2. The given posterior distribution is comprised of more than two parameters, giving rise to intractable grid approximations.
3. Having full conditionals (part or all of it) dissimilar from any known distributions, hence, Gibbs sampling does not exist for any unknown full conditionals.

Metropolis-Hastings algorithm can be employed in such situation where all other MCMC algorithms fail, as it will definitely work if we have any of the aforementioned conditions. Therefore, we introduce the Metropolis-Hastings algorithm steps as follows.

1. Select an initial value $\theta^{(0)}$. This is essentially the same as taking draws from our starting stationary distribution. It is essential to note that our initial value $\theta^{(0)}$ is highly recommended to possess positive probability, otherwise, we will be initiating with a value that is impossible to draw (i.e. $P(\theta^{(0)}|y) > 0$).
2. At the time component t analogous to iteration t, we draw a candidate parameter denoted as θ^* from $J_t(\theta^*|\theta^{(t-1)})$ a jumping distribution. This jumping distribution $J_t(\theta^*|\theta^{(t-1)})$ indicates where we transition to at our next Markov chain iteration (this is analogous to the Markov chain transition kernel). The jumping distribution's support must also comprise the posterior distribution's support.

The initially developed ***Metropolis algorithm*** necessitated that the jumping distribution $J_t(\theta^*|\theta^{(t-1)})$, must be a symmetrical distribution (for instance a normal distribution).

$$J_t(\theta^*|\theta^{(t-1)}) = J_t(\theta^{(t-1)}|\theta^*) \tag{3.43}$$

It remains a fact that symmetry is non-essential in the use Metropolis-Hastings algorithm. Peradventure our jumping distribution possesses symmetry, which implies that the distribution is dependent on $\theta^{(t-1)}$ as seen in Equation 3.43, hence, what we have is recognized as ***random walk Metropolis sampling*** according to literature. On the other hand, whenever our jumping distribution is independent of $\theta^{(t-1)}$, as expressed in Equation 3.44, therefore, we have what is referred to as ***independent Metropolis-Hastings sampling***.

$$J_t(\theta^*|\theta^{(t-1)}) = J_t(\theta^*) \tag{3.44}$$

Fundamentally, irrespective of the position of our previous draw, our entire candidate parameter draws θ^* are always obtained from indistinguishable (same) distribution. How extremely efficient or extremely inefficient this is, is dependent upon the closeness of the jumping distribution with the posterior distribution.

Typically speaking, the Markov chain's behavior is good, if and only if our jumping distribution possesses heavier tails compared to the posterior distribution.

3. The next step is the computation of an acceptance ratio (i.e. probability of acceptance) mathematically expressed as follows.

   For a symmetric jumping distribution scenario, our acceptance ratio is expressed mathematically as

$$r = \frac{P(\theta^*|y)}{P(\theta^{(t-1)}|y)} \tag{3.45}$$

   Whenever we have a higher probability for our candidate draw than we have for our present draw, we unquestionably accept the candidate draw because it is better. Otherwise, the acceptance of our candidate draw is based upon the ratio of the candidate's draw and present draws probabilities. It is essential to note that because r is a ratio, all that is needed is our posterior distribution, $P(\theta|y)$, (*up to a constant of proportionality*), based on the fact that the probability of our observed data denoted by $P(y)$ crosses out each other in both the numerator and denominator.

For a non-symmetric jumping distribution case, our acceptance ratio r is expressed mathematically as follows.

$$r = \frac{\frac{P(\theta^*|y)}{J_t(\theta^*|\theta^{(t-1)})}}{\frac{P(\theta^{(t-1)}|y)}{J_t(\theta^{(t-1)}|\theta^*)}} \tag{3.46}$$

It is required that our evaluations of draws made at the posterior densities is weighed by how possible each of our draws are drawn. Let's assume we have a potential of jumping or transitioning to some candidate draw, θ^*, hence, there is possibility of a high jumping distribution, $J_t(\theta^*|\theta^{(t-1)})$, all we need to do is to accept less of these θ^*, than several other θ^* that we have less possibility of transitioning or jumping to.

For an ***independent Metropolis-Hastings sampling*** scenario, our acceptance ratio is expressed as follows.

$$r = \frac{\frac{P(\theta^*|y)}{J_t(\theta^*)}}{\frac{P(\theta^{(t-1)}|y)}{J_t(\theta^{(t-1)})}} \tag{3.47}$$

4. At this step, a decision is made about which candidate draw θ^* will be accepted. We accept candidate draw θ^* with a probability $\min(r, 1)$ as $\theta^{(t)}$, otherwise, if unacceptable, consequently $\theta^{(t)} = \theta^{(t-1)}$.

   (a) For individual candidate draw θ^*, we draw from the Uniform(0,1) distribution a value denoted as u.

   (b) If $u \leq r$, then the candidate draw is accepted, θ^* is accepted as $\theta^{(t)}$. Otherwise, $\theta^{(t-1)}$ is used as $\theta^{(t)}$.

   We accept candidate draws θ^* having higher density than our present or current draw. Each iteration will ever produce either a candidate draw θ^* or $\theta^{(t-1)}$ in contrast to what we have in rejection sampling.

5. In order to acquire M draws from our posterior distribution $P(\theta|y)$, we then reiterate steps two to four M times. Burn-in and thinning process can then be performed, but these two processes are always optional.

In terms of our ***Acceptance Rates***: monitoring of the acceptance rate (fraction of accepted θ^*) of our Metropolis-Hastings algorithm is crucial. If we have a very high acceptance rate, this implies that the Markov chain is not well mixed (i.e. the movement of the chain all over the parameter space is not quick enough). In contrast, a very low acceptance rate

indicates that our algorithm is very inefficient leading to too many θ^* being rejected. The particular algorithm used determines what is very high and very low, but typically, according to literature, recommended acceptance rate for ***random walk Metropolis sampling*** is between 0.25 and 0.50, while that preferred for the ***independent Metropolis-Hastings sampling*** is somewhere close to 1.

In [155], Alasseur et al. used the Metropolis-Hastings algorithm, an MCMC method combined with k-means classification for parameter estimation of HMM from experimental data to account for the time fluctuations of received power experienced in a mobile satellite service context. The author used the k-means classification method to refine change-points location by detecting false change-point because the MCMC method used provided raw change-points as a result of fewer iteration used.

According to [156], Yu-Zhong Jiang, Xiu-lin, Xu and Zhai derived and computed an efficient Bayesian estimator of the Middleton Class A interference model parameters utilizing the Gibbs sampler, another form of MCMC method. The authors proved that the use of small sample sizes for the simulation of the estimator ascertains that this technique is efficient and near optimal performance can be achieved. Rong-Rong et al. in [157] reported the application of Gibbs sampler MCMC method to both MIMO detection and channel equalization. The authors showed that using an MCMC-based MIMO detector could bring them within 2 dB of the channel capacity with a great degree of reduced complexity compared to the use of sphere-decoding based detectors. In this paper, it was also demonstrated that an MCMC-based equalizer achieves very good performance even in the presence of ISI (inter-symbol-interference) for a frequency-selective channel. In [158], Hong et al. developed over a time-varying frequency-selective channel, MCMC methods for both joint data detection and channel estimation. In this work, the MCMC-list channel estimates (MCMC-LCE) was proposed as the detector. This detector adopted the Gibbs sampler MCMC method to discover a list of likeliest sequences transmitted and then matches the CIR (channel estimates/impulse responses) to calculate the log-likelihood ratio of bits transmitted. In [159], a Metropolis-Hastings adaptation referred to as reversible jump MCMC (RJ-MCMC) sampler solved the problem of signal detection and parameter estimation.

CHAPTER 4

The NB-PLC Transceiver System, Modeling Methodology

Majority of the conventional communication transceiver systems currently accessible utilize hardware-based wiring of application specific integrated circuits (ASICs). This configuration constrains the modulation and FEC techniques required for a particular standard to a hardware based architecture. As a result, continuous technological development and evolution in various communication system technologies causes many transceiver implementation to become obsolete with time. Similarly, interoperability becomes difficult due to the emergence of new communication standards in the communication industry. Consequently, frequent replacement of communication equipment becomes a norm.

Thus, to tackle this problem, flexibility has been introduced into the adopted PLC transceiver system, as we opted for the software defined approach. An advanced software programmable modulation is utilized in the implementation of the NB-PLC transceiver systems, hence, modifications due to emerging standards and technological developments are implementable in the software domain to enhance PLC system performance without the need for hardware architectural changes or replacement. Therefore, a reconfigurable software-defined single carrier and multi-carrier OFDM transceivers, utilizing Matlab packages interfaced with the Ettus universal software radio peripheral (USRP) is developed. With this flexibility employed in developing the transceiver systems, digital signal processing codes for the NB-PLC transceiver systems are brought closer to both the transmitting and receiving front ends. To the best of the author's knowledge, the reconfigurable software-defined NB-PLC transceiver developed in this work using USRP is a novel approach for NB-PLC applications, as several other transceivers developed in literatures are simulation-based or hardware-based design.

The functionality of the NB-PLC transceiver system testbed is verified in an in-home residential and laboratory CENELEC "A" narrowband low voltage (LV) power line environment,

using a suitable differential capacitive mode coupling specified for LV PLC applications, by transmitting and receiving digital complex base-band OFDM frames.

The following hardware and software components were utilized in developing the reconfigurable software defined single-carrier (BPSK, DBPSK, QPSK and DQPSK) and multi-carrier (QPSK-OFDM, DQPSK-OFDM and D8PSK-OFDM) NB-PLC transceiver adopted in this project.

1. Universal software radio peripheral version 2 (USRP2) with LFTX and LFRX daughterboard.
2. Bandpass filters (The transmitter and receiver coupling circuit).
3. The transmitter and receiver host computer (Windows PC).
4. Power line network (residential and laboratory in-home topology).
5. Gigabit Ethernet cables.
6. Matlab/Simulink communications systems toolbox support package for USRP.

This Chapter thus provides basic definitions and introduction of the major constituents (both hardware and software) of the NB-PLC transceiver design. Furthermore, how the various hardware are configured and suitable software installed is presented. The modeling methodology/approach employed is also discussed in this Chapter.

4.1 The Universal Software Radio Peripheral (USRP)

The USRP families are range of SDRs designed and sold by Ettus Research and its parent organization the National Instruments. They are designed as a flexible, affordable, reconfigurable and reusable hardware modules or peripherals capable of transmitting and receiving arbitrary baseband signals and also enabling universal purpose computers to operate as high bandwidth SDRs [160]. As a result of its modularization into a motherboard and a daughterboard, USRPs can be adopted to an extensive range of operational frequencies. The first generation of USRPs is connected to a host computer through a USB 2.0 port, while the next generation USRPs is connected via fast Gigabit Ethernet connection and embedded

USRP peripheral do not need external computers as they possess embedded Linux operating system.

The modularized USRP daughterboards gives the USRP device direct access to the radio frequency world and comprise analog radio frequency front-end and intermediate frequency (IF) mixing functionality for the SDR. Several range of daughterboards exist for the USRP modules and are designed for particular frequency spectrum with the capability of a center frequency tunable via software. The obtainable USRP daughterboards frequency spans from DC-5.9 GHz [161, 162].

4.1.1 The Universal Software Radio Peripheral Version 2

The second generation of USRP modules is comprised of few changes made to the first generation USRP1. The new modules can house two daughterboards and possesses two input and output channels. The FPGA of this new generation USRPs can be reconditioned for additional control of the signal processing ahead of decimation operation and transmission to the host receiver computer. Alongside USRP version 2 (USRP2), we have the USRP N200 and N210 with the 10 in the later model indicating a superior FPGA than the former allowing additional space for custom pre-processing code [161].

The USRP2 used in this research allows multiple USRP modules to be linked and to function as a single USRP with additional channels (MIMO capability). The USRP2 is still operational but discontinued for the N2x0 versions. The USRP2 box houses both the motherboard, daughterboard and has the following features: standalone operation, a gigabit Ethernet interface, a one transceiver daughterboard slot or 1 RX and 1 TX daughterboard slot, a Xilinx Spartan 3 XC3S2000 FPGA, 25 MHz of instantaneous RF bandwidth to/from host, Dual 400 MHz 16-bit DACs Dual 100 MHz 14-bit ADCs, SD card reader, MIMO expansion slot, 1 pulse per second input and external reference clock capability.

4.1.2 Motherboards

The motherboard is the heart of a USRP module as it manages the communication with the host and is able to perform digital signal processing task up to the 25 MHz bandwidth at

an IF [161], [163]. Positioned on the motherboard are the following: Gigabit Ethernet interface for communicating between host PCs and the USRP module, MIMO expansion slot for MIMO capabilities, SD card reader slot for storage of FPGA configuration and microprocessor firmware on standard SD cards, two 100 MS/s 14-bit ADCs (LTC2284) for analog to digital conversion of signals, two 400 MS/s 16-bit DACs (AD9777) for digital to analog conversion of signals, a reprogrammable Xilinx Spartan 3-2000 FPGA on which baseband digital signal processing tasks are performed at intermediate frequency. Also built into the FPGA are; two digital down-converters (DDC) having programmable decimation rates for digital down conversion task and two digital up-converters (DUC) having programmable interpolation rates for digital up-conversion task. The RF front-end is realized through modular daughterboard interfaced with the motherboard. The attainable modular functional frequency is from DC-5.9 Gigahertz [163].

4.1.3 Daughterboards

The USRP, a family of SDR is characterized by a modularized architecture having daughterboards which are interchangeable and able to function as the radio frequency (RF) front-end. Several categories of daughterboard modules with specific frequency range are obtainable as follows: transceivers, transmitters and receivers, but focus will be on the transmitter and receiver only versions used in this project [163].

Two receive and two transmit channel are accessible on each daughterboard for either a complex or two real valued data streams in the receive and transmit directions with full duplex communication capabilities [161]. On the motherboard, a 10 MHz fixed frequency oscillator is employed in generating an oscillator on to the daughterboard's target frequency. This oscillator then carries out a modulation of the signal from the operational receive frequency to the intermediate frequency and the transmit streams from the intermediate frequency into the operational transmit frequency [161]. For real valued data streams, one can connect the two data streams to dissimilar antennas with the same operational frequency. Majority of daughterboards possess the capability of suppressing aliasing effects by filtering of the received signal [161].

The LFTX and LFRX daughterboards operate in the DC-30 MHz frequency range and are therefore suitable candidates for the NB-PLC operational frequency (9-95 kHz) considered in this project. These boards possess the following [164].

- They both have four front-ends labeled A, B, AB and BA. A and B are for real signals and are connected to antennas RXA and RXB for the receiver and to TXA and TXB for the transmitter. On the other hands, AB and BA are quadrature front-ends utilizing both antennas (IQ) and (QI).
- The gains of LFRX and LFTX are not tunable but with aliasing one can down-convert and up-convert signals greater than the Nyquist rate of the ADC and DAC respectively.
- The LFRX and LFTX bandwidths are 33 MHz for front-end A or B and 66 MHz for front-end AB or BA.

4.2 The Transmit and Receive Coupling Circuits

In order to transmit and receive on the NB-PLC channel, appropriate transmit and receive coupling interface must be developed. These coupling interfaces are not just any piece of circuitry, but the most important part of PLC transmission.

The TX and RX couplers are designed basically as high-order bandpass filters with the following fundamental functions: couple onto and decouple signals from the power line while concurrently providing galvanic isolation and blocking the AC main 50/60 Hz current from damaging the sensitive USRP transmitter and receiver modules. Apart from its filtering functionality, the coupling interface must guarantee an impedance matching characteristic in order to adapt to the ever changing impedance experienced at the coupling point and on the power line. Therefore, careful consideration must be made in the selection of its components and its design in order to adhere to stipulated regulatory standards.

In this Section, the choice of coupling mode and component selection compatible with the target NB-PLC frequency is justified as well as detailed description of the coupler design provided.

4.2.1 Coupling modes

Coupling of signals onto the power line can be realized through two different closed current paths, the differential mode and common mode coupling [5, 98]. Furthermore, for a practical implementation of coupling circuits, the use of either a capacitive or inductive coupling is employed. In this project, a suitable differential capacitive transmitter and receiver coupling circuits for transmission on the LV in-home NB-PLC network is developed. Refer to [149] for a detailed description of the differential mode, common mode, capacitive and inductive coupling.

The differential mode is implemented by connecting the live terminal of the plug to one end of the cable, while the neutral terminal is the other end of the cable. This mode is realized on a low voltage network where there is provision for a neutral line [149].

Capacitive coupling: In this mode, a capacitor is utilized in injecting or coupling of the signal onto the power line. This is accomplished by modulating the signal onto the power line voltage waveform. A capacitive coupler is highly recommended and specified for LV applications due to power restrictions (maximum allowable power) stipulated by regulatory bodies for the LV network [5, 98].

4.2.2 Components Selection and Its Function

To achieve a reliable communication on the power line, deliberate attention must be paid to the design of a coupling interface connecting the power circuitry (operating at low frequencies, high power, current and voltage levels) and the communication circuitry (operating at high frequencies, low power, current and voltage levels) for optimal compatibility since these two systems operate at differing extremes [98]. Hence, selection of appropriate components for the chosen application is crucial in the design of the coupling interface in order to achieve optimal compatibility and reliable real time transmission.

Capacitor: For proper coupling, a high pass filter (bandpass filter) is essential for blocking the AC main voltage and vital part of its harmonics from the sensitive communication URSP modules. Thus, a capacitor is positioned in series with the transformer. This capacitor should be a high voltage, high frequency capacitor rated 230 vac (50/60 Hz) and possess a

nominal value adhering to the maximum reactive power stipulated for power line applications [27, 165].

Transformer: In a coupling interface, a transformer provides galvanic isolation between the USRP transmit and receive modules to prevent damage to this sensitive equipment. A suitable transformer must offer a compromise between robust coupling at the transmitting side in order to avoid signal attenuation and a weak coupling at the receiving side for adequate filtering of interferences. Dimensioning the winding inductance and the leakage inductance must be done with care in order to achieve an effective coupling interface [98, 165]. In actual fact, the HV capacitor in combination with the series leakage inductance of the transformer produces a series-resonant bandpass filter (coupling circuit) given by the equation (4.1) as follows, where L_{Leak} is the leakage inductance of the transformer and C_{HV} is the series HV capacitance [98].

$$f_{res} = \frac{1}{2\pi\sqrt{L_{Leak}C_{HV}}} \tag{4.1}$$

4.2.3 Schematic of the TX and RX Coupling Interface

The coupling interface design schematic for the transmitter and the receiver is as shown in Figure 4.1 and Figure 4.2 respectively. It is comprised of a high voltage capacitor connected in series with the transformer (possess leakage inductance).

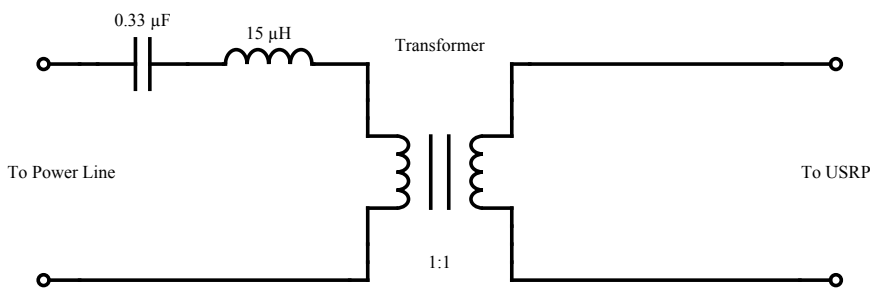

FIGURE 4.1: Proposed design schematic for the transmitter coupling circuit

These proposed coupling interfaces are fundamentally high order bandpass filter allowing high frequency communication signals within the 9-500 kHz range to be coupled onto the power line, while blocking the AC main 50 Hz low frequency. Apart from its function as

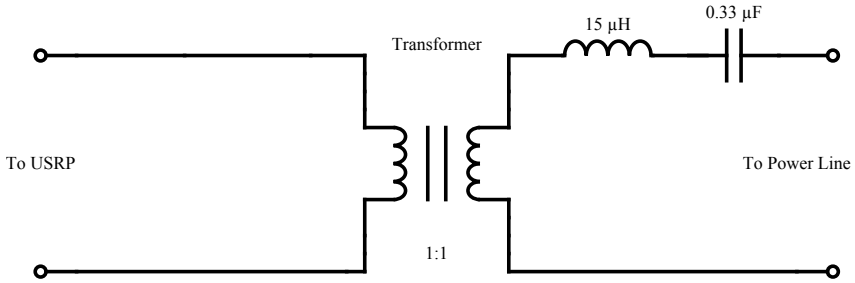

FIGURE 4.2: Proposed design schematic for the transmitter coupling circuit

a filter, these interfaces ensure impedance matching with the 50 ohms USRP transmit and receive modules in order to guarantee a maximum signal transfer.

The frequency range covered by the coupling interfaces is decided by the respective -3 dB low cut-off frequency denoted by (f_{lc}) in equation (4.2) and high cut-off frequency denoted by (f_{hc}) in equation (4.3), where R is the terminating resistance [98].

$$f_{lc} = \frac{1}{2\pi R C_{HV}} \tag{4.2}$$

$$f_{hc} = \frac{R}{2\pi L_{Leak}} \tag{4.3}$$

In our design, we have utilized a HV capacitor rated 0.33 μF and a custom designed 1:1 wideband transformer with leakage inductance of 15 μH.

(a) Tx and Rx coupling termination (b) Picture of complete Tx and Rx Coupler

FIGURE 4.3: Photograph of Tx and Rx coupler termination and complete implementation

Figure 4.3(a) and Figure 4.3(b) show the transmitter and the receiver coupling circuit termination and complete transmitter and receiver coupler implementation picture respectively.

4.3 Transmitter and Receiver Host Computer

The transmitter (TX) and receiver (RX) host computers house the Matrix laboratory (MATLAB) software, a multi-paradigm numerical computing environment and communication toolbox support package for interacting with the USRP. The host TX and RX is used to load the correct firmware and FPGA images onto the SD cards of the USRP2 modules through the gigabit Ethernet. Furthermore, the host TX and RX controls and interact with the USRP2 modules through the gigabit Ethernet cable connection. The digital signal processing (both pre-processing and post-processing) of the complex baseband signals is carried out in software domain on the host computers.

4.4 Power Line Network Topology and Scenarios

It is vital to give a description of the power line network where the functionality of the implemented NB-PLC transceiver test-beds was ascertained/utilized for real-time transmission, experimental measurement and for modeling of the NB-PLC channel. This is essential due to variations in noise parameters often obtained from country-to-country resulting from dissimilar mains voltage (in some cases), power line topology, power line frequency bandwidth considered, place or locality and time.

The CENELEC A NB-PLC spectrum is the chosen operational frequency spectrum for the NB-PLC transceiver. This band is the most susceptible to noise impairment amidst the stipulated CENELEC NB-PLC spectrum. Power electronic end-user appliances connected across the network are the major cause of noise impairments which results to burst errors inhibiting reliable data transmission.

The NB-PLC transceiver were thus utilized at two urban locations, the in-home *residential* and *laboratory* environment in Johannesburg, South Africa. These two in-home environments are both radially wired but differ with regards to the number of multi-paths and the number of un-coordinated end-user power electronic devices operated on the network. Therefore, these distinguishing factors impacts and determines the level and severity of noise, perturbation, disturbances, fading and attenuation experienced in both environment. Power electronics devices available on the residential in-home environment include: incandescent

lamps, electric cooker, electric kettle, washing machine, TV, pressing iron, shaving machine, microwave and geyser. In the in-home laboratory environment, equipment such as: oscilloscope, spectrum analyzer, function generator, table power supply, tower computers with monitor, air conditioning unit, soldering Irons and switch mode power supplies are present on the network.

Two distinct measurement scenarios were considered at the two urban locations namely: the "mildly disturbed" and "heavily disturbed" scenarios as defined in Section 7.4. Note also that some of the interfering end-user appliances were positioned close to the transceiver during the "heavily disturbed" scenario, hence more disturbance were recorded. This is because, in real life communication, the closer the interferers are to the receiver, the more severe the interference level and consequently more received data are corrupted.

4.5 Gigabit Ethernet Cable

The gigabit Ethernet cable is used to connect the host TX and RX computers to the TX and RX USRP2 modules respectively. Both the host computers and the USRP modules have gigabit Ethernet cards which are configured with a static IP address in order to interact with each other. It should be noted that the USRP modules exclusively functions with a 1000 megabits per second ($10^9 bits/s$) network adapters. The Cat 5E Ethernet cable was utilized in connecting the USRP2 modules to their corresponding host computers. This cable is able to handle 1000 Mbps of data speed from the computer's Ethernet controller and is capable of handling full-duplex operation.

4.6 Matlab/Simulink

The hardware part of SDR systems are completed by the USRP modules and the host computers, but for the purpose of interoperability, compatible software packages such as Matlab Simulink, LabVIEW and GNU's Not UNIX (GNU) radio must be installed on the host computers in order to control the USRP modules. The MathWorks Matrix laboratory (MATLAB) offers the Simulink, digital signal processing and communications systems toolbox support package for the USRP modules. These packages utilize the universal hardware

driver (UHD), the only supported USRP driver that allows the interaction between USRPs and Matlab/Simulink. The UHD enables the USRP to transmit and receive. The Matlab environment consists of wrapper functions for the UHD commands such that the USRP can be easily controlled. Preparation of codes and creating of the baseband signal to be transmitted as well as digital signal processing (including both pre-processing and post-processing) of the complex baseband signals is carried out in Matlab on the corresponding host TX and RX computers. Other supporting functions of Matlab and Simulink toolboxes include: setting and configuration of the TX and RX parameters such as frequency range, sampling frequency, sampling rate, gain, decimation and interpolation. Matlab version R2012b (8.0.0.783) is utilized in this project.

4.7 Hardware and Software Setup and Configuration

This Section gives a step-by-step guide on setting up of the hardware and software components of the transceiver in order to ensure that the TX and RX USRP modules are correctly interfaced with the Matlab. After the correct daughterboard LFTX and LFRX is installed on both the TX and RX USRP modules respectively, the following three steps were carried out: First, the installation of the Matlab/Simulink support package for USRP on the host computers, followed by configuration of the gigabit Ethernet card on the host computers and finally the loading of the correct and compatible firmware and FPGA images onto the TX and RX USRP hardware modules.

4.7.1 Hardware Setup

First and foremost, the correct network adapter is installed on both the host TX and RX computers. This is to facilitate a fast transfer rate of communication between the host computers and the TX and RX USRP2 modules and also because the USRP2 and the USRP2x10 modules exclusively functions with a 1000 megabits per second (Mbps) network adapters. It is vital to also connect the host computers to the USRP2 modules with the appropriate gigabit Ethernet cables that can handle the bandwidth in use.

A compatible daughterboard capable of operating in the NB-PLC frequency spectrum considered in this research is chosen and installed onto both the TX and RX USRP2 modules. The

choice of daughterboard corresponding and working in the NB-PLC operating frequency chosen for this research is the LFTX and LFRX daughterboard operating in the DC-30 MHz frequency spectrum.

Another important hardware that needs to be properly configured is the TX and RX coupling circuits. The coupling circuits are designed to operate within specified NB-PLC frequencies. Tests are carried out to ascertain the transfer function of the couplers and also ensure that the coupling circuit provides galvanic isolation and prevent excessive AC mains voltage from damaging the sensitive USRP modules.

4.7.2 Gigabit Ethernet Card Configuration

A dedicated gigabit Ethernet network card is required for the USRP2 hardware module. If the need for internet access is required, a second gigabit Ethernet network card should be installed on the host computers. The following tasks are performed in order to configure the Ethernet card for the USRP2 TX and RX modules.

- Navigate to "Control Panel" from the windows operating system through the windows icon on the lower left-hand side of the host TX and RX computer monitor.
- From the list of Control Panel items, navigate and select the "Network and Sharing Center" and then click on "Change adapter settings" located on the left-hand sidebar.
- Select the correct network device from the list of the network connection adapters, in this case the local area connection representing the gigabit network connection adapter. And then right-click and click on "properties" at the lower part of the local area connection status interface.
- Under the "Networking" tab, navigate and click on the "Internet Protocol Version 4 (TCP/IPv4)" under the "this connection uses the following items:" list and check the "Use the following IP address" option.
- Set the IP address to the following static IPs: 192.168.30.1 and 192.168.10.1 for the host TX and RX computer respectively. A click on the subnet mask box automatically sets it to 255.255.255.0 for both TX and RX computer. Click "ok" to save and

exit. Note that the TX and RX host IP addresses are configured based on the TX and RX USRP module IP addresses preconfigured as 192.168.30.2 and 192.168.10.2 respectively, but can also be changed using the NI-USRP configuration utility software.

4.7.3 Installation of USRP Support Package

- Visit http://www.mathworks.com/discovery/sdr/usrp.html to download the USRP communication systems toolbox supporting package.
- Click on get support package and then click on download hardware support package on the subsequent web page. This downloads an installer file for the USRP communication systems toolbox supporting package.
- Open the .mlpkginstall installation file via your host computer operating system or from inside the Matlab environment prompting an installation procedure to be initiated for acquiring the latest hardware support package obtainable for the release you possess. Note that the .mlpkginstall installer file is only compatible and operational for Matlab version R2013a and other version beyond.
- After a complete installation, typing "help sdru" from within the Matlab user interface gives information on the use of the communication toolbox package with the USRP module.
- For subsequent Matlab sessions, it is highly recommended to run setupsdru in order to utilize the communication toolbox with the USRP2 modules. Automation of this step is also possible by adding setupsdru to the startup.m Matlab file or otherwise a manual setting will involve using the "Add sdru" provided on the shortcut bar of Matlab.

4.7.4 Firmware and FPGA Images Loading onto the USRP2

The USRP2 firmware and FPGA images are loaded onto the SD card plugged into the SD card slot of the USRP modules. Due to compatibility issues with the use of some third-party SD card, it is recommended that the SD card shipped with the USRP modules be

utilized. In order to update the firmware and FPGA images of the USRP2 modules an SD card interface having read and write capability is required. Note that you do not format the disk if prompted by the SD card interface to do so. Find as follows procedural steps to update the USRP2 firmware and FPGA images [166].

- Download and install NI-USRP configuration utility version 1.2 from [166].
- Remove the SD card from the SD card slot of the USRP2 and insert into the SD card interface of the computer.
- Navigate to and open the installed NI-USRP configuration utility under programs. Choose the USRP2 SD Card Burner tab and this would spontaneously populate the firmware image and FPGA image environments with the default firmware and FPGA image file paths. For a different version of firmware and FPGA images, browse and navigate to the appropriate firmware and FPGA images file you are required to use, in this case usrp2 fw (003.002.003) and usrp2 fpga (003.002.003) respectively.
- Confirm that the correct firmware and FPGA image paths are chosen as both images are loaded the same time.
- Refresh device list and choose the correct drive name that matches the SD card inserted into the SD card interface.
- Click on the "WRITE IMAGES" tab to load the images onto the SD card and a status update is shown via a progress bar and once the firmware and FPGA images are completely loaded onto the SD card, a dialog box is shown to this effect.
- Close the NI-USRP utility interface and remove the SD card from the computer SD card interface to be returned and slotted onto the USRP2 modules. To verify that the firmware and FPGA images are successfully loaded, power on the USRP2 device and a lit LED indicator D shows a successful update.

4.8 The NB-PLC Transceiver System Testbed

In this section, the aim is to describe the NB-PLC transceiver systems implemented as a testbed for real time transmission and as a tool for modeling the NB-PLC channel in this

project. First, the hardware architecture of the reconfigurable software-defined transceiver system is shown, followed by the photograph of the overall NB-PLC transceiver system testbed. A simplified but holistic system model of the developed single-carrier and multi-carrier transceiver systems is further presented in subsequent sections.

Pairing of a USRP with an appropriate host computer produces a complete software-defined system. The USRP motherboards utilize high processing power to carry the following task in the FPGA: amplification, up-conversion and down-conversion, decimation and interpolation operation with slight knowledge about the signal. The daughterboard is tasked with modulation and filtering while all DSP and waveform-specific operation are performed on the host computers, thus enabling high diversity of transmission system using the same hardware [161, 162].

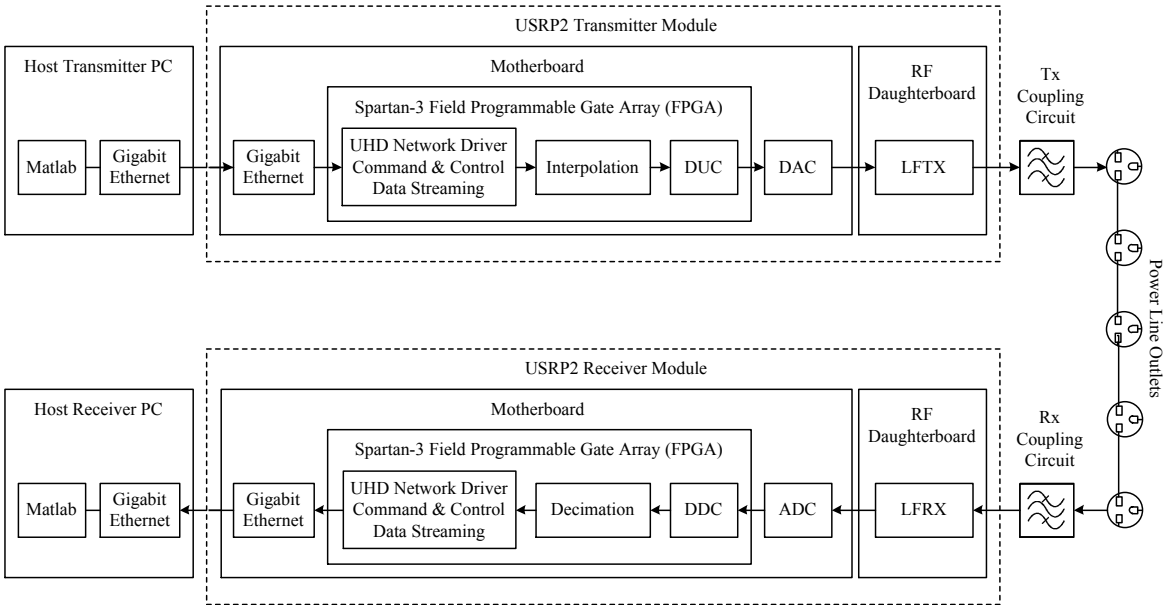

FIGURE 4.4: The hardware architecture of the NB-PLC transceiver system.

Figure 4.4 shows the hardware architecture of the software-defined NB-PLC transceiver system and an elaborate view of how the entire unit is integrated to function together as a system.

The USRP2 module communicates with the transmitter and receiver PC via the gigabit Ethernet control port as shown on the left-hand side of Figure 4.4. Baseband signal processing tasks are performed on the Matlab application installed on both the host transmitter and receiver PC workstation. The USRP2 transmitter and receiver module and its LFTX and LFRX daughterboards adopted are shown in the dotted blocks of Figure 4.4. The USRP2

contains a Xilinx Spartan-3 XC3S2000-4 FPGA, on which interpolation and digital up-conversion task are performed on the transmitter side, while digital down-conversion and decimation task are performed on the receiver side. This Xilinx Spartan-3 FPGA interfaces with the digital-analog-converter (DAC) chip for the digital to analog conversion of the signal on the transmitter side, and likewise interfaces with the analog-to-digital converter (ADC) chip for the analog to digital conversion of the signal at 100 MHz (for the DAC 400 MSps is often written as interpolation is automatically carried out by a factor of four). On the right-hand side, the modulated signal is coupled onto and received through the PLC channel via the transmit and receive coupling interface respectively.

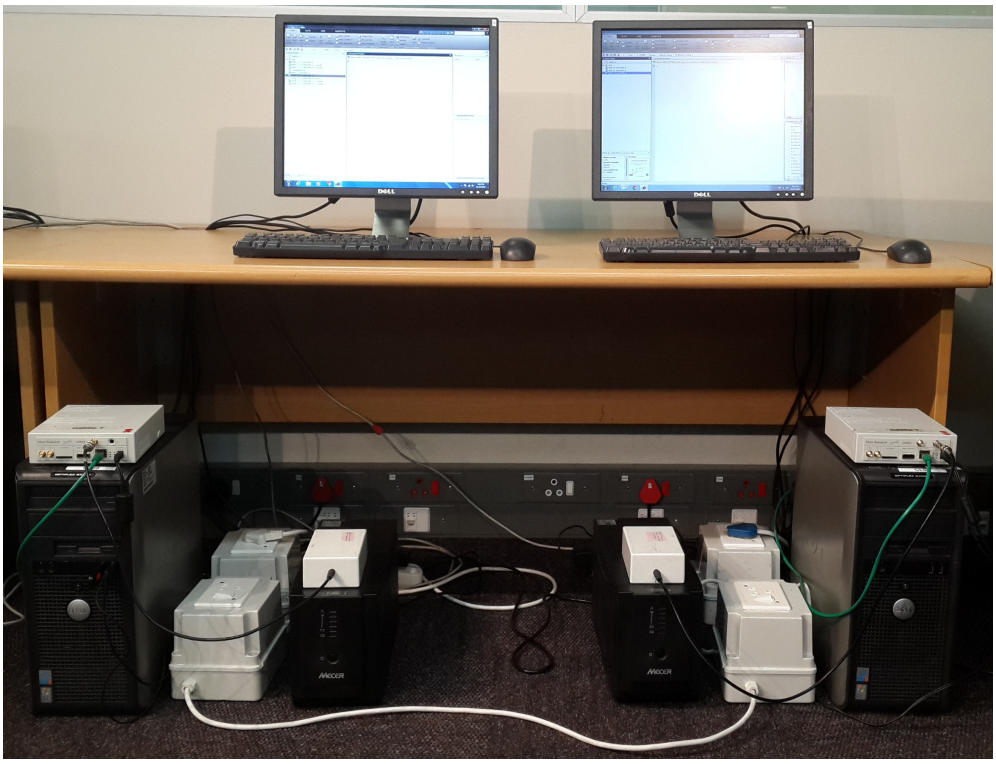

FIGURE 4.5: Photograph of the overall NB-PLC transceiver system testbed

Figure 4.5 depicts the overall NB-PLC transceiver testbed. The host transmitter and receiver PCs, the USRP2 transmitter and receiver modules, the transmitter and receiver coupling interfaces and the PLC outlets are all shown as units constituting the overall NB-PLC transceiver testbed.

Two dedicated uninterrupted power supply (UPS) are being used to power both the host PCs and the USRP modules as shown in Figure 4.5. The RF output of the USRP2 module configured as transmitter on the left-hand side is connected to the corresponding transmitter

coupling circuit via which the transmitted signal is injected onto the PLC channel. Similarly, the RF input of the USRP2 module configured as receiver on the right-hand side is connected to the corresponding receiver coupling circuit via which the transmitted signal is received from the power line and coupled to the RF input port of the receiving USRP2 module for baseband processing, and subsequently sent to the host receiver PC through the gigabit Ethernet port for further baseband signal post-processing.

4.8.1 Single-Carrier NB-PLC Transceiver System

A single-carrier un-coded NB-PLC transceiver system is implemented using the following digital modulation schemes, BPSK, DBPSK, QPSK and DQPSK for real time signal transmission.Figure 4.6 shows the system model for the single-carrier NB-PLC transceiver.

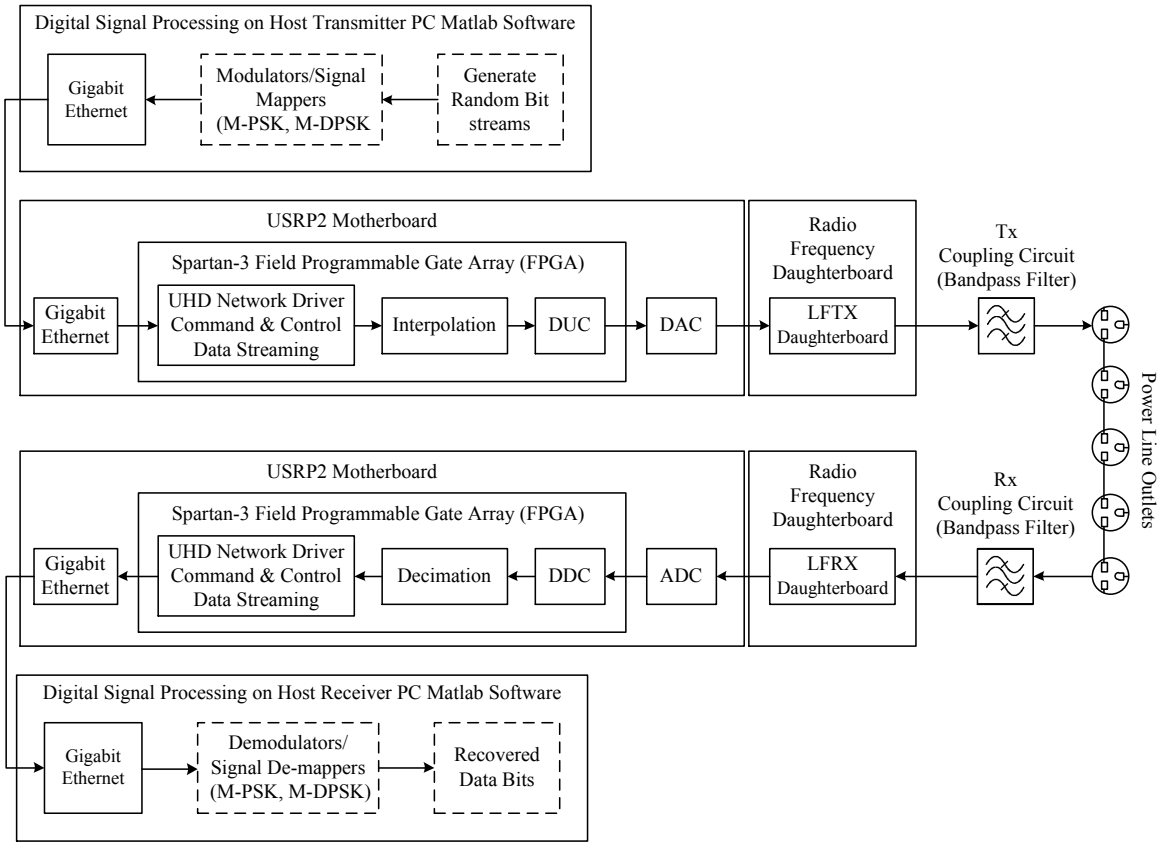

FIGURE 4.6: The single-carrier NB-PLC transceiver system.

The DBPSK and the DQPSK are more or less similar to the conventional BPSK and QPSK respectively, except that, for every successive baseband symbol, the differentially encoded

symbol for DBPSK and DQPSK is derived based on the current and on the previously mapped or encoded symbol. Note that henceforth, communication elements with dotted blocks lines are implemented in software, while elements with solid block line are hardware-based implementation.

In the BPSK and QPSK systems, the input signal are modulated and mapped onto the constellation points of the BPSK and QPSK using the BPSK and QPSK modulator or signal mapper respectively. In the DBPSK and DQPSK systems, the input signal are first differentially encoded before being modulated and mapped onto the BPSK and QPSK constellation points using the BPSK and QPSK modulator or signal mapper respectively.

At the transmitting side, the transmit USRP receives the pre-processed modulated signal from the host transmitter PC via the gigabit Ethernet interface after which it is stored in a buffer for baseband processing. The samples are then interpolated, up-sampled and then modulated to the IF from the buffer by sine and cosine or cosine wave for complex samples and real samples respectively. In essence, the digital up-converter translates the digital complex baseband signal to real digital passband signal [167]. The yet to be up-converted complex baseband input signal is normally sampled at a comparatively lower sampling rate. Thus, the complex baseband signal is filtered and translated at a much higher sampling rate subsequent to being modulated onto a direct digitally synthesized (DDS) carrier frequency. The digital up-converter executes pulse shaping task on the incoming signal as well as modulating to an appropriate intermediate carrier frequency suitable for driving a final analog up-converter [167]. The DAC finally converts the digital signal into analog format than can transmitted on the PLC channel before sending it to the LFTX daughterboard. The USRP LFTX daughterboard manages the modulation of the TX streams from the IF to the NB-PLC operating transmit frequency. The resultant continuous analog signal is then coupled onto the voltage waveform of the PLC channel via the TX capacitive coupling interface.

At the receiving side, the transmitted signal is received and decoupled via the RX capacitive coupling interface after which it is passed to the USRP module through the LFRX daughterboard. The LFRX daughterboard filters and modulate the received analog signals (RX streams) from the operating RX frequency to the intermediate frequency by first sampling and then multiplying with a discrete time sine and cosine or cosine wave for complex samples

and real samples respectively [161]. Subsequently, the ADC converts the signal from analog to digital bit for baseband processing. The resultant digital signal is further filtered by the DDC and decimated in order to obliterate the dual frequency parts and reduce the sample rate. The resultant baseband signal samples are then stored in a buffer and sent to the host receiver PC through the gigabit Ethernet interface for baseband signal post-processing task [167]. Finally, the baseband signals are demodulated by demodulators or signal de-mappers corresponding to the modulator used at the transmitter and then the original transmitted signal is recovered correctly in the absence of channel or noise impairments.

4.8.2 OFDM NB-PLC Transceiver System

The OFDM system utilizes the conventional M-ary PSK (M-PSK) and Differential-MPSK (D-MPSK) single-carrier modulators for its signal mapping. Figure 4.7 shows the developed multi-carrier OFDM NB-PLC transceiver system and its respective transmitter and receiver communication elements.

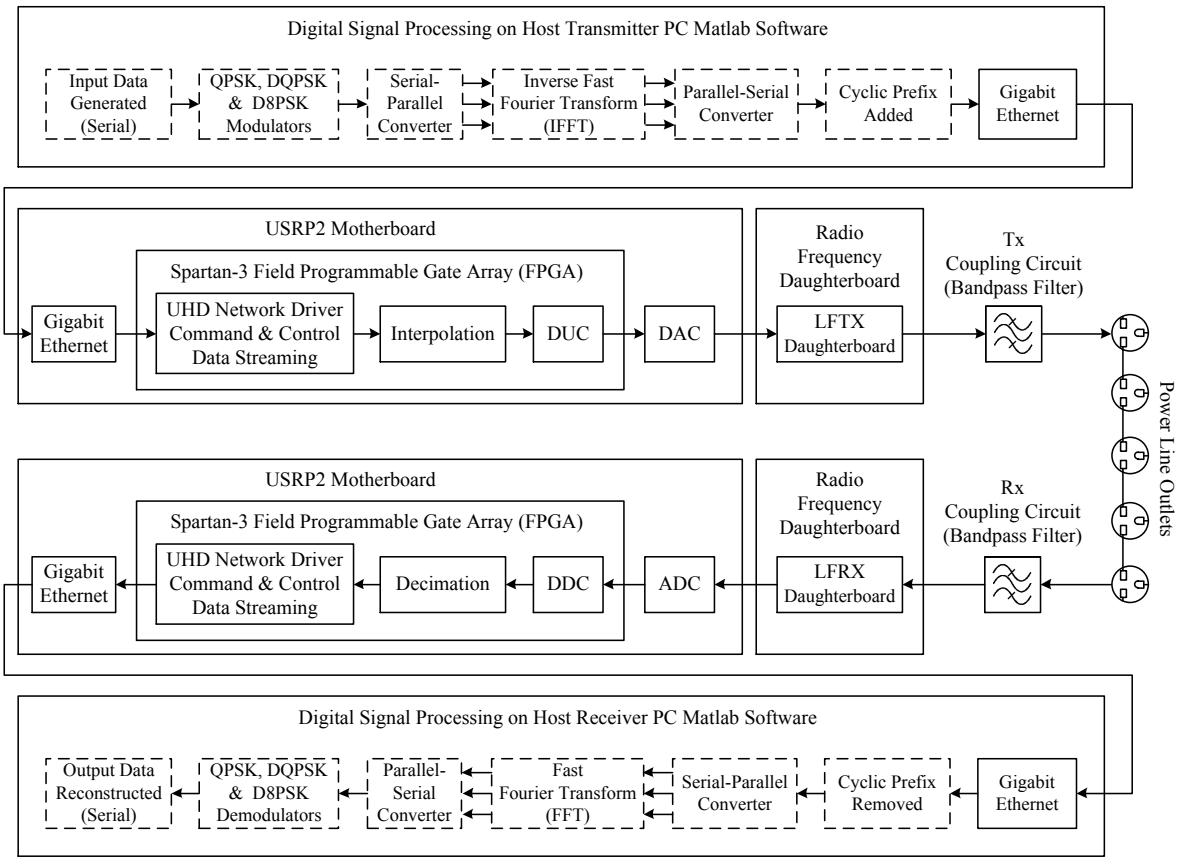

FIGURE 4.7: The multi-carrier OFDM NB-PLC transceiver system.

The serial input data stream generated is first mapped by the modulator/signal mapper onto the constellation symbol of the chosen modulator. The chosen modulation (e.g. M-PSK, M-DPSK and M-QAM) is influenced by the number of bits designated to the signal mapper.

In an M-PSK OFDM system (such as QPSK-OFDM), the serial input signal is directly modulated and mapped onto the QPSK modulator/signal mapper's constellation points, while on the other hand, in D-MPSK OFDM systems (such as DQPSK and D8PSK-OFDM), the serial input signal is first differentially encoded before being modulated and mapped onto either the QPSK or 8PSK modulator/signal mapper's constellation points in frequency domain.

The output of the modulator/signal mapper are a set of complex baseband symbols further de-multiplexed by the serial-to-parallel converter, resulting into parallel streams of complex baseband symbols. A modulation of the complex number in the baseband is subsequently carried out by the IFFT block. The resulting samples produced by the IFFT block typify the OFDM symbol that is a time domain depiction of all the multiplexed symbols. In essence, the IFFT block converts N modulated sub-carriers into an equivalent sampled time domain signal for transmission on the PLC channel. The equivalent time domain OFDM symbols are multiplexed by the parallel-to-serial converter, resulting into serial data stream. A guard interval in the form of cyclic prefix is then added to the time domain OFDM signal by appending a copy, typically 10% - 25% of the last few samples to the beginning of the OFDM symbol as illustrated in Figure 4.8, in order to combat ISI, the effect of multipath delays.

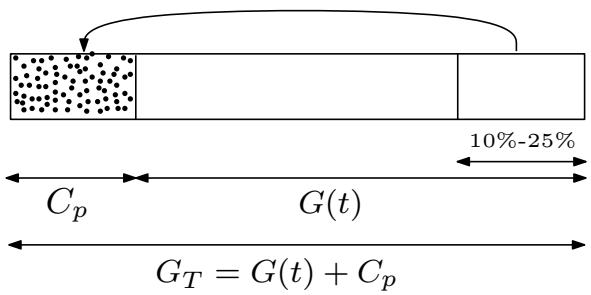

FIGURE 4.8: Cyclic prefix addition to $G(t)$ time domain OFDM signal.

The discrete output waveform is received from the host transmitter PC by the transmitting USRP via the gigabit Ethernet interface, where it is stored in a buffer for further

baseband processing. The samples are interpolated and digitally up-converted. The digital up-converter (DUC) translates the digital complex baseband signal to real digital passband signal. The resultant passband signal is then converted to time domain analog signal by the DAC block. In essence, the DAC block converts the discrete output waveform into continuous time domain waveform. The USRP LFTX daughterboard manages the modulation of the TX streams from the IF to the NB-PLC operating transmit frequency. The continuous time domain waveform or analog signal is then coupled onto the voltage waveform of the PLC channel via the transmitter capacitive coupling interface after which, it is continuously transmitted over the time-varying frequency-selective PLC channel.

At the receiver, the transmitted signal is received and decoupled onto the receiving USRP via the receiver capacitive coupling interface. The LFRX daughterboard filters and modulates the received analog signals (RX streams) from the operating RX frequency to the intermediate frequency. The received data, a continuous time domain analog signal is sampled and transformed back into digital or discrete samples by the ADC block. The resultant digital signal is further filtered by the digital down-converter (DDC) and decimated in order to obliterate the dual frequency parts and reduce the sample rate. The resultant baseband signal samples are then stored in a buffer and sent to the host receiver PC through the gigabit Ethernet interface for baseband signal post-processing task [167]. The cyclic prefix is subsequently removed from the received time domain OFDM signal as shown in Figure 4.9.

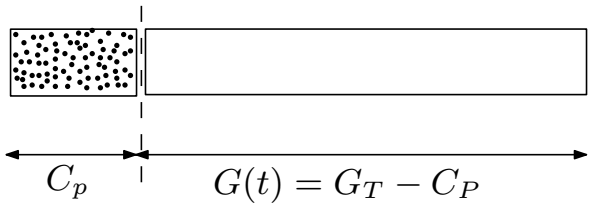

FIGURE 4.9: Cyclic prefix removal from G_T time domain OFDM signal.

The serial data stream is further de-multiplexed by the serial-to-parallel converter in order for individual frames to be formed from the buffered samples. Furthermore, the transmitted frequency domain information are extracted by the FFT block from the OFDM frame before a multiplexing is carried out by the parallel-to-serial converter. The resulting frequency domain serial data stream is finally passed through the symbol demodulation or de-mapping stage. The demodulator or symbol de-mapper estimates the transmitted symbol from a set of known symbols and yields the respective bit pattern e.g. QPSK-2 bit pattern, BPSK-1 bit pattern and 8PSK-3 bit pattern. The estimated serial data stream obtained from the

demodulator or signal de-mapper is a reconstruction of the transmitted signal and in practice often contains errors introduced by noise impairments or channel irregularities.

4.9 Modeling Methodology/Approach

In this section, a holistic view of the modeling methodology/approach adopted in this project is presented. First, a discussion of how the SHFMM parameters are initialized is presented, followed by a holistic view of how the parameters of the SHFMM are re-estimated and trained using BWA in order to obtain the most probable SHFMM parameter sets that depict the empirical error sequences obtained from both the single-carrier and NB-PLC OFDM systems taking into consideration the mildly and heavily disturbed noise scenarios and the two measurement sites considered.

4.9.1 SHFMM Parameterization

The state cross-over probabilities for a First-Order and Second-Order SHFMM denoted by A_1 and A_2 is presented in Section 3.3.2 and Section 3.3.3 respectively.

Three approaches exist in literature for initializing the model parameters: the count-based initial model, random initial model and uniform initial model. The random initialization approach frequently used in literature is adopted in this project. The elements of A_1 are randomly and uniquely chosen for this application such that probability of crossover to an error-free state denoted by the matrix elements a_{11}, a_{22}, a_{31} and a_{32} is high, while the crossover probability to an error state denoted by the matrix elements a_{13}, a_{23} and a_{33} is low in order to depict the empirical data (error sequence).

Similarly, elements of A_2 are randomly and uniquely chosen for this application such that probability of crossover to an error-free state denoted by the matrix elements a_{111}, a_{122}, a_{131}, a_{132}, a_{211}, a_{222}, a_{231}, a_{232}, a_{311}, a_{322}, a_{331}, a_{332} is high, while the crossover probability to an error state denoted by the matrix elements a_{113}, a_{123}, a_{133}, a_{213}, a_{223}, $a_{23,3}$, $a_{31,3}$, $a_{32,3}$ and $a_{33,3}$ is low in order to depict the observed data. The error symbol probability B is in binary format due to the uniqueness of the SHFMM model adopted as depicted in Equation (3.19)

and Equation (3.22). The prior state probabilities denoted by Π is also uniquely chosen with lower error probability for state three, the error state to depict the empirical error sequence.

Furthermore, in order to determine the number of assumed initial state crossover probabilities to be randomly generated as input to the Baum-Welch algorithm, first, the value of the crossover probabilities in A_1 are categorized into three (3) main classes: high (0.8), mid (0.5) and low probability (0.3). Second, we check the First-Order SHFMM state crossover probability matrix A_1 and determine the number of state cross-over probability elements that are involved in generating A_1. From Equation (4.4), it can be seen that four (4) matrix elements: a_{11}, a_{22}, a_{31} and a_{32} are the main matrix elements involved in generating A_1, as other elements a_{13}, a_{23} and a_{33} are obtained through subtraction. Thus the number of assumed initial state crossover probabilities is $3^4 = 81$. This invariably implies that 81 SHFMM parameters are randomly obtained for each empirical error sequence from which the most probable is chosen after training with the Baum-Welch algorithm.

$$A_1 = \begin{bmatrix} a_{11} & 0 & a_{13} \\ 0 & a_{22} & a_{23} \\ a_{31} & a_{32} & a_{33} \end{bmatrix} = \begin{bmatrix} a_{11} & 0 & 1 - a_{11} \\ 0 & a_{22} & 1 - a_{22} \\ a_{31} & a_{32} & 1 - a_{31} - a_{32} \end{bmatrix} \tag{4.4}$$

4.9.2 Modeling Methodology

In this project, SHFMM is implemented to model the empirical burst error sequence produced in the NB-PLC channel for a multi-carrier OFDM system as shown in Figure 4.10. Note, that Figure 4.10 also applies to the modeling of the empirical burst error sequence produced by the single-carrier NB-PLC system also adopted in this project.

The process of modeling the empirical burst error sequence as depicted in Figure 4.10 are thus enumerated as follows.

1. The empirical error sequences are obtained based on the comparison between the transmitted and the received bit streams for both single-carrier and multi-carrier OFDM NB-PLC systems, under the influence of additive, impulse, narrowband and background noise as well as multipath frequency selective fading.

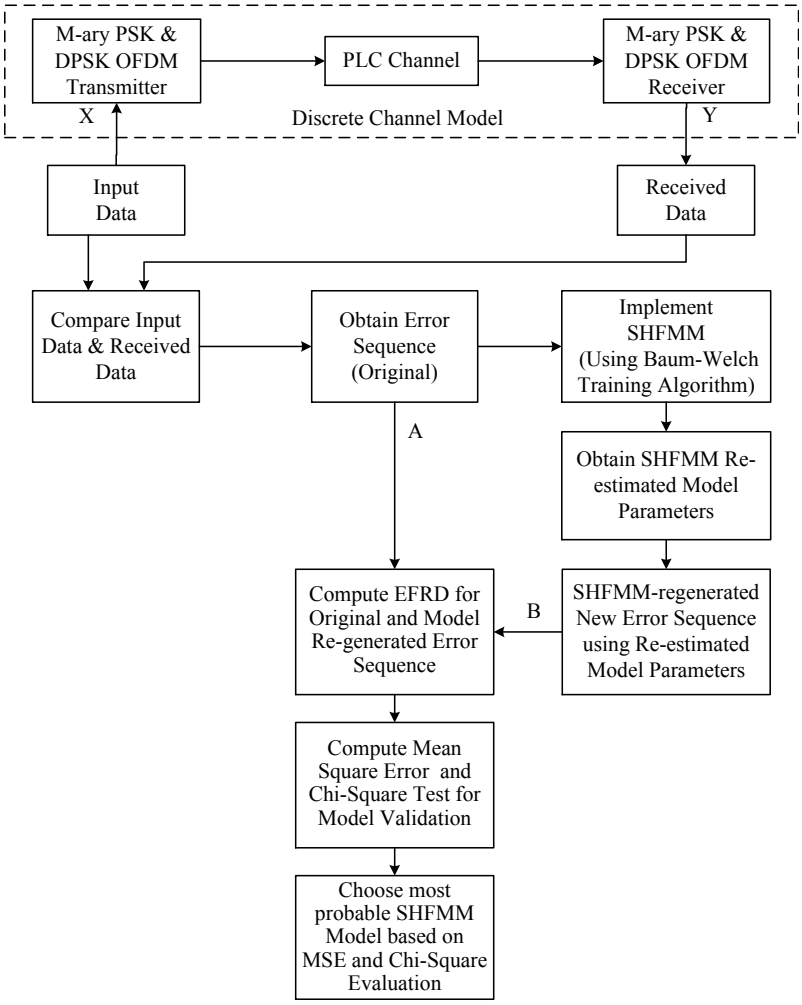

FIGURE 4.10: Block diagram of SHFMM parameter estimation for the NB-PLC OFDM system.

2. Eighty-one (81) initial SHFMM parameters are randomly assumed for each empirical error sequence (training data) as input to the Baum-Welch algorithm. The Baum-Welch algorithm is implemented and used to re-estimate the 81 SHFMM parameters using the forward and backward path probabilities as illustrated in Section 3.4.3 of Chapter 3 in order to obtain parameter set that better fits the empirical error sequence.

3. The 81 SHFMM re-estimated parameters are used to generate 81 new error sequences having the same length as the original empirical error sequence.

4. The error-free run distribution (EFRD) denoted by $\Pr(0^m|1)$ is then computed for both the original empirical error sequence and the 81 newly regenerated error sequences. Note that the EFRD ($Pr(0^m|1)$) is a monotonically decreasing function of m in such a way that $Pr(0^0|1) = 1$ and $Pr(0^m|1) \to 0$, which implies that it consistently

decreases and never increases in value as would be observed at the model analysis stage [168].

5. Compute the Mean Square Error (MSE) and Chi-Square χ^2 for each of the 81 obtained EFRD with respect to the EFRD of the original empirical error sequence. Where the EFRD for the original empirical error sequence is the observed data, while the EFRD for the 81 newly regenerated error sequences is the expected data.

   Apart from the popular error-free run distribution (EFRD) metric used in validating the accuracy of SHFMM, the Mean Square Error (MSE) and the Chi-Square (χ^2) test are another popular metrics used to carry out the fitness or accuracy check of SHFMMs in order to ascertain the closeness between the measured original empirical error sequences and the SHFMM statistically re-generated error sequences. The values of χ^2 and MSE are invariably non-negative, with values closer to zero indicating a better fitting model (indicating close agreement between empirical error sequence and model re-generated error sequence), hence, the estimated SHFMM with the best (smallest) χ^2 and MSE values is chosen to have produced the empirical error sequence (observed data). Find as follows the mathematical expression for computing MSE and χ^2 values.

$$MSE = \frac{\sum_{i=1}^{N}(O_i - E_i)^2}{N} \tag{4.5}$$

$$\chi^2 = \sum_{i=1}^{N}\left[\frac{(O_i - E_i)^2}{E_i}\right] \tag{4.6}$$

   Where O_i is the observed EFRD, in other words, the EFRD for the original empirical error sequence, while E_i is the expected EFRD, in other words, the EFRD of the SHFMM regenerated error sequence and N denotes the length of the EFRD, which is the same for both observed and expected EFRD.

6. The most probable SHFMM given the original empirical error sequence is chosen amongst the 81 SHFMM, based on the use of MSE and Chi-Square χ^2 values to validate the most probable model that depicts each empirical error sequence.

Note that the computation of the recursive forward probability function (α) and backward probability function (β) requires the order of N^2T operations for the First-Order compared

to the order of (N^3T) operations for the Second-Order estimation as shown in Table 4.1, where N is the number of model states, T is the length of the experimentally obtained error sequences. Consequently, the overall computational complexity for both the First and the Second-Order SHFMM parameters using the Baum-Welch algorithm is shown in Table 4.2, where O is the experimentally obtained error sequences. This implies that a First-Order SHFMM and a Second-order SHFMM requires $O(N^2T)$ and $O(N^3T)$ time respectively in computing the probability of the experimentally obtained sequence given the model. Hence, there is a trade-off in terms of computational complexity, as training of a Second-Order model is more computationally intensive than training it's First-Order counterpart.

TABLE 4.1: Computational complexity comparison of the recursive forward probability function (α) and backward probability function (β)

First-Order SHFMM	Second-Order SHFMM
N^2T	N^3T

TABLE 4.2: Overall time computational complexity comparison between First-Order and Second-Order SHFMM parameter estimation

First-Order SHFMM	Second-Order SHFMM
$O(N^2T)$	$O(N^3T)$

CHAPTER 5

Narrowband PLC Channel Modeling using USRP and PSK Modulations

The indoor narrowband power line communication (NB-PLC) suffers from noise impairments, which emanate from several end-user electrical devices connected across the PLC channel. These noise impairments result into burst errors, which consequently lead to data corruption. Therefore, in order to implement robust communication techniques that will thrive on the noisy PLC channel, a full knowledge and modeling of the noise that exists on the NB-PLC channel is inevitable. This Chapter thus reports a First-order Markov modeling of NB-PLC channel noise, based on experimental measurements. For the modeling, BPSK, DBPSK, QPSK and DQPSK modulation schemes were implemented using Universal Software Radio Peripheral (USRP). The resulting channel models are useful for improving the robustness of the above modulation schemes as well as designing forward error correction techniques for mitigating the effect of noise impairments. The results are also useful in optimizing NB-PLC system design, thereby, enhancing the accuracy and improving the overall PLC system performance.

5.1 Introduction

PLC technology utilizes the ubiquitous network of existing power lines that are universally accessible in almost every room in homes and offices across the globe for data communication purposes. The low-voltage in-house CENELEC A-band is one of the sub-bands of the four classified European CENELEC standard with frequency bandwidth between 3-95 kHz for narrowband applications [1]. The power line network was originally meant for electrical energy distribution to end-user devices. Its recent use as a medium of data communication inherits the harsh intrinsic attributes of power line accompanied by noise and disturbances that originate from un-coordinated use of end-user electrical devices connected onto the network. External noise sources such as broadcast stations and other devices sharing the

same frequency as the PLC modulating frequency also introduce noise and disturbances onto the network. Thus, the CENELEC A-band is plagued with a lot of noise impairments, which result in burst errors that can corrupt the transmitted data, thereby, making reliable data communication almost impossible. To achieve a reliable communication as well as mitigate the performance degradation caused by the effect of noise impairments on the channel, modeling of the channel is vital.

In modeling other communication channels such as wireless, twisted pair, co-axial cables, an Additive White Gaussian Noise (AWGN) is usually assumed. However, such is not the case for PLC channel in general. The attributes of the noise existing on the NB-PLC channel are characterized and modeled as non-white, non-Gaussian and unstable. Therefore, this work is motivated by the need to model NB-PLC noise and disturbances, by using USRP to implement the modulation schemes specified in the NB-PLC standards. The USRP is a computer-hosted software defined radio designed by Ettus Research.

The two NB-PLC narrowband standards (i.e. PLC G3 and PRIME) have suggested Phase-Shift Keying (PSK) as the OFDM component in their specifications [10]. As such, this work has chosen to implement M-ary Phase-Shift Keying (M-PSK) and M-ary Differential Phase-Shift Keying (M-DPSK).

In this work, Binary Phase Shift Keying (BPSK), Differential BPSK (DBPSK), Quadrature Phase Shift Keying (QPSK) and Differential QPSK (DQPSK) were implemented to be used for first-order Markov modeling of NB-PLC channel, using USRP. A single-error state first-order Fritchman model is used in this work. The resulting models for each modulation schemes were analyzed and hereby presented in this Chapter. These can be employed to improve the robustness of modulation schemes and, in addition, used to design forward error correction techniques for mitigating the effect of noise impairments on NB-PLC channels. Furthermore, the results can be used to optimize NB-PLC system design, thus enhancing PLC systems' overall performance.

The remaining part of this Chapter is structured thus. In Section 5.2, a concise discussion of the following is presented: PLC noise classifications, PSK modulation schemes, Fritchman model and Baum-Welch algorithm. A detailed discussion of the experimental setup and methodology is done in Section 5.3. In Section 5.4, a statistical analysis of the modeling results is carried out under the following headings: error sequence generation, estimated state

transition matrix, log-likelihood ratio plots, and error-free run distribution plots. Finally, Section 5.5 concludes the Chapter.

5.2 Background

5.2.1 PLC Noise Classification

The noise associated with the PLC channel has been classified into background noise, impulsive noise and frequency disturbance (or narrowband noise) [79, 169, 170].

Background noise results from various sources of low power noise, which are usually household devices like computers, hair dryers and light dimmers. This noise category has an increasing effect, as the frequency of transmission reduces and vice versa.

Frequency disturbance, otherwise known as narrowband noise (NBN), is caused by interference from foreign signals in the spectrum of interest. The amplitude of this class of noise is usually time dependent, and it only dominates a narrow portion of the spectrum of interest [79]. As demonstrated in [79], NBN can be expressed as modulated sinusoidal signals, whose amplitude is coupled to the network. This noise class majorly originates from TV vertical scanning frequency and harmonics, AM transmissions and amateur radio connected to the same network as the transmitter [5].

Impulsive noise is a noise with flat PSD (power spectral density) which can affect all frequency components at a particular duration [171].

5.2.2 PSK Modulation Scheme

PSK is the process of encoding digital data bits onto an analogue form, by altering the phase of a sinusoidal carrier signal. It is possible to map more than one digital bit onto a sinusoidal carrier wave. Binary phase shift keying (BPSK) is the fundamental type of PSK, which maps only one bit of data onto the carrier, using two possible phases- bit 0 for 0 radian and bit 1 for π radians. Quadrature phase shift keying (QPSK) maps two bits onto a sinusoidal carrier phase, using four possible phases $-\pi/4$, $3\pi/4$, $5\pi/4$ and $7\pi/4$. As

described in [172], BPSK has one-dimensional constellation point ($N = 1$), having two equally spaced message points ($M = 2$) as the signal constellation. With QPSK, $N = 2$ and $M = 4$. As such, QPSK (or 4-PSK) is said to be a special case of M-ary PSK, in which the carrier phase has $M = 4$ possible values described by $2(i-1)\pi/M$, with i being $1, 2, \ldots, M$. In order to demodulate any PSK modulated symbol, a coherent reference signal is needed at the receiving end, for ensuring carrier recovery, which computes and equalizes phase and frequency imbalances between the received carrier wave and the local oscillator of the receiver. Symbol synchronization is achievable by using a suitable timing recovery algorithm.

DPSK is a non-coherent version of PSK modulation, which does not require coherent demodulation. However, to achieve symbol synchronization, there is need for timing recovery [173]. As such, it is relatively easy and cheap to implement DPSK receivers, as compared to those of ordinary PSK receivers. When a modulated DPSK symbol is received, it is more or less equivalent to a signal with unknown phase information, due to the way it is being modulated. Detailed information about M-PSK and M-DPSK modulation schemes can be accessed in any digital communication literature like [172], [173].

5.2.3 Fritchman Model

Hidden Markov models (HMMs), are usually utilized in several applications such as automatic speech recognition, digital signal processing, queuing theory, control theory, weather prediction, modeling of burst error channels, and a host of other interesting applications. Gilbert and Elliot [174], [175] proposed a HMM type regarded as the Gilbert-Elliot model. They assumed a two-state Markov model grouped into a good and a bad state, but this model does not depict the bursty nature of the NB-PLC channel. However, Fritchman, in [16], proposed a more advanced channel model which better depicts the actual long burst error nature of the NB-PLC channel.

For a binary channel, Fritchman grouped the state space into k good states and $N - k$ bad states. An error-free transmission occurs in a good state, while a bad state is characterized by a frequently occurring transmission error.

According to Vogler [176], a single-error state Fritchman model offers a fair compromise between the analytic intractability of sophistication and the non-realism of a two-state Markov model. Hence, a single-error state Fritchman model with two error-free states is assumed in this work as shown in Figure 5.1.

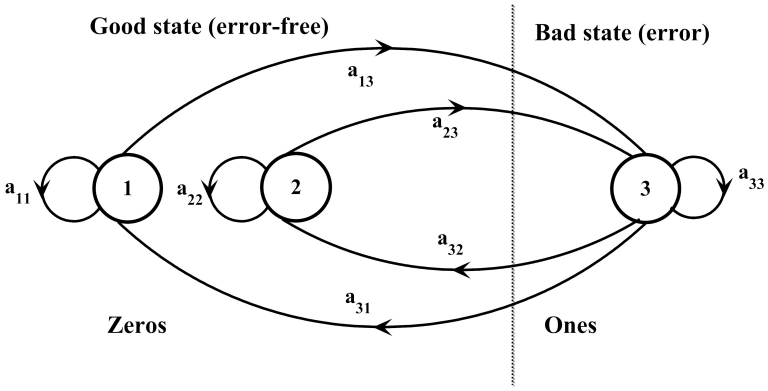

FIGURE 5.1: A three-state Fritchman Markov model.

In Figure 5.1, it is evident that for the three-state partitioned Fritchman model, transitions are not permissible between states of the same group. This implies the availability of multiple degrees of memory. Hence, modeling of real communication channels is made possible.

The assumption of a single-error state Fritchman model allows for the models error-free distribution $Pr(0^m|1)$ to distinctively indicate the single-error state. Hence, the model parameters are obtainable from the error-free run distributions and vice versa [177]. In general, the First-Order state transition probabilities, A_1 for Figure 5.1 can be expressed in matrix form as:

$$\mathbf{A_1} = \begin{bmatrix} a_{11} & 0 & a_{13} \\ 0 & a_{22} & a_{23} \\ a_{31} & a_{32} & a_{33} \end{bmatrix}, \quad \mathbf{B} = \begin{bmatrix} 1 & 1 & 0 \\ 0 & 0 & 1 \end{bmatrix}.$$

The values of elements a_{12} and a_{21} are zeros. This is due to the uniqueness of the Fritchman Markov chain chosen, based on the fact that transitions are not permissible between states of the same group. Hence, the output symbol probability matrix, B is expressed as shown above. The elements of the B matrix contains zeros and ones, because no transitions is allowed between states of the same group, hence an error only occurs in the bad state, while the good states are error-free. Therefore, the entries are not to be estimated [21]. The prior

or initial state probabilities is denoted by π and expressed as:

$$\mathbf{\Pi} = [\pi_1,\ \pi_2,\ \ \ldots, \pi_N].$$

where, N is the number of states which is three for this work.

5.2.4 Baum-Welch Algorithm

Baum-Welch algorithm [20, 21] is a method that uses the maximum likelihood estimation approach to estimate the model parameters, $\Gamma = (A_1, B, \Pi)$, such that the likelihood of the observed sequence $\bar{E}$ is maximized. The expectation maximization (EM) method is used to solve the maximum likelihood estimation problem. The EM approach is an iterative method that begins with an initial assumption of the model parameters, Γ and updates of these model parameters are carried out iteratively in such a manner that the likelihood does not decrease for each step. For detailed steps of how the model parameters are re-estimated, refer to Section 3.4.2.

5.3 Experimental Setup and Methodology

Figure 5.2 shows the architecture of the experimental setup involved in this work.

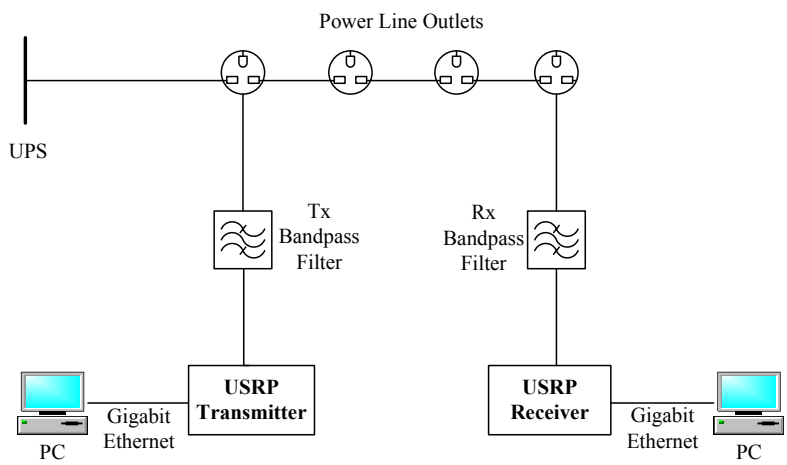

FIGURE 5.2: Block diagram of the experimental setup showing the end-to-end connection

The experiment was setup in the Convergence Laboratory at the University of the Witwatersrand, Johannesburg. Two distinct noise scenarios were considered: the mildly and the heavily disturbed scenarios.

The USRP hardware at the right hand side of the topology was configured as the transmitter, whose RF (radio frequency) output is connected to a PLC coupling circuit, and the receiving USRP sits at the left hand side of the topology. The two host PCs connected to the USRPs are equipped with a software (MATLAB), capable of some functionalities (like modulation, filtering and amplification, etc.), which are normally carried out by electronic components. This therefore provides flexibility in the system, and as well, gives room for experimenting some new concepts like forward error correction schemes (e.g., Permutation code [178]). The implementation is carried out in the MATLAB environment depending on whether the new concepts are based on modulation or forward error correction as shown in the transmitter and the receiver constituent block of Figure 2.2. The photograph of the transceiver testbed used to obtained empirical error sequence can be seen in Figure 4.5 showing the different hardware components of the transceiver system.

5.3.1 Host-based Software Description

The SDRU (Software Defined Radio uhd) Simulink Target and communication toolbox, developed by Mathworks, are the software components used in this work. The toolbox is equipped with some signal processing blocks, which can either be used directly or developed from scratch, depending on the user's application requirements. These blocks can be connected together to form the signal processing flow graph.

The SDRU Target contains two main boxes, which are either used as the signal sink (for the USRP TX) or source (for the USRP RX). The SDRU boxes are what are used to configure the hardware's parameters like the signal level, operating frequency, decimation and interpolation.

USRPs are loaded with FPGA and firmware images to provide compatibility with the software version to be used. Table 5.1 contains the important modulation and configuration parameters used in our implementation.

Table 5.1: Software configuration

PARAMETER	VALUE
Tx gain & Rx gain	Default (not tunable)
USRP Firmware revision	usrp2_fw (003.002.003)
USRP FPGA revision	usrp2_fpga (003.002.003)
Centre frequency	92 kHz
Sample time	5 μs
Sampling frequency	0.2 MHz
Transmitted bits	5256
Decimation & Interpolation factors	1e8/Sampling frequency
Modulation schemes	BPSK, DBPSK, QPSK & DQPSK
Host Tx & Rx Operating System	Windows 7, 64 bits, Ver. 6.1
Host-based Software Version	Matlab R2012b (8.0.0.783)

5.3.2 Hardware Description

The USRP hardware used is the Ettus-USRPs (as transmitter, TX and receiver, RX). USRP generally has digital to analogue (D/A) and analogue to digital (A/D) converters for respectively up-converting and down-converting the signals, FPGA (field programmable gate array) which is used for interpolation and decimation, and Ethernet interface for interfacing the hardware with the computer. The Cat 5E Ethernet cable used is capable of handling 1000 Mbps of data speed from the PC's Ethernet controller, and it can handle full-duplex operation.

The USRPs also contains daughterboards (RF front ends), whose specifications determine the frequency of operation of the hardware setup. The TX and RX daughterboards used are respectively LFTX and LFRX, each with respective operating frequency range of 0-30 MHz and 0-50 MHz.

For good performance, it is advised to ensure that the hardware sample time and the source block (the software block that conveys the data received by the RX hardware to other software processing blocks) are matched [179]. As such, the sample time used is calculated as Decimation rate/1e8, where 1e8 is the hardwares A/D sampling rate (in Hz). The TX

Table 5.2: Hardware configuration

ITEMS	CONFIGURATION
TX and RX USRP Hardware Rev. no.	USRP2, version 4.0
TX daughterboard model	LFTX, rev 2.2 (0-30 MHz)
RX daughterboard model	LFRX, rev 2.2 (0-50 MHz)
Host TX IP & USRP TX IP	192.168.10.1 & 192.168.10.2
Host RX IP & USRP RX IP	192.168.30.1 & 192.168.30.2

gain value determines the amplitude level of the signal sent into the channel, from the transmitting USRP. Table 5.2 shows the hardware parameters and configurations used for the implementation.

5.3.3 First-order Markov Model Parameters

The initially assumed model parameters for the adopted three-state Fritchman model are expressed in matrix form as:

$$\mathbf{A_1} = \begin{bmatrix} a_{11} & 0 & a_{13} \\ 0 & a_{22} & a_{23} \\ a_{31} & a_{32} & a_{33} \end{bmatrix}, \qquad B = \begin{bmatrix} 1 & 1 & 0 \\ 0 & 0 & 1 \end{bmatrix}, \qquad \pi = \begin{bmatrix} 0.47 \; 0.47 \; 0.06 \end{bmatrix}.$$

The 81 initialized First-Order SHFMM state transition probabilities fed as input to the Baum-Welch algorithm to train the model can be found in Appendix C. The above-defined model parameters are fed as input into the Baum-Welch algorithm, together with the training error sequence.

5.4 Results and Analysis

This section presents the realized First-Order SHFMM results. The First-Order estimated error statistics of the realized First-Order SHFMM have been analytically validated in terms of performance metrics such as: log-likelihood, error-free run distribution, error probabilities,

mean square error (MSE) and Chi-square (χ^2) test. The reliability of the model results is also confirmed by an excellent match between the empirically obtained error sequence and the SHFMM regenerated error sequence as shown by the error-free run distribution plot.

5.4.1 The Estimated State Transition Probabilities

Table 5.3 and Table 5.4 show the most probable First-Order SHFMM estimated state transition probabilities out of the 81 regenerated model that depicts the empirical error sequence for the mildly and heavily disturbed scenario respectively.

TABLE 5.3: Estimated state transition matrix (Mildly disturbed scenario).

a	BPSK	DBPSK	QPSK	DQPSK
a_{11}	0.9469	0.9466	0.9397	0.9323
a_{13}	0.0531	0.0534	0.0603	0.0677
a_{22}	0.9471	0.9347	0.8972	0.9317
a_{23}	0.0529	0.0653	0.1028	0.0683
a_{31}	0.3453	0.7518	0.7168	0.5588
a_{32}	0.5811	0.1783	0.1901	0.3555
a_{33}	0.0736	0.0698	0.0932	0.0857

TABLE 5.4: Estimated state transition matrix (Heavily disturbed scenario)

a	BPSK	DBPSK	QPSK	DQPSK
a_{11}	0.9236	0.9327	0.9032	0.9475
a_{13}	0.0764	0.0673	0.0968	0.0525
a_{22}	0.9487	0.9613	0.9705	0.8786
a_{23}	0.0513	0.0387	0.0295	0.1214
a_{31}	0.5465	0.5587	0.6086	0.4172
a_{32}	0.3618	0.3558	0.2765	0.4778
a_{33}	0.0917	0.0855	0.1149	0.1051

The re-estimated state transition probabilities depicts the transition of the channel from one state to another depending on the input-to-output symbol probability matrix, which is

influenced by the channel status. The model parameters depicts the probability distribution of both the transmission errors and non-error transmissions as obtained through empirical measurement. The probabilities distribution are non-uniform as seen in Table 5.3 and Table 5.4 but are exact probabilities distribution that depict the empirical error sequence obtained for each single-carrier modulation scheme.

5.4.2 The Log-likelihood Ratio Plots

Figure 5.3 and Figure 5.4 show the log-likelihood plots for the model realized for the mildly disturbed scenario and the heavily disturbed scenario. The values of log-likelihood ratio are constantly negative with higher log-likelihood ratio values (closer to zero) establishing a better fitting model. These log-likelihood values cannot be used exclusively as an index of fitness because these values are a function of data size but can be utilized in comparing the fitness of different model parameter given an empirical data. Thus, Figure 5.3 and Figure 5.4 show the log-likelihood plot of the most probable First-Order SHFMM out of the 81 estimated SHFMM for the mildly disturbed scenario and the heavily disturbed scenario respectively.

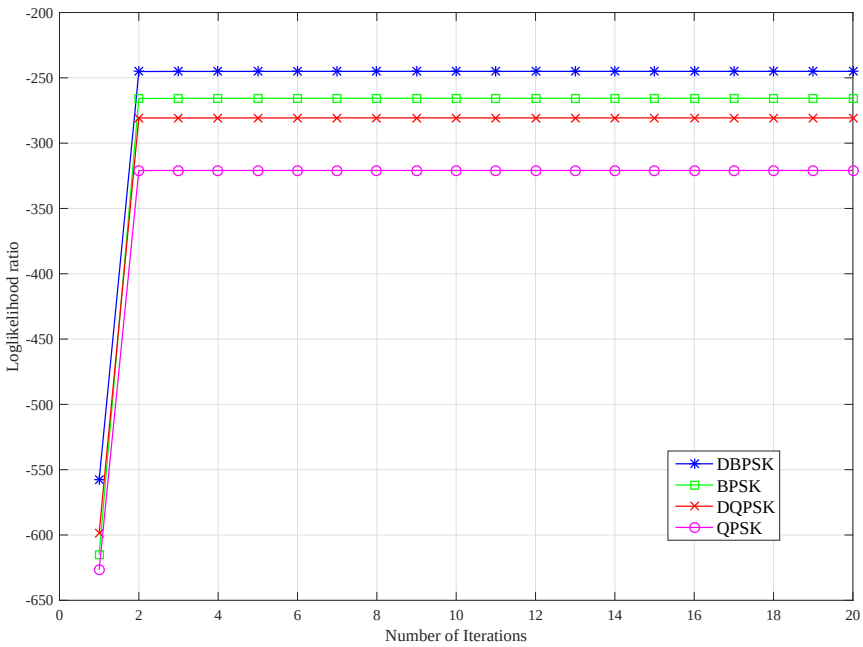

FIGURE 5.3: The Log-likelihood ratio plot (mildly disturbed scenario)

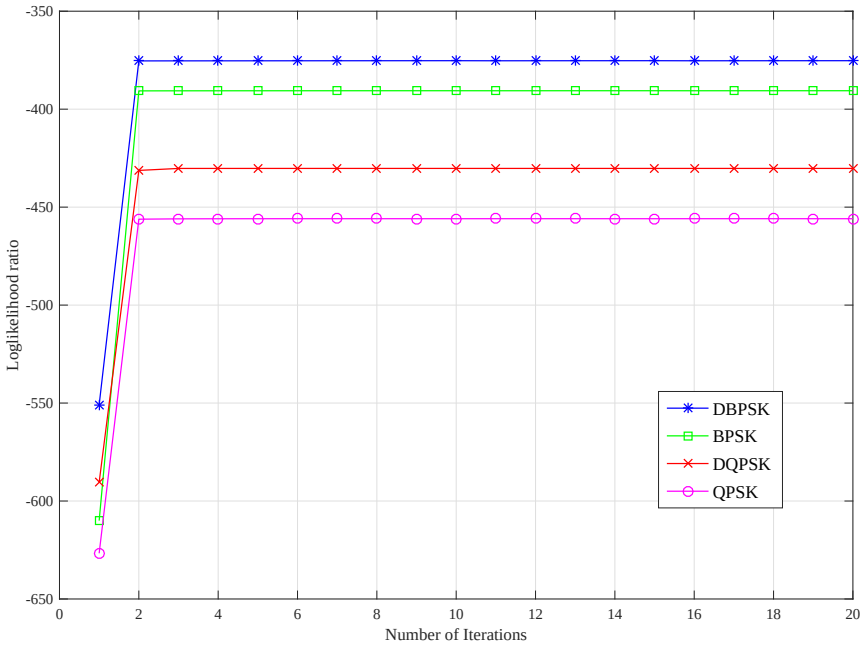

FIGURE 5.4: The Log-likelihood ratio plot (heavily disturbed scenario)

It can also be deduced from Figure 5.3 and Figure 5.4 that convergence is achieved at the 2nd iteration, but the desired level of accuracy is reached after 2nd iteration. The difference in the log-likelihood values of the models in Figure 5.3 and Figure 5.4 is as a result of differing error pattern and the number of errors that exist in each error sequence. These dissimilar error pattern is as a result of the dissimilarities in the characteristics (e.g symbol energy and euclidean distance on the constellation graph) of the modulation schemes used [180].

5.4.3 The Error-free Run Distribution Plots

The error-free run plot indicates the runs of m consecutive error-free distribution following an error state.

Figure 5.5 and Figure 5.6 show the error-free run distribution (EFRD) of the most probable First-Order SHFMM out of the 81 model estimated First-Order SHFMM. The reliability of both First-Order SHFMMs (mildly and heavily disturbed scenario) is confirmed by a close match between the empirical error sequence and SHFMM re-generated error sequence as shown in Figure 5.5 and Figure 5.6.

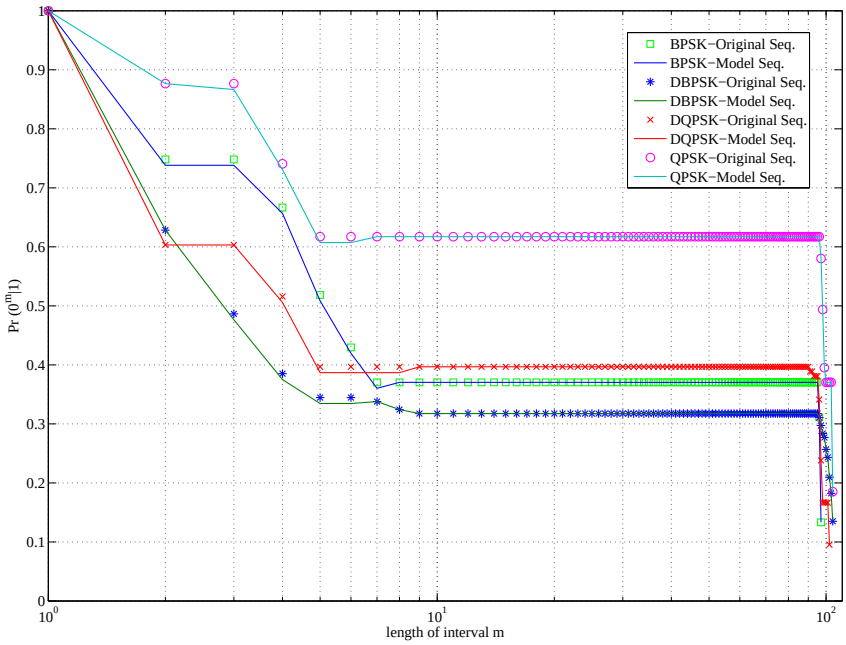

FIGURE 5.5: The error-free run distribution plot (mildly disturbed scenario)

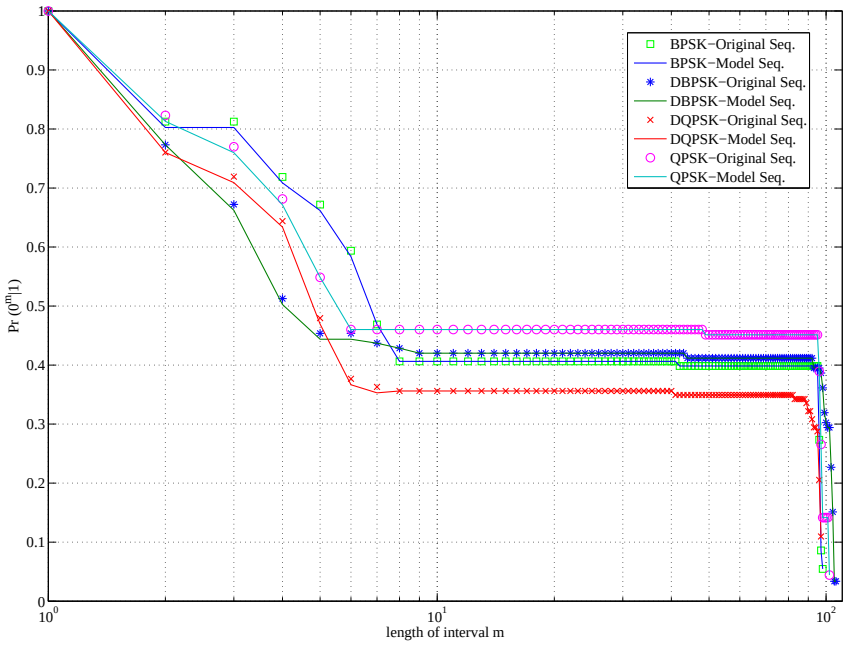

FIGURE 5.6: The error-free run distribution plot (heavily disturbed scenario)

In Figure 5.5 and Figure 5.6, the close match between the EFRD of the empirical error sequence and that of the SHFMM re-generated error sequence can be seen especially in the

lower range of length of interval m.

5.4.4 First-Order Error Probabilities Comparison

The error probability is another performance metric used to validate and ascertain the fitness of a model. An excellent or close match between the error probability of the empirical error sequences and the model regenerated error sequence validates the fitness of the model. Table 5.5 shows the most probable First-Order SHFMM out of the 81 estimated First-Order SHFM for the mildly disturbed scenarios, while Table 5.6 shows the most probable First-Order SHFMM out of the 81 estimated First-Order SHFM for the heavily disturbed scenarios. Table 5.5 and Table 5.6 show a close agreement between the error probability of the empirical error sequence and the model regenerated error sequence, in other words this depicts a correlation between both error probability, hence validating the fitness of the models.

TABLE 5.5: Error probabilities for measured original error sequence (P_e) and model regenerated error sequence ($\bar{P}_e$)- (mildly disturbed scenario)

	BPSK	DBPSK	QPSK	DQPSK
P_e	0.0431	0.0320	0.0615	0.0583
$\bar{P}_e$	0.0420	0.0309	0.0604	0.0572

TABLE 5.6: Error probabilities for measured original error sequence (P_e) and model regenerated error sequence ($\bar{P}_e$)- (heavily disturbed scenario)

	BPSK	DBPSK	QPSK	DQPSK
P_e	0.0781	0.0657	0.0923	0.0812
$\bar{P}_e$	0.0769	0.0645	0.0911	0.0801

A close look at Table 5.5 and Table 5.6 shows the performance of each single-carrier modulation schemes in terms of which modulation has the highest and lowest error probability using the empirical error sequences. It can be deduced from both Table 5.5 and Table 5.6 that the most robust single-carrier modulation scheme is the DBPSK scheme, while QPSK has the

least performance in terms of robustness. The difference in performance can be attributed to the fact that based on the differing robustness of each modulation scheme, no two error sequences can be identical as the modulation scheme with the most superior spatial proximity and angular separation or euclidean distance on the constellation graph performs better and is to a degree robust against noise impairments.

5.4.5 The Mean Square Error (MSE) and Chi-Square Test

The Chi-Square (χ^2) test and the Mean Square Error (MSE) are two analytical metrics often used to validate the fitness and accuracy of a model. These two metrics help to ascertain if there is close correlation between two data, in this case, the empirically obtained error sequences and the model re-generated error sequences. Table 5.7 shows a comparison of the computed Chi-Square and MSE values for the First-Order SHFMM (mildly and heavily disturbed scenarios). The First-Order SHFMM chi-Square and MSE values represents the best fit model, in other words, the First-Order SHFMM chi-Square and MSE values depict the most probable First-Order SHFMM out of the 81 estimated SHFMM thus validating the model accuracy.

Table 5.7: Chi-Square and MSE values for the most probable model parameters (mildly and heavily disturbed scenarios)

	Chi-Square (χ^2)		MSE	
	Mildly	Heavily	Mildly	Heavily
BPSK	0.2118	0.4912	2.5709e-04	4.0161e-04
DBPSK	0.1191	0.3516	1.2118e-04	3.2356e-04
QPSK	0.4929	0.6829	5.4715e-04	7.3062e-04
DQPSK	0.3579	0.5512	3.9531e-04	5.1822e-04

The smaller the (χ^2) and MSE values, the more fitter the model, hence, the reason for training each experimentally obtained measured sequences with 81 different initial model parameters in order to analytically obtain the most probable parameters that produced the empirically obtained error sequences.

Note, optimized model results obtained based on M-H algorithm for the modeling effort in this Chapter is presented in Section B.1 of Appendix B.

5.5 Conclusion

Implementation of PSK modulation for NB-PLC channel modeling using USRP has been presented in this work. A three-state Fritchman model was employed to model the NB-PLC channel and the resulting statistical models are precise channel models obtained from experimental measurements. The resulting model for each modulation scheme were analytically validated. The error statistics of the realized First-Order SHFMMs were analytically validated in terms of log-likelihood, error-free run distribution, error probabilities, mean square error (MSE) and Chi-square (χ^2) test. The reliability of the First-Order model results were also confirmed by an excellent match between the empirical error sequences and SHFMM re-generated error sequences as shown Figure 5.5 and Figure 5.6. Performance analysis shows that DBPSK-OFDM is the most robust scheme, while QPSK-OFDM is the least robust scheme. The realized models are useful for improving the robustness of the modulation schemes as well as facilitating the design of FEC such as permutation trellis coding to exploit and mitigate noise for enhanced transmission reliability over the NB-PLC channel.

CHAPTER 6

A Semi-Hidden Markov Modeling of a Low Complexity FSK-OOK In-House PLC and VLC Integration

The integration of power line communication (PLC) and visible light communication (VLC) is increasingly receiving a lot of research interest with the advent of (IEEE 1901, ITUT G.9960/61) and IEEE 802.15.7 standards for PLC and VLC respectively. In particular, there is an underlying gain that could be achieved by leveraging the existing ubiquitous power line network infrastructure to render connectivity, while we also exploit the illumination system of power-saving Light Emitting Diodes (LEDs) for wireless data communication. The ubiquitous nature of these two systems makes us believe that VLC can offer a good complementary wireless data transmission technology to the existing In-House PLC in a similar manner broad-band Ethernet connection enjoys the support of Wi-Fi. This Chapter thus reports an implementation of a low complexity FSK-OOK In-House PLC and VLC Integration, as well as its Second-Order Semi-Markov Model. The resulting statistical models facilitates the design and evaluation of forward error correcting codes to mitigate burst error occurrences, as well as optimizing the performance of the overall system.

6.1 Introduction

PLC wire-line technology affords us the luxury of harnessing the existing ubiquitous power line network for data transmission. This technology offers a wide variety of services such as home inter-networking and automation, as well as providing a medium for internet connectivity, hence solving the last mile problem. On the other hand, VLC technology is a short-range optical wireless communication (OWC) technology that utilizes the visible light spectrum for data transmission. It exploits visible light sources such as White LEDs for both illumination and communication purposes. The ubiquitous nature and advantages these two

medium of communication possess can be harnessed, such that VLC is made to offer a good complementary wireless data communication to the existing ubiquitous In-House PLC channel. Therefore, this Chapter thus reports an implementation of a low cost, low complexity FSK-OOK In-House PLC and VLC Integration utilizing Mamba power line communication shield. A First and Second-Order Semi-Markov Modeling of the burst error that occurs on the overall system is also carried out, based on the need to mitigate these burst errors. The resulting statistical Markov models furnishes us with information about the distribution of the burst errors, which can be used to facilitate the design and evaluation of forward error correcting codes for burst error mitigation, as well as useful in optimizing the overall system performance.

The rest of the Chapter is organized as follows. Section 6.2 discusses background details on the following: Visible light communication, the implementation of the VLC module, a concise description of the low cost PLC module used, the Semi-Hidden Markov model, a Second-Order model and the algorithm for the parameterization of the model. Section 6.3 presents and discusses the experimental setup showing how the PLC and VLC modules are integrated. The Semi-Hidden Markov model results are in Section 6.4. Section 6.5 concludes the Chapter.

6.2 Background

6.2.1 Visible Light Communication

White LEDs are gradually taking over a great deal of our everyday life. Visible light communication is thus defined as a short-range OWC (optical wireless communication) employing visible light source (e.g White LEDs) for both illumination and high speed wireless data transmission purposes [124]. An attractive aspect of these LED devices is the fact that apart from its original use for lighting purposes, it can also be used for data communication purposes. Data transmission at high speed is fast becoming part of what is playing a major role in our day-to-day life in this modern century. Availability of multimedia data/information is envisioned to be within our reach at different places at any given time. A key element in the realization and achievement of this feat is the wireless access networks (WANs).

Nevertheless, there is scarcity of frequency ranges in the radio frequency spectrum where practical spatial coverage could be achieved, hence it poses a limiting factor. Consequently, other wireless communication means needed to be explored. Visible light communication (VLC) utilizing solid-state visible light sources such as white LEDs, offers a possible alternative with the following advantages [115]: Possible integration with existing power line network, Visible light transmitters and receivers are inexpensive, Free from external intruders and eavesdroppers as the light-waves are only concentrated in a particular region and can not penetrate opaque objects and Radiations from the visible light sources are not harmful to human also free from radio frequency interference, hence, its use in air planes is safe. A comprehensive literature on VLC systems, its underlying fundamentals and its integration with PLC systems can be found in the following literatures: [115, 121, 128]

6.2.2 Visible Light Communication System Architecture

The VLC transmission system architecture is depicted in Figure 6.1 as follows. A concise

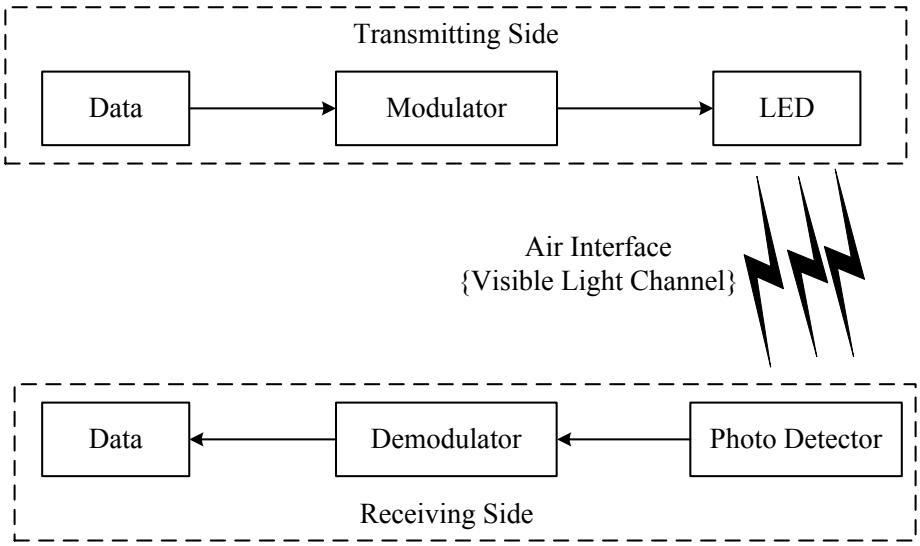

FIGURE 6.1: Visible light communication system architecture

discussion of the major building block of the VLC system (the transmitter, the channel and the receiver) are presented as follows.

The transmitter: The VLC transmitter has the signal conditioning module, the modulation module and the LED. The combination of the LED and a modulation scheme depend on two main factors: the application of the communication system and the utilization of the lighting

system. Two important constraints are to be met by the transmitter: Firstly, the optical power must remain constant during data transmission and, secondly, the communication throughput must be optimized.

The channel: In VLC, the channel is represented by the air interface between the transmitter and the receiver. The channel is influenced by different sources of impairment, such as noise and interference sources, which must be distinguished from each other. The most important noise in the VLC channel is the shot noise modeled using poisson distribution.

The receiver: The main element in the VLC receiver is the photo-detector used to collect the light radiation. Two main types of photo-detectors are used in VLC receivers: the photo-diode and the photo-transistors. Components such as concentrator, optical filter, amplifier and equalizer are added to the photo-detector to build a complete VLC receiver. In VLC, the transmission is governed by the following equation:

$$r(t) = h(t) * s(t) + n(t),$$

where $r(t)$, $h(t)$, $s(t)$ and $n(t)$ are the received signal, the channel impulse response, the transmitted signal and the channel noise respectively.

The Modulator (On-off keying modulation technique): Different modulation techniques are available to be used in VLC. Most of them are dedicated for specified situations. One distinguishes the variable pulse position modulation (VPPM) [181], which is a variance of PPM, the color shift keying (CSK) [182] and the on-off keying (OOK) [183] to mention only a few [126], [183]. By definition, IEEE 802.15.7 is the standard that gives rules and regulation for VLC [2]. According to this standard, OOK must be employed for low data rate applications. OOK is a special case of binary amplitude modulation using two voltage levels, where the second amplitude is null. It maps bit "0" to "0 volt" and bit "1" to "A volt", A being the amplitude of the OOK signal. The OOK signal will be used as a baseband signal to control the LEDs. The problem of flickering and dimming will rise when OOK is used in VLC: Since the LEDs are powered using a squared wave corresponding to the OOK signal, at very low bit frequency, the human eyes can detect the flickering. It is the important to produce data at a frequency greater than 200Hz. In the case of consecutive zeros, the lighting system will challenge a dimming situation. In this case compensation is needed, this could be done by varying the width of the pulses controlling the LEDs.

6.2.3 Visible Light Communication Module Implementation

The circuit used to convey the information through the VLC channel is shown on Figure 6.2.

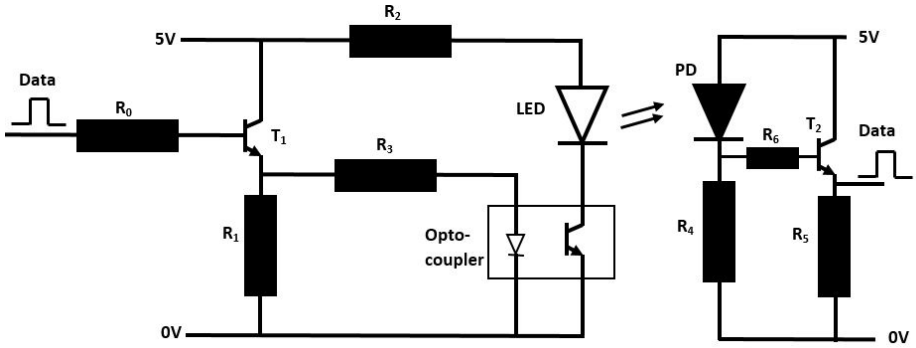

FIGURE 6.2: Schematic diagram of the VLC module implementation.

It shows on one side a simple VLC transmitter composed of an LED in series with an opto-coupler and the control part. The control part uses the incoming data to switch the opto-coupler. On the receiver side, we have a photo-detector (PD), together with a transistor. The PD collects the message from the channel and the transistor tries to polish the receive signal to produce a pure square wave.

6.2.4 Mamba Narrowband Power Line Communication (NB-PLC) Shield

The Mamba NB-PLC shield utilized for the PLC-VLC integration in this work, is a shield that allows the Arduino to get access to this convenient network for data transmission and home automation applications. The Mamba shield developed by LinkSprite is pre-built with a Frequency Shift Keying (FSK) modulation scheme and is designed to work under the 110/240V, 50/60Hz supply. The shield is controlled by an Arduino UNO REV3 board utilizing a simple SPI interface.

In order to use the Mamba, two Mamba shields and two Arduino UNO REV3 are required, but for the purpose of this work we use four of both the Arduino UNO REV3 and the Mamba shield because of our desire to integrate with a VLC system as discussed in the overall system setup in Section 6.3. A 5V, 1A wall adaptor is required to power the Mamba shield for it

to work accurately or alternatively, it can be powered via the USB port on the arduino. A Mamba Arduino code written in C++ is used to initialize the module. The code is a simple Universal Asynchronous Receiver/Transmitter (UART) to PLC bridge, as it allows whatever we send to the UART (Transmitter) to be transmitted on the power line, and then displayed on the UART (Receiver) at the other end. The following steps are carried out to prepare the module for transmission, while Figure 6.3 shows a picture of the Mamba NB-PLC shield coupled with the Arduino UNO.

1. Install the Arduino-1.0.6-windows IDE version.
2. Install the X-CTU serial terminal software.
3. Plug the Mamba Shield to the computers to be used as a transmitter and Receiver.
4. Open the X-CTU software, the two Arduinos are detected with their precise COM ports.
5. Load the code onto the four Arduino UNOs via the Arduino-1.0.6-windows IDE by selecting the right COM ports.
6. The LED on the shield turns green, an indication that the PLC chip has been initialized and is ready.

FIGURE 6.3: Photograph of mamba narrowband power-line communication shield.

6.2.5 Semi-Hidden Markov Model

A Fritchman model also regarded as a Semi-Hidden Markov model is used for both the First and Second-order Semi-Hidden Markov modeling in this work. The choice of Fritchman model is based on the fact that it typifies the long bursty error nature of the PLC channel.

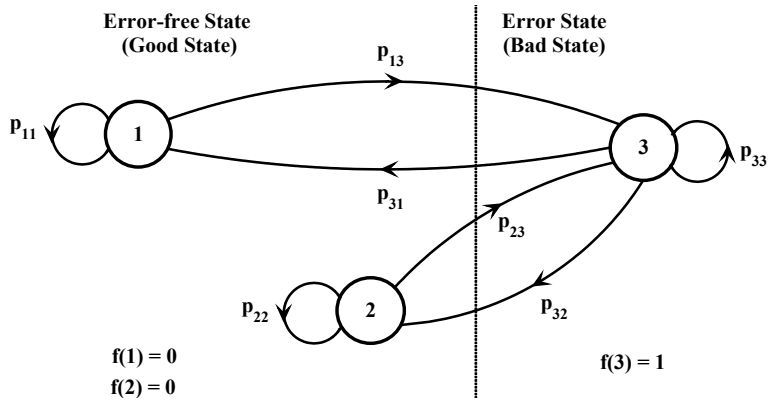

FIGURE 6.4: A semi-hidden Markov model (Fritchman model).

Fritchman [16], characterized binary communication channel utilizing functions of finite-state Markov chain (FSMC). He proposed the grouping of an N-state model into two major partitions namely an error-free state (good states) and an error state (bad states). A good state is synonymous to an error-free transmission and denoted as "0", while a bad state depicts an occurrence of transmission error, which is denoted by a "1" as shown in Figure 6.4. For modeling of the burst error PLC-VLC system in this work, a three-state model is proposed with two good states and one bad state. Figure 6.4 shows the Markov chain representation of the Fritchman model.

6.2.6 A First and Second-Order Semi-Hidden Markov Model

Figure 6.5 shows a First-Order hidden Markov model structure. A First-Order Markov chain model, is one for which the probability of an observation at a particular time t is dependent only on the immediate preceding one. For example, in Figure 6.5, a current state say S_3 at time t depends on previous state S_2 at time $t-1$ and is mathematically represented as $Pr\ [S_t|S_{t-1}] = Pr\ [S_3|S_2]$. The conditional probability of the first-order Markov model takes the form $p_{ij} = Pr\ [S_{t+1} = j|S_t = i]$ which denotes the probability of transitioning from state i at time t to state j at time $t+1$. Hence the first-order transition matrix A_1 for a three-state

model assumed for the burst error model is a stochastic 3×3 sized matrix whose rows sum up to 1 ($\sum_{j=1}^{N} p_{ij} = 1$). The First-Order state transition matrix is presented in matrix form in Section 6.3.

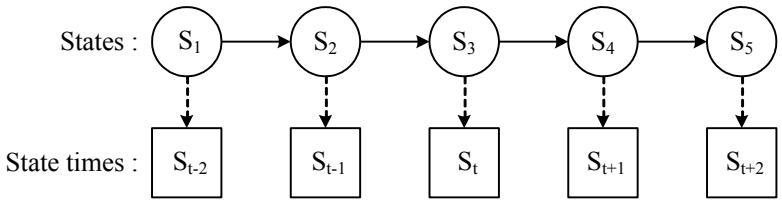

FIGURE 6.5: A First-Order hidden Markov model.

On the other hand, for a Second-Order Markov chain assumption, the probability of an observation at time t depends on two preceding ones. For example, according to Figure 6.6, current state say S_3 at time t depends on previous states S_2 and S_1 at times $t-1$ and $t-2$ respectively, and is mathematically represented as $Pr\ [S_t|S_{t-1}, S_{t-2}] = Pr\ [S_3|S_2, S_1]$. Hence, the conditional probability of the Second-Order Markov model is denoted as $p_{ijk} = Pr\ [S_{t+2} = k|S_{t+1} = j, S_t = i]$, which denotes the probability of transitioning from state i at time t to state j at time $t+1$ and to state k at time $t+2$. The Second-Order state transition matrix A_2 is also a stochastic $3 \times 3 \times 3$ sized matrix shown in Section 6.3.

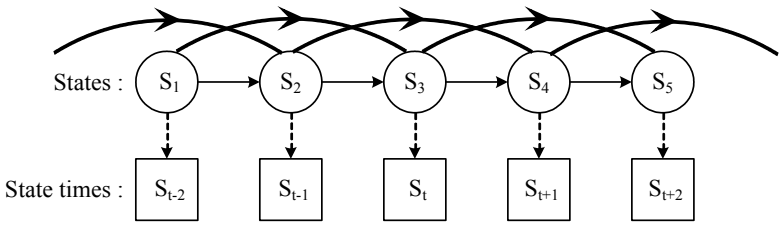

FIGURE 6.6: A Second-Order hidden Markov model.

The basic training procedures for obtaining the most probable First and Second-Order SHFMM that depicts the empirical error sequences is discussed in Section 3.4.2 and Section 3.4.3 respectively. Refer to Section 4.9 for the modeling methodology and procedure for obtaining an accurate First-Order SHFMM parameter sets.

6.3 Experimental Setup and Methodology

Figure 6.7 shows the PLC-VLC integrated architecture.

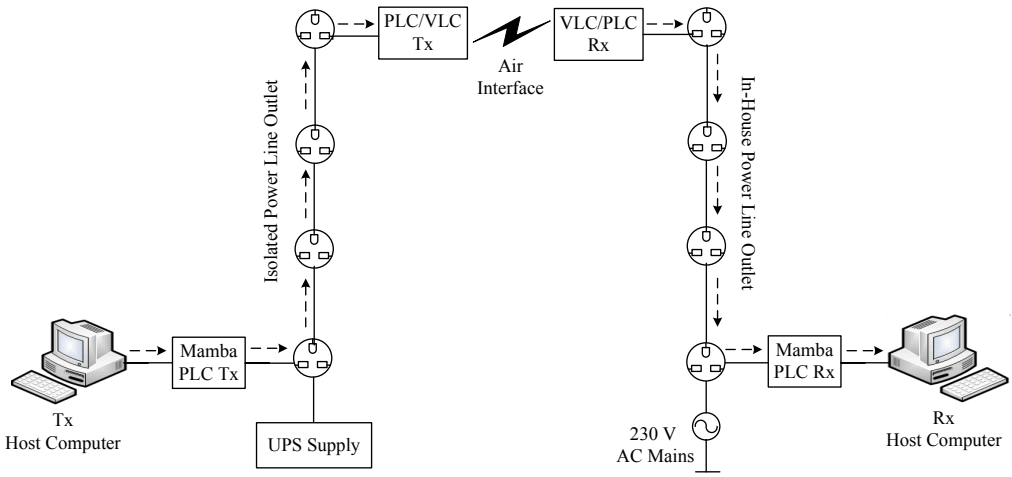

FIGURE 6.7: PLC-VLC integrated architecture showing data flow.

FIGURE 6.8: The hybrid PLC-VLC testbed.

A close look at Figure 6.7, shows the separation and connection of the PLC main transmitter (TX) and receiver (RX) onto different power line outlets. The main TX is connected to an isolated power line outlet powered through a UPS, while the main RX is connected to the normal In-House power line topology. This is to ensure that the received data are obtained via the VLC receiver and not from the power line, were they to be connected to the same PLC topology. The dotted arrows shows the data flow direction. Figure 6.8 illustrates the hybrid PLC-VLC testbed setup showing the PLC white boxes and the integrated PLC-VLC modlues between the PLC white boxes.

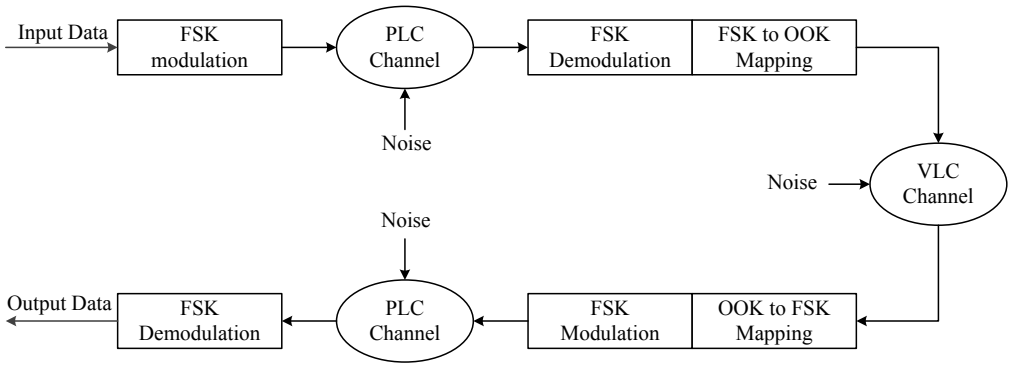

FIGURE 6.9: PLC-VLC model showing PLC and VLC interface and modulators.

Figure 6.9 shows a simplified form of the PLC-VLC integration. The Mamba PLC shield is plugged onto the power line and the FSK modulated signal is coupled onto the power line through it. The signal is then captured and demodulated by the PLC receiver. The demodulated signal is routed to the visible light transmitter using the micro-controller. An OOK modulation is then utilized by the VLC transmitter to transmit in a simplex mode. At this stage, the LED converts the received electrical signal into optical signal sent via air interface and received by the VLC receiver through the photo diode which then converts the signal back into electrical form.

The system mainly consists of power line and visible light section. PLC employs the infrastructure of electrical power distribution system as communication medium. Power line modem is plugged into the existing power line network and the ASK modulated signal is transmitted through it. This signal is captured by the PLC receiver and it is demodulated. This is routed to the visible light section using micro-controller. FSK modulation is used in VLC and the communication is simplex. Here the LED will convert the electrical signal into optical signal which is received using a photo-diode and convert back into electrical signal and sends it to the PLC module, which modulates the signal using FSK. The modulated signal is then coupled unto the power line network, after which it is demodulated and reconstructed back into the original sent message by the receiving PLC module.

First and Second-Order Initial Model Parameters The Baum-Welch algorithm used to parameterize the SHFMM takes the measured error sequence as training data, and the model's initial parameter as input for the re-estimation of the model parameters. The initial model parameters used are stated as follows.

$$\mathbf{A_1} = \begin{bmatrix} a_{11} & 0 & a_{13} \\ 0 & a_{22} & a_{23} \\ a_{31} & a_{32} & a_{33} \end{bmatrix}, \quad \mathbf{A_2} = \begin{bmatrix} 0.95 & 0 & 0.05 \\ 0 & 0.87 & 0.13 \\ 0.38 & 0.50 & 0.12 \\ 0.90 & 0 & 0.10 \\ 0 & 0.85 & 0.15 \\ 0.45 & 0.45 & 0.10 \\ 0.89 & 0 & 0.11 \\ 0 & 0.90 & 0.10 \\ 0.67 & 0.27 & 0.06 \end{bmatrix}, \quad \mathbf{B} = \begin{bmatrix} 1 & 1 & 0 \\ 0 & 0 & 1 \end{bmatrix}.$$

The First-Order SHFMM state transition probability matrix is denoted by A_1. The initialized values for A_1 can be found in Appendix C.

The Second-Order SHFMM state transition probability matrix is denoted by A_2. Since a Semi-Hidden Fritchman Markov model is assumed for this work, the output symbol or error probability matrix B (representing the input-to-output symbol transition) is written in binary form as shown above. The first two columns typifies the two error-free state (good states), while the last column symbolizes the error-state (bad state). The initial state probability matrix, which denotes a prior or initial probability of being in any of the state is also written as follows. All the element of the prior probability matrix must sum up to one.

$$\mathbf{\Pi} = [\pi_1 \ \pi_2 \ \pi_3] = [0.47 \ 0.47 \ 0.06]. \tag{6.1}$$

6.4 Results and Analysis

This section discusses the realized model results, the First and Second-Order SHFMM estimated state transition probabilities in Section 6.4.1. The error statistics of the realized First and Second-Order SHFMMs have been analytically validated in terms of log-likelihood, error-free run distribution, error probabilities, mean square error (MSE) and Chi-square (χ^2) test in Sections 6.4.2, 6.4.3, 6.4.4 and 6.4.5 respectively. The Second-Order SHFMMs have also been analytically validated to be superior to the First-Order SHFMMs although at the expense of more computational complexity. The reliability of both First and Second-Order

model results is confirmed by an excellent match between the empirical error sequences and SHFMM re-generated error sequences as shown by the error-free run distribution plot.

6.4.1 The Estimated State Transition Probabilities

Table 6.1 and Table 6.2 show the most probable First and Second-Order SHFMM estimated state transition probabilities that depicts the empirical error sequence. In Table 6.1, the estimated state transition probabilities shown are the most probable First-Order SHFMM estimated state transition probabilities out of the 81 regenerated model that depicts the empirical error sequence.

TABLE 6.1: First-Order estimated state transition matrix for residential and laboratory site (Morning, Afternoon and Evening)

	Residential			Laboratory		
	Morn.	Aftn.	Even.	Morn.	Aftn.	Even.
a_{11}	0.9383	0.9110	0.9205	0.9466	0.9431	0.9496
a_{13}	0.0617	0.0890	0.0795	0.0534	0.0569	0.0504
a_{22}	0.9705	0.9721	0.9646	0.9226	0.9429	0.9522
a_{23}	0.0295	0.0279	0.0354	0.0774	0.0571	0.0478
a_{31}	0.1173	0.0085	0.2280	0.5698	0.3853	0.5501
a_{32}	0.8289	0.9554	0.7065	0.4074	0.5416	0.4071
a_{33}	0.0538	0.0361	0.0656	0.0228	0.0731	0.0428

The re-estimated state transition probabilities depicts the transition of the channel from one state to another depending on the input-to-output symbol probability matrix, which is influenced by the channel status. The model parameters depicts the probabilities distribution of both the transmission errors and non-error transmissions as obtained on the channel through measurement. The probability distribution are non-uniform as seen from the state transition probabilities values for the First and Second-Order models.

Based on analytical validation using performance metrics like log-likelihood ratio, error-free run, error probabilities, mean square error (MSE) and Chi-square (χ^2) test, it can be categorically stated that the Second-Order SHFMM are superior to the First-Order SHFMM.

TABLE 6.2: Second-Order estimated state transition matrix for residential and laboratory site (Morning, Afternoon and Evening)

	Residential			Laboratory		
	Morn.	Aftn.	Even.	Morn.	Aftn.	Even.
a_{111}	0.9406	0.9499	0.9479	0.9473	0.9483	0.9494
a_{113}	0.0594	0.0501	0.0521	0.0527	0.0517	0.0506
a_{122}	0.9532	0.9408	0.9414	0.9412	0.9494	0.9544
a_{123}	0.0468	0.0592	0.0586	0.0588	0.0506	0.0456
a_{131}	0.1493	0.1496	0.1419	0.1417	0.1418	0.1421
a_{132}	0.7590	0.7576	0.7597	0.7593	0.7588	0.7580
a_{133}	0.0917	0.0928	0.0984	0.0990	0.0994	0.0979
a_{211}	0.9139	0.9155	0.9153	0.9165	0.9160	0.9156
a_{213}	0.0861	0.0845	0.0847	0.0835	0.0840	0.0844
a_{222}	0.8816	0.8817	0.8825	0.8814	0.8819	0.8812
a_{223}	0.1184	0.1183	0.1175	0.1186	0.1181	0.1188
a_{231}	0.6588	0.6577	0.6588	0.6596	0.6589	0.6570
a_{232}	0.2606	0.2627	0.2623	0.2618	0.2619	0.2602
a_{233}	0.0806	0.0796	0.0789	0.0786	0.0792	0.0828
a_{311}	0.8815	0.8829	0.8834	0.8827	0.8824	0.8824
a_{313}	0.1185	0.1171	0.1166	0.1173	0.1176	0.1176
a_{322}	0.9881	0.9872	0.9882	0.9884	0.9895	0.9887
a_{323}	0.0119	0.0128	0.0118	0.0116	0.0105	0.0113
a_{331}	0.0614	0.0908	0.0440	0.0985	0.0125	0.0403
a_{332}	0.8645	0.8520	0.8715	0.8521	0.8890	0.8913
a_{333}	0.0741	0.0572	0.0845	0.0494	0.0985	0.0684

6.4.2 The Log-likelihood Ratio Plots

Figure 6.10 and Figure 6.11 show the log-likelihood ratio plot for the First and Second-Order SHFMM respectively. Log-likelihood values are always negative, with higher log-likelihood values (closer to zero) establishing a better fitting model. These values cannot be utilized alone as an index of fitness because these values are a function of data size but can be utilized in comparing the fitness of different model parameter given an empirical data.

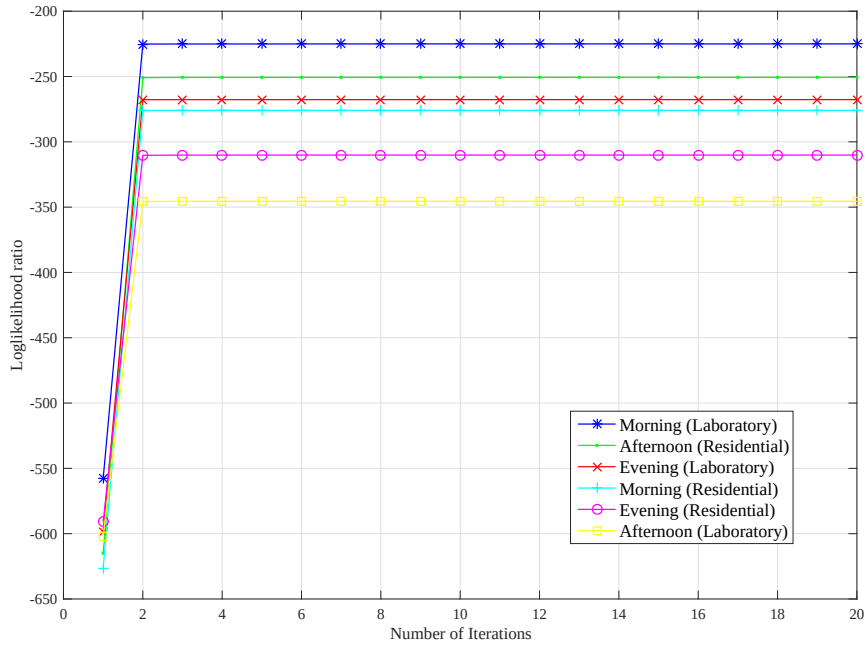

FIGURE 6.10: Log-likelihood ratio plot for the First-Order SHFMM.

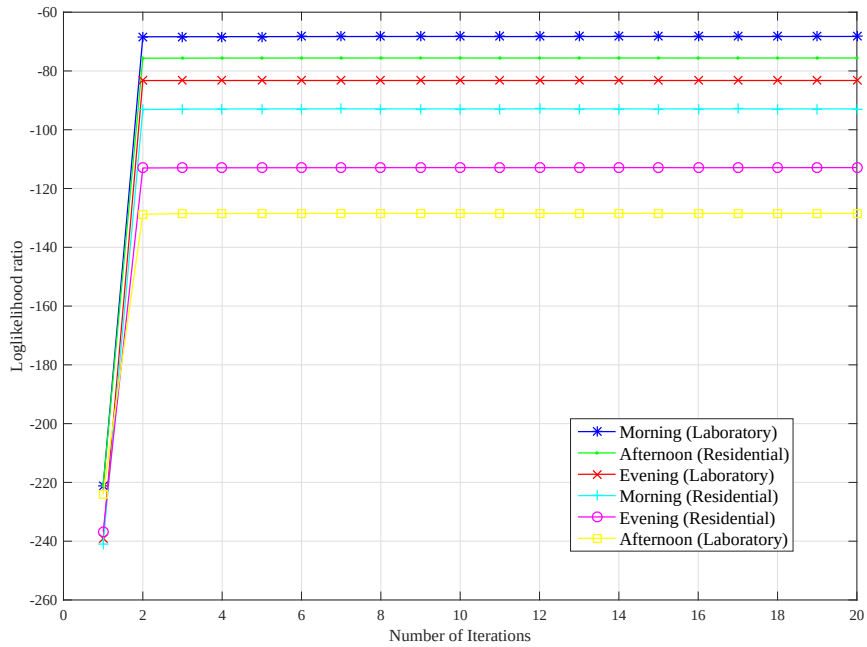

FIGURE 6.11: Log-likelihood ratio plot for the Second-Order SHFMM.

Thus, Figure 6.10 shows the log-likelihood plot of the most probable First-Order SHFMM out of the 81 estimated SHFMM. A comparison of Figure 6.10 and Figure 6.11 show a better

fit for the Log-likelihood of the Second-Order SHFMM thus validating the superiority of the Second-Order SHFMMs over the First-Order SHFMMs.

6.4.3 The Error-free Run Distribution Plots

Figure 6.12 and Figure 6.13 show the First and Second-Order error-free run distribution plot respectively.

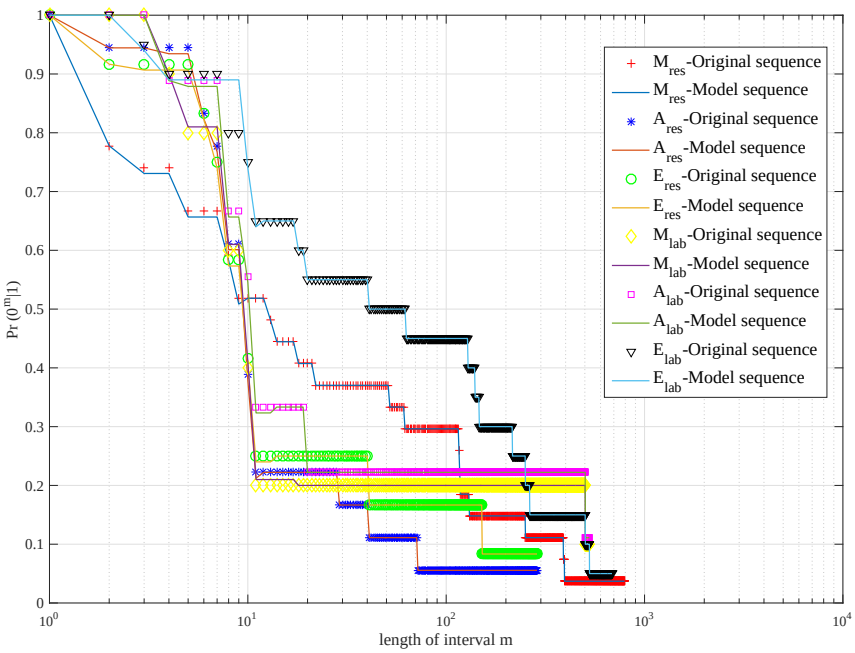

FIGURE 6.12: Error-free run distribution plot for the First-Order SHFMM.

The error-free run plot indicates the runs of m consecutive error-free distribution following an error state. Figure 6.12 depicts the error-free run distribution of the most probable First-Order SHFMM out of the 81 model estimated First-Order SHFMM.

The reliability of both First and Second-Order model results is confirmed by a close match between the empirical error sequence and SHFMM re-generated error sequence as shown by the error-free run distribution plots in Figure 6.12 and Figure 6.13. A closer look shows that error-free run distribution plot for the Second-Order SHFMM has a more excellent match between the empirical error sequence and SHFMM re-generated error sequence compared to the error-free run distribution plot for the First-Order SHFMM. This thus validates the superiority of the Second-Order SHFMM over the First-Order SHFMM.

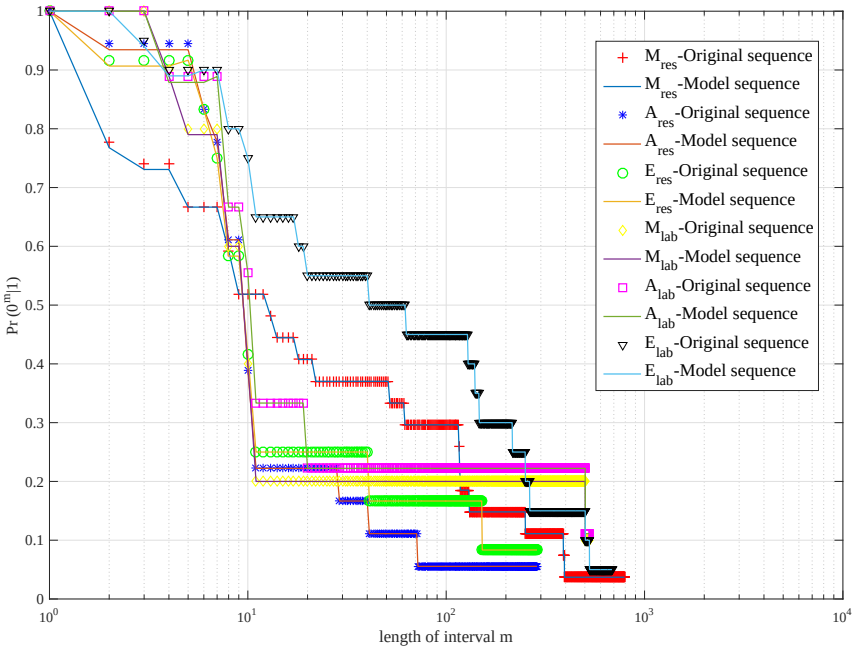

FIGURE 6.13: Error-free run distribution plot for the Second-Order SHFMM.

6.4.4 The First and Second-Order Model Error Probabilities

A comparison between error probabilities of the empirical error sequence and the model regenerated error sequence is another way of ascertaining the fitness of a model.

TABLE 6.3: Error probabilities for measured original error sequence (P_e) and model regenerated error sequence ($\bar{P}_e$)- First-Order SHFMM

	Residential			Laboratory		
	Morn.	Aftn.	Even.	Morn.	Aftn.	Even.
P_e	0.0511	0.0333	0.0662	0.0287	0.0789	0.0478
$\bar{P}_e$	0.0501	0.0320	0.0651	0.0276	0.0778	0.0467

Tables 6.3 and Table 6.4 show the error probability of the empirical error sequence versus the model regenerated error sequence for the First and Second-Order SHFMM respectively. Tables 6.3 shows the error probabilities for the most probable First-Order SHFMM out of the 81 estimated First-Order SHFMM. Tables 6.3 and Table 6.4 show a close agreement between the error probability of the empirical error sequence and the model regenerated error

TABLE 6.4: Error probabilities for measured original error sequence (P_e) and model regenerated error sequence ($\bar{P}_e$)- Second-Order SHFMM

	Residential			Laboratory		
	Morn.	Aftn.	Even.	Morn.	Aftn.	Even.
P_e	0.0511	0.0333	0.0662	0.0287	0.0789	0.0478
$\bar{P}_e$	0.0509	0.0330	0.0659	0.0284	0.0785	0.0475

sequence, in other words this depicts a correlation between both error probability, hence validating the model. Table 6.4 shows a more excellent agreement between error probability of the empirical error sequence and the model regenerated error sequence thus validating the superiority of the Second-order SHFMM over the First-Order SHFMM.

TABLE 6.5: Chi-square and MSE values for the First and Second-Order SHFMMs (morning, afternoon and evening)

		Chi-Square (χ^2)	MSE
$MORNING_{LAB}$	1st Order	4.4582e-04	7.5670e-07
	2nd Order	3.3321e-04	2.5580e-07
$AFTERNOON_{RES}$	1st Order	4.2505e-04	1.3235e-06
	2nd Order	3.1993e-04	2.7346e-07
$EVENING_{LAB}$	1st Order	4.0784e-04	9.4354e-07
	2nd Order	3.6669e-04	3.2348e-07
$MORNING_{RES}$	1st Order	5.5829e-04	1.3320e-06
	2nd Order	2.6387e-04	4.1181e-07
$EVENING_{RES}$	1st Order	5.8490e-04	1.6785e-06
	2nd Order	3.2551e-04	5.7892e-07
$AFTERNOON_{LAB}$	1st Order	4.6705e-04	2.1155e-06
	2nd Order	3.4209e-04	6.1572e-07

6.4.5 The Mean Square Error (MSE) and Chi-Square Test

Table 6.5 shows a comparison of the computed Chi-Square and MSE values for the First and Second-Order SHFMM. The mean square error (MSE) and Chi-square (χ^2) test are two other performance metrics used to validate the correlation between empirical error sequence

(the observed sequence) and model regenerated sequence (the expected sequence). The χ^2 and MSE values ascertain the quality of the estimate and are always positive values, with χ^2 and MSE values closer to zero establishing a better fit. The First-Order SHFMM chi-Square and MSE values represents the best fit model, in other words, the First-Order SHFMM chi-Square and MSE values depict the most probable First-Order SHFMM out of the 81 estimated SHFMM.

It can be deduced from Table 6.5 that the chi-Square and MSE values for the Second-Order SHFMMs represent a better fitting model as the values are closer to zero than the chi-Square and MSE values for the First-Order SHFMMs. This thus validates and establishes the superiority of the Second-Order SHFMMs over the First-Order SHFMMs.

Note, optimized model results obtained based on M-H algorithm for the modeling effort in this Chapter is presented in Section B.2 of Appendix B.

6.5 Conclusion

In this Chapter, a novel low-cost, low-complexity FSK-OOK In-House hybrid PLC-VLC system is developed. We derived a First and Second-Order SHFMM to model the burst error on the channel. The error statistics of the realized First and Second-Order SHFMMs were analytically validated in terms of performance metrics such as: log-likelihood, error-free run distribution, error probabilities, mean square error (MSE) and Chi-square (χ^2) test. The Second-Order SHFMMs were also analytically validated and results show it is superior to the First-Order SHFMMs although at the expense of additional computational complexity. The reliability of both First and Second-Order model results were also confirmed by an excellent match between the empirical error sequences and SHFMM re-generated error sequences as shown by the error-free run distribution plot.

CHAPTER 7

First and Second-Order Semi-Hidden Fritchman Markov Models for a multi-carrier based Indoor Narrowband Power Line Communication System

The realization of a Semi-Hidden Fritchman Markov models (SHFMMs) that capture the statistical distribution of errors on the power line communication (PLC) channel is only practicable if combined with efficient algorithms for learning and inference. This article thus reports a First and Second-Order SHFMM of an Orthogonal Frequency Division Multiplexing (OFDM) based indoor narrowband PLC (NB-PLC) system. Accurate SHFMMs have been derived utilizing the efficient iterative Baum-Welch algorithm for a "mildly disturbed" and "heavily disturbed" noise scenario in both residential and laboratory settings. The estimated error statistics of the realized SHFMMs have been validated analytically in terms of log-likelihood, error-free run distribution, mean square error (MSE) and Chi-Square (χ^2) test. The estimated Second-Order SHFMMs have been analytically ascertained and validated to be superior than the First-Order SHFMMs, although at the expense of more computational complexity. The reliability of the SHFMMs realized is confirmed by an excellent match between the empirical data and SHFMM generated data as shown by the error-free run distribution plots.

7.1 Introduction

Due to the varying nature of the power line network as a result of multipath, noise impairments leading to burst error thus inhibiting reliable and efficient transmission, there is need to capture the statistical distribution of such errors in order to enhance the transmission reliability of the PLC channel. Efficient, flexible and reliable channel models are thus valuable in developing robust modulation schemes (preferably multi-carrier) and forward error correcting codes capable of exploiting and mitigating noise and fading on the channel.

Graphical models such as SHFMMs offer a powerful, universal framework for formulating statistical models of communication channel problems (such as noise, perturbation and interference). However, the formulation of SHFMM is only practicable if combined with efficient algorithms for learning and inference. Due to the varying noise parameters obtained from country to country, based on the fact that noise impairments are dependent on mains voltages, topology of power line, place and time, hence the need for constant measurement campaigns before statistical mathematical models are derived.

This Chapter thus reports First and Second-Order SHFMM of an OFDM NB-PLC channel based on empirical data. This is achieved through a novel development of a reconfigurable software-defined QPSK, DQPSK and D8PSK OFDM NB-PLC transceiver systems, utilizing the Universal Software Radio Peripheral (USRP). Empirical data are obtained at both residential and laboratory sites, taking into consideration two noise scenarios: "mildly disturbed" and "heavily disturbed". The empirically obtained error sequences (training data) and the initial SHFMM parameters are inputs to the iterative Baum-Welch maximum likelihood estimation (MLE) algorithm [21] for parameter re-estimation in order to realize the most probable First and Second-Order SHFMM parameters that depicts the empirical data (error sequences) for each of the OFDM scheme considered. Accurate First and Second-Order SHFMMs have been derived and analytically validated to ascertain the precision of the realized model through performance metrics such as: log-likelihood, error-free run distribution, mean square error (MSE) and Chi-square (χ^2) test. The estimated Second-Order SHFMMs have been analytically validated and ascertained to be a more superior model than the First-Order SHFMMs, although this comes at the expense of more computational complexity. A performance comparison of the different OFDM modulation schemes considered in the presence of similar interferers for the two noise scenarios considered were also carried out.

The remaining part of this Chapter is structured as follows. Section 7.2 gives a concise description of the adopted OFDM NB-PLC transceiver system and a discrete channel model elements. The SHFMM and the iterative Baum-Welch algorithm is presented in Section 7.3. Specifically, the 3-state First and Second-Order SHFMM used in this article is presented in Section 7.3.1, while "Baum-Welch" an iterative algorithm used in estimating the parameter of the First and Second-Order SHFMMs is discussed in Section 7.3.2. The NB-PLC transceiver

testbed used for obtaining the empirical error sequences is discussed in Section 7.4. In Section 7.5, results and performance analysis of the OFDM modulation schemes used in the presence of similar interferers is carried out. Furthermore, a comparison of the First and Second-Order models for each of the modulation scheme considered is also carried out. Section 7.6 gives a brief summary of this Chapter with concluding remarks.

7.2 Narrowband PLC Transceiver Description

The degradation in performance over NB-PLC systems is majorly caused by multipath-induced dispersion and impulse noise [8], [79]. Impulse noise (IN) poses as the most difficult noise impairment on PLC channels. PLC-G3 and PRIME PLC standards [10–12] have established OFDM, a multi-carrier digital modulation system to be more robust against such noise when compared to single carrier modulation systems. This is due to attribute of the OFDM in spreading the noise energy over the available sub-carriers [15], hence, the reason for the use of PLC-G3 standard in this work.

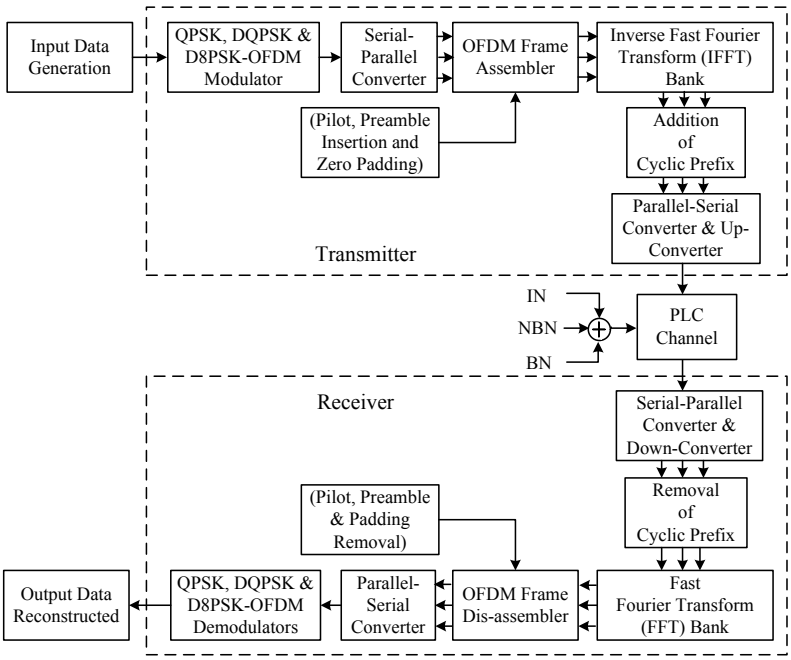

FIGURE 7.1: OFDM PLC transceiver system building blocks

Figure 7.1 clearly shows a typical OFDM PLC transceiver system, its basic building blocks and the different stages of digital signal processing of an OFDM transceiver system. The upper building blocks of Figure 7.1 shows the transmitting side, while the lower part shows the

receiving side of the transceiver. The constellation mapping in the modulator and demodulator block of the OFDM system is done utilizing the conventional single carrier modulators, thus, a QPSK, DQPSK and D8PSK-OFDM is implemented [184, 185]. The fundamental communication system model as illustrated in Fig. 7.2, is generally comprised of a data source (discrete), a source and channel encoder for error control purposes, a modulator and transmitter, a channel, a demodulator and receiver, and a source and channel decoder. The terminology finite state channel model (FSCM) or discrete channel model (DCM) [186] is basically used to refer to the communication elements that lies between points X and Y, where at point X, the input sequence comprises a vector of discrete symbols, while at point Y, the output sequence is a similar vector of discrete symbols [21]. Refer to Section 4.8.2 for an elaborate description of the OFDM NB-PLC transceiver functionality.

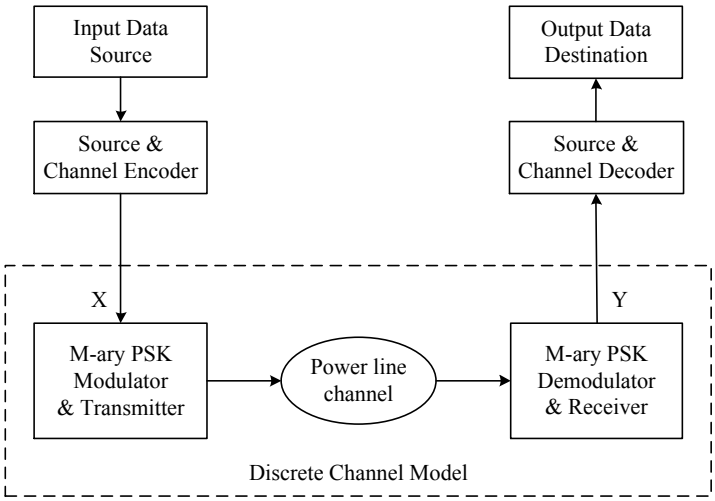

FIGURE 7.2: PLC discrete channel model (DCM) building blocks

7.3 SHFMM and Baum-Welch Algorithm

7.3.1 Semi-Hidden Fritchman Markov Model

Recently, SHFMM has received a lot of attention for modeling burst error communication channels [18, 19]. Errors measured on such channels appear in cluster, hence, are not independent. Consequently, such channels exhibit memory, which invariably means error occurrences are statistically dependent, therefore, classical memoryless binary symmetric channel models

such as Gilbert-Elliot cannot satisfactorily depict such channel. This motivated the use of SHFMM, a memory channel model in this work [134].

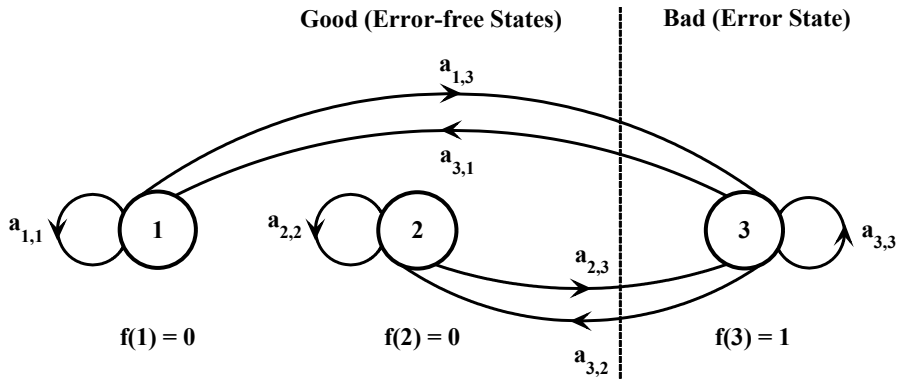

FIGURE 7.3: The First-Order semi-hidden Fritchman model

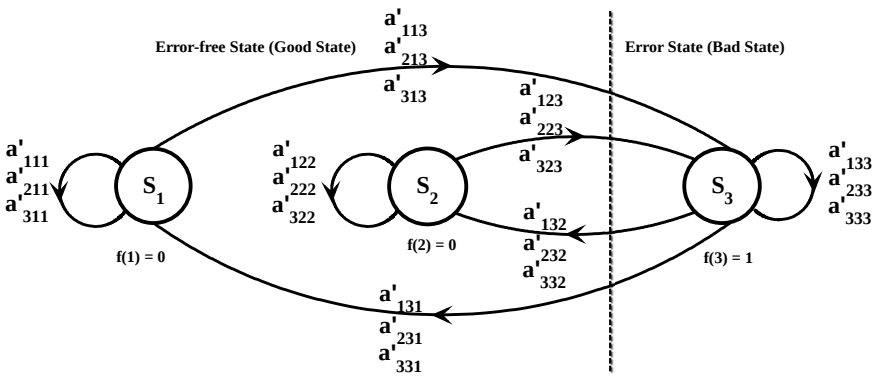

FIGURE 7.4: The Second-Order semi-hidden Fritchman model

Fritchman model is an important class of generative error model based on semi-hidden Markov model principles, this model can precisely typify the statistical patterns of the burst errors that occurs on the NB-PLC channel [186]. Figure 7.3 and Figure 7.4 show the structure of the First and Second-Order 3-state SHFMM adopted in this work respectively. In the application of Fritchman model to channel modeling, the established practice entails a First-Order Markov assumption as detailed in [149]. The First-Order SHFMM state transition probability matrix denoted by $\mathbf{A_1}$ for the three-state model in Figure 7.3 is thus a stochastic 3×3 sized matrix with the rows summing up to one ($\sum_{j=1}^{3} a_{ij} = 1$) and represented as follows [21]. Refer to Appendix C for the 81 initialized First-Order SHFMM state transition probabilities.

$$\mathbf{A_1} = \begin{bmatrix} a_{11} & 0 & a_{13} \\ 0 & a_{22} & a_{23} \\ a_{31} & a_{32} & a_{33} \end{bmatrix} \tag{7.1}$$

In contrast, a *Second-Order semi-hidden Markov* model entails an alteration in the First-Order semi-hidden Markov assumption as depicted in Figure 7.4, such that, *"at any observation time, t, transition occurs to a new state based on the transition probability, which is dependent not only upon the preceding state but dependent on two preceding states at time instant $t-1$ and $t-2$"*. This is refered to as the Second-Order semi-hidden Markov assumption, and is mathematically represented in general form as follows.

$$Pr\ [s_t|s_{t-1}, s_{t-2}] = Pr\ [S_k|S_j, S_i]. \tag{7.2}$$

This expression implies that, transition to state S_k at time instant t is dependent on previous states S_j and S_i at time instants $t-1$ and $t-2$ respectively. Therefore, the conditional probability of the Second-Order model a_{ijk} is mathematically represented as follows.

$$a_{ijk} = Pr[s_{t+2} = S_k|s_{t+1} = S_j, s_t = S_i] \tag{7.3}$$

This expression implies that, the chance of making a transition to state k at time $t+2$ is conditioned on the previous state transitions to states j and i at time instants $t+1$ and t respectively. Hence, the assumed Second-Order SHFMM state transition matrix denoted as $\mathbf{A_2}$ is also a stochastic $3 \times 3 \times 3$ sized matrix having the rows summing up to one as shown in (7.4).

$$\mathbf{A_2} = \begin{bmatrix} a_{111} & 0 & a_{113} \\ 0 & a_{122} & a_{123} \\ a_{131} & a_{132} & a_{133} \\ a_{211} & 0 & a_{213} \\ 0 & a_{222} & a_{223} \\ a_{231} & a_{232} & a_{233} \\ a_{311} & 0 & a_{313} \\ 0 & a_{322} & a_{323} \\ a_{331} & a_{332} & a_{333} \end{bmatrix} = \begin{bmatrix} 0.95 & 0 & 0.05 \\ 0 & 0.87 & 0.13 \\ 0.38 & 0.50 & 0.12 \\ 0.90 & 0 & 0.10 \\ 0 & 0.85 & 0.15 \\ 0.45 & 0.45 & 0.10 \\ 0.89 & 0 & 0.11 \\ 0 & 0.90 & 0.10 \\ 0.67 & 0.27 & 0.06 \end{bmatrix}. \tag{7.4}$$

Note, that for the 3-state SHFMM adopted for modeling in this work, transmission errors are only produced in the single error state, while any error-free transmission can emanate from any of the two error-free states. Hence, if a transmission error occurs, this implies that

the error is produced from the single error state. Consequently, an error generation matrix denoted as **B** is formed. This error generation matrix represents the input-to-output symbol transition and is written as follows [21].

$$\mathbf{B} = \begin{bmatrix} 1 & 1 & 0 \\ 0 & 0 & 1 \end{bmatrix} \tag{7.5}$$

The first two columns represents the good error-free states and the third column represents the bad error-state. Row one represents no transmission error, while row two indicates a transmission error and the probability value one and zero indicates certainty and impossibility respectively.

The final Fritchman model parameter is the initial state probability denoted by π which is a $1 \times N$ vector, where N is the number of states. This probability depicts the prior probability of sitting in any of the three states, hence, for the three states SHFMM adopted π is written as follows with the values indicating the assumed initial prior probability [21].

$$\mathbf{\Pi} = [\pi_1 \ \pi_2 \ \pi_3] = [0.47 \ 0.47 \ 0.06]. \tag{7.6}$$

7.3.2 Baum-Welch Algorithm Training of the SHFMM

Finding model parameter estimates that best describes the observation sequence has been a major problem in SHMMs parameterization. Baum-Welch algorithm offers a solution to this difficulty [20], [21]. BWA is designed as an iterative algorithm based on the MLE principle and is thus used to estimate the parameters of the First and Second-Order SHFMM $\Gamma = (A_1, A_2, B, \pi)$ based on empirically obtained data (error sequence). The Baum-Welch algorithm converges to the maximum likelihood estimator of $\Gamma = (A_1, A_2, B, \pi) = (\hat{A}_1, \hat{A}_2, \hat{B}, \hat{\pi})$ which maximizes $\Pr(\bar{E}|\Gamma)$, where $\bar{E}$ is the empirically obtained error sequences. The basic training procedures for obtaining the most probable First and Second-Order SHFMM that depicts the empirical error sequences is discussed in Section 3.4.2 and Section 3.4.3 respectively. Furthermore, Section 4.9 describes an end-to-end methodology and procedure for obtaining an accurate First-Order SHFMM parameter sets analytically validated through performance metrics such as: log-likelihood error-free run distribution, error probabilities, mean square error (MSE) and Chi-square (χ^2) test.

7.4 Experimental Setup

In [19], we study an NB-PLC channel modeling using the USRP for single-carrier M-ary Phase Shift Keying (M-PSK) NB-PLC transceiver development. The same arrangement of the measurement testbed is adopted in this work, but with a novel development of a reconfigurable software-defined NB-PLC transceiver using multi-carrier OFDM modulations as discussed in Section 4.8.2. No alteration is done to the hardware setup in [19], but changes are made in the implementation of the signal processing algorithms since a multi-carrier OFDM modulation is adopted here.

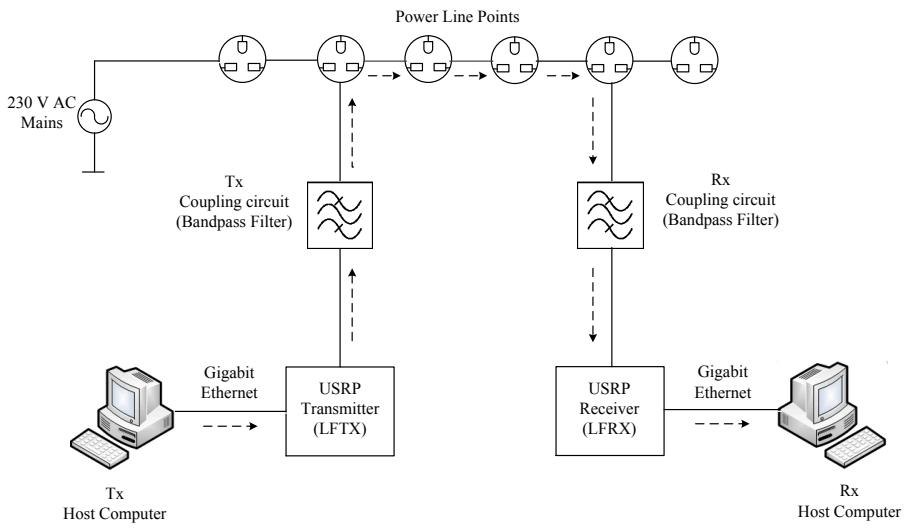

FIGURE 7.5: Experimental setup architecture showing data flow

An architecture of the experimental testbed deployed is shown in Figure 7.5, illustrating the direction of flow of the transmitted signal/data from the host TX computer to the host RX computer. The USRP modules with the LFTX and LFRX daughterboard are configured as the transmitter (TX) and the receiver (RX) respectively and are controlled by their individual Host computer through a gigabit Ethernet cable. The transmitting USRP is connected through its radio frequency (RF) output port to a coupling circuit designed as a bandpass filter (differential mode coupling) and utilized in coupling the transmitted data onto the PLC channel. On the receiving side, the receiver coupling circuit which is also a differential mode bandpass filter (capacitive coupler) decouples the signal from the PLC network and couples it onto the RF input port of the receiving USRP, and sent through the gigabit Ethernet cable to the RX host computer for post-processing and analysis.

In [79], three distinctive measurement scenarios were identified namely, the *"heavily disturbed"* scenario, the *"medium disturbed"*scenario and the "*weakly disturbed*" scenario. Here, we defined and considered only two distinct scenarios, the "*mildly disturbed*" and "*heavily disturbed*" because significant number of error events are needed in order for the error sequence to accurately define the model. In the "mildly disturbed" scenario, empirical data were captured in the morning between the hours of 10-12am when some of the appliances are not active on the network and interfering end-user appliances are at their normal positions on the network while, for the "heavily disturbed" scenario, empirical data were obtained in the evening between 5-7pm when several end-user appliances were active on the network with some closer to the receiver. Table 7.1 shows the OFDM parameters used.

Table 7.1: OFDM parameters set

Parameter	**Value**
Modulation	QPSK, DQPSK and D8PSK
Frequency band	Start: 35.9 kHz and Stop: 90.6 kHz
Sampling frequency	400 kHz
Sub-carrier spacing	1.5625 kHz
FFT Size	64
Cyclic prefix length	16
OFDM symbol duration	695 μs
Sample Duration	2.5 μs

7.5 Results and Analysis

This section discusses the analytical validation of the realized model results, the First-Order and Second-Order SHFMM estimated state transition probabilities documented in Appendix D. The estimated error statistics of the realized SHFMMs have been analytically validated in terms of log-likelihood, error-free run distribution, error probabilities, mean square error (MSE) and Chi-square (χ^2) test. The estimated Second-Order SHFMMs have been analytically validated to be superior to the First-Order SHFMMs although at the expense of more computational complexity. The reliability of the model is confirmed by an excellent match between the empirical data and SHFMM generated data as shown by the error-free run distribution plot.

7.5.1 The Log-likelihood Ratio Plots

Figure 7.6 and Figure 7.7 show the First and Second-Order log-likelihood ratio plot for the mildly disturbed scenario. The goal of any communication model is to derive the most likely parameter values given the empirical or simulated data, in essence, to determine a set of parameter estimates that depicts the empirical data. Lots of procedures utilize the log-likelihood, rather than the likelihood itself, based on the fact that it is easier to work with.

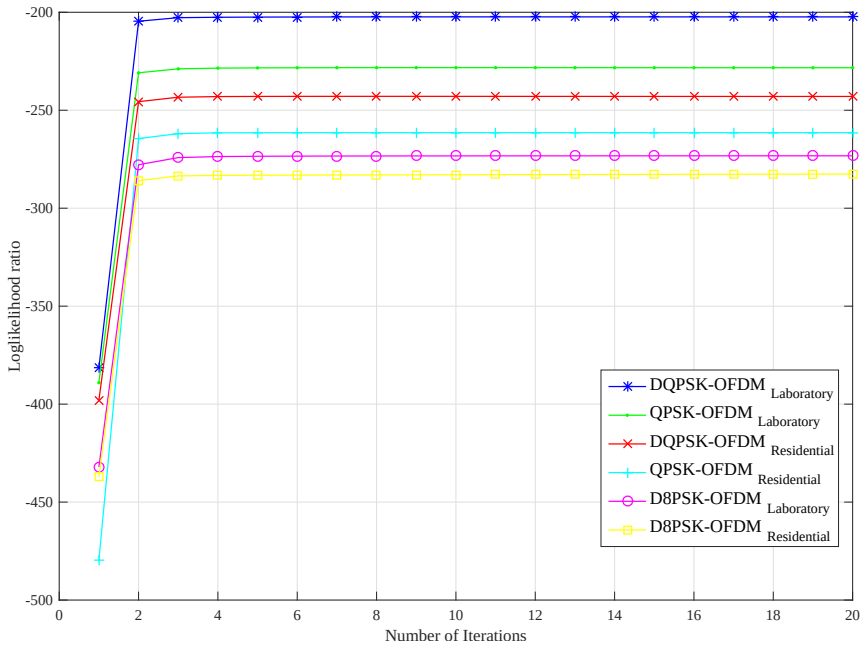

FIGURE 7.6: First-Order log-likelihood ratio plot (mildly disturbed scenario)

In essence, log-likelihood ratio is employed to access a model's fitness. Log-likelihood values are constantly negative, with high values (closer to zero) establishing a better fitting model. These values cannot be utilized alone as an index of fitness because these values are a function of data size but can be utilized in comparing the fitness of different model parameter given an empirical data. Thus, Figure 7.6 shows the log-likelihood plot of the most probable First-Order SHFMM out of the 81 estimated SHFMM for the mildly disturbed scenario. A comparison of Figure 7.6 and Figure 7.7 show that the Second-Order SHFMM is a better fitting model as the Log-likelihood value is closer to zero than that of the First-Order SHFMM, thus validating the superiority of the Second-Order SHFMMs over the First-Order SHFMMs.

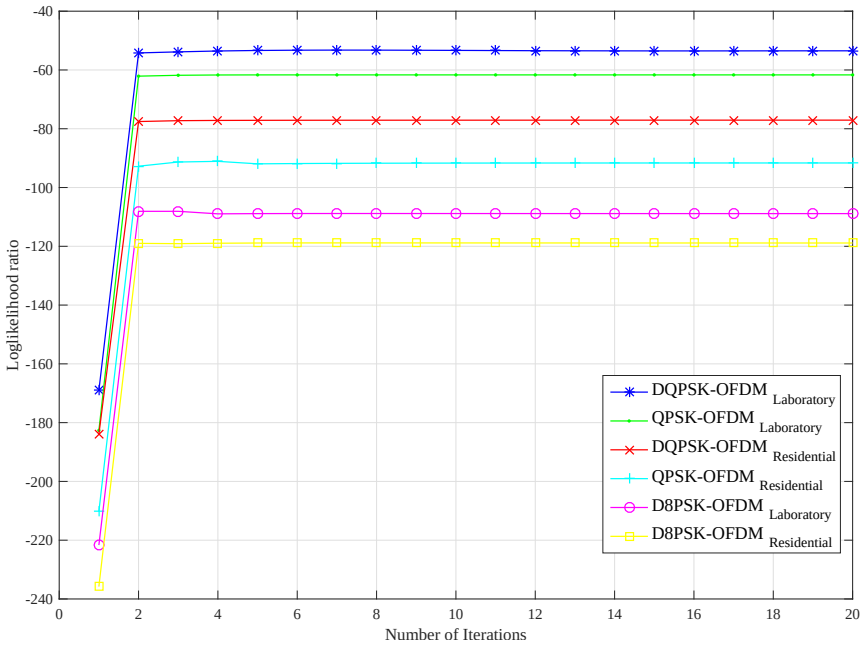

FIGURE 7.7: Second-Order log-likelihood ratio plot (mildly disturbed scenario)

Furthermore, In Figure 7.6, it can be deduced that the OFDM scheme with the best fit model is the DQPSK-OFDM laboratory, while the D8PSK-OFDM residential has a log-likelihood value that is the farthest from zero. Likewise, in Figure 7.7, a similar trend is recorded.

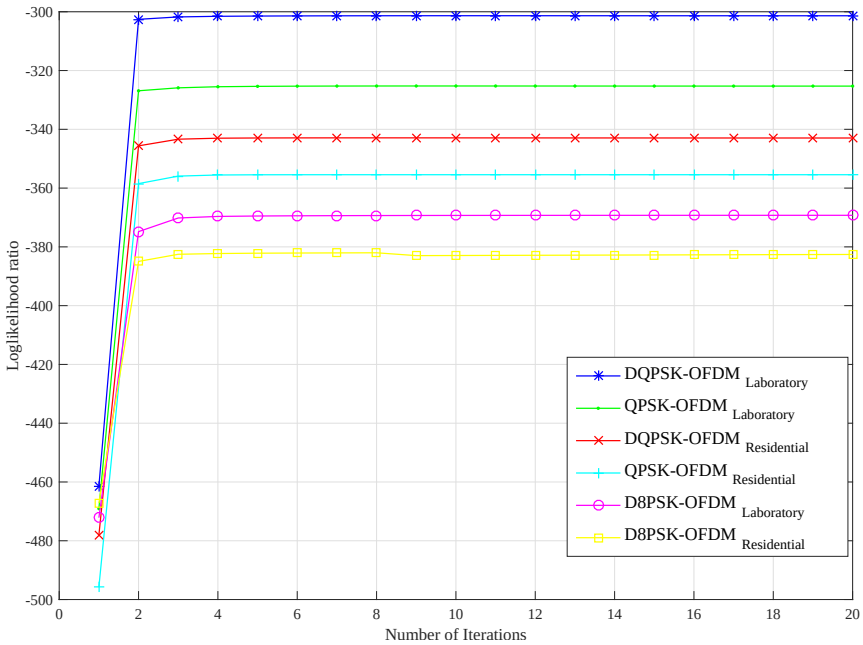

FIGURE 7.8: First-Order log-likelihood ratio plot (heavily disturbed scenario)

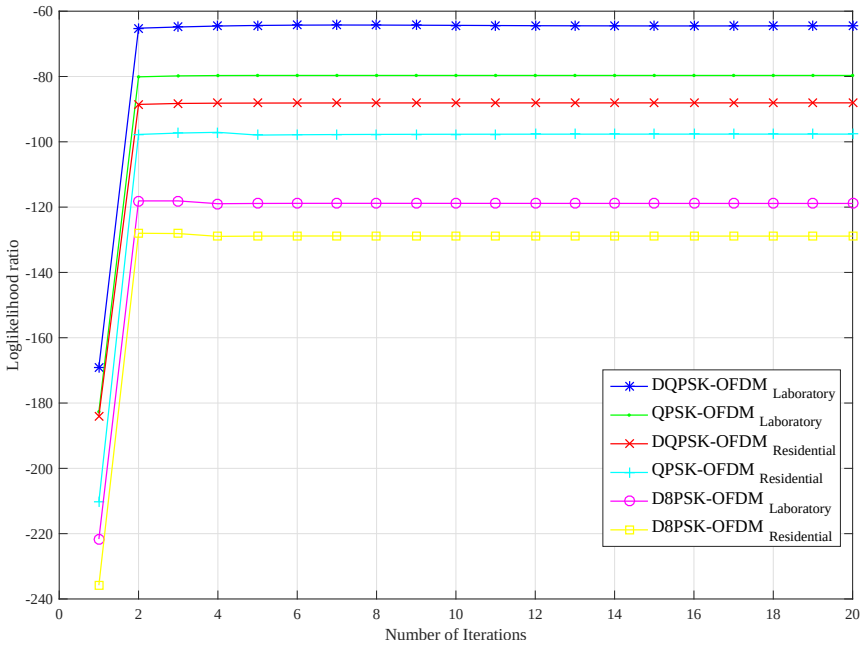

FIGURE 7.9: Second-Order log-likelihood ratio plot (heavily disturbed scenario)

Figure 7.8 and Figure 7.9 show the First and Second-Order log-likelihood ratio plot for the heavily disturbed scenario. Figure 7.8 shows the log-likelihood plot of the most probable First-Order SHFMM out of the 81 estimated SHFMM for the heavily disturbed scenario. A comparison of Figure 7.8 and Figure 7.9 show that the Second-Order SHFMM is a better fitting model as the Log-likelihood value is closer to zero than that of the First-Order SHFMM, thus validating the superiority of the Second-Order SHFMMs over the First-Order SHFMMs. It can also be deduced from Figure 7.8 and Figure 7.9 that OFDM scheme with the best fit model is the DQPSK-OFDM laboratory, while the D8PSK-OFDM residential has a log-likelihood value that is the farthest from zero.

7.5.2 The Error-free Run Distribution Plots

The error-free run distribution denoted by $Pr(0^m|1)$ is another performance metric used to validate the fitness of a model. The error-free run distribution depicts the probability of transitioning to m consecutive error-free state following the occurrence of an error.

Figure 7.10 and Figure 7.11 show the First and Second-Order SHFMM error-free run distribution plot for the mildly disturbed scenario. Figure 7.10 depicts the error-free run distribution of the most probable First-Order SHFMM out of the 81 model estimated First-Order

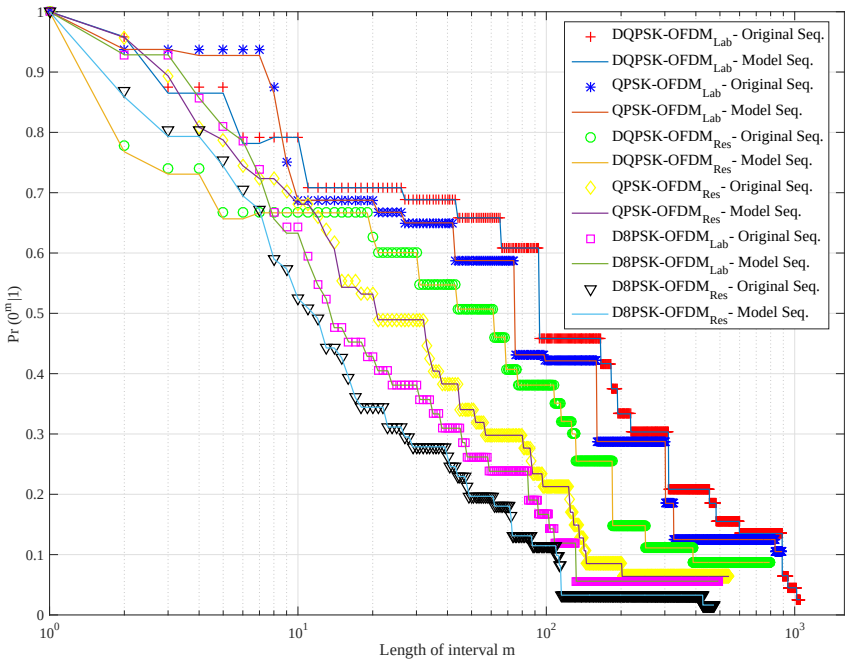

FIGURE 7.10: First-Order error-free run distribution plot (mildly disturbed scenario)

SHFMM. The reliability of both First and Second-Order SHFMM results is confirmed by a close match between the empirical error sequence and SHFMM re-generated error sequence as shown by the error-free run distribution plots in Figure 7.10 and Figure 7.11.

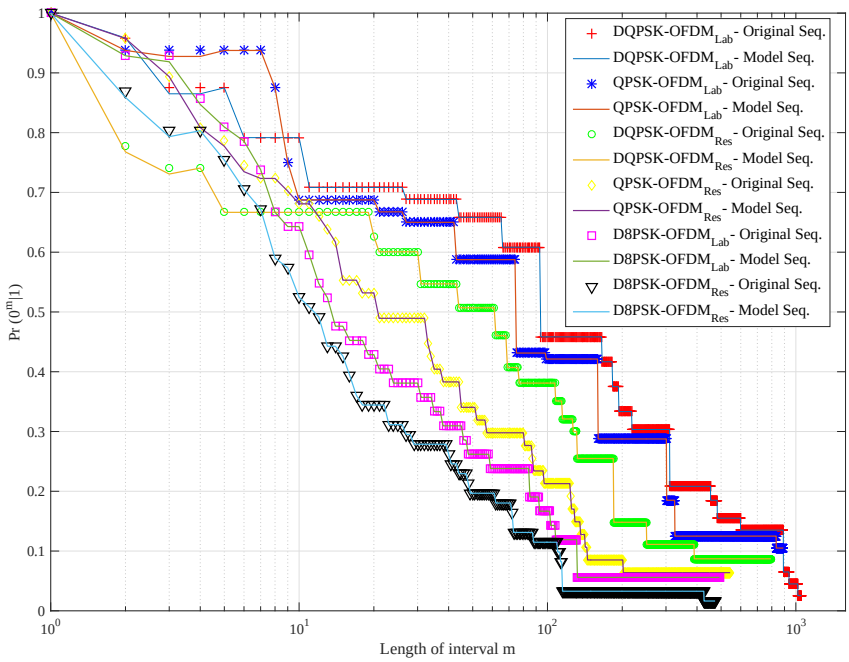

FIGURE 7.11: Second-Order error-free run distribution plot (mildly disturbed scenario)

A closer look shows that error-free run distribution plot for the Second-Order SHFMM in Figure 7.11 has a more excellent match between the empirical error sequence and SHFMM re-generated error sequence compared to the error-free run distribution plot for the First-Order SHFMM in Figure 7.10. This thus validates the superiority of the Second-Order SHFMM over the First-Order SHFMM.

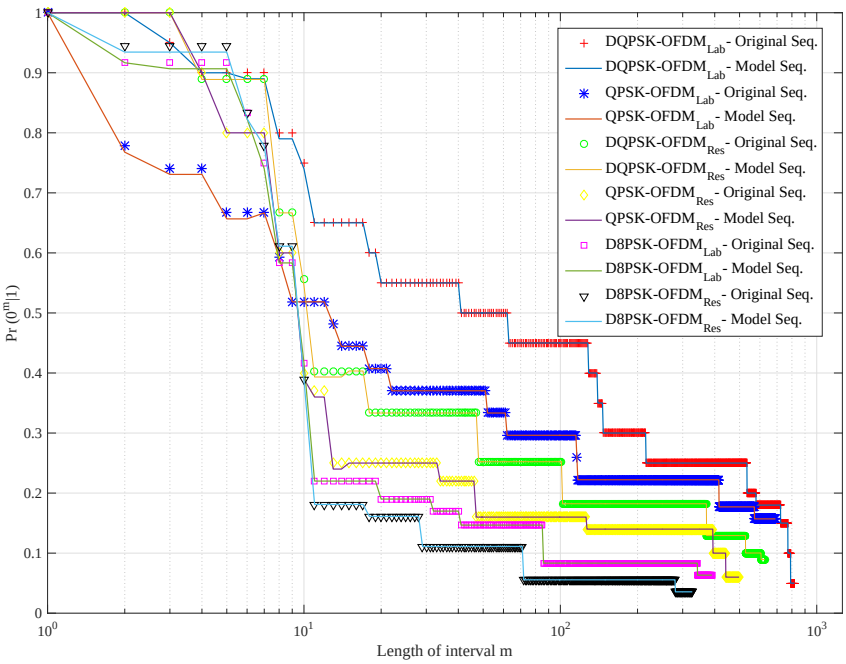

FIGURE 7.12: First-Order error-free run distribution plot (heavily disturbed scenario)

Figure 7.12 and Figure 7.13 show the First and Second-Order SHFMM error-free run distribution plot for the mildly disturbed scenario. Figure 7.12 depicts the error-free run distribution of the most probable First-Order SHFMM out of the 81 model estimated First-Order SHFMM. The reliability of both First and Second-Order SHFMM results is confirmed by a close match between the empirical error sequence and SHFMM re-generated error sequence as shown by the error-free run distribution plots in Figure 7.12 and Figure 7.13. A closer look shows that error-free run distribution plot for the Second-Order SHFMM in Figure 7.13 has a more excellent match between the empirical error sequence and SHFMM re-generated error sequence compared to the error-free run distribution plot for the First-Order SHFMM in Figure 7.12. This thus validates the superiority of the Second-Order SHFMM over the First-Order SHFMM. It is evident that the EFRD ($Pr(0^m|1)$) is a monotonically decreasing function of m in such a way that $Pr(0^0|1) = 1$ and $Pr(0^m|1) \rightarrow 0$, which implies that it consistently decreases and never increases in value [168], as seen in EFRD plots.

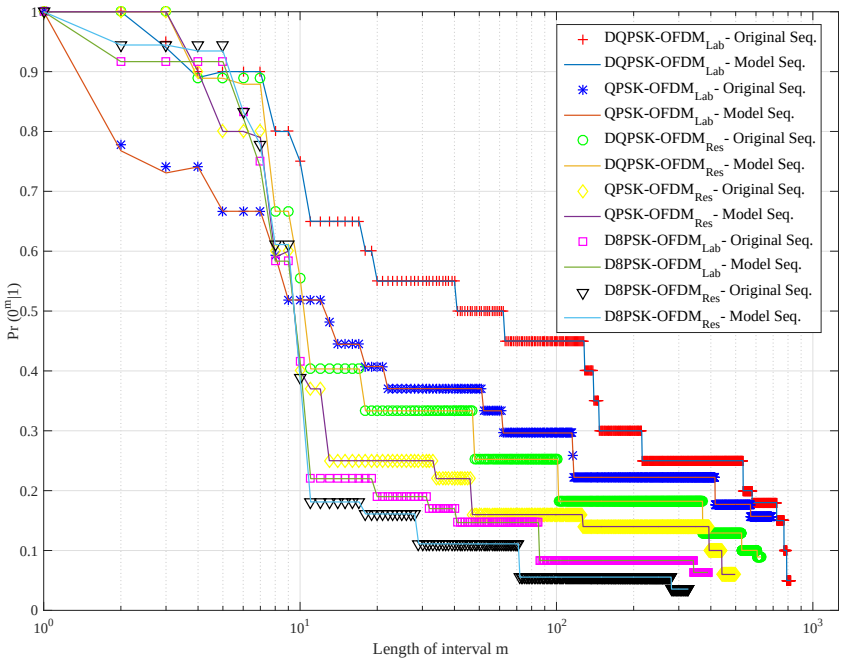

FIGURE 7.13: Second-Order error-free run distribution plot (heavily disturbed scenario)

7.5.3 The First and Second-Order Model Error Probabilities

The error probability of a model is also used to ascertain the fitness of a model. A perfect or close agreement between the error probability of the empirical error sequences and the model regenerated error sequence validates the fitness of the model.

TABLE 7.2: First and Second-Order Error probabilities for measured original error sequence (P_e) and model regenerated error sequence ($\bar{P}_e$)- (mildly disturbed scenario)

	Residential			Laboratory		
	QPSK OFDM	DQPSK OFDM	D8PSK OFDM	QPSK OFDM	DQPSK OFDM	D8PSK OFDM
P_e (1st-Order)	0.0444	0.0325	0.0580	0.0290	0.0141	0.0509
$\bar{P}_e$ (1st-Order)	0.0432	0.0313	0.0569	0.0279	0.0130	0.0499
P_e (2nd-Order)	0.0444	0.0325	0.0580	0.0290	0.0141	0.0509
$\bar{P}_e$ (2nd-Order)	0.0441	0.0322	0.0578	0.0287	0.0139	0.0506

Table 7.2 shows the First and Second-Order Error probabilities for the mildly disturbed scenarios, while Table 7.3 shows the First and Second-Order Error probabilities for the

TABLE 7.3: First and Second-Order error probabilities for measured original error sequence (P_e) and model regenerated error sequence ($\bar{P}_e$)- (heavily disturbed scenario)

	Residential			Laboratory		
	QPSK OFDM	DQPSK OFDM	D8PSK OFDM	QPSK OFDM	DQPSK OFDM	D8PSK OFDM
P_e (1st-Order)	0.0525	0.0429	0.0699	0.0356	0.0231	0.0613
$\bar{P}_e$ (1st-Order)	0.0514	0.0417	0.0687	0.0343	0.0220	0.0601
P_e (2nd-Order)	0.0525	0.0429	0.0699	0.0356	0.0231	0.0613
$\bar{P}_e$ (2nd-Order)	0.0521	0.0426	0.0696	0.0353	0.0229	0.0610

heavily disturbed scenarios. Table 7.2 shows the error probabilities for the most probable First-Order SHFMM out of the 81 estimated First-Order SHFMM. Table 7.2 and Table 7.3 show a close agreement between the error probability of the empirical error sequence and the model regenerated error sequence, in other words this depicts a correlation between both error probability, hence validating the fitness of the model. Table 7.3 shows a more excellent agreement between error probability of the empirical error sequence and the model regenerated error sequence thus validating the superiority of the Second-order SHFMM over the First-Order SHFMM.

A close look at Table 7.2 shows that DQPSK-OFDM laboratory has the best performance (lowest error) in terms of the probability of error recorded, while D8PSK-OFDM residential has the worst performance as it has the highest error probability. A similar trend is deduced from Table 7.3 except for larger error probabilities recorded for this scenario due to the heavily disturbed scenario considered. Otherwise, DQPSK-OFDM laboratory has the best performance (lowest error probability), while D8PSK-OFDM residential has the worst performance as it has the highest error probability. The difference in error probabilities between the different OFDM scheme utilized can be attributed to the fact that practically no two error vectors can be identical. This is because each of the modulation scheme used in this article are more robust than each other, hence, in the presence of similar noise impairment levels they perform better than each other. The modulation scheme with the most superior spatial proximity and angular separation or Euclidean distance on the constellation graph performs better [102].

Note also, that the computation of the recursive Forward probability function (α) and backward probability function (β) requires the order of N^2T operations for the First-Order compared to the order of (N^3T) operations for the Second-Order estimation. Hence, there is a trade-off in terms of computational complexity, as training of a Second-Order model is more computationally intensive than training it's First-Order counterpart.

7.5.4 The Mean Square Error (MSE) and Chi-square Test

The mean square error (MSE) and Chi-square (χ^2) test are two other useful metrics used in ascertaining and validating a model's accuracy and fitness. The χ^2 and MSE values ascertains and validate the correlation between empirical error sequence (the observed sequence) and model regenerated sequence (the expected sequence). Refer to the later part of Section 4.9.2 for the mathematical equation used in computing the mean square error (MSE) and Chi-square (χ^2).

TABLE 7.4: Chi-square and MSE for the First and Second-Order models (mildly and heavily disturbed scenarios)

		Chi-Square (χ^2)		MSE	
		Mildly	Heavily	Mildly	Heavily
$DQPSK_{OFDM-LAB}$	1st Order	3.4682e-04	8.5705e-04	2.8517e-07	7.3260e-07
	2nd Order	2.3121e-04	2.1874e-04	1.9011e-07	2.4420e-07
$QPSK_{OFDM-LAB}$	1st Order	3.2345e-04	1.0000e-03	3.3708e-07	1.0145e-06
	2nd Order	2.1563e-04	2.6709e-04	2.2472e-07	2.8986e-07
$DQPSK_{OFDM-RES}$	1st Order	4.0394e-04	1.4000e-03	3.7831e-07	9.5694e-07
	2nd Order	2.6709e-04	2.2756e-04	2.5221e-07	3.1898e-07
$QPSK_{OFDM-RES}$	1st Order	5.5229e-04	1.6000e-03	5.5147e-07	1.0040e-06
	2nd Order	2.6477e-04	2.9607e-04	3.6765e-07	4.0161e-07
$D8PSK_{OFDM-LAB}$	1st Order	4.8690e-04	7.6189e-04	6.0852e-07	1.5385e-06
	2nd Order	2.2691e-04	2.5659e-04	4.0568e-07	5.1282e-07
$D8PSK_{OFDM-RES}$	1st Order	3.6855e-04	1.0000e-03	6.3425e-07	2.4465e-06
	2nd Order	2.4249e-04	2.1403e-04	4.2283e-07	6.1162e-07

Table 7.4 shows a comparison of the computed Chi-Square and MSE values for the First and Second-Order SHFMM (mildly and heavily disturbed scenarios). The First-Order SHFMM

chi-Square and MSE values represents the best fit model, in other words, the First-Order SHFMM chi-Square and MSE values depict the most probable First-Order SHFMM out of the 81 estimated SHFMM. It can be deduced from Table 7.4 that the chi-Square and MSE values for the Second-Order SHFMMs represent a better fitting model as the values are closer to zero than the chi-Square and MSE values for the First-Order SHFMMs. This thus validates and establishes the superiority of the Second-Order SHFMMs over the First-Order SHFMMs.

Note, optimized model results obtained based on M-H algorithm for the modeling effort in this Chapter is presented in Section B.3 of Appendix B.

7.6 Conclusion

In this Chapter, we have reported a novel implementation of a QPSK, DQPSK and D8PSK-OFDM NB-PLC systems, utilizing the Universal Software Radio Peripheral (USRP) as a tool for the transceiver design. We also report an experimental NB-PLC channel burst error measurement based on real life transmission at two urban locations (residential and laboratory) in Johannesburg taking into consideration two interference scenarios (mildly and heavily disturbed). And contrary to simulation based modeling often reported in literatures, we have reported an empirical based First and Second-Order SHFMM of the burst-error obtained on the CENELEC A-Band NB-PLC channel. The popular iterative Baum-Welch algorithm is employed in obtaining the re-estimated First and Second-Order model parameters for the empirically obtained error sequences for the three OFDM schemes used. The error statistics of the realized First and Second-Order SHFMMs were analytically validated in terms of log-likelihood, error-free run distribution, error probabilities, mean square error (MSE) and Chi-square (χ^2) test. Results showed through analytical validation the superiority of the Second-Order SHFMMs over the First-Order SHFMMs although at the expense of additional computational complexity. The reliability of both First and Second-Order model results were also confirmed by an excellent match between the empirical error sequences and SHFMM re-generated error sequences as shown by the error-free run distribution plot. Performance analysis shows that DQPSK-OFDM is the most robust scheme, while D8PSK-OFDM is the least robust scheme. The realized models can be used to facilitate the design of FEC to exploit and mitigate noise on the NB-PLC channel.

CHAPTER 8

Metropolis-Hastings Algorithm for Parameter Optimization of Semi-Hidden Fritchman Markov Model for NB-PLC Channel

The problem of models realized through EM algorithms such as the iterative Baum-Welch algorithm is the problem of locally maximized model results and not the sort after near optimal model results (global maxima). This chapter presents a novel Metropolis-Hastings algorithm for optimizing the parameters of the proposed SHFMM. The optimized modeling results are guaranteed to have optimized parameter sets which are globally maximized as opposed to locally maximized parameter sets obtained by the use of only a maximum likelihood parameter estimation techniques such as Baum-Welch algorithm.

8.1 Metropolis-Hastings Conventional Derivation

MetropolisHastings (M-H) algorithm is aimed at generating a group of states according to a desired distribution $P(\theta^{(t-1)})$. In order to achieve this, M-H algorithm utilizes a Markov process that asymptotically arrives at a distinct stationary distribution $\pi(\theta^{(t-1)})$ in a way that $\pi(\theta^{(t-1)}) = P(\theta^{(t-1)})$.

Markov processes are unambiguously defined by their crossover probabilities, $P(\theta^*|\theta^{(t-1)})$, which implies the probability of crossing over from any given state $\theta^{(t-1)}$, to another given state θ^*. They possess a distinct stationary distribution denoted by $\pi(\theta^{(t-1)})$, should the following conditions be satisfied.

1. *A stationary distribution* $\pi(\theta^{(t-1)})$*, must exist*: "detailed balance" is a sufficient but not essential condition which demands reversibility for each transition, that is transitions $\theta^{(t-1)} \rightarrow \theta^*$ and $\theta^* \rightarrow \theta^{(t-1)}$ is possible. Thus, for all pair of states $\theta^{(t-1)}$,

θ^*, the probability of being in state $\theta^{(t-1)}$ and crossing over to state θ^* must be equivalent to the probability of being in state θ^* and crossing over to state $\theta^{(t-1)}$, $\pi(\theta^{(t-1)})P(\theta^*|\theta^{(t-1)}) = \pi(\theta^*)P(\theta^{(t-1)}|\theta^*)$.

2. *Unique stationary distribution*: a unique stationary distribution $\pi(\theta^{(t-1)})$ must exist. The ergodicity of the Markov process ensures this, and this demands that all state must: (i) be Aperiodic- that is the Markov chain is not expected to return to the same state at fixed intervals; and (ii) be positive recurrent- that is, the anticipated number of steps required to return to the same state is finite.

The M-H algorithm entails the design of a Markov chain process (by creating transition or crossover probabilities) fulfilling the above two conditions, in such a way that $\pi(\theta^{(t-1)})$, its unique stationary distribution is selected to be $P(\theta^{(t-1)})$. The derivation of the M-H algorithm begins with writing out an expression for the detailed balance condition.

$$P(\theta^*|\theta^{(t-1)})P(\theta^{(t-1)}) = P(\theta^{(t-1)}|\theta^*)P(\theta^*) \tag{8.1}$$

Rewriting Equation (8.1), we have

$$\frac{P(\theta^*|\theta^{(t-1)})}{P(\theta^{(t-1)}|\theta^*)} = \frac{P(\theta^*)}{P(\theta^{(t-1)})} \tag{8.2}$$

The end goal is the separation of the transition into two sub-steps; first the proposal sub-step, and then the acceptance-rejection sub-step. The conditional probability that a state θ^* is proposed given $\theta^{(t-1)}$ represents the *proposal distribution* denoted by $g(\theta^*|\theta^{(t-1)})$, while the conditional probability of accepting θ^* the proposed state is represented by the *acceptance distribution* denoted by $A(\theta^*|\theta^{(t-1)})$. The transition probability can thus be expressed as a product of the proposal and acceptance distribution as follows.

$$P(\theta^*|\theta^{(t-1)}) = g(\theta^*|\theta^{(t-1)})A(\theta^*|\theta^{(t-1)}) \tag{8.3}$$

Similarly,

$$P(\theta^{(t-1)}|\theta^*) = g(\theta^{(t-1)}|\theta^*)A(\theta^{(t-1)}|\theta^*) \tag{8.4}$$

Substituting Equations (8.3) and (8.4) into Equation (8.2), we have

$$\frac{g(\theta^*|\theta^{(t-1)})}{g(\theta^{(t-1)}|\theta^*)}\frac{A(\theta^*|\theta^{(t-1)})}{A(\theta^{(t-1)}|\theta^*)} = \frac{P(\theta^*)}{P(\theta^{(t-1)})} \tag{8.5}$$

$$\frac{A(\theta^*|\theta^{(t-1)})}{A(\theta^{(t-1)}|\theta^*)} = \frac{P(\theta^*)}{P(\theta^{(t-1)})}\frac{g(\theta^{(t-1)}|\theta^*)}{g(\theta^*|\theta^{(t-1)})} \tag{8.6}$$

The subsequent derivation step is the choice of acceptance that satisfies the condition above. A common option is the Metropolis choice:

$$A(\theta^*|\theta^{(t-1)}) = min\left(1, \frac{P(\theta^*)}{P(\theta^{(t-1)})}\frac{g(\theta^{(t-1)}|\theta^*)}{g(\theta^*|\theta^{(t-1)})}\right) \tag{8.7}$$

In essence, when the acceptance is bigger than 1, we accept, else we reject if the acceptance is smaller than 1. The M-H algorithm practical realization thus consist of the following steps.

1. *Initialization step*: An initial state $\theta^{(t-1)}$ is randomly selected;
2. *Proposal step*: random selection of a state θ^* according to the proposal distribution $g(\theta^*|\theta^{(t-1)})$;
3. *Acceptance and rejection step*: the proposed state is accepted according to the acceptance ratio $A(\theta^*|\theta^{(t-1)})$. If the proposed state is rejected, no transition, hence no update is required. Else, acceptance of the proposed state will effect a transition to the proposed state θ^*;
4. Return to step 2 until T number of states are generated;
5. Save the state $\theta^{(t-1)}$ and then return to 2.

Note, in principle, the saved states are pulled or drawn from the distribution $P(\theta^{(t-1)})$, while step 4 of the M-H algorithm guarantees they are de-correlated. Furthermore, the choice of T must be according to factors like the proposal distribution and conventionally, of the order of the autocorrelation time of the Markovian process.

In a general problem, there is no clear definition of the proposal distribution $g(\theta^*|\theta^{(t-1)})$ one ought to utilize, hence, its a free parameter of the M-H algorithm that must be carefully adapted to the peculiar problem in hand.

8.2 Metropolis-Hastings Algorithm Procedure

In this Section, a step-by-step procedure of how the M-H algorithm is used to optimize SHFMM parameters is presented, as well a block diagram representation of these procedures. Before applying the M-H algorithm for parameter optimization of the SHFMM models, the following tasks must be carried out in order to obtain the input data fed into the M-H algorithm.

1. Generate and obtain error sequence based on real-time experimental measurement on the NB-PLC channel.
2. Assume 81 initial SHMM parameters.
3. Train the Baum-Welch algorithm with the 81 initial model parameters using the above generated error sequence as training input to obtain 81 re-estimated SHMM model parameters.
4. Utilize the 81 model regenerated parameters to generate 81 error sequences with the same length as the original experimentally obtained error sequence. The original experimentally obtained error sequence and 81 model regenerated error sequences are fed as input to the Metropolis-Hasting algorithm as presented as follows.

The following procedural steps depicts how the Metropolis-Hastings algorithm is used to optimize the SHMM parameters in order to obtain an optimized parameter set guaranteed to have a global maximized likelihood as opposed to parameter sets obtained using maximum likelihood estimation techniques which are locally maximized.

1. Load the input: both experimentally obtained error sequence and the 81 model regenerated error sequences.
2. Assume a proposal distribution. A uniform distribution is assumed in this case as the proposed prior. Define some constants: nSamples representing the number of samples and burnIn number to discard some of the first draws. Burnin =500, while nSamples = 10,000 (same as length of error sequence).

3. Toss a coin or randomly sample from between 1-81, representing the number of generated models from the original measured error sequence.

4. Compute the posterior probability of the chosen model with respect to the original measured sequence.

5. Compute the corrected acceptance ratio as follows:

   The correction factor denoted by "c" is mathematically written as:

$$c = \frac{g(\theta^{(t-1)}|\theta^*)}{g(\theta^*|\theta^{(t-1)})} \tag{8.8}$$

   The corrected acceptance ratio formula is thus written as follows.

$$alpha = min\left(1, \frac{P(\theta^*)}{P(\theta^{(t-1)})}\frac{g(\theta^{(t-1)}|\theta^*)}{g(\theta^*|\theta^{(t-1)})}\right) \tag{8.9}$$

   Where $P(\theta^*)$ is the current posterior probability and $P(\theta^{(t-1)})$ is the previous posterior probability. Since the proposed prior is assumed as a uniform distribution, the correction factor "c" is thus equals to 1. Consequently, Equation (8.9) is thus simplified as follows.

$$alpha = min\left(1, \frac{P(\theta^*)}{P(\theta^{(t-1)})}\right) \tag{8.10}$$

6. Generate U from a uniform distribution (0,1). Toss a coin or sample to either accept or reject based on the computed acceptance ratio. If u $\leq$ alpha, accept the $P(\theta^*)$ and save, else reject. This results into a sequence of accepted models. Return to step 3 until T number of states are generated, where T is equivalent to nSamples which is equals to 10,000 and until convergence is achieved.

7. Plot the Markov chain showing the sampling path and a histogram showing the exact prior as opposed to assumed proposed prior. In other words, the histogram shows the model with the highest probablity of occurence, which invariably is the model closest to the global maximum, hence, the near optimal model amongst the 81 models obtained models.

8.3 Results and Analysis

In this section analysis of optimized model results is presented. The Markov chain for the M-H sampling shows the sampling path, while the corresponding histogram shows the exact prior given the empirical error sequence and the 81 model re-generated error sequences. In otherwords, the M-H algorithm converges to the most probable model.

Figure 8.1, Figure 8.3 and Figure 8.5 show the Markov chain sampling path for the converged samples, while Figures 8.2, 8.4 and Figure 8.6 show the converged model samples with the exact distribution as opposed to the uniform distribution assumed.

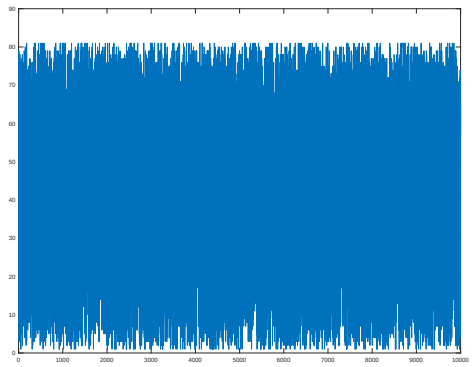

FIGURE 8.1: Markov chain showing sampling path

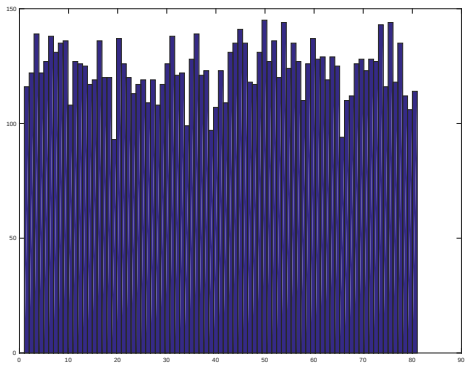

FIGURE 8.2: Histogram showing the exact distribution given observed data

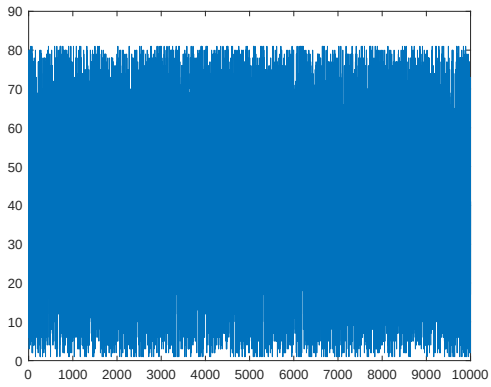

FIGURE 8.3: Markov chain showing sampling path

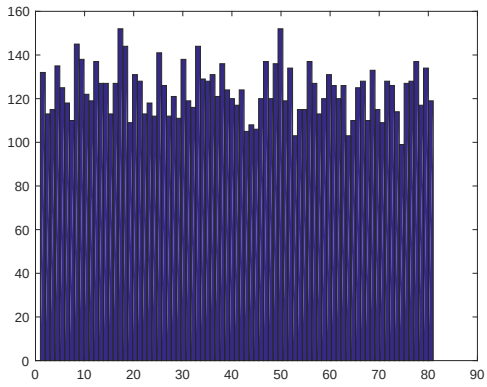

FIGURE 8.4: Histogram showing the exact distribution given observed data

It can be deduced from Figures 8.2, 8.4 and Figure 8.6 that model 50 has the highest occurence from the converged sampling results. This implies that model 50 is invariably the model closest to the global maximum, hence, its the near optimal model amongst the 81 Baum-Welch regenerated models obtained from experimentally obtained error sequence. In contrast, model 18 was analytically chosen based on the use of the iterative Baum-Welch algorithm to select the model that is the most probable given the $QPSK - OFDM$ empirically obtained error sequence and the initial model.

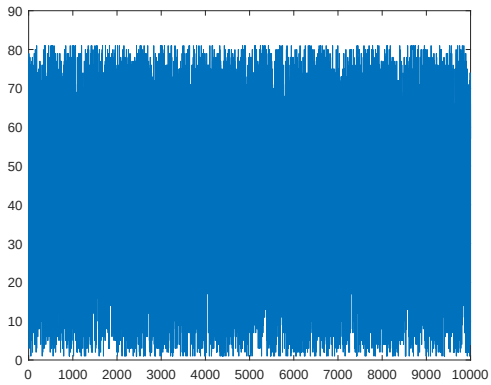

FIGURE 8.5: Markov chain showing sampling path

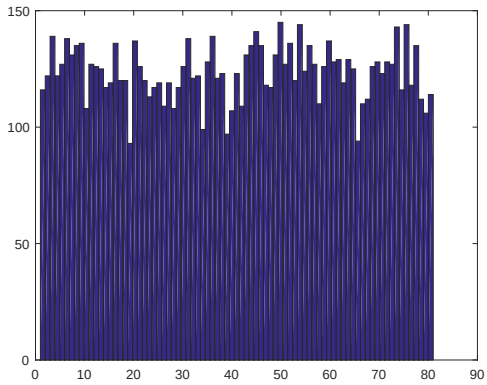

FIGURE 8.6: Histogram showing the exact distribution given observed data

8.4 Conclusion

The problem of locally maximized model results is often associated with Maximum likelihood estimation algorithm such as Baum-Welch algorithm used to adjust the parameters of semi-hidden Fritchman Markov models. In this chapter, an improved method for optimization of model results obtained based on MLE algorithm is proposed. A Metropolis-Hastings algorithm based on Markov Chain Monte Carlo Bayesian inference techniques is developed. As deduced from the results analysis, the algorithm is used to obtain a near optimal model from amongst 81 regenerated models for a particular experimentally obtained error sequence. The near optimal chosen model is guaranteed to have model parameter set that is globally maximized and depict the measured error sequence.

CHAPTER 9

Conclusion

This Chapter concludes and gives final remarks on this thesis. This Chapter delineates the overall contribution of this work by first presenting an abridged overview of the aim and achievement of this work. Subsequently, the outcome of each Chapter is concisely discussed to provide a general outlook of the precise contributions presented in each Chapter. Future research possibilities and recommendations are further stated, while final remarks are given to conclude this Chapter.

9.1 Thesis Summary and Key Results

This thesis title "Classification and Modeling of Power Line Noise using Machine Learning Techniques" expatiates the overall aim and objectives of this study. More realistically, this thesis is aimed at the realization of a flexible, interoperable and reconfigurable software defined NB-PLC transceiver utilizing a USRP. Furthermore, the aim of this work is also to realize and achieve optimized and precise channel models for the NB-PLC channel with the intent of using these precise channel model to first improve the modulation scheme and furthermore facilitate a more robust and reliable communication on the noisy channel through design and evaluation of FEC codes capable of exploiting the noise impairments on the channel to achieve improved overall system performance. The problem of noise, perturbation and interferences experienced on the NB-PLC channel is first introduced in Chapter 1, while the need for a flexible and reconfigurable NB-PLC transceiver as well as precise and optimized channel models based on experimental measurement rather than simulation based approach is also justified.

In Chapter 2, technical background details and review of power line communication and visible light communication are presented. PLC frequency bands classification and topologies, PLC regulations, PLC specifications and standards, PLC channel characteristics, PLC

channel modeling, PLC noise characteristics and classification, PLC single-carrier and multi-carrier modulation and background on visible light communications and the advantages it offers are well expounded.

Chapter 3 presents a technical background on conventional HMMs and the adopted First and Second-Order SHFMM used in modeling the NB-PLC channel errors resulting from noise impairments. Chapter 3 also delineates the First and Second-Order Baum-Welch algorithm, a class of Maximum Likelihood Estimation (MLE) algorithm utilized in training the SHFMM given empirical data in order to realize the most probable SHFMM that depicts the empirical data. In addition, Metropolis-Hastings (M-H)algorithm, a Bayesian inference statistical algorithm based on Markov Chain Monte Carlo technique used in optimizing model results obtained based on MLE is discussed. The capability of the M-H algorithm to solve the problem of locally maximized model results obtained from MLE approach and to realize models with rich parameter sets guaranteed to be near optimal and closer to the global maxima is reiterated.

Chapter 4 presents a detailed step-by-step guide on the development of the novel reconfigurable NB-PLC transceivers for both single-carrier (BPSK, DBPSK, QPSK and DQPSK) and multi-carrier OFDM modulation (QPSK-OFDM, DQPSK-OFDM and D8PSK-OFDM) from the hardware to the software setup and configuration. The development of the NB-PLC coupling circuits, the most important piece of hardware in the NB-PLC transceiver testbed is also discussed. Furthermore, an end-to-end depiction of the modeling methodology/approach adopted in estimating the parameters of the SHFMM based on MLE technique is discussed.

A Narrowband PLC Channel Modeling using USRP and PSK Modulations is developed in Chapter 5. The reconfigurable single-carrier NB-PLC transceiver testbed developed in Chapter 4 is used to obtain empirical error sequence used to model the burst error on the NB-PLC channel. A First-Order SHFMM of the burst error obtained empirically from the channel is carried out utilizing the efficient Baum-Welch algorithm to realize the model parameter estimates for the SHFMM. The SHFMMs are validated through analytical analysis with the validated SHFMMs depicting the most probable and precise channel models that depicts the empirical data obtained. Furthermore, the performance of the different single-carrier schemes (BPSK, DBPSK, QPSK and DQPSK) considered were compared in the

presence of similar interferers. The resulting models can be used to facilitate the design and evaluation of robust adaptive modulation and/or FEC codes capable of exploiting and mitigating errors on the noisy NB-PLC channel for an improved overall system performance for the single-carrier application.

In Chapter 6, a Semi-Hidden Markov Modeling of a Low Complexity FSK-OOK In-House PLC and VLC Integration is developed. A low cost hybrid PLC-VLC test-bed is first developed to harness the advantages of two ubiquitous communication technology, the PLC and the VLC in order to achieve both illumination and data communication. The resulting test-bed implementation leverage the existing ubiquitous power line network infrastructure to render connectivity, while we also exploit the illumination system of power-saving Light Emitting Diodes (LEDs) for wireless data communication. Thus, VLC is harnessed to offer a good complementary wireless data transmission technology to the existing In-House PLC in a similar manner broad-band Ethernet connection enjoys the support of Wi-Fi. A First and Second-Order SHFMM of the hybrid system is realized, while the superiority of the Second-Order SHFMM is validated through analytical analysis. Precise channel models obtained for the hybrid system shows a correlation between the empirical data and model regenerated data. The realized statistical model results can be used to facilitate an improved overall communication through FEC code design and evaluation as well as adapted for software reconfigurable test-bed, a robust multi-carrier scheme or adaptive modulation.

Performance Analysis of First and Second Order Fritchman Semi-Hidden Markov Model for an OFDM-based Indoor Narrowband Power Line Channel using USRP is presented in Chapter 7. The reconfigurable multi-carrier NB-PLC transceiver testbed developed in Chapter 4 is used for real-time experimental measurement to obtain empirical error sequence used to model the burst error on the NB-PLC channel. A First and a Second-Order SHFMM of the OFDM systems are realized. The performance of the different OFDM schemes (QPSK-OFDM, DQPSK-OFDM and D8PSK-OFDM) considered were compared in the presence of similar interferers. The realized SHFMMs were validated through analytical analysis with the validated SHFMMs depicting the most probable and precise SHFMM models that depicts the empirical data obtained. Moreover, the superiority of the Second-Order SHFMM is established through analytical analysis. The resultant precise channel model can be used to facilitate the design of a coded NB-PLC transceiver (such as permutation coded time

diversity scheme) to exploit and mitigate noise and resulting burst errors experienced on the NB-PLC channel.

Metropolis-Hastings Algorithm for Parameter Optimization of Semi-Hidden Fritchman Markov Model for NB-PLC is developed in Chapter 8. The problem of models obtained through MLE or Expectation Maximization (EM) algorithms is the locally maximized results and not the sort after near-optimal results (global maximum). In this Chapter, a novel M-H algorithm utilized in solving this problem is developed and used to optimize model results obtained in Chapters 5, 6, 7. The optimized models realized in this Chapter are models with rich parameter sets guaranteed to converge closer to a global maxima as opposed to locally maximized parameter sets obtained using just the maximum likelihood estimation techniques such as Baum-Welch algorithm.

Fundamentally, this study proffers solutions to the problem of non-reconfigurable, inflexible hardware based PLC transceivers by developing a flexible, reconfigurable software-defined NB-PLC transceiver system to cater for the demands of the unstable and harsh NB-PLC channel with the possibility of implementing different waveforms for several real-time scenarios without making architectural changes to the hardware. Moreover, the problem of locally maximized solutions obtained by using MLE algorithms is solved through the development of a Metropolis-Hastings algorithm based on MCMC Bayesian inference approach with guaranteed fast convergence and realization of globally maximized model parameter sets. Results in Chapters 4, 5, 6, 7 and Chapter 8 answer these thesis research questions. In general, the following significant points were deduced from this thesis:

- A flexible, reconfigurable software-defined NB-PLC transceiver system proffers a solution to the problem of hardware changes in hardware-based PLC transceiver systems as it is capable of being adapted to cater for the demands of the unstable and harsh NB-PLC channel as implementation of different waveforms for several real-time scenarios are made possible at low cost and without the need for making architectural changes to the hardware.
- A low-cost hybrid PLC-VLC system is achievable to leverage the existing ubiquitous power line network infrastructure to render connectivity, while we also exploit the illumination system of power-saving Light Emitting Diodes (LEDs) for wireless data transmission. The resulting model can be used to facilitate the design of a more flexible,

reconfigurable software-defined hybrid PLC-VLC OFDM system to achieve a more robust communication.

- The multi-carrier OFDM modulation is a more robust scheme than the single-carrier PSK modulation, thus making OFDM a modulation of choice for NB-PLC communications due to its robustness against the noise, perturbation and interferences encountered on the NB-PLC channel. Further, robustness can be achieved with the introduction of suitable and robust FEC codes in order to exploit and mitigate noise impairments on the channel. Other variants of OFDM such as constant envelope OFDM and vector OFDM can also be exploited to overcome major problems with the conventional OFDM.
- SHFMMs are suitable models for obtaining statistical models that depicts empirical measured data on the bursty NB-PLC channel.
- The superiority of the Second-Order SHFMMs over First-Order SHFMMs have been validated through analytical analysis, although at the expense of more computational complexity.
- SHFMM realized through the use of maximum likelihood estimation algorithms can be further optimized utilizing the developed Metropolis-Hastings algorithm, an MCMC Bayesian inference approach to obtain parameter sets guaranteed to be near-optimal and globally maximized.

9.2 Future Research Possibilities and Recommendations

In order to absolutely exploit the reconfigurable software-defined PLC transceiver, the validated optimized NB-PLC model results obtained and presented in this thesis, recommendations stated as follows can be carefully weighed as valuable and useful direction for prospective research possibilities.

- The modeling results can be used to design and evaluate FEC codes such as a concatenation of Reed-Solomon and Permutation codes and other robust codes suitable for noise mitigation on the low voltage NB-PLC, where OFDM is the modulation scheme of choice.

- The modeling results can also facilitate the implementation and evaluation of Time-Diversity Permutation coding scheme for simple but robust and practicable NB-PLC systems as reported in [86]. As well as consideration given to implementation of other diversity schemes such as Frequency Diversity and Spatial Diversity.

Furthermore, other future research possibilities are itemized as follows.

- Experimental implementation and performance evaluation of a constant envelope OFDM reported in [187] using the reconfigurable NB-PLC transceiver realized in this research project.
- Experimental implementation and the performance evaluation of the Adaptive Permutation Coded Differential OFDM System reported in [188] using the reconfigurable NB-PLC transceiver realized in this work
- Implementation and performance evaluation of an OFDM-based Hybrid PLC-VLC for an in-home scenario, with the possibility of also implementing software-defined hybrid system using USRP. The block diagrams of the proposed hybrid system are shown in Figure 9.1 and Figure 9.2 as follows.

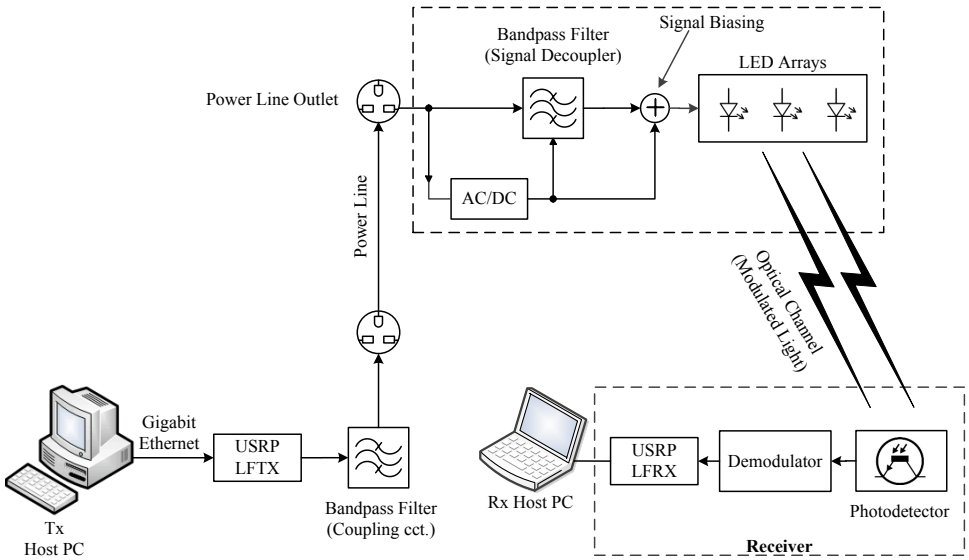

FIGURE 9.1: Schematic of the PLC-VLC hybrid system.

- The reconfigurable NB-PLC transceiver realized in this research project can also be utilized for future measurement campaign and to implement different waveforms for several real-time scenarios performance analysis.

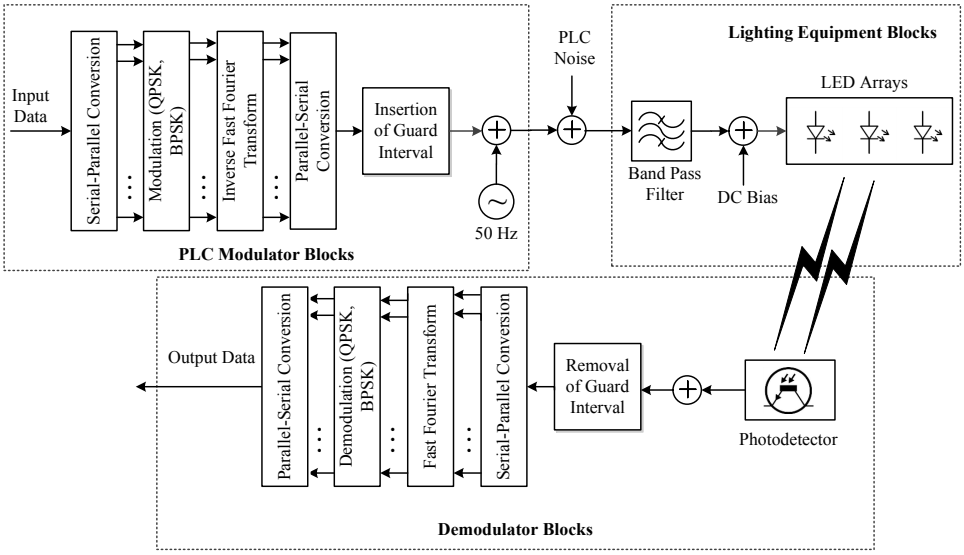

FIGURE 9.2: PLC-VLC hybrid OFDM system.

- The reconfigurable NB-PLC transceiver test-bed realized in this research project can also be adapted for MIMO power line communication.

Appendix A

Second-Order Baum-Welch Algorithm for Second-Order SHFMM Parameter Estimation

An empirical error sequence $\bar{E}$ of length T = 5 and a three-state semi-hidden Fritchman Markov model is adopted to show how the model parameters are re-estimated using the second-order Baum-Welch algorithm. Note that, no transition exist between states of the same group (i.e. no transition between the two good states). Therefore, the First-Order state transition matrix A_1 and second-order state transition matrix A_2 for the three state model takes the form written as follows. Note that the matrix elements a_{12} and a_{21} for the first-order and matrix elements a_{112}, a_{121}, a_{212}, a_{221}, a_{312} and a_{321} all are zeros because of the cross-over restriction.

$$\mathbf{A_1} = \begin{bmatrix} a_{11} & a_{12} & a_{13} \\ a_{21} & a_{22} & a_{23} \\ a_{31} & a_{32} & a_{33} \end{bmatrix} = \begin{bmatrix} a_{11} & 0 & a_{13} \\ 0 & a_{22} & a_{23} \\ a_{31} & a_{32} & a_{33} \end{bmatrix} \tag{A.1}$$

$$\mathbf{A_2} = \begin{bmatrix} a_{111} & a_{112} & a_{113} \\ a_{121} & a_{122} & a_{123} \\ a_{131} & a_{132} & a_{133} \\ a_{211} & a_{212} & a_{213} \\ a_{221} & a_{222} & a_{223} \\ a_{231} & a_{232} & a_{233} \\ a_{311} & a_{312} & a_{313} \\ a_{321} & a_{322} & a_{323} \\ a_{331} & a_{332} & a_{333} \end{bmatrix} = \begin{bmatrix} a_{111} & 0 & a_{113} \\ 0 & a_{122} & a_{123} \\ a_{131} & a_{132} & a_{133} \\ a_{211} & 0 & a_{213} \\ 0 & a_{222} & a_{223} \\ a_{231} & a_{232} & a_{233} \\ a_{311} & 0 & a_{313} \\ 0 & a_{322} & a_{323} \\ a_{331} & a_{332} & a_{333} \end{bmatrix}. \tag{A.2}$$

According to Fritchman for a three state model with two good states and a bad state, the two good states do not produce any error. Therefore, an observation of errors implies that

these errors are generated from the only bad state [16]. Hence, the B matrix which is the error generation matrix is represented in binary form with the matrix notation as follows.

$$\mathbf{B} = \begin{bmatrix} 1 & 1 & 0 \\ 0 & 0 & 1 \end{bmatrix}. \tag{A.3}$$

$$\pi = [\pi_1 \ \pi_2 \ \pi_3]. \tag{A.4}$$

A.1 Forward Probabilities Computation

This is denoted by $\alpha_t(i,j)$, and is defined as the probability of the partial observation sequence from 1 to time t, and transition $S_i \rightarrow S_j$ at times t-1, t given the model Γ_2=(A_2, B, π)

$$\alpha_t(i,j) = Pr(e_1, e_2, e_3, \cdots, e_t, \ S_{t-1} = i, S_t = j|\Gamma) \tag{A.5}$$

Solving for $\alpha_t(i,j)$ recursively, we have

$$\alpha_1(i) = \pi_i \ b_i \ (e_1) \tag{A.6}$$

1. **Initialization**

$$\alpha_2(i,j) = \alpha_1(i) a_{ij} b_j(e_2), \quad for \ 1 \leq i,j \leq N \tag{A.7}$$

2. **Recursive computation** for $2 \leq t \leq T-1$

$$\alpha_{t+1}(j,k) = \left[\sum_i^N \alpha_t(i,j) a_{ijk} \right] b_k(e_{t+1}) \tag{A.8}$$

3. **Termination of forward variable**

$$Pr(\bar{E}|\Gamma) = \sum_{i=1}^N \sum_{j=1}^N \alpha_T(i,j) \tag{A.9}$$

Similarly the backward probabilities is defined and derived as follows.

A.2 Backward Probabilities Computation

The backward function denoted as $\beta_t(i,j)$, is defined as the probability of the partial observation sequence t+1 to T, given the transition S_iS_j at times t-1, t and the model Γ_2=(A_2, B, π).

$$\beta_t(i,j) = Pr(e_{t+1}, e_{t+2}, e_{t+3}, \cdots, e_T | S_{t-1} = S_i, S_t = S_j, \Gamma_2) \tag{A.10}$$

Solving $\beta_t(i,j)$ recursively, we have

1. **Initialization**

$$\beta_t(i,j) = 1, \quad for\ 1 \leq i,j \leq N \tag{A.11}$$

2. **Recursive computation** for $T-1 \geq t \geq 2$

$$\beta_t(i,j) = \sum_{k=1}^{N} a_{ijk} b_k(e_{t+1}) \beta_{t+1}(j,k) \tag{A.12}$$

Computation of both forward and backward functions requires in the order of N^3T calculations.

A.3 Parameter Re-estimation Variables Computation

Eta (η): The first parameter re-estimation variable eta denoted by $\eta_t(i,j,k)$, is defined as the probability of being in states S_i, S_j and S_k respectively at times t-1, t and t+1 given the model Γ_2=(A_2, B, π) and empirical error sequence $\bar{E}$.

$$\eta_t(i,j,k) = Pr(S_{t-1} = i, S_t = j, S_{t+1} = k | \bar{E}, \Gamma_2) \tag{A.13}$$

$$\eta_t(i,j,k) = \frac{\alpha_t(i,j) a_{ijk} b_k(e_{t+1}) \beta_{t+1}(j,k)}{Pr(\bar{E}|\Gamma_2)} \tag{A.14}$$

$$\eta_{t+1}(i,j,k) = \frac{\alpha_{t+1}(i,j) a_{ijk} b_k(e_{t+2}) \beta_{t+2}(j,k)}{Pr(\bar{E}|\Gamma_2)} \tag{A.15}$$

Xi (ξ): This variable is denoted by $\xi_t(i,j)$, and is defined as the probability of being in state S_i at time t and in state S_j at time t+1 given the model and the observation sequence.

$$\xi_t(i,j) = Pr(S_t = i, S_{t+1} = j|\bar{E}, \Gamma_2) \tag{A.16}$$

$$\xi_t(i,j) = \sum_{k=1}^{N} \eta_{t+1}(i,j,k) \tag{A.17}$$

$$\xi_t(i,j) = \sum_{k=1}^{N} \left[\frac{\alpha_{t+1}(i,j) a_{ijk} b_k(e_{t+2}) \beta_{t+2}(j,k)}{Pr(\bar{E}|\Gamma_2)} \right] \tag{A.18}$$

Gamma (γ): The final parameter re-estimation variable denoted by $\gamma_t(i)$, is defined as the probability of being in state S_i at time t, given the model and the observation sequence.

$$\gamma_t(i) = Pr(S_t = i|\bar{E}, \Gamma) \tag{A.19}$$

$$\gamma_t(i) = \sum_{j=1}^{N} \xi_t(i,j) \tag{A.20}$$

$$\gamma_t(i) = \sum_{j=1}^{N} \sum_{k=1}^{N} \left[\frac{\alpha_{t+1}(i,j) a_{ijk} b_k(e_{t+2}) \beta_{t+2}(j,k)}{Pr(\bar{E}|\Gamma_2)} \right] \tag{A.21}$$

$\eta_t(i,j,k)$, $\xi_t(i,j)$ and $\gamma_t(i)$ are computed from the forward and backward variables given the above formulas.

A.4 Parameter Re-estimation equations

1. The re-estimated first-order state transition probabilities is computed as follows.

$$\hat{a}_{ij} = \frac{\xi_1(i,j)}{\gamma_1(i)} \tag{A.22}$$

2. The computation of the re-estimated second-order state transition probabilities is carried out by the equation shown as follows

$$\hat{a}_{ijk} = \frac{\sum_{t=1}^{T-3} \eta_{t+1}(i,j,k)}{\sum_{t=1}^{T-3} \xi_t(i,j)} \tag{A.23}$$

3. The re-estimated output symbol probability matrix is computed using the equation shown as follow.

$$\hat{b_k}(l) = \frac{\sum_{t=1,e_t=V_l}^{T} \gamma_t(k)}{\sum_{t=1}^{T} \gamma_t(k)} \tag{A.24}$$

4. The re-estimated initial state probability is computed as follows.

$$\hat{\pi}_i = \frac{\gamma_1(i)}{\sum_{i=1}^{N} \gamma_1(i)} \tag{A.25}$$

A summary of the procedural steps in carrying out model parameter re-estimation using the extended Second-Order Baum-Welch algorithm is as follows.

1. The initialization of π_i^0, a_{ij}^0, a_{ijk}^0 and ${b_k}^0(l)$, for $1 \leq i, \quad j,k \leq N, \quad 1 \leq l \leq M$.

2. Computation of the forward and backward probabilities.

3. Computation of the re-estimation formulas: $\eta_t(i,j,k)$, $\xi_t(i,j)$ and $\gamma_t(i)$, for $1 \leq i, \quad j,k \leq N, \quad 2 \leq t \leq T-1$ using the computed forward and backward probabilities.

4. Computation of the new re-estimated parameters: $\hat{\pi}_i$, $\hat{a}_{ij}$, $\hat{a}_{ijk}$ and $\hat{b_k}(l)$ for $1 \leq i, \quad j,k \leq N, \quad 1 \leq l \leq M$ utilizing the parameter re-estimation formulas.

5. Reiteration of steps 2-4 with the re-estimated parameters until the desired level of convergence is reached, that is, $\pi_i = \hat{\pi}_i$, $a_{ij} = \hat{a}_{ij}$, $a_{ijk} = \hat{a}_{ijk}$ and $b_k(l) = \hat{b_k}(l)$ for $1 \leq i, \quad j,k \leq N, \quad 1 \leq l \leq M$.

A.5 Forward Probabilities Computation

Computation of the forward probability variables is performed in three steps as follows: the initialization, the recursive computation and termination.

1. **Initialization**: Initialize for $t = 1$

$$\alpha_t(i) = \pi_i \; b_i \; (e_t) \tag{A.26}$$

$$\alpha_1(1) = \pi_1 \; b_1 \; (e_1), \quad for \; i = 1 \tag{A.27}$$

$$\alpha_1(2) = \pi_2 \; b_2 \; (e_1), \quad for \; i = 2 \tag{A.28}$$

$$\alpha_1(3) = \pi_3 \; b_3 \; (e_1), \quad for \; i = 3 \tag{A.29}$$

$$\alpha_2(i,j) = \alpha_1(i) a_{ij} b_j(e_2) \tag{A.30}$$

$$\alpha_2(1,1) = \alpha_1(1) a_{11} b_1(e_2) \tag{A.31}$$

$$\alpha_2(1,2) = \alpha_1(1) a_{12} b_2(e_2) \tag{A.32}$$

$$\alpha_2(1,3) = \alpha_1(1) a_{13} b_3(e_2) \tag{A.33}$$

$$\alpha_2(2,1) = \alpha_1(2) a_{21} b_1(e_2) \tag{A.34}$$

$$\alpha_2(2,2) = \alpha_1(2) a_{22} b_2(e_2) \tag{A.35}$$

$$\alpha_2(2,3) = \alpha_1(2) a_{23} b_3(e_2) \tag{A.36}$$

$$\alpha_2(3,1) = \alpha_1(3) a_{31} b_1(e_2) \tag{A.37}$$

$$\alpha_2(3,2) = \alpha_1(3) a_{32} b_2(e_2) \tag{A.38}$$

$$\alpha_2(3,3) = \alpha_1(3) a_{33} b_3(e_2) \tag{A.39}$$

2. **Recursive Computation**

$$\alpha_{t+1}(j,k) = \left[\sum_{i=1}^{N} \alpha_t(i,j) a_{ijk} \right] b_k(e_{t+1}) 2 \leq t \leq T-1 \tag{A.40}$$

For T = 5, we have

$$\alpha_3(j,k) = \left[\sum_{i=1}^{N} \alpha_2(i,j) a_{ijk} \right] b_k(e_3), \; for \; t = 2 \tag{A.41}$$

$$\alpha_4(j,k) = \left[\sum_{i=1}^{N} \alpha_3(i,j) a_{ijk} \right] b_k(e_4), \; for \; t = 3 \tag{A.42}$$

$$\alpha_5(j,k) = \left[\sum_{i=1}^{N} \alpha_4(i,j) a_{ijk} \right] b_k(e_5), \; for \; t = 4 \tag{A.43}$$

Therefore, for $\alpha_3(j,k)$, we have

$$\alpha_3(1,1) = \alpha_2(1,1)a_{111}b_1(e_3) + \alpha_2(2,1)a_{211}b_1(e_3) + \alpha_2(3,1)a_{311}b_1(e_3) \tag{A.44}$$

$$\alpha_3(1,2) = \alpha_2(1,1)a_{112}b_2(e_3) + \alpha_2(2,1)a_{212}b_2(e_3) + \alpha_2(3,1)a_{312}b_2(e_3) \tag{A.45}$$

$$\alpha_3(1,3) = \alpha_2(1,1)a_{113}b_3(e_3) + \alpha_2(2,1)a_{213}b_3(e_3) + \alpha_2(3,1)a_{313}b_3(e_3) \tag{A.46}$$

$$\alpha_3(2,1) = \alpha_2(1,2)a_{121}b_1(e_3) + \alpha_2(2,2)a_{221}b_1(e_3) + \alpha_2(3,2)a_{321}b_1(e_3) \tag{A.47}$$

$$\alpha_3(2,2) = \alpha_2(1,2)a_{122}b_2(e_3) + \alpha_2(2,2)a_{222}b_2(e_3) + \alpha_2(3,2)a_{322}b_2(e_3) \tag{A.48}$$

$$\alpha_3(2,3) = \alpha_2(1,2)a_{123}b_3(e_3) + \alpha_2(2,2)a_{223}b_3(e_3) + \alpha_2(3,2)a_{323}b_3(e_3) \tag{A.49}$$

$$\alpha_3(3,1) = \alpha_2(1,3)a_{131}b_1(e_3) + \alpha_2(2,3)a_{231}b_1(e_3) + \alpha_2(3,3)a_{331}b_1(e_3) \tag{A.50}$$

$$\alpha_3(3,2) = \alpha_2(1,3)a_{132}b_2(e_3) + \alpha_2(2,3)a_{232}b_2(e_3) + \alpha_2(3,3)a_{332}b_2(e_3) \tag{A.51}$$

$$\alpha_3(3,3) = \alpha_2(1,3)a_{133}b_3(e_3) + \alpha_2(2,3)a_{233}b_3(e_3) + \alpha_2(3,3)a_{333}b_3(e_3) \tag{A.52}$$

Likewise, $\alpha_4(j,k)$ is computed as follows.

$$\alpha_4(1,1) = \alpha_3(1,1)a_{111}b_1(e_4) + \alpha_3(2,1)a_{211}b_1(e_4) + \alpha_3(3,1)a_{311}b_1(e_4) \tag{A.53}$$

$$\alpha_4(1,2) = \alpha_3(1,1)a_{112}b_2(e_4) + \alpha_3(2,1)a_{212}b_2(e_4) + \alpha_3(3,1)a_{312}b_2(e_4) \tag{A.54}$$

$$\alpha_4(1,3) = \alpha_3(1,1)a_{113}b_3(e_4) + \alpha_3(2,1)a_{213}b_3(e_4) + \alpha_3(3,1)a_{313}b_3(e_4) \tag{A.55}$$

$$\alpha_4(2,1) = \alpha_3(1,2)a_{121}b_1(e_4) + \alpha_3(2,2)a_{221}b_1(e_4) + \alpha_3(3,2)a_{321}b_1(e_4) \tag{A.56}$$

$$\alpha_4(2,2) = \alpha_3(1,2)a_{122}b_2(e_4) + \alpha_3(2,2)a_{222}b_2(e_4) + \alpha_3(3,2)a_{322}b_2(e_4) \tag{A.57}$$

$$\alpha_4(2,3) = \alpha_3(1,2)a_{123}b_3(e_4) + \alpha_3(2,2)a_{223}b_3(e_4) + \alpha_3(3,2)a_{323}b_3(e_4) \tag{A.58}$$

$$\alpha_4(3,1) = \alpha_3(1,3)a_{131}b_1(e_4) + \alpha_3(2,3)a_{231}b_1(e_4) + \alpha_3(3,3)a_{331}b_1(e_4) \tag{A.59}$$

$$\alpha_4(3,2) = \alpha_3(1,3)a_{132}b_2(e_4) + \alpha_3(2,3)a_{232}b_2(e_4) + \alpha_3(3,3)a_{332}b_2(e_4) \tag{A.60}$$

$$\alpha_4(3,3) = \alpha_3(1,3)a_{133}b_3(e_4) + \alpha_3(2,3)a_{233}b_3(e_4) + \alpha_3(3,3)a_{333}b_3(e_4) \tag{A.61}$$

Lastly, $\alpha_5(j,k)$ is recursively computed as follows.

$$\alpha_5(1,1) = \alpha_4(1,1)a_{111}b_1(e_5) + \alpha_4(2,1)a_{211}b_1(e_5) + \alpha_4(3,1)a_{311}b_1(e_5) \tag{A.62}$$

$$\alpha_5(1,2) = \alpha_4(1,1)a_{112}b_2(e_5) + \alpha_4(2,1)a_{212}b_2(e_5) + \alpha_4(3,1)a_{312}b_2(e_5) \tag{A.63}$$

$$\alpha_5(1,3) = \alpha_4(1,1)a_{113}b_3(e_5) + \alpha_4(2,1)a_{213}b_3(e_5) + \alpha_4(3,1)a_{313}b_3(e_5) \tag{A.64}$$

$$\alpha_5(2,1) = \alpha_4(1,2)a_{121}b_1(e_5) + \alpha_4(2,2)a_{221}b_1(e_5) + \alpha_4(3,2)a_{321}b_1(e_5) \tag{A.65}$$

$$\alpha_5(2,2) = \alpha_4(1,2)a_{122}b_2(e_5) + \alpha_4(2,2)a_{222}b_2(e_5) + \alpha_4(3,2)a_{322}b_2(e_5) \tag{A.66}$$

$$\alpha_5(2,3) = \alpha_4(1,2)a_{123}b_3(e_5) + \alpha_4(2,2)a_{223}b_3(e_5) + \alpha_4(3,2)a_{323}b_3(e_5) \tag{A.67}$$

$$\alpha_5(3,1) = \alpha_4(1,3)a_{131}b_1(e_5) + \alpha_4(2,3)a_{231}b_1(e_5) + \alpha_4(3,3)a_{331}b_1(e_5) \tag{A.68}$$

$$\alpha_5(3,2) = \alpha_4(1,3)a_{132}b_2(e_5) + \alpha_4(2,3)a_{232}b_2(e_5) + \alpha_4(3,3)a_{332}b_2(e_5) \tag{A.69}$$

$$\alpha_5(3,3) = \alpha_4(1,3)a_{133}b_3(e_5) + \alpha_4(2,3)a_{233}b_3(e_5) + \alpha_4(3,3)a_{333}b_3(e_5) \tag{A.70}$$

3. **Termination of Forward probabilities**

$$Pr(O|\Gamma) = \sum_{i=1}^{N}\sum_{j=1}^{N} \alpha_T(i,j) \tag{A.71}$$

Since $\alpha_t(i,j) = \alpha_t(i)a_{ij}b_j(e_t)$ and $t = T$, hence we have, $\alpha_T(i,j) = \alpha_T(i)a_{ij}b_j(e_T)$.

$$\alpha_T(i) = \pi_i \; b_i \; (e_T) \tag{A.72}$$

$$\alpha_5(1) = \pi_1 \; b_1 \; (e_5), \; for \; i = 1 \tag{A.73}$$

$$\alpha_5(2) = \pi_2 \; b_2 \; (e_5), \; for \; i = 2 \tag{A.74}$$

$$\alpha_5(3) = \pi_3 \; b_3 \; (e_5), \; for \; i = 3 \tag{A.75}$$

Furthermore, we compute $\alpha_T(i,j) = \alpha_T(i)a_{ij}b_j(e_T)$, as follows.

$$\alpha_5(1,1) = \alpha_5(1)a_{11}b_1(e_5) \tag{A.76}$$

$$\alpha_5(1,2) = \alpha_5(1)a_{12}b_2(e_5) \tag{A.77}$$

$$\alpha_5(1,3) = \alpha_5(1)a_{13}b_3(e_5) \tag{A.78}$$

$$\alpha_5(2,1) = \alpha_5(2)a_{21}b_1(e_5) \tag{A.79}$$

$$\alpha_5(2,2) = \alpha_5(2)a_{22}b_2(e_5) \tag{A.80}$$

$$\alpha_5(2,3) = \alpha_5(2)a_{23}b_3(e_5) \tag{A.81}$$

$$\alpha_5(3,1) = \alpha_5(3)a_{31}b_1(e_5) \tag{A.82}$$

$$\alpha_5(3,2) = \alpha_5(3)a_{32}b_2(e_5) \tag{A.83}$$

$$\alpha_5(3,3) = \alpha_5(3)a_{33}b_3(e_5) \tag{A.84}$$

Therefore,

$$Pr(O|\Gamma) = \alpha_5(1,1) + \alpha_5(1,2) + \alpha_5(1,3) + \alpha_5(2,1) + \alpha_5(2,2) + \alpha_5(2,3) + \alpha_5(3,1) + \alpha_5(3,2) + \alpha_5(3,3) \tag{A.85}$$

A.6 Backward Probabilities Computation

1. **Initialization**: $\beta_T(i,j) = 1$, for $i \leq i,\ j \leq N$. Therefore, we have

$$\beta_5(1,1) = 1; \quad \beta_5(2,1) = 1; \quad \beta_5(3,1) = 1 \tag{A.86}$$

$$\beta_5(1,2) = 1; \quad \beta_5(2,2) = 1; \quad \beta_5(3,2) = 1 \tag{A.87}$$

$$\beta_5(1,3) = 1; \quad \beta_5(2,3) = 1; \quad \beta_5(3,3) = 1 \tag{A.88}$$

2. **Recursive computation of** β, for $T-1 \geq t \geq 2$

$$\beta_t(i,j) = \sum_{k=1}^{N} a_{ijk}b_k(e_{t+1})\beta_{t+1}(j,k) \tag{A.89}$$

$$\beta_4(i,j) = \sum_{k=1}^{N} a_{ijk}b_k(e_5)\beta_5(j,k),\ \ for\ t = 4 \tag{A.90}$$

$$\beta_3(i,j) = \sum_{k=1}^{N} a_{ijk}b_k(e_4)\beta_5(j,k),\ \ for\ t = 3 \tag{A.91}$$

$$\beta_2(i,j) = \sum_{k=1}^{N} a_{ijk}b_k(e_3)\beta_5(j,k),\ \ for\ t = 2 \tag{A.92}$$

Computing $\beta_4(i,j)$, we have,

$$\beta_4(1,1) = a_{111}b_1(e_5)\beta_5(1,1) + a_{112}b_2(e_5)\beta_5(1,2) + a_{113}b_3(e_5)\beta_5(1,3) \quad \text{(A.93)}$$

$$\beta_4(1,2) = a_{121}b_1(e_5)\beta_5(2,1) + a_{122}b_2(e_5)\beta_5(2,2) + a_{123}b_3(e_5)\beta_5(2,3) \quad \text{(A.94)}$$

$$\beta_4(1,3) = a_{131}b_1(e_5)\beta_5(3,1) + a_{132}b_2(e_5)\beta_5(3,2) + a_{133}b_3(e_5)\beta_5(3,3) \quad \text{(A.95)}$$

$$\beta_4(2,1) = a_{211}b_1(e_5)\beta_5(1,1) + a_{212}b_2(e_5)\beta_5(1,2) + a_{213}b_3(e_5)\beta_5(1,3) \quad \text{(A.96)}$$

$$\beta_4(2,2) = a_{221}b_1(e_5)\beta_5(2,1) + a_{222}b_2(e_5)\beta_5(2,2) + a_{223}b_3(e_5)\beta_5(2,3) \quad \text{(A.97)}$$

$$\beta_4(2,3) = a_{231}b_1(e_5)\beta_5(3,1) + a_{232}b_2(e_5)\beta_5(3,2) + a_{233}b_3(e_5)\beta_5(3,3) \quad \text{(A.98)}$$

$$\beta_4(3,1) = a_{311}b_1(e_5)\beta_5(1,1) + a_{312}b_2(e_5)\beta_5(1,2) + a_{313}b_3(e_5)\beta_5(1,3) \quad \text{(A.99)}$$

$$\beta_4(3,2) = a_{321}b_1(e_5)\beta_5(2,1) + a_{322}b_2(e_5)\beta_5(2,2) + a_{323}b_3(e_5)\beta_5(2,3) \quad \text{(A.100)}$$

$$\beta_4(3,3) = a_{331}b_1(e_5)\beta_5(3,1) + a_{332}b_2(e_5)\beta_5(3,2) + a_{333}b_3(e_5)\beta_5(3,3) \quad \text{(A.101)}$$

Computing $\beta_3(i,j)$, we have,

$$\beta_3(1,1) = a_{111}b_1(e_4)\beta_4(1,1) + a_{112}b_2(e_4)\beta_4(1,2) + a_{113}b_3(e_4)\beta_4(1,3) \quad \text{(A.102)}$$

$$\beta_3(1,2) = a_{121}b_1(e_4)\beta_4(2,1) + a_{122}b_2(e_4)\beta_4(2,2) + a_{123}b_3(e_4)\beta_4(2,3) \quad \text{(A.103)}$$

$$\beta_3(1,3) = a_{131}b_1(e_4)\beta_4(3,1) + a_{132}b_2(e_4)\beta_4(3,2) + a_{133}b_3(e_4)\beta_4(3,3) \quad \text{(A.104)}$$

$$\beta_3(2,1) = a_{211}b_1(e_4)\beta_4(1,1) + a_{212}b_2(e_4)\beta_4(1,2) + a_{213}b_3(e_4)\beta_4(1,3) \quad \text{(A.105)}$$

$$\beta_3(2,2) = a_{221}b_1(e_4)\beta_4(2,1) + a_{222}b_2(e_4)\beta_4(2,2) + a_{223}b_3(e_4)\beta_4(2,3) \quad \text{(A.106)}$$

$$\beta_3(2,3) = a_{231}b_1(e_4)\beta_4(3,1) + a_{232}b_2(e_4)\beta_4(3,2) + a_{233}b_3(e_4)\beta_4(3,3) \quad \text{(A.107)}$$

$$\beta_3(3,1) = a_{311}b_1(e_4)\beta_4(1,1) + a_{312}b_2(e_4)\beta_4(1,2) + a_{313}b_3(e_4)\beta_4(1,3) \quad \text{(A.108)}$$

$$\beta_3(3,2) = a_{321}b_1(e_4)\beta_4(2,1) + a_{322}b_2(e_4)\beta_4(2,2) + a_{323}b_3(e_4)\beta_4(2,3) \quad \text{(A.109)}$$

$$\beta_3(3,3) = a_{331}b_1(e_4)\beta_4(3,1) + a_{332}b_2(e_4)\beta_4(3,2) + a_{333}b_3(e_4)\beta_4(3,3) \quad \text{(A.110)}$$

Computing $\beta_2(i,j)$, we have,

$$\beta_2(1,1) = a_{111}b_1(e_3)\beta_3(1,1) + a_{112}b_2(e_3)\beta_3(1,2) + a_{113}b_3(e_3)\beta_3(1,3) \quad \text{(A.111)}$$

$$\beta_2(1,2) = a_{121}b_1(e_3)\beta_3(2,1) + a_{122}b_2(e_3)\beta_3(2,2) + a_{123}b_3(e_3)\beta_3(2,3) \quad \text{(A.112)}$$

$$\beta_2(1,3) = a_{131}b_1(e_3)\beta_3(3,1) + a_{132}b_2(e_3)\beta_3(3,2) + a_{133}b_3(e_3)\beta_3(3,3) \quad \text{(A.113)}$$

$$\beta_2(2,1) = a_{211}b_1(e_3)\beta_3(1,1) + a_{212}b_2(e_3)\beta_3(1,2) + a_{213}b_3(e_3)\beta_3(1,3) \quad \text{(A.114)}$$

$$\beta_2(2,2) = a_{221}b_1(e_3)\beta_3(2,1) + a_{222}b_2(e_3)\beta_3(2,2) + a_{223}b_3(e_3)\beta_3(2,3) \quad \text{(A.115)}$$

$$\beta_2(2,3) = a_{231}b_1(e_3)\beta_3(3,1) + a_{232}b_2(e_3)\beta_3(3,2) + a_{233}b_3(e_3)\beta_3(3,3) \quad \text{(A.116)}$$

$$\beta_2(3,1) = a_{311}b_1(e_3)\beta_3(1,1) + a_{312}b_2(e_3)\beta_3(1,2) + a_{313}b_3(e_3)\beta_3(1,3) \quad \text{(A.117)}$$

$$\beta_2(3,2) = a_{321}b_1(e_3)\beta_3(2,1) + a_{322}b_2(e_3)\beta_3(2,2) + a_{323}b_3(e_3)\beta_3(2,3) \quad \text{(A.118)}$$

$$\beta_2(3,3) = a_{331}b_1(e_3)\beta_3(3,1) + a_{332}b_2(e_3)\beta_3(3,2) + a_{333}b_3(e_3)\beta_3(3,3) \quad \text{(A.119)}$$

A.7 Parameter Re-estimation Variables Computation

Computation of η for $1 \leq t \leq T-1$:

$$\eta_t(i,j,k) = \left[\frac{\alpha_t(i,j)a_{ijk}b_k(e_{t+1})\beta_{t+1}(j,k)}{Pr(\bar{E}|\Gamma_2)}\right] \quad \text{(A.120)}$$

$$\eta_{t+1}(i,j,k) = \left[\frac{\alpha_{t+1}(i,j)a_{ijk}b_k(e_{t+2})\beta_{t+2}(j,k)}{Pr(\bar{E}|\Gamma_2)}\right] \quad \text{(A.121)}$$

For simplicity, the denominator is omitted, hence, we have

$$\eta_{t+1}(i,j,k) = \alpha_{t+1}(i,j)a_{ijk}b_k(e_{t+2})\beta_{t+2}(j,k) \quad \text{(A.122)}$$

$$\eta_2(i,j,k) = \alpha_2(i,j)a_{ijk}b_k(e_3)\beta_3(j,k) \quad \text{(A.123)}$$

$$\eta_3(i,j,k) = \alpha_3(i,j)a_{ijk}b_k(e_4)\beta_4(j,k) \quad \text{(A.124)}$$

$$\eta_4(i,j,k) = \alpha_4(i,j)a_{ijk}b_k(e_5)\beta_5(j,k) \quad \text{(A.125)}$$

$$\eta_5(i,j,k) = \alpha_5(i,j)a_{ijk}b_k(ee_6)\beta_6(j,k) \quad \text{(A.126)}$$

Computation of $\eta_2(i,j,k)$, for $i,j,k = 1,2,3$, we have,

$$\eta_2(1,1,1) = \alpha_2(1,1)a_{111}b_1(e_3)\beta_3(1,1) \tag{A.127}$$

$$\eta_2(1,1,2) = \alpha_2(1,1)a_{112}b_2(e_3)\beta_3(1,2) \tag{A.128}$$

$$\eta_2(1,1,3) = \alpha_2(1,1)a_{113}b_3(e_3)\beta_3(1,3) \tag{A.129}$$

$$\eta_2(1,2,1) = \alpha_2(1,2)a_{121}b_1(e_3)\beta_3(2,1) \tag{A.130}$$

$$\eta_2(1,2,2) = \alpha_2(1,2)a_{122}b_2(e_3)\beta_3(2,2) \tag{A.131}$$

$$\eta_2(1,2,3) = \alpha_2(1,2)a_{123}b_3(e_3)\beta_3(2,3) \tag{A.132}$$

$$\eta_2(1,3,1) = \alpha_2(1,3)a_{131}b_1(e_3)\beta_3(3,1) \tag{A.133}$$

$$\eta_2(1,3,2) = \alpha_2(1,3)a_{132}b_2(e_3)\beta_3(3,2) \tag{A.134}$$

$$\eta_2(1,3,3) = \alpha_2(1,3)a_{133}b_3(e_3)\beta_3(3,3) \tag{A.135}$$

$$\eta_2(2,1,1) = \alpha_2(2,1)a_{211}b_1(e_3)\beta_3(1,1) \tag{A.136}$$

$$\eta_2(2,1,2) = \alpha_2(2,1)a_{212}b_2(e_3)\beta_3(1,2) \tag{A.137}$$

$$\eta_2(2,1,3) = \alpha_2(2,1)a_{213}b_3(e_3)\beta_3(1,3) \tag{A.138}$$

$$\eta_2(2,2,1) = \alpha_2(2,2)a_{221}b_1(e_3)\beta_3(2,1) \tag{A.139}$$

$$\eta_2(2,2,2) = \alpha_2(2,2)a_{222}b_2(e_3)\beta_3(2,2) \tag{A.140}$$

$$\eta_2(2,2,3) = \alpha_2(2,2)a_{223}b_3(e_3)\beta_3(2,3) \tag{A.141}$$

$$\eta_2(2,3,1) = \alpha_2(2,3)a_{231}b_1(e_3)\beta_3(3,1) \tag{A.142}$$

$$\eta_2(2,3,2) = \alpha_2(2,3)a_{232}b_2(e_3)\beta_3(3,2) \tag{A.143}$$

$$\eta_2(2,3,3) = \alpha_2(2,3)a_{233}b_3(e_3)\beta_3(3,3) \tag{A.144}$$

$$\eta_2(3,1,1) = \alpha_2(3,1)a_{311}b_1(e_3)\beta_3(1,1) \tag{A.145}$$

$$\eta_2(3,1,2) = \alpha_2(3,1)a_{312}b_2(e_3)\beta_3(1,2) \tag{A.146}$$

$$\eta_2(3,1,3) = \alpha_2(3,1)a_{313}b_3(e_3)\beta_3(1,3) \tag{A.147}$$

$$\eta_2(3,2,1) = \alpha_2(3,2)a_{321}b_1(e_3)\beta_3(2,1) \tag{A.148}$$

$$\eta_2(3,2,2) = \alpha_2(3,2)a_{322}b_2(e_3)\beta_3(2,2) \tag{A.149}$$

$$\eta_2(3,2,3) = \alpha_2(3,2)a_{323}b_3(e_3)\beta_3(2,3) \tag{A.150}$$

$$\eta_2(3,3,1) = \alpha_2(3,3)a_{331}b_1(e_3)\beta_3(3,1) \tag{A.151}$$

$$\eta_2(3,3,2) = \alpha_2(3,3)a_{332}b_2(e_3)\beta_3(3,2) \tag{A.152}$$

$$\eta_2(3,3,3) = \alpha_2(3,3)a_{333}b_3(e_3)\beta_3(3,3) \tag{A.153}$$

Computation of $\eta_3(i,j,k)$, for $i,j,k = 1,2,3$, we have,

$$\eta_3(1,1,1) = \alpha_3(1,1)a_{111}b_1(e_4)\beta_4(1,1) \tag{A.154}$$

$$\eta_3(1,1,2) = \alpha_3(1,1)a_{112}b_2(e_4)\beta_4(1,2) \tag{A.155}$$

$$\eta_3(1,1,3) = \alpha_3(1,1)a_{113}b_3(e_4)\beta_4(1,3) \tag{A.156}$$

$$\eta_3(1,2,1) = \alpha_3(1,2)a_{121}b_1(e_4)\beta_4(2,1) \tag{A.157}$$

$$\eta_3(1,2,2) = \alpha_3(1,2)a_{122}b_2(e_4)\beta_4(2,2) \tag{A.158}$$

$$\eta_3(1,2,3) = \alpha_3(1,2)a_{123}b_3(e_4)\beta_4(2,3) \tag{A.159}$$

$$\eta_3(1,3,1) = \alpha_3(1,3)a_{131}b_1(e_4)\beta_4(3,1) \tag{A.160}$$

$$\eta_3(1,3,2) = \alpha_3(1,3)a_{132}b_2(e_4)\beta_4(3,2) \tag{A.161}$$

$$\eta_3(1,3,3) = \alpha_3(1,3)a_{133}b_3(e_4)\beta_4(3,3) \tag{A.162}$$

$$\eta_3(2,1,1) = \alpha_3(2,1)a_{211}b_1(e_4)\beta_4(1,1) \tag{A.163}$$

$$\eta_3(2,1,2) = \alpha_3(2,1)a_{212}b_2(e_4)\beta_4(1,2) \tag{A.164}$$

$$\eta_3(2,1,3) = \alpha_3(2,1)a_{213}b_3(e_4)\beta_4(1,3) \tag{A.165}$$

$$\eta_3(2,2,1) = \alpha_3(2,2)a_{221}b_1(e_4)\beta_4(2,1) \tag{A.166}$$

$$\eta_3(2,2,2) = \alpha_3(2,2)a_{222}b_2(e_4)\beta_4(2,2) \tag{A.167}$$

$$\eta_3(2,2,3) = \alpha_3(2,2)a_{223}b_3(e_4)\beta_4(2,3) \tag{A.168}$$

$$\eta_3(2,3,1) = \alpha_3(2,3)a_{231}b_1(e_4)\beta_4(3,1) \tag{A.169}$$

$$\eta_3(2,3,2) = \alpha_3(2,3)a_{232}b_2(e_4)\beta_4(3,2) \tag{A.170}$$

$$\eta_3(2,3,3) = \alpha_3(2,3)a_{233}b_3(e_4)\beta_4(3,3) \tag{A.171}$$

$$\eta_3(3,1,1) = \alpha_3(3,1)a_{311}b_1(e_4)\beta_4(1,1) \tag{A.172}$$

$$\eta_3(3,1,2) = \alpha_3(3,1)a_{312}b_2(e_4)\beta_4(1,2) \tag{A.173}$$

$$\eta_3(3,1,3) = \alpha_3(3,1)a_{313}b_3(e_4)\beta_4(1,3) \tag{A.174}$$

$$\eta_3(3,2,1) = \alpha_3(3,2)a_{321}b_1(e_4)\beta_4(2,1) \tag{A.175}$$

$$\eta_3(3,2,2) = \alpha_3(3,2)a_{322}b_2(e_4)\beta_4(2,2) \tag{A.176}$$

$$\eta_3(3,2,3) = \alpha_3(3,2)a_{323}b_3(e_4)\beta_4(2,3) \tag{A.177}$$

$$\eta_3(3,3,1) = \alpha_3(3,3)a_{331}b_1(e_4)\beta_4(3,1) \tag{A.178}$$

$$\eta_3(3,3,2) = \alpha_3(3,3)a_{332}b_2(e_4)\beta_4(3,2) \tag{A.179}$$

$$\eta_3(3,3,3) = \alpha_3(3,3)a_{333}b_3(e_4)\beta_4(3,3) \tag{A.180}$$

Computation of $\eta_4(i,j,k)$, for $i,j,k = 1,2,3$, we have,

$$\eta_4(1,1,1) = \alpha_4(1,1)a_{111}b_1(e_5)\beta_5(1,1) \tag{A.181}$$

$$\eta_4(1,1,2) = \alpha_4(1,1)a_{112}b_2(e_5)\beta_5(1,2) \tag{A.182}$$

$$\eta_4(1,1,3) = \alpha_4(1,1)a_{113}b_3(e_5)\beta_5(1,3) \tag{A.183}$$

$$\eta_4(1,2,1) = \alpha_4(1,2)a_{121}b_1(e_5)\beta_5(2,1) \tag{A.184}$$

$$\eta_4(1,2,2) = \alpha_4(1,2)a_{122}b_2(e_5)\beta_5(2,2) \tag{A.185}$$

$$\eta_4(1,2,3) = \alpha_4(1,2)a_{123}b_3(e_5)\beta_5(2,3) \tag{A.186}$$

$$\eta_4(1,3,1) = \alpha_4(1,3)a_{131}b_1(e_5)\beta_5(3,1) \tag{A.187}$$

$$\eta_4(1,3,2) = \alpha_4(1,3)a_{132}b_2(e_5)\beta_5(3,2) \tag{A.188}$$

$$\eta_4(1,3,3) = \alpha_4(1,3)a_{133}b_3(e_5)\beta_5(3,3) \tag{A.189}$$

$$\eta_4(2,1,1) = \alpha_4(2,1)a_{211}b_1(e_5)\beta_5(1,1) \tag{A.190}$$

$$\eta_4(2,1,2) = \alpha_4(2,1)a_{212}b_2(e_5)\beta_5(1,2) \tag{A.191}$$

$$\eta_4(2,1,3) = \alpha_4(2,1)a_{213}b_3(e_5)\beta_5(1,3) \tag{A.192}$$

$$\eta_4(2,2,1) = \alpha_4(2,2)a_{221}b_1(e_5)\beta_5(2,1) \tag{A.193}$$

$$\eta_4(2,2,2) = \alpha_4(2,2)a_{222}b_2(e_5)\beta_5(2,2) \tag{A.194}$$

$$\eta_4(2,2,3) = \alpha_4(2,2)a_{223}b_3(e_5)\beta_5(2,3) \tag{A.195}$$

$$\eta_4(2,3,1) = \alpha_4(2,3)a_{231}b_1(e_5)\beta_5(3,1) \tag{A.196}$$

$$\eta_4(2,3,2) = \alpha_4(2,3)a_{232}b_2(e_5)\beta_5(3,2) \tag{A.197}$$

$$\eta_4(2,3,3) = \alpha_4(2,3)a_{233}b_3(e_5)\beta_5(3,3) \tag{A.198}$$

$$\eta_4(3,1,1) = \alpha_4(3,1)a_{311}b_1(e_5)\beta_5(1,1) \tag{A.199}$$

$$\eta_4(3,1,2) = \alpha_4(3,1)a_{312}b_2(e_5)\beta_5(1,2) \tag{A.200}$$

$$\eta_4(3,1,3) = \alpha_4(3,1)a_{313}b_3(e_5)\beta_5(1,3) \tag{A.201}$$

$$\eta_4(3,2,1) = \alpha_4(3,2)a_{321}b_1(e_5)\beta_5(2,1) \tag{A.202}$$

$$\eta_4(3,2,2) = \alpha_4(3,2)a_{322}b_2(e_5)\beta_5(2,2) \tag{A.203}$$

$$\eta_4(3,2,3) = \alpha_4(3,2)a_{323}b_3(e_5)\beta_5(2,3) \tag{A.204}$$

$$\eta_4(3,3,1) = \alpha_4(3,3)a_{331}b_1(e_5)\beta_5(3,1) \tag{A.205}$$

$$\eta_4(3,3,2) = \alpha_4(3,3)a_{332}b_2(e_5)\beta_5(3,2) \tag{A.206}$$

$$\eta_4(3,3,3) = \alpha_4(3,3)a_{333}b_3(e_5)\beta_5(3,3) \tag{A.207}$$

Computation of ξ for $1 \leq t \leq T-1$:

$$\xi_t(i,j) = \sum_{k=1}^{N} \eta_{t+1}(i,j,k) \tag{A.208}$$

$$\xi_t(i,j) = \eta_{t+1}(i,j,1) + \eta_{t+1}(i,j,2) + \eta_{t+1}(i,j,3) \tag{A.209}$$

$$\xi_1(i,j) = \eta_2(i,j,1) + \eta_2(i,j,2) + \eta_2(i,j,3), \;\; for \; t = 1 \tag{A.210}$$

$$\xi_2(i,j) = \eta_3(i,j,1) + \eta_3(i,j,2) + \eta_3(i,j,3), \;\; for \; t = 2 \tag{A.211}$$

$$\xi_3(i,j) = \eta_4(i,j,1) + \eta_4(i,j,2) + \eta_4(i,j,3), \;\; for \; t = 3 \tag{A.212}$$

Computation of $\xi_1(i,j)$, for $i,j = 1,2,3$, we have,

$$\xi_1(1,1) = \eta_2(1,1,1) + \eta_2(1,1,2) + \eta_2(1,1,3) \tag{A.213}$$

$$\xi_1(1,2) = \eta_2(1,2,1) + \eta_2(1,2,2) + \eta_2(1,2,3) \tag{A.214}$$

$$\xi_1(1,3) = \eta_2(1,3,1) + \eta_2(1,3,2) + \eta_2(1,3,3) \tag{A.215}$$

$$\xi_1(2,1) = \eta_2(2,1,1) + \eta_2(2,1,2) + \eta_2(2,1,3) \tag{A.216}$$

$$\xi_1(2,2) = \eta_2(2,2,1) + \eta_2(2,2,2) + \eta_2(2,2,3) \tag{A.217}$$

$$\xi_1(2,3) = \eta_2(2,3,1) + \eta_2(2,3,2) + \eta_2(2,3,3) \tag{A.218}$$

$$\xi_1(3,1) = \eta_2(3,1,1) + \eta_2(3,1,2) + \eta_2(3,1,3) \tag{A.219}$$

$$\xi_1(3,2) = \eta_2(3,2,1) + \eta_2(3,2,2) + \eta_2(3,2,3) \tag{A.220}$$

$$\xi_1(3,3) = \eta_2(3,3,1) + \eta_2(3,3,2) + \eta_2(3,3,3) \tag{A.221}$$

Computation of $\xi_2(i,j)$, for $i,j = 1,2,3$, we have,

$$\xi_2(1,1) = \eta_3(1,1,1) + \eta_3(1,1,2) + \eta_3(1,1,3) \tag{A.222}$$

$$\xi_2(1,2) = \eta_3(1,2,1) + \eta_3(1,2,2) + \eta_3(1,2,3) \tag{A.223}$$

$$\xi_2(1,3) = \eta_3(1,3,1) + \eta_3(1,3,2) + \eta_3(1,3,3) \tag{A.224}$$

$$\xi_2(2,1) = \eta_3(2,1,1) + \eta_3(2,1,2) + \eta_3(2,1,3) \tag{A.225}$$

$$\xi_2(2,2) = \eta_3(2,2,1) + \eta_3(2,2,2) + \eta_3(2,2,3) \tag{A.226}$$

$$\xi_2(2,3) = \eta_3(2,3,1) + \eta_3(2,3,2) + \eta_3(2,3,3) \tag{A.227}$$

$$\xi_2(3,1) = \eta_3(3,1,1) + \eta_3(3,1,2) + \eta_3(3,1,3) \tag{A.228}$$

$$\xi_2(3,2) = \eta_3(3,2,1) + \eta_3(3,2,2) + \eta_3(3,2,3) \tag{A.229}$$

$$\xi_2(3,3) = \eta_3(3,3,1) + \eta_3(3,3,2) + \eta_3(3,3,3) \tag{A.230}$$

Computation of $\xi_3(i,j)$, for $i,j = 1,2,3$, we have,

$$\xi_3(1,1) = \eta_4(1,1,1) + \eta_4(1,1,2) + \eta_4(1,1,3) \tag{A.231}$$

$$\xi_3(1,2) = \eta_4(1,2,1) + \eta_4(1,2,2) + \eta_4(1,2,3) \tag{A.232}$$

$$\xi_3(1,3) = \eta_4 41,3,1) + \eta_4(1,3,2) + \eta_4(1,3,3) \tag{A.233}$$

$$\xi_3(2,1) = \eta_4(2,1,1) + \eta_4(2,1,2) + \eta_4(2,1,3) \tag{A.234}$$

$$\xi_3(2,2) = \eta_4(2,2,1) + \eta_4(2,2,2) + \eta_4(2,2,3) \tag{A.235}$$

$$\xi_3(2,3) = \eta_4(2,3,1) + \eta_4(2,3,2) + \eta_4(2,3,3) \tag{A.236}$$

$$\xi_3(3,1) = \eta_4(3,1,1) + \eta_4(3,1,2) + \eta_4(3,1,3) \tag{A.237}$$

$$\xi_3(3,2) = \eta_4(3,2,1) + \eta_4(3,2,2) + \eta_4(3,2,3) \tag{A.238}$$

$$\xi_3(3,3) = \eta_4(3,3,1) + \eta_4(3,3,2) + \eta_4(3,3,3) \tag{A.239}$$

Computation of γ for $1 \leq t \leq T-1$:

$$\gamma_t(i) = \sum_{j=1}^{N} \xi_t(i,j) \tag{A.240}$$

$$\gamma_t(i) = \xi_t(i,1) + \xi_t(i,2) + \xi_t(i,3) \tag{A.241}$$

Computation of $\gamma_t(i)$, for $t = 1, 2, 3$, we have,

$$\gamma_1(1) = \xi_1(1,1) + \xi_1(1,2) + \xi_1(1,3) \tag{A.242}$$

$$\gamma_1(2) = \xi_1(2,1) + \xi_1(2,2) + \xi_1(2,3) \tag{A.243}$$

$$\gamma_1(3) = \xi_1(3,1) + \xi_1(3,2) + \xi_1(3,3) \tag{A.244}$$

$$\gamma_2(1) = \xi_2(1,1) + \xi_2(1,2) + \xi_2(1,3) \tag{A.245}$$

$$\gamma_2(2) = \xi_2(2,1) + \xi_2(2,2) + \xi_2(2,3) \tag{A.246}$$

$$\gamma_2(3) = \xi_2(3,1) + \xi_2(3,2) + \xi_2(3,3) \tag{A.247}$$

$$\gamma_3(1) = \xi_3(1,1) + \xi_3(1,2) + \xi_3(1,3) \tag{A.248}$$

$$\gamma_3(2) = \xi_3(2,1) + \xi_3(2,2) + \xi_3(2,3) \tag{A.249}$$

$$\gamma_3(3) = \xi_3(3,1) + \xi_3(3,2) + \xi_3(3,3) \tag{A.250}$$

A.8 Parameter Re-estimation Computation

Computation of first-order state transition matrix $\hat{a}_{ij}$, is carried out as follows.

$$\hat{a}_{ij} = \frac{\xi_1(i,j)}{\gamma_1(i)} \tag{A.251}$$

$$\hat{a}_{11} = \frac{\xi_1(1,1)}{\gamma_1(1)} \tag{A.252}$$

$$\hat{a}_{12} = \frac{\xi_1(1,2)}{\gamma_1(1)} \tag{A.253}$$

$$\hat{a}_{13} = \frac{\xi_1(1,3)}{\gamma_1(1)} \tag{A.254}$$

$$\tag{A.255}$$

$$\hat{a}_{21} = \frac{\xi_1(2,1)}{\gamma_1(2)} \tag{A.256}$$

$$\hat{a}_{22} = \frac{\xi_1(2,2)}{\gamma_1(2)} \tag{A.257}$$

$$\hat{a}_{23} = \frac{\xi_1(2,3)}{\gamma_1(2)} \tag{A.258}$$

$$\tag{A.259}$$

$$\hat{a}_{31} = \frac{\xi_1(3,1)}{\gamma_1(3)} \tag{A.260}$$

$$\hat{a}_{32} = \frac{\xi_1(3,2)}{\gamma_1(3)} \tag{A.261}$$

$$\hat{a}_{33} = \frac{\xi_1(3,3)}{\gamma_1(3)} \tag{A.262}$$

Computation of second-order state transition matrix $\hat{a}_{ijk}$, is carried out as follows.

$$\hat{a}_{ijk} = \frac{\sum_{t=1}^{T-3} \eta_{t+1}(i,j,k)}{\sum_{t=1}^{T-3} \xi_t(i,j)} \tag{A.263}$$

$$= \frac{\eta_2(i,j,k) + \eta_3(i,j,k)}{\xi_1(i,j) + \xi_2(i,j)} \tag{A.264}$$

Therefore, for $i, j, k = 1, 2, 3$, we have,

$$\hat{a}_{111} = \frac{\eta_2(1,1,1) + \eta_3(1,1,1)}{\xi_1(1,1) + \xi_2(1,1)} \tag{A.265}$$

$$\hat{a}_{112} = \frac{\eta_2(1,1,2) + \eta_3(1,1,2)}{\xi_1(1,1) + \xi_2(1,1)} \tag{A.266}$$

$$\hat{a}_{113} = \frac{\eta_2(1,1,3) + \eta_3(1,1,3)}{\xi_1(1,1) + \xi_2(1,1)} \tag{A.267}$$

$$\hat{a}_{121} = \frac{\eta_2(1,2,1) + \eta_3(1,2,1)}{\xi_1(1,2) + \xi_2(1,2)} \tag{A.268}$$

$$\hat{a}_{122} = \frac{\eta_2(1,2,2) + \eta_3(1,2,2)}{\xi_1(1,2) + \xi_2(1,2)} \tag{A.269}$$

$$\hat{a}_{123} = \frac{\eta_2(1,2,3) + \eta_3(1,2,3)}{\xi_1(1,2) + \xi_2(1,2)} \tag{A.270}$$

$$\hat{a}_{131} = \frac{\eta_2(1,3,1) + \eta_3(1,3,1)}{\xi_1(1,3) + \xi_2(1,3)} \tag{A.271}$$

$$\hat{a}_{132} = \frac{\eta_2(1,3,2) + \eta_3(1,3,2)}{\xi_1(1,3) + \xi_2(1,3)} \tag{A.272}$$

$$\hat{a}_{133} = \frac{\eta_2(1,3,3) + \eta_3(1,3,3)}{\xi_1(1,3) + \xi_2(1,3)} \tag{A.273}$$

$$\hat{a}_{211} = \frac{\eta_2(2,1,1) + \eta_3(2,1,1)}{\xi_1(2,1) + \xi_2(2,1)} \tag{A.274}$$

$$\hat{a}_{212} = \frac{\eta_2(2,1,2) + \eta_3(2,1,2)}{\xi_1(2,1) + \xi_2(2,1)} \tag{A.275}$$

$$\hat{a}_{213} = \frac{\eta_2(2,1,3) + \eta_3(2,1,3)}{\xi_1(2,1) + \xi_2(2,1)} \tag{A.276}$$

$$\hat{a}_{221} = \frac{\eta_2(2,2,1) + \eta_3(2,2,1)}{\xi_1(2,2) + \xi_2(2,2)} \tag{A.277}$$

$$\hat{a}_{222} = \frac{\eta_2(2,2,2) + \eta_3(2,2,2)}{\xi_1(2,2) + \xi_2(2,2)} \tag{A.278}$$

$$\hat{a}_{223} = \frac{\eta_2(2,2,3) + \eta_3(2,2,3)}{\xi_1(2,2) + \xi_2(2,2)} \tag{A.279}$$

$$\hat{a}_{231} = \frac{\eta_2(2,3,1) + \eta_3(2,3,1)}{\xi_1(2,3) + \xi_2(2,3)} \tag{A.280}$$

$$\hat{a}_{232} = \frac{\eta_2(2,3,2) + \eta_3(2,3,2)}{\xi_1(2,3) + \xi_2(2,3)} \tag{A.281}$$

$$\hat{a}_{233} = \frac{\eta_2(2,3,3) + \eta_3(2,3,3)}{\xi_1(2,3) + \xi_2(2,3)} \tag{A.282}$$

$$\hat{a}_{311} = \frac{\eta_2(3,1,1) + \eta_3(3,1,1)}{\xi_1(3,1) + \xi_2(3,1)} \tag{A.283}$$

$$\hat{a}_{312} = \frac{\eta_2(3,1,2) + \eta_3(3,1,2)}{\xi_1(3,1) + \xi_2(3,1)} \tag{A.284}$$

$$\hat{a}_{313} = \frac{\eta_2(3,1,3) + \eta_3(3,1,3)}{\xi_1(3,1) + \xi_2(3,1)} \tag{A.285}$$

$$\hat{a}_{321} = \frac{\eta_2(3,2,1) + \eta_3(3,2,1)}{\xi_1(3,2) + \xi_2(3,2)} \tag{A.286}$$

$$\hat{a}_{322} = \frac{\eta_2(3,2,2) + \eta_3(3,2,2)}{\xi_1(3,2) + \xi_2(3,2)} \tag{A.287}$$

$$\hat{a}_{323} = \frac{\eta_2(3,2,3) + \eta_3(3,2,3)}{\xi_1(3,2) + \xi_2(3,2)} \tag{A.288}$$

$$\hat{a}_{331} = \frac{\eta_2(3,3,1) + \eta_3(3,3,1)}{\xi_1(3,3) + \xi_2(3,3)} \tag{A.289}$$

$$\hat{a}_{332} = \frac{\eta_2(3,3,2) + \eta_3(3,3,2)}{\xi_1(3,3) + \xi_2(3,3)} \tag{A.290}$$

$$\hat{a}_{333} = \frac{\eta_2(3,3,3) + \eta_3(3,3,3)}{\xi_1(3,3) + \xi_2(3,3)} \tag{A.291}$$

Appendix B

Optimized M-H Model Results for the First-Order SHFMMs obtained in Chapters 5, 6, 7

B.1 M-H Results for Chapter 5

In this section analysis of optimized model results obtained for the First-Order SHFMM presented in Chapters 5 is presented. The Markov chain for the M-H sampling shows the sampling path, while the corresponding histogram shows the optimized model results after training the M-H algorithm with the observed data and semi-hidden Fritchman model regenerated data.

Table B.1: Model Comparison (M-H algorithm vs. Baum-Welch algorithm)- mildly disturbed scenario

	Model Selected M-H Algorithm	Model Selected Baum-Welch Algorithm
QPSK	A_1^{49}	A_1^{79}
DQPSK	A_1^{8}	A_1^{68}
DBPSK	A_1^{40}	A_1^{38}
BPSK	A_1^{50}	A_1^{69}

Table B.2: Model Comparison (M-H algorithm vs. Baum-Welch algorithm)- heavily disturbed scenario

	Model Selected M-H Algorithm	Model Selected Baum-Welch Algorithm
QPSK	A_1^{8}	A_1^{50}
DQPSK	A_1^{37}	A_1^{60}
DBPSK	A_1^{16}	A_1^{42}
BPSK	A_1^{63}	A_1^{39}

Table B.1 and Table B.2 show a comparison between model selected by the M-H algorithm and Baum-Welch training algorithm for mildly disturbed and heavily disturbed scenario respectively. The optimized model selected by the M-H algorithm in Table B.1 and Table B.2 are near optimal models that depict the empirical error sequence modeled.

B.1.1 M-H Results for Mildly Disturbed Empirical Data

The Figure B.2, Figure B.4, Figure B.6 and Figure B.8 show the optimized model selected for each of the corresponding modulation scheme used to model the NB-PLC channel for the mildly disturbed noise scenario. Although a prior with uniform distribution is assumed but the histogram shows that the M-H algorithm converged to the exact prior, given the empirical sequence and the 81 SHFMM generated error sequences. Hence, the selected model depicts the most probable model that generated the empirically obtained error sequences.

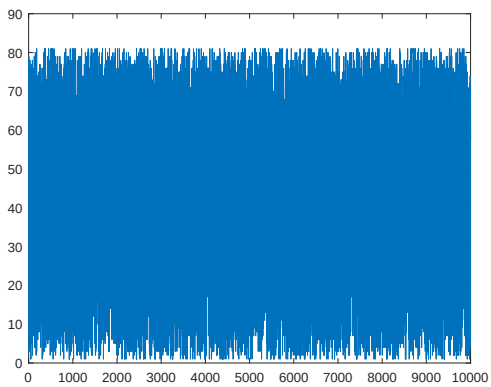

FIGURE B.1: Markov chain showing sampling path (QPSK)

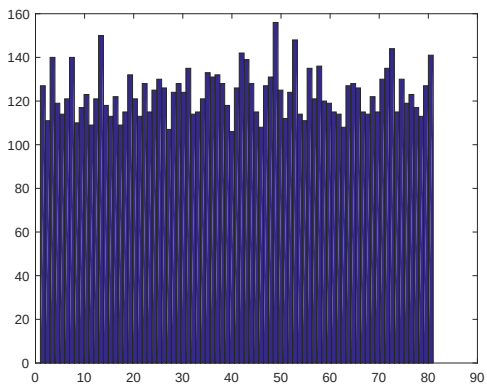

FIGURE B.2: Exact distribution given observed data (QPSK)

Figure B.1 shows the Markov chain sampling path for the converged samples, given the empirical sequence and the 81 SHFMM generated error sequence for the $QPSK$ modulation scheme. Figure B.2 shows that the M-H algorithm converges to model A_1^{49} as the most probable and optimized model that produced the empirically obtained $QPSK$ error sequence.

Figure B.3 shows the Markov chain sampling path for the converged samples, given the empirical sequence and the 81 SHFMM generated error sequence for the $DQPSK$ modulation scheme. Figure B.4 shows that the M-H algorithm converges to model A_1^{8} as the

most probable and optimized model that produced the empirically obtained $DQPSK$ error sequence.

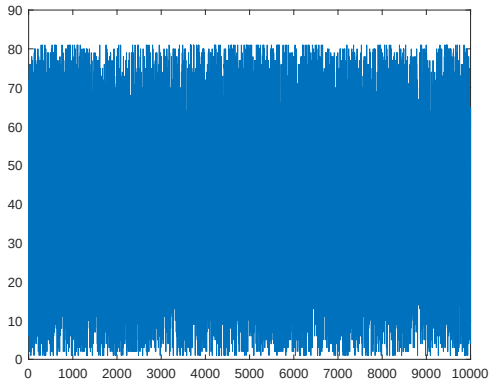

FIGURE B.3: Markov chain showing sampling path (DQPSK)

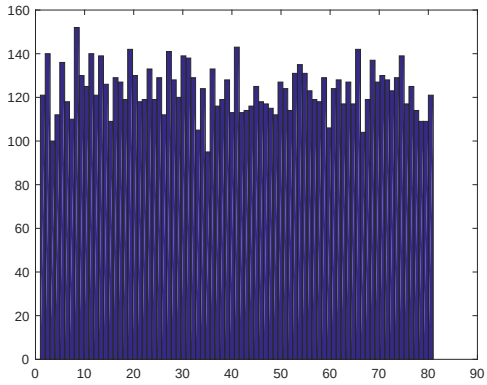

FIGURE B.4: Exact distribution given observed data (DQPSK)

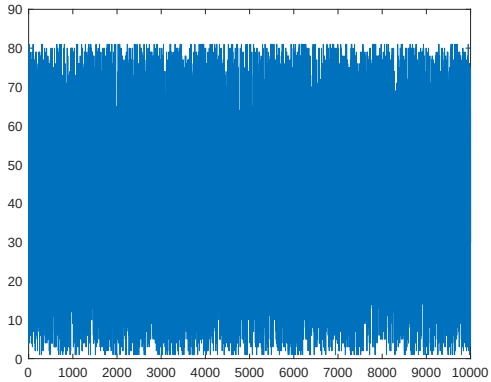

FIGURE B.5: Markov chain showing sampling path (DBPSK)

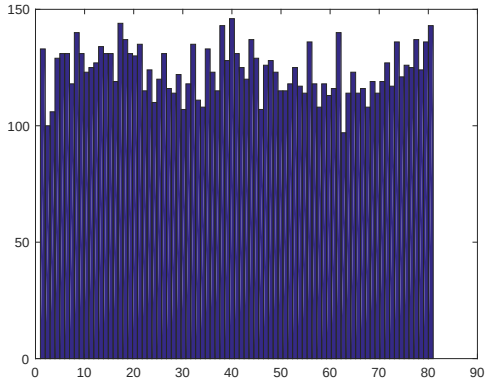

FIGURE B.6: Exact distribution given observed data (DBPSK)

Figure B.5 shows the Markov chain sampling path for the converged samples, given the empirical sequence and the 81 SHFMM generated error sequence for the $DBPSK$ modulation scheme. Figure B.6 shows that the M-H algorithm converges to model A_1^{40} as the most probable and optimized model that produced the empirically obtained $DBPSK$ error sequence.

Figure B.7 shows the Markov chain sampling path for the converged samples, given the empirical sequence and the 81 SHFMM generated error sequence for the $BPSK$ modulation

scheme. Figure B.8 shows that the M-H algorithm converges to model A_1^{50} as the most probable and optimized model that produced the empirically obtained $BPSK$ error sequence.

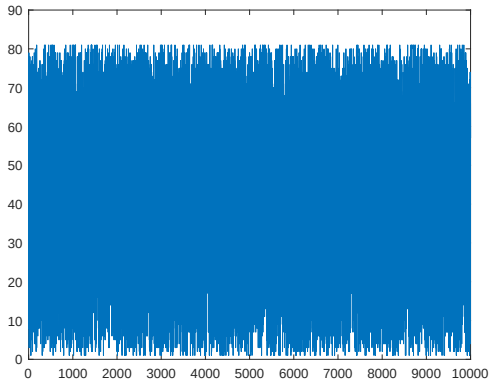

FIGURE B.7: Markov chain showing sampling path (BPSK)

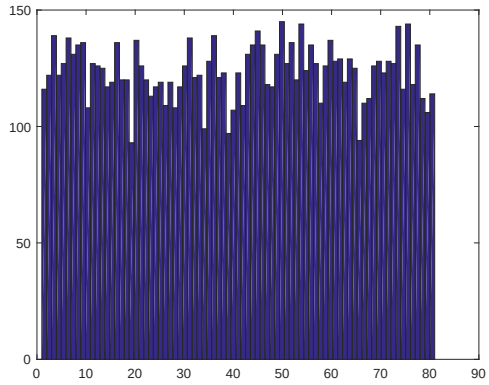

FIGURE B.8: Exact distribution given observed data (BPSK)

B.1.2 M-H Results for Heavily Disturbed Empirical Data

Figure B.10, Figure B.12, Figure B.14 and Figure B.16 show the near optimal model selected for each of the corresponding modulation scheme considered for modeling the NB-PLC channel taking into consideration a heavily disturbed noise scenario. While a prior with uniform distribution is initially assumed, it can be seen that the histogram shows that the M-H algorithm converged to the exact prior, given the empirical sequence and the 81 SHFMM generated error sequences.

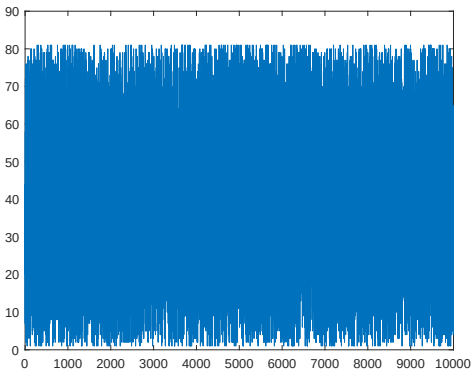

FIGURE B.9: Markov chain showing sampling path (QPSK)

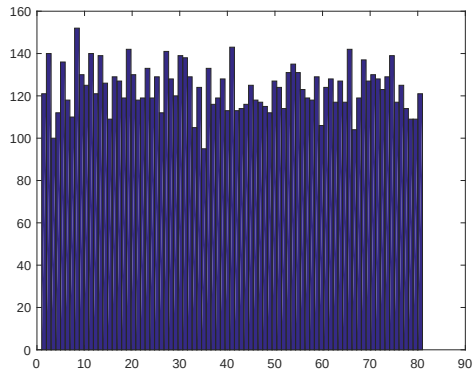

FIGURE B.10: Exact distribution given observed data (QPSK)

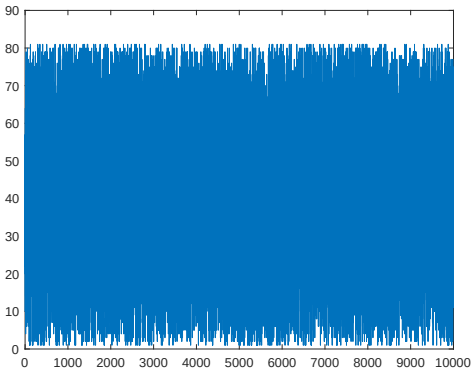

FIGURE B.11: Markov chain showing sampling path (DQPSK)

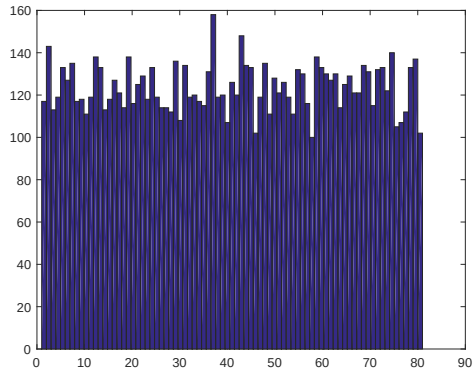

FIGURE B.12: Exact distribution given observed data (DQPSK)

Figure B.9 shows the Markov chain sampling path for the converged samples, given the empirical sequence and the 81 SHFMM generated error sequence for the $QPSK$ modulation scheme. Figure B.10 shows that the M-H algorithm converges to model A_1^8 as the most probable and optimized model that produced the empirically obtained $QPSK$ error

sequence. Figure B.11 shows the Markov chain sampling path for the converged samples, given the empirical sequence and the 81 SHFMM generated error sequence for the $DQPSK$ modulation scheme. Figure B.12 shows that the M-H algorithm converges to model A_1^{37} as the most probable and optimized model that produced the empirically obtained $DQPSK$ error sequence.

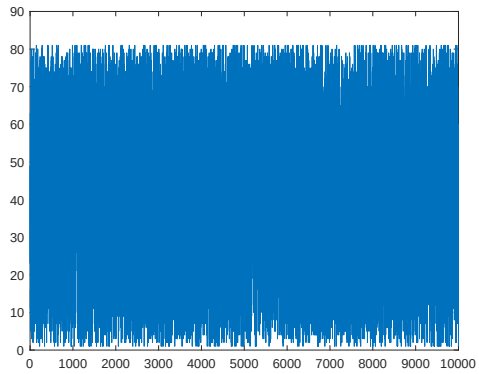

FIGURE B.13: Markov chain showing sampling path (DBPSK)

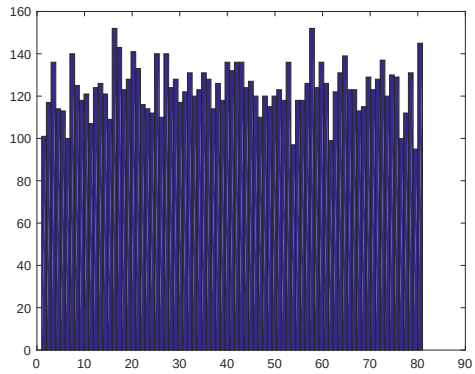

FIGURE B.14: Exact distribution given observed data (DBPSK)

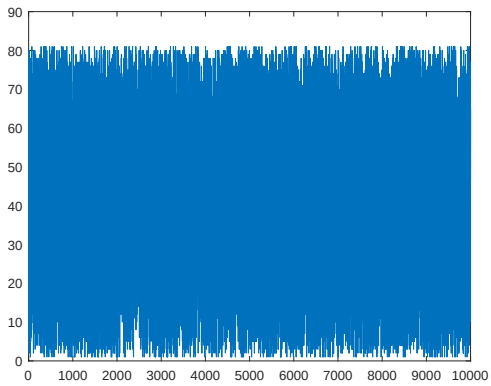

FIGURE B.15: Markov chain showing sampling path (BPSK)

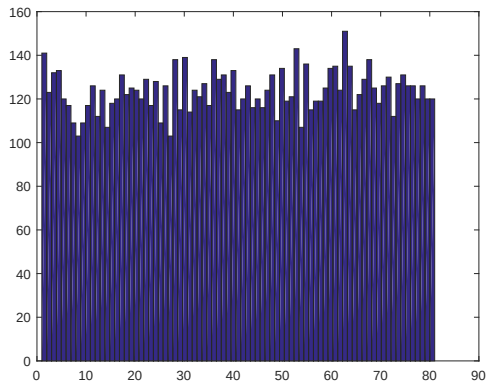

FIGURE B.16: Exact distribution given observed data (BPSK)

Figure B.13 shows the Markov chain sampling path for the converged samples, given the empirical sequence and the 81 SHFMM generated error sequence for the $DBPSK$ modulation scheme. Figure B.14 shows that the M-H algorithm converges to model A_1^{16} as the most probable and optimized model that produced the empirically obtained $DBPSK$ error sequence. Figure B.15 shows the Markov chain sampling path for the converged samples, given the empirical sequence and the 81 SHFMM generated error sequence for the $BPSK$ modulation scheme. Figure B.16 shows that the M-H algorithm converges to model A_1^{63} as

the most probable and optimized model that produced the empirically obtained $BPSK$ error sequence.

B.2 M-H Results for Chapter 6

In this section analysis of optimized model results obtained for the First-Order SHFMM presented in Chapters 6 is presented. The Markov chain for the M-H sampling shows the sampling path, while the corresponding histogram shows the optimized model results after training the M-H algorithm with the observed data and semi-hidden Fritchman model regenerated data.

Table B.3 show a comparison between model selected by the M-H algorithm and Baum-Welch training algorithm. The optimized model selected by the M-H algorithm in Table B.3 are near optimal models that depict the empirical error sequence modeled.

Table B.3: Model Comparison (M-H algorithm vs. Baum-Welch algorithm)

	Model Selected M-H Algorithm	Model Selected Baum-Welch Algorithm
Morning (Lab)	A_1^{43}	A_1^{35}
Afternoon (Res)	A_1^{39}	A_1^{78}
Evening (Lab)	A_1^{72}	A_1^{68}
Morning (Res)	A_1^{18}	A_1^{57}
Evening (Res)	A_1^{27}	A_1^{58}
Afternoon (Lab)	A_1^{51}	A_1^{39}

The Figure B.18, Figure B.20, Figure B.22, Figure B.24, Figure B.26 and Figure B.28 show the optimized model selected for each empirical error sequence corresponding to the time of the day measurement were taken for modeling the hybrid FSK-OOK PLC-VLC taking into consideration the laboratory (Lab) and residential (Res) site.

Although a prior with uniform distribution is assumed but the histogram shows that M-H converged to the exact prior given the empirical sequence and the 81 SHFMM generated error sequence. Hence the selected model depicts the most probable model that generated the empirical error sequences.

Figure B.17 shows the Markov chain sampling path for the converged samples, given the empirical sequence and the 81 SHFMM generated error sequence for $(Morning - Lab)$. Figure B.18 shows that the M-H algorithm converges to model A_1^{43} as the most probable and optimized model that produced the empirically obtained error sequence for $(Morning - Lab)$. Figure B.19 shows the Markov chain sampling path for the converged samples, given the empirical sequence and the 81 SHFMM generated error sequence for $(Afternoon - Res)$. Figure B.20 shows that the M-H algorithm converges to model A_1^{39} as the most probable and optimized model that produced the empirically obtained error sequence for $(Afternoon - Res)$.

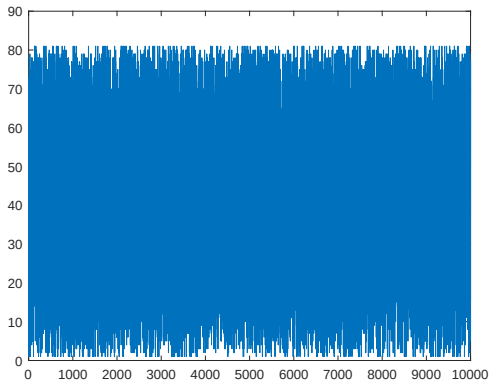

FIGURE B.17: Markov chain showing sampling path (Morning-Lab)

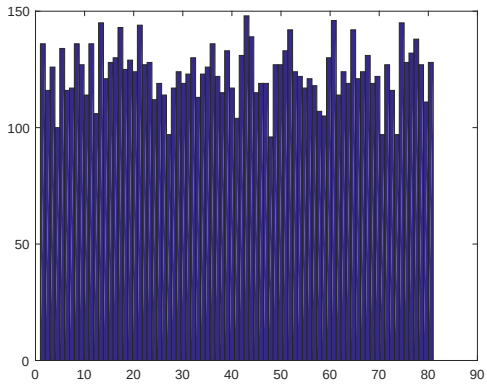

FIGURE B.18: Exact distribution given observed data (Morning-Lab)

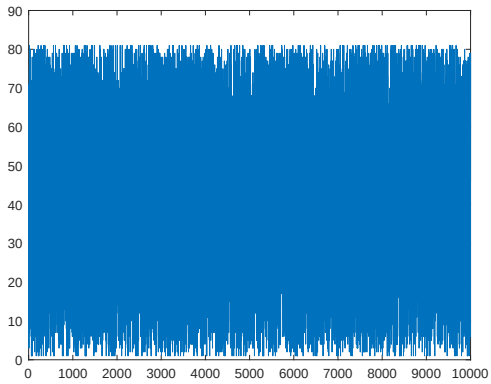

FIGURE B.19: Markov chain showing sampling path (Afternoon-Res)

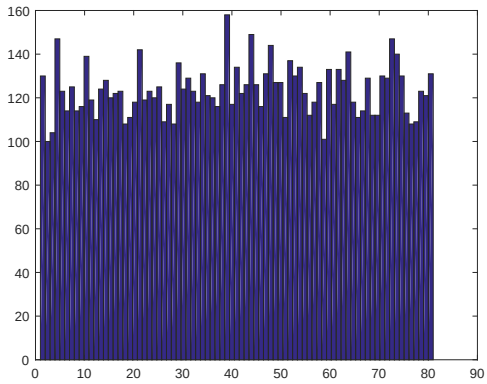

FIGURE B.20: Exact distribution given observed data (Afternoon-Res)

Figure B.21 shows the Markov chain sampling path for the converged samples, given the

empirical sequence and the 81 SHFMM generated error sequence for $(Evening - Lab)$. Figure B.22 shows that the M-H algorithm converges to model A_1^{72} as the most probable and optimized model that produced the empirically obtained error sequence for $(Evening - Lab)$. Figure B.23 shows the Markov chain sampling path for the converged samples, given the empirical sequence and the 81 SHFMM generated error sequence for $(Morning - Res)$. Figure B.24 shows that the M-H algorithm converges to model A_1^{18} as the most probable and optimized model that produced the empirically obtained error sequence for $(Morning - Res)$.

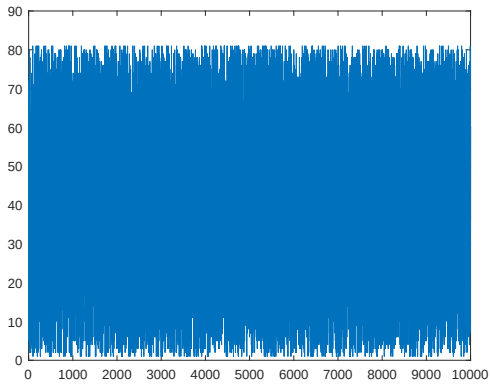

FIGURE B.21: Markov chain showing sampling path (Evening-Lab)

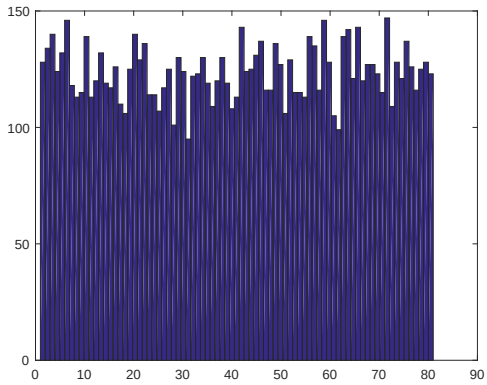

FIGURE B.22: Exact distribution given observed data (Evening-Lab)

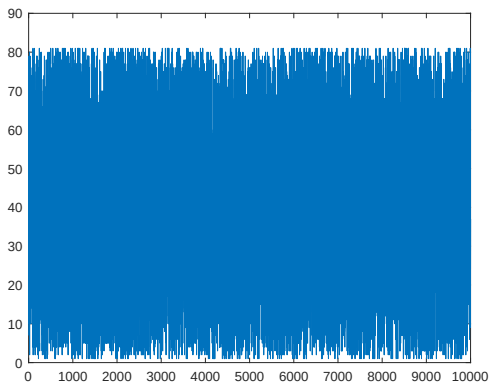

FIGURE B.23: Markov chain showing sampling path (Morning-Res)

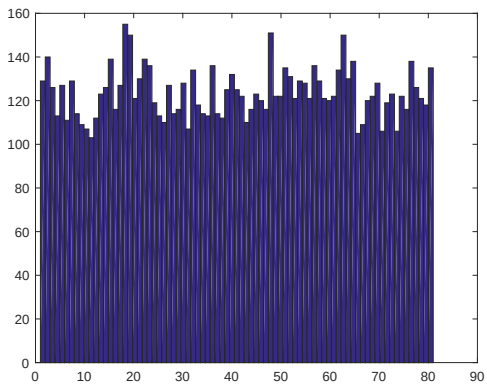

FIGURE B.24: Exact distribution given observed data (Morning-Res)

Figure B.25 shows the Markov chain sampling path for the converged samples, given the

empirical sequence and the 81 SHFMM generated error sequence for $(Evening - Res)$. Figure B.26 shows that the M-H algorithm converges to model A_1^{27} as the most probable and optimized model that produced the empirically obtained error sequence for $(Evening - Res)$. Figure B.27 shows the Markov chain sampling path for the converged samples, given the empirical sequence and the 81 SHFMM generated error sequence for $(Afternoon - Lab)$. Figure B.28 shows that the M-H algorithm converges to model A_1^{51} as the most probable and optimized model that produced the empirically obtained error sequence for $(Afternoon - Lab)$.

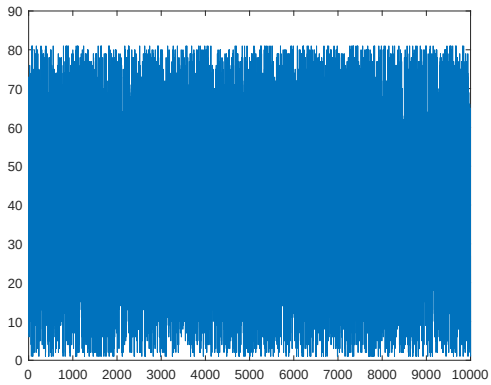

FIGURE B.25: Markov chain showing sampling path (Evening-Res)

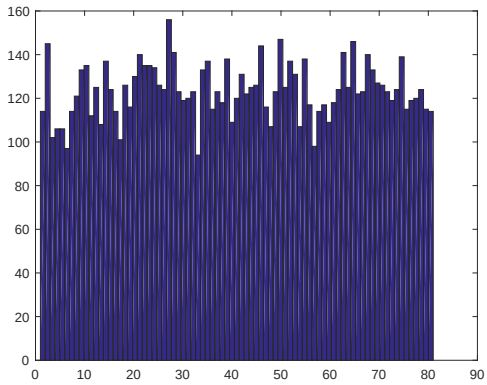

FIGURE B.26: Exact distribution given observed data (Evening-Res)

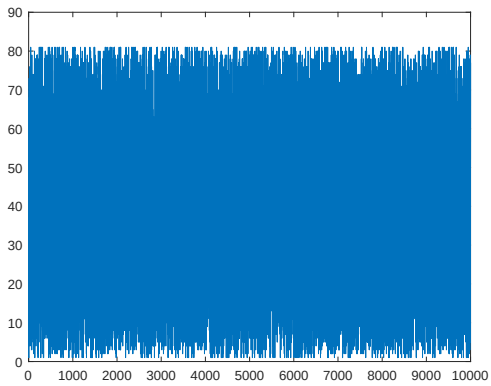

FIGURE B.27: Markov chain showing sampling path (Afternoon-Lab)

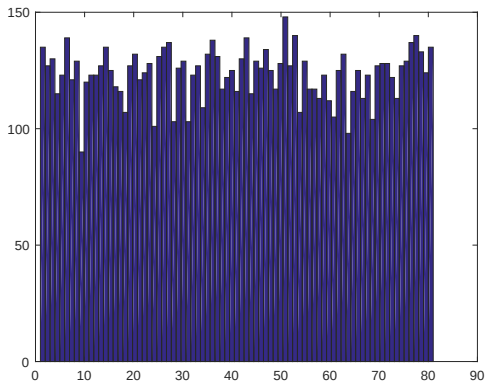

FIGURE B.28: Exact distribution given observed data (Afternoon-Lab)

B.3 M-H Results for Chapter 7

In this section analysis of optimized model results obtained for the First-Order SHFMM presented in Chapters 7 is presented. The Markov chain for the M-H sampling shows the sampling path, while the corresponding histogram shows the optimized model results after training the M-H algorithm with the observed data and semi-hidden Fritchman model regenerated data.

Table B.4 and Table B.5 show a comparison between model selected by the M-H algorithm and Baum-Welch training algorithm for mildly disturbed and heavily disturbed scenario respectively. The optimized model selected by the M-H algorithm in Table B.4 and Table B.5 are near optimal models that depict the empirical error sequence modeled.

Table B.4: Model Comparison (M-H algorithm vs. Baum-Welch algorithm) - mildly disturbed scenario

	Model Selected M-H Algorithm	Model Selected Baum-Welch Algorithm
DQPSK-OFDM (Lab)	A_1^{58}	A_1^{70}
QPSK-OFDM (Lab)	A_1^{49}	A_1^{58}
DQPSK-OFDM (Res)	A_1^{26}	A_1^{39}
QPSK-OFDM (Res)	A_1^{20}	A_1^{78}
D8PSK-OFDM (Lab)	A_1^{12}	A_1^{38}
D8PSK-OFDM (Res)	A_1^{54}	A_1^{50}

Table B.5: Model Comparison (M-H algorithm vs. Baum-Welch algorithm) - heavily disturbed scenario

	Model Selected M-H Algorithm	Model Selected Baum-Welch Algorithm
DQPSK-OFDM (Lab)	A_1^{16}	A_1^{58}
QPSK-OFDM (Lab)	A_1^{53}	A_1^{59}
DQPSK-OFDM (Res)	A_1^{52}	A_1^{62}
QPSK-OFDM (Res)	A_1^{50}	A_1^{78}
D8PSK-OFDM (Lab)	A_1^{47}	A_1^{47}
D8PSK-OFDM (Res)	A_1^{51}	A_1^{62}

B.3.1 M-H Results for Mildly Disturbed Scenario

Figure B.30, Figure B.32, Figure B.34, Figure B.36, Figure B.38 and Figure B.40 show the near optimal model selected for each of the corresponding modulation scheme considered for modeling the NB-PLC channel taking into consideration a mildly disturbed noise scenario.

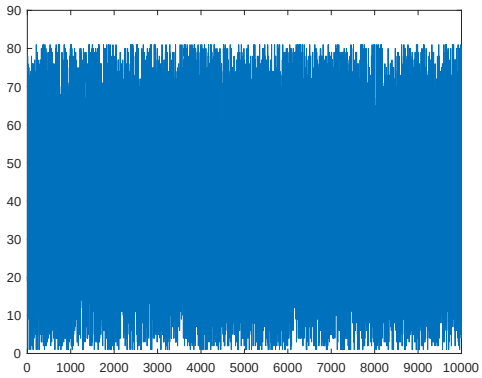

FIGURE B.29: Markov chain showing sampling path (DQPSK-OFDM Lab)

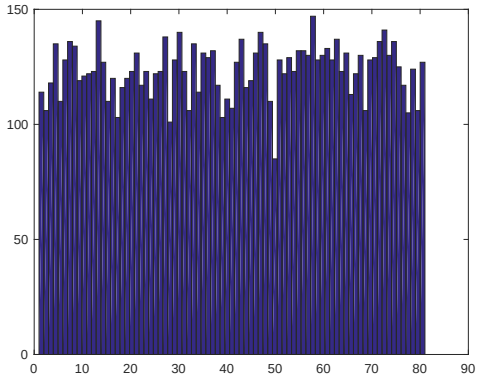

FIGURE B.30: Exact distribution given data (DQPSK-OFDM Lab)

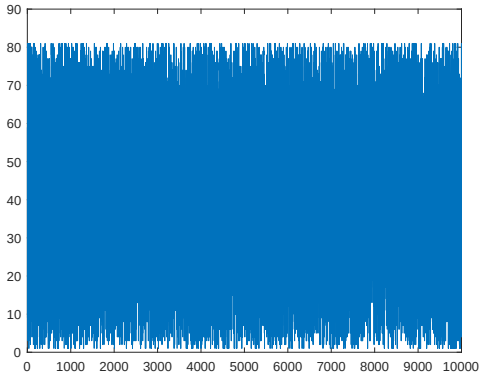

FIGURE B.31: Markov chain showing sampling path (QPSK-OFDM Lab)

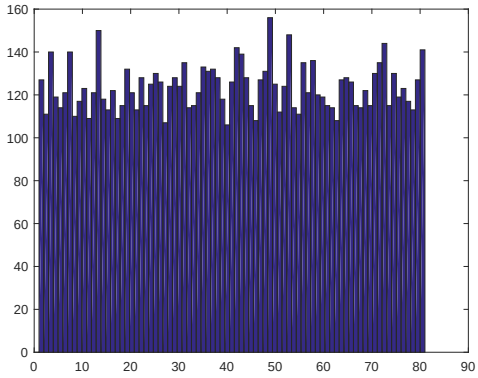

FIGURE B.32: Exact distribution given data (QPSK-OFDM Lab)

Figure B.29 shows the Markov chain sampling path for the converged samples, given the empirical sequence and the 81 SHFMM generated error sequence for the $DQPSK-OFDMLab$ modulation scheme. Figure B.30 shows that the M-H algorithm converges to model A_1^{58} as the most probable and optimized model that produced the empirically obtained $DQPSK-OFDMLab$ error sequence. Figure B.31 shows the Markov chain sampling path for the converged samples, given the empirical sequence and the 81 SHFMM generated error sequence

for the $QPSK - OFDMLab$ modulation scheme. Figure B.32 shows that the M-H algorithm converges to model A_1^{49} as the most probable and optimized model that produced the empirically obtained $QPSK - OFDMLab$ error sequence.

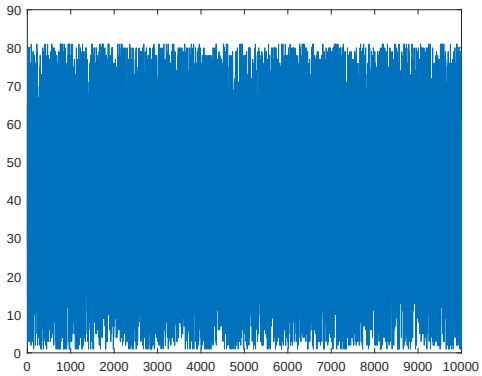

FIGURE B.33: Markov chain showing sampling path (DQPSK-OFDM Res)

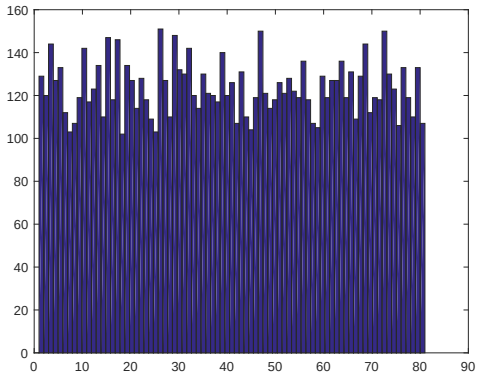

FIGURE B.34: Exact distribution given data (DQPSK-OFDM Res)

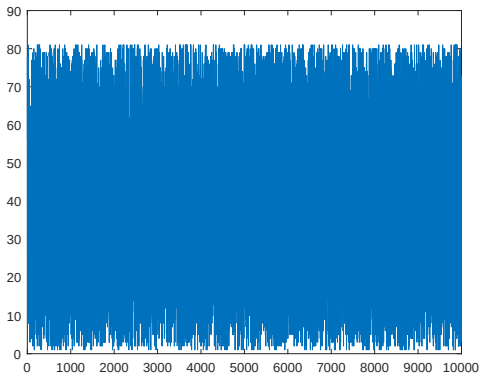

FIGURE B.35: Markov chain showing sampling path (QPSK-OFDM Res)

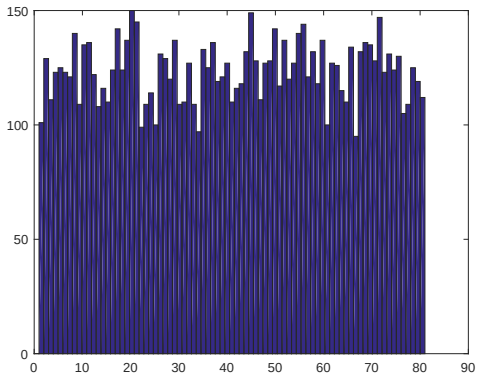

FIGURE B.36: Exact distribution given data (QPSK-OFDM Res)

Figure B.33 shows the Markov chain sampling path for the converged samples, given the empirical sequence and the 81 SHFMM generated error sequence for the $DQPSK - OFDMRes$ modulation scheme. Figure B.34 shows that the M-H algorithm converges to model A_1^{26} as the most probable and optimized model that produced the empirically obtained $DQPSK - OFDMRes$ error sequence. Figure B.35 shows the Markov chain sampling path for the converged samples, given the empirical sequence and the 81 SHFMM generated error sequence

for the $QPSK - OFDMRes$ modulation scheme. Figure B.36 shows that the M-H algorithm converges to model A_1^{20} as the most probable and optimized model that produced the empirically obtained $QPSK - OFDMRes$ error sequence.

Figure B.37 shows the Markov chain sampling path for the converged samples, given the empirical sequence and the 81 SHFMM generated error sequence for the $D8PSK - OFDMLab$ modulation scheme. Figure B.38 shows that the M-H algorithm converges to model A_1^{12} as the most probable and optimized model that produced the empirically obtained $D8PSK - OFDMLab$ error sequence.

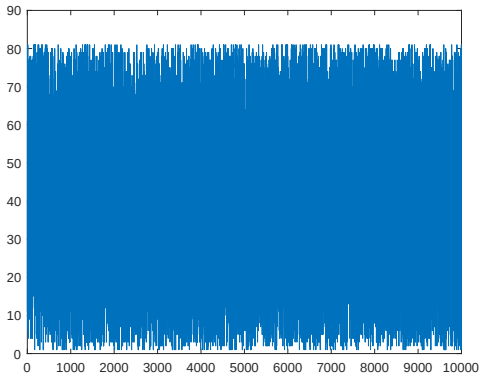

FIGURE B.37: Markov chain showing sampling path (D8PSK-OFDM Lab)

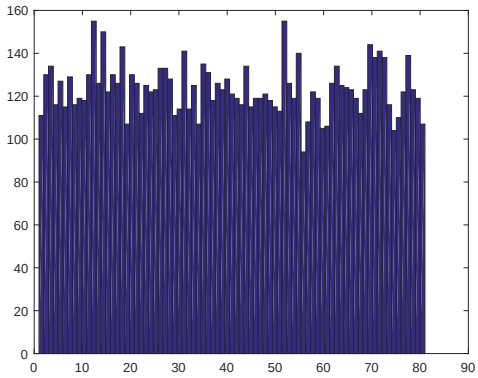

FIGURE B.38: Exact distribution given data (D8PSK-OFDM Lab)

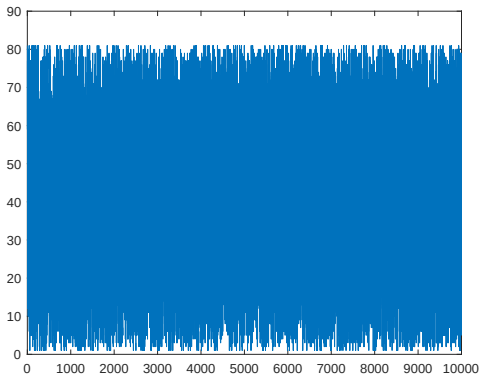

FIGURE B.39: Markov chain showing sampling path (D8PSK-OFDM Res)

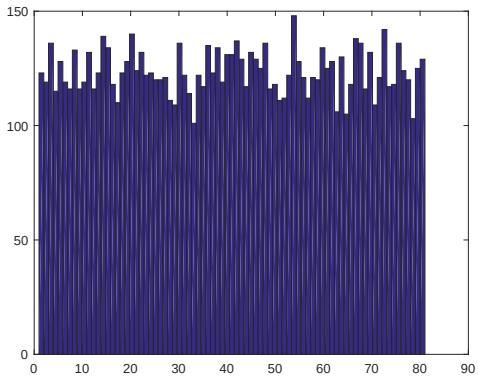

FIGURE B.40: Exact distribution given data (D8PSK-OFDM Res)

Figure B.39 shows the Markov chain sampling path for the converged samples, given the empirical sequence and the 81 SHFMM generated error sequence for the $D8PSK - OFDMRes$ modulation scheme. Figure B.40 shows that the M-H algorithm converges to model A_1^{54} as

the most probable and optimized model that produced the empirically obtained $D8PSK - OFDMRes$ error sequence.

B.3.2 M-H Results for Heavily Disturbed Scenario

Figures B.42, B.44, B.46, B.48, B.50 and Figure B.52 show the near optimal model selected for each of the corresponding modulation scheme considered for modeling the NB-PLC channel taking into consideration a heavily disturbed noise scenario.

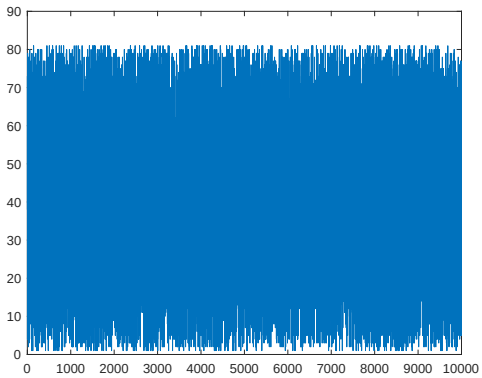

FIGURE B.41: Markov chain showing sampling path (DQPSK-OFDM Lab)

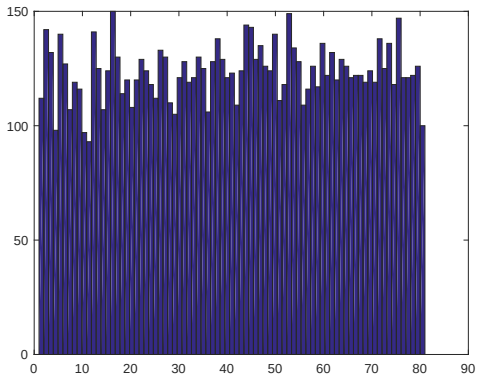

FIGURE B.42: Exact distribution given data (DQPSK-OFDM Lab)

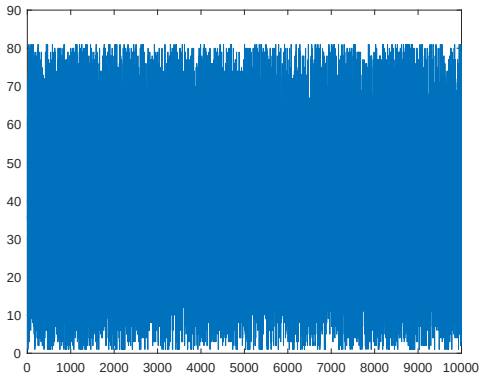

FIGURE B.43: Markov chain showing sampling path (QPSK-OFDM Lab)

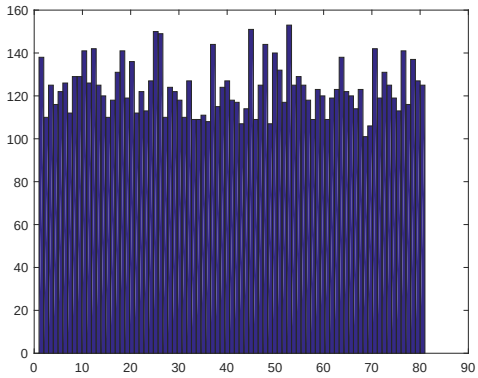

FIGURE B.44: Exact distribution given data (QPSK-OFDM Lab)

Figure B.41 shows the Markov chain sampling path for the converged samples, given the empirical sequence and the 81 SHFMM generated error sequence for the $DQPSK-OFDMLab$ modulation scheme. Figure B.42 shows that the M-H algorithm converges to model A_1^{16} as the most probable and optimized model that produced the empirically obtained $DQPSK-OFDMLab$ error sequence. Figure B.43 shows the Markov chain sampling path for the converged samples, given the empirical sequence and the 81 SHFMM generated error sequence

for the $QPSK - OFDMLab$ modulation scheme. Figure B.44 shows that the M-H algorithm converges to model A_1^{53} as the most probable and optimized model that produced the empirically obtained $QPSK - OFDMLab$ error sequence.

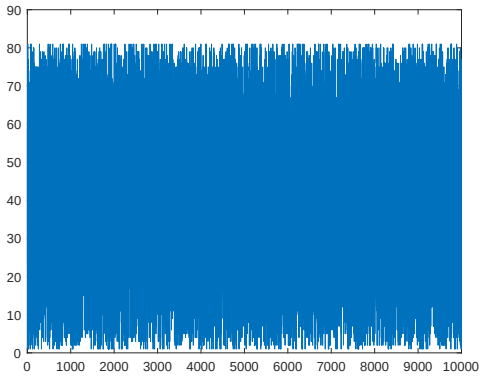

FIGURE B.45: Markov chain showing sampling path (DQPSK-OFDM Res)

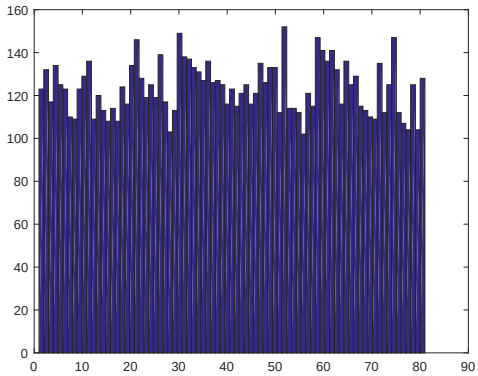

FIGURE B.46: Exact distribution given data (DQPSK-OFDM Res)

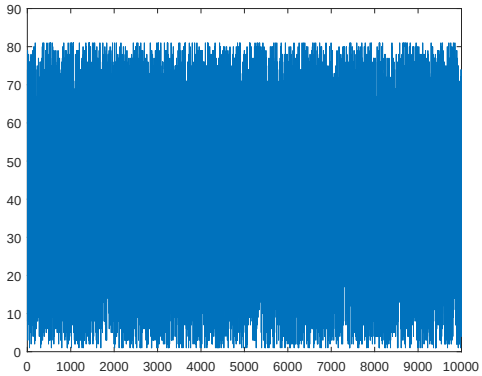

FIGURE B.47: Markov chain showing sampling path (QPSK-OFDM Res)

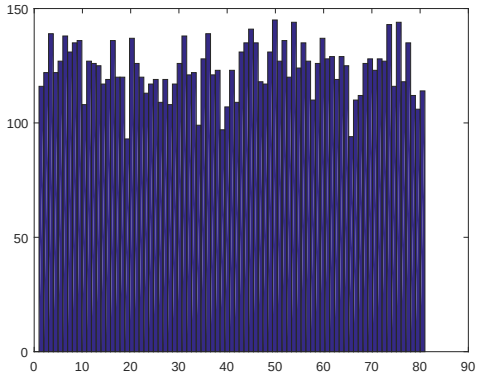

FIGURE B.48: Exact distribution given data (QPSK-OFDM Res)

Figure B.45 shows the Markov chain sampling path for the converged samples, given the empirical sequence and the 81 SHFMM generated error sequence for the $DQPSK - OFDMRes$ modulation scheme. Figure B.46 shows that the M-H algorithm converges to model A_1^{52} as the most probable and optimized model that produced the empirically obtained $DQPSK - OFDMRes$ error sequence. Figure B.47 shows the Markov chain sampling path for the converged samples, given the empirical sequence and the 81 SHFMM generated error sequence

for the $QPSK - OFDMRes$ modulation scheme. Figure B.48 shows that the M-H algorithm converges to model A_1^{50} as the most probable and optimized model that produced the empirically obtained $QPSK - OFDMRes$ error sequence.

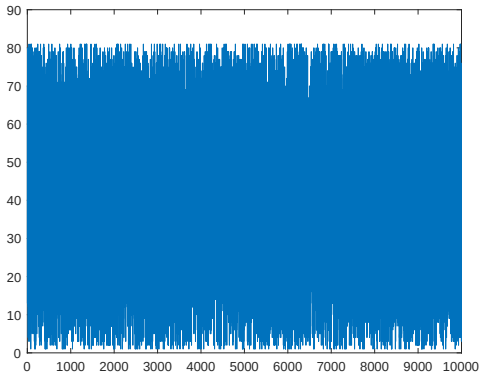

FIGURE B.49: Markov chain showing sampling path (D8PSK-OFDM Lab)

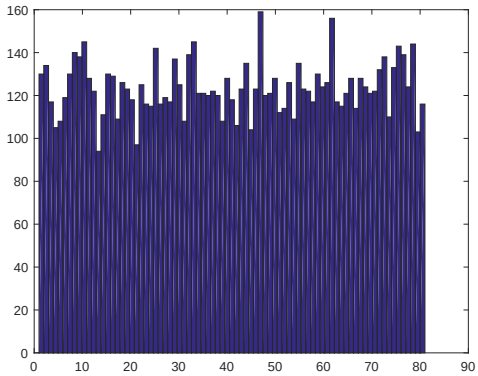

FIGURE B.50: Exact distribution given data (D8PSK-OFDM Lab)

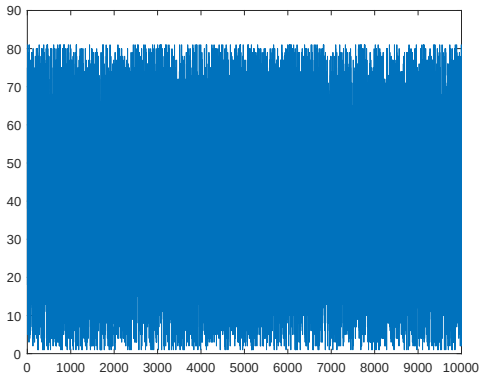

FIGURE B.51: Markov chain showing sampling path (D8PSK-OFDM Res)

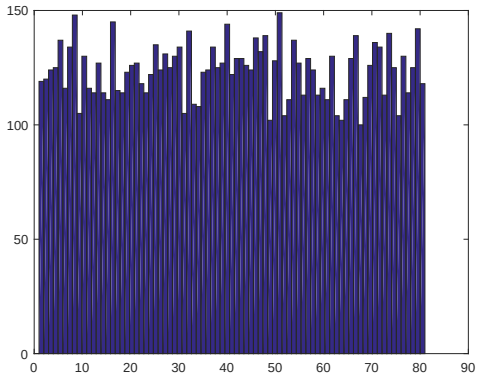

FIGURE B.52: Exact distribution given data (D8PSK-OFDM Res)

Figure B.49 shows the Markov chain sampling path for the converged samples, given the empirical sequence and the 81 SHFMM generated error sequence for the $D8PSK - OFDMLab$ modulation scheme. Figure B.50 shows that the M-H algorithm converges to model A_1^{47} as the most probable and optimized model that produced the empirically obtained $D8PSK - OFDMLab$ error sequence. Figure B.51 shows the Markov chain sampling path for the converged samples, given the empirical sequence and the 81 SHFMM generated error sequence

for the $D8PSK - OFDMRes$ modulation scheme. Figure B.52 shows that the M-H algorithm converges to model A_1^{51} as the most probable and optimized model that produced the empirically obtained $D8PSK - OFDMRes$ error sequence.

Appendix C

Initial State Transition Probabilities for the First-Order SHFMMs

Table C.1: First-Order SHFMM initial state transition probabilities (model 1 - 20)

	A_1^1	A_1^2	A_1^3	A_1^4	A_1^5	A_1^6	A_1^7	A_1^8	A_1^9	A_1^{10}	A_1^{11}	A_1^{12}	A_1^{13}	A_1^{14}	A_1^{15}	A_1^{16}	A_1^{17}	A_1^{18}	A_1^{19}	A_1^{20}
a_{11}	0.65	0.75	0.85	0.95	0.90	0.80	0.89	0.79	0.95	0.85	0.92	0.90	0.95	0.65	0.85	0.75	0.88	0.98	0.90	0.95
a_{13}	0.35	0.25	0.15	0.05	0.10	0.20	0.11	0.21	0.05	0.15	0.08	0.10	0.05	0.25	0.15	0.25	0.12	0.02	0.10	0.05
a_{22}	0.75	0.85	0.85	0.87	0.85	0.95	0.89	0.95	0.85	0.75	0.95	0.85	0.95	0.95	0.85	0.88	0.85	0.95	0.95	0.85
a_{23}	0.25	0.15	0.15	0.13	0.15	0.05	0.11	0.05	0.15	0.25	0.05	0.15	0.05	0.05	0.15	0.12	0.15	0.05	0.05	0.15
a_{31}	0.35	0.46	0.45	0.38	0.50	0.40	0.65	0.55	0.50	0.46	0.55	0.45	0.55	0.20	0.37	0.55	0.45	0.55	0.23	0.30
a_{32}	0.50	0.45	0.41	0.50	0.40	0.50	0.25	0.32	0.38	0.39	0.35	0.45	0.35	0.65	0.52	0.35	0.44	0.30	0.68	0.60
a_{33}	0.15	0.09	0.14	0.12	0.10	0.10	0.10	0.13	0.12	0.15	0.10	0.10	0.10	0.15	0.11	0.10	0.11	0.15	0.09	0.10

Table C.2: First-Order SHFMM initial state transition probabilities (model 21 - 40)

	A_1^{21}	A_1^{22}	A_1^{23}	A_1^{24}	A_1^{25}	A_1^{26}	A_1^{27}	A_1^{28}	A_1^{29}	A_1^{30}	A_1^{31}	A_1^{32}	A_1^{33}	A_1^{34}	A_1^{35}	A_1^{36}	A_1^{37}	A_1^{38}	A_1^{39}	A_1^{40}
a_{11}	0.80	0.90	0.95	0.90	0.95	0.90	0.80	0.90	0.80	0.95	0.70	0.80	0.90	0.69	0.79	0.99	0.89	0.59	0.89	0.83
a_{13}	0.20	0.10	0.05	0.10	0.05	0.10	0.20	0.10	0.20	0.05	0.30	0.20	0.10	0.31	0.21	0.01	0.11	0.41	0.11	0.17
a_{22}	0.90	0.92	0.85	0.80	0.90	0.85	0.72	0.82	0.92	0.62	0.90	0.92	0.92	0.85	0.82	0.92	0.82	0.92	0.95	0.93
a_{23}	0.10	0.08	0.15	0.20	0.10	0.15	0.28	0.18	0.08	0.38	0.10	0.08	0.08	0.15	0.18	0.08	0.18	0.08	0.05	0.07
a_{31}	0.35	0.45	0.15	0.45	0.45	0.50	0.40	0.45	0.50	0.60	0.70	0.50	0.40	0.40	0.30	0.50	0.30	0.50	0.65	0.40
a_{32}	0.50	0.45	0.75	0.48	0.50	0.42	0.50	0.43	0.40	0.35	0.20	0.45	0.51	0.52	0.65	0.40	0.60	0.40	0.26	0.52
a_{33}	0.15	0.10	0.10	0.07	0.05	0.08	0.10	0.12	0.10	0.05	0.10	0.05	0.09	0.08	0.05	0.10	0.10	0.10	0.09	0.08

Table C.3: First-Order SHFMM initial state transition probabilities (model 41 - 60)

	A_1^{41}	A_1^{42}	A_1^{43}	A_1^{44}	A_1^{45}	A_1^{46}	A_1^{47}	A_1^{48}	A_1^{49}	A_1^{50}	A_1^{51}	A_1^{52}	A_1^{53}	A_1^{54}	A_1^{55}	A_1^{56}	A_1^{57}	A_1^{58}	A_1^{59}	A_1^{60}
a_{11}	0.83	0.93	0.73	0.63	0.95	0.88	0.93	0.95	0.75	0.98	0.93	0.99	0.68	0.93	0.88	0.96	0.68	0.78	0.95	0.83
a_{13}	0.17	0.07	0.27	0.37	0.05	0.12	0.07	0.05	0.25	0.02	0.07	0.01	0.32	0.07	0.12	0.04	0.32	0.22	0.05	0.17
a_{22}	0.99	0.95	0.79	0.89	0.79	0.88	0.79	0.89	0.83	0.95	0.85	0.89	0.79	0.75	0.94	0.98	0.75	0.95	0.85	0.99
a_{23}	0.01	0.05	0.21	0.11	0.21	0.12	0.21	0.11	0.17	0.05	0.15	0.11	0.21	0.25	0.06	0.02	0.25	0.05	0.15	0.01
a_{31}	0.40	0.50	0.40	0.60	0.50	0.30	0.50	0.49	0.45	0.37	0.40	0.55	0.48	0.75	0.65	0.50	0.25	0.60	0.70	0.40
a_{32}	0.45	0.45	0.50	0.35	0.40	0.55	0.55	0.45	0.45	0.53	0.55	0.30	0.45	0.15	0.28	0.48	0.65	0.25	0.25	0.45
a_{33}	0.15	0.05	0.10	0.05	0.10	0.15	0.05	0.06	0.10	0.10	0.05	0.15	0.07	0.10	0.07	0.02	0.10	0.15	0.05	0.15

Table C.4: First-Order SHFMM initial state transition probabilities (model 61-81)

	A_1^{61}	A_1^{62}	A_1^{63}	A_1^{64}	A_1^{65}	A_1^{66}	A_1^{67}	A_1^{68}	A_1^{69}	A_1^{70}	A_1^{71}	A_1^{72}	A_1^{73}	A_1^{74}	A_1^{75}	A_1^{76}	A_1^{77}	A_1^{78}	A_1^{79}	A_1^{80}	A_1^{81}
a_{11}	0.77	0.82	0.93	0.96	0.91	0.99	0.75	0.76	0.97	0.55	0.81	0.97	0.75	0.88	0.85	0.95	0.79	0.89	0.91	0.99	0.74
a_{13}	0.23	0.18	0.07	0.04	0.09	0.01	0.25	0.24	0.03	0.45	0.19	0.03	0.25	0.12	0.15	0.05	0.29	0.11	0.09	0.01	0.26
a_{22}	0.89	0.91	0.92	0.87	0.91	0.89	0.91	0.94	0.77	0.89	0.81	0.97	0.78	0.87	0.74	0.71	0.79	0.87	0.88	0.79	0.74
a_{23}	0.11	0.09	0.08	0.13	0.09	0.11	0.09	0.06	0.23	0.11	0.19	0.03	0.22	0.13	0.26	0.29	0.29	0.13	0.12	0.21	0.26
a_{31}	0.50	0.37	0.50	0.75	0.36	0.40	0.71	0.61	0.52	0.62	0.73	0.64	0.72	0.52	0.47	0.79	0.69	0.62	0.52	0.23	0.76
a_{32}	0.41	0.61	0.46	0.15	0.45	0.52	0.19	0.29	0.40	0.27	0.20	0.28	0.17	0.45	0.48	0.17	0.21	0.23	0.35	0.69	0.18
a_{33}	0.09	0.02	0.04	0.10	0.19	0.08	0.10	0.10	0.08	0.11	0.07	0.08	0.11	0.03	0.05	0.04	0.10	0.15	0.13	0.08	0.06

Appendix D

First-Order and Second-Order Estimated State Transition Probabilities for Chapter 7

D.1 Estimated State Transition Probabilities

This section shows the estimated state transition probability matrices for both the First and Second-Order Semi-Hidden Fritchman Markov models (SHFMMs) for the different OFDM modulation schemes utilized, for both residential and laboratory sites taking into consideration the two distinct noise scenarios considered: the "mildly disturbed" and the "heavily disturbed".

D.1.1 First-Order SHFMM Estimated State Transition Probabilities

Table D.1 and Table D.2 show the table for the First-Order SHFMM estimated state transition probabilities for both residential and laboratory sites taking into consideration the mildly and heavily disturbed noise scenarios respectively.

The estimated state transition probability values shown in Table D.1 and Table D.2 are the most probable First-Order SHFMM estimated state transition probabilities out of the 81 regenerated model given the empirical error sequence. These estimated state transition probabilities depicts the statistical probability distribution of both the transmission errors and non-occurrence of transmission error as empirically obtained for the different OFDM modulation schemes.

A close look at Table D.1 and Table D.2 shows a non-uniform probability distributions typical of the narrowband PLC channel. The non-uniformity in probability distribution can be attributed to differing channel characteristics as at the time of transmission and the fact that practically no two error sequences can be identical as the OFDM modulation schemes used are more robust than each other in the presence of similar interferers, hence

Table D.1: First-order SHFMM estimated state transition probabilities (mildly disturbed scenario)

	Residential			Laboratory		
	QPSK OFDM	DQPSK OFDM	D8PSK OFDM	QPSK OFDM	DQPSK OFDM	D8PSK OFDM
a_{11}	0.9501	0.9522	0.9547	0.9623	0.9375	0.9569
a_{13}	0.0499	0.0478	0.0430	0.0377	0.0625	0.0431
a_{22}	0.8936	0.9401	0.8979	0.9724	0.9372	0.9036
a_{23}	0.1064	0.0599	0.1021	0.0276	0.0628	0.0964
a_{31}	0.7061	0.7963	0.6562	0.0339	0.5098	0.6857
a_{32}	0.2396	0.1615	0.2368	0.9298	0.4644	0.2113
a_{33}	0.0543	0.0422	0.1070	0.0363	0.0259	0.0930

the modulation scheme with the most superior spatial proximity and angular separation or euclidean distance on the constellation graph performs better [102]. Other factors that contribute to the non-uniformity of the probability distributions includes: topology of the power line at different measurement sites, the duration of noise impairments, source, place and time of measurement. Hence, the need for constant measurement campaigns before statistical mathematical models are derived in order to capture rich parameters sets that depicts the channel and can be used to exploit and mitigate performance degradation on the PLC channel.

Table D.2: First-order SHFMM estimated state transition probabilities (heavily disturbed scenario)

	Residential			Laboratory		
	QPSK OFDM	DQPSK OFDM	D8PSK OFDM	QPSK OFDM	DQPSK OFDM	D8PSK OFDM
a_{11}	0.9536	0.9607	0.9873	0.9662	0.9574	0.9948
a_{13}	0.0464	0.0393	0.0127	0.0338	0.0426	0.0052
a_{22}	0.9360	0.9550	0.9380	0.9312	0.9489	0.9011
a_{23}	0.0640	0.0450	0.0620	0.0688	0.0511	0.0989
a_{31}	0.2981	0.5707	0.6435	0.6062	0.1500	0.6364
a_{32}	0.6285	0.3623	0.2449	0.3260	0.7954	0.2551
a_{33}	0.0734	0.0670	0.1116	0.0677	0.0546	0.1085

D.1.2 Second-Order SHFMM Estimated State Transition Probabilities

Table D.3 and Table D.4 show the Second-Order SHFMM estimated state transition probabilities for both residential and laboratory sites taking into consideration the mildly and heavily disturbed noise scenarios respectively. The estimated state transition probability values shown in Table D.3 and Table D.4 are the most probable Second-Order SHFMM estimated transition probability values out of the 81 regenerated model given the empirical error sequence.

Table D.3: Second-Order SHFMM estimated state transition probabilities (mildly disturbed scenario)

	Residential			Laboratory		
	QPSK OFDM	DQPSK OFDM	D8PSK OFDM	QPSK OFDM	DQPSK OFDM	D8PSK OFDM
a_{111}	0.9506	0.9594	0.9583	0.9599	0.9573	0.9579
a_{113}	0.0494	0.0406	0.0417	0.0401	0.0427	0.0421
a_{122}	0.9532	0.9544	0.9494	0.9408	0.9412	0.9414
a_{123}	0.0468	0.0456	0.0506	0.0592	0.0588	0.0586
a_{131}	0.1493	0.1421	0.1418	0.1496	0.1417	0.1419
a_{132}	0.7590	0.7580	0.7588	0.7576	0.7593	0.7597
a_{133}	0.0917	0.0979	0.0994	0.0928	0.0990	0.0984
a_{211}	0.9039	0.9056	0.9060	0.9055	0.9065	0.9053
a_{213}	0.0961	0.0944	0.0940	0.0945	0.0935	0.0947
a_{222}	0.8816	0.8812	0.8819	0.8817	0.8814	0.8825
a_{223}	0.1184	0.1188	0.1181	0.1183	0.1186	0.1175
a_{231}	0.6588	0.6570	0.6589	0.6577	0.6596	0.6588
a_{232}	0.2406	0.2402	0.2419	0.2427	0.2418	0.2423
a_{233}	0.1006	0.1028	0.0992	0.0996	0.0986	0.0989
a_{311}	0.8815	0.8824	0.8824	0.8829	0.8827	0.8834
a_{313}	0.1185	0.1176	0.1176	0.1171	0.1173	0.1166
a_{322}	0.9889	0.9883	0.9896	0.9878	0.9885	0.9888
a_{323}	0.0111	0.0117	0.0104	0.0122	0.0115	0.0112
a_{331}	0.0714	0.0803	0.0195	0.0908	0.0985	0.0440
a_{332}	0.8641	0.8614	0.8825	0.8622	0.8624	0.8820
a_{333}	0.0645	0.0583	0.0980	0.0470	0.0391	0.0740

These estimated state transition probabilities depicts the statistical probability distribution

of both the transmission errors and non-occurrence of transmission error as empirically obtained for the different OFDM modulation schemes. A close look at Table D.3 and Table D.4 shows a non-uniform probability distributions. The non-uniformity in probability distribution can be attributed to differing channel characteristics, superior spatial proximity and angular separation or euclidean distance on the constellation graph of the OFDM modulation scheme used, hence, non-identical empirical error sequences are obtained. Other factors contributing to the non-uniformity of the probability distribution includes: power line topology, sources of noise impairments and other factors mentioned in the concluding part of Section D.1.1. It is important to note that the Second-Order SHFMM estimated state transition probabilities in Table D.3 and Table D.4 are the most probable estimated state transition probabilities out of the 81 regenerated model that depict the empirical error sequence been modeled.

Table D.4: Second-Order SHFMM estimated state transition probabilities (Heavily disturbed scenario)

	Residential			Laboratory		
	QPSK OFDM	DQPSK OFDM	D8PSK OFDM	QPSK OFDM	DQPSK OFDM	D8PSK OFDM
a_{111}	0.9006	0.9004	0.9013	0.9001	0.9021	0.9011
a_{113}	0.0994	0.0996	0.0987	0.0999	0.0979	0.0989
a_{122}	0.9832	0.9834	0.9894	0.9802	0.9838	0.9816
a_{123}	0.0168	0.0166	0.0106	0.0198	0.0162	0.0184
a_{131}	0.1453	0.1451	0.1488	0.1486	0.1483	0.1484
a_{132}	0.7860	0.7850	0.7818	0.7836	0.7827	0.7827
a_{133}	0.0687	0.0699	0.0694	0.0678	0.0690	0.0689
a_{211}	0.8939	0.8959	0.8960	0.8958	0.8962	0.8957
a_{213}	0.1061	0.1041	0.1040	0.1042	0.1038	0.1043
a_{222}	0.8814	0.8818	0.8819	0.8813	0.8814	0.8826
a_{223}	0.1186	0.1182	0.1181	0.1187	0.1186	0.1174
a_{231}	0.6888	0.6870	0.6889	0.6879	0.6886	0.6883
a_{232}	0.2105	0.2108	0.2112	0.2124	0.2118	0.2118
a_{233}	0.1005	0.1022	0.0999	0.0997	0.0996	0.0999
a_{311}	0.8813	0.8822	0.8826	0.8821	0.8823	0.8836
a_{313}	0.1187	0.1178	0.1174	0.1179	0.1177	0.1164
a_{322}	0.9588	0.9583	0.9594	0.9572	0.9584	0.9582
a_{323}	0.0412	0.0417	0.0406	0.0428	0.0416	0.0418
a_{331}	0.0428	0.0448	0.0064	0.0519	0.0668	0.0085
a_{332}	0.8841	0.8844	0.8925	0.8881	0.8828	0.9020
a_{333}	0.0731	0.0708	0.1011	0.0600	0.0504	0.0895

Bibliography

[1] E. C. for Electrotechnical Standardization (CENELEC). "EN 50065-1 Signalling on low voltage electrical installations in the frequency range 3 kHz to 148.5 kHz - Part 1: General requirments, frequency bands and electromagnetic disturbances.", 2011.

[2] I. 1901.2. "*Draft standard for low frequency (less than 500 kHz) narrow band power line communications for Smart Grid applications.*", 2013. http://grouper.ieee.org/groups/1901/2/ [Accessed: 2016-08-31].

[3] H. C. Emissions. "Guidelines to the standard EN 61000-3-2.", 2010.

[4] A. Mengi. *On combined coding and modulation*. Ph.D. thesis, Duisburg, Essen, Univ., Diss., 2010.

[5] H. Ferreira, L. Lampe, J. Newbury, and T. Swart. *Power line communications: Theory and applications for narrowband and broadband communications over power lines*. John Wiley & Sons, 2011.

[6] Y.-H. Kim, K.-H. Kim, H.-M. Oh, K.-H. Kim, and S.-C. Kim. "Mitigation of effect of impulsive noise for OFDM systems over power line channels." In *Power Line Communications and Its Applications, 2008. ISPLC 2008. IEEE International Symposium on*, pp. 386–390. IEEE, 2008.

[7] M. Zimmermann and K. Dostert. "An analysis of the broadband noise scenario in powerline networks." In *International Symposium on Powerline Communications and its Applications (ISPLC2000)*, pp. 5–7. 2000.

[8] M. Ghosh. "Analysis of the effect of impulse noise on multicarrier and single carrier QAM systems." *IEEE Transactions on Communications*, vol. 44, no. 2, pp. 145–147, 1996.

[9] A. H. Vinck and J. Häring. "Coding and modulation for power-line communications." In *Proc. Int. Symp. Power Line Communication*, pp. 5–7. 2000.

[10] M. Hoch. "Comparison of PLC G3 and PRIME." In *IEEE International Symposium on Power Line Communications and Its Applications*, pp. 165–169. 2011.

[11] I. Berganza, A. Sendin, and J. Arriola. "PRIME: Powerline intelligent metering evolution." In *CIRED Seminar*, pp. 1–3. Citeseer, 2008.

[12] S. Galli and T. Lys. "Next generation narrowband (under 500 kHz) power line communications (PLC) standards." *China Communications*, vol. 12, no. 3, pp. 1–8, 2015.

[13] C. Sonntag. *Orthogonal frequency division multiplexing (OFDM) implementation as part of a software devined radio (SDR) environment*. Ph.D. thesis, Stellenbosch: University of Stellenbosch, 2005.

[14] A. B. Narasimhamurthy, M. K. Banavar, and C. Tepedelenliouglu. "OFDM systems for wireless communications." *Synthesis Lectures on Algorithms and Software in Engineering*, vol. 2, no. 1, pp. 1–78, 2010.

[15] Y. Ma, P. So, and E. Gunawan. "Performance analysis of OFDM systems for broadband power line communications under impulsive noise and multipath effects." *IEEE Transactions on Power Delivery*, vol. 20, no. 2, pp. 674–682, 2005.

[16] B. Fritchman. "A binary channel characterization using partitioned Markov chains." *IEEE Transactions on Information Theory*, vol. 13, no. 2, pp. 221–227, 1967.

[17] J.-Y. Chouinard, M. Lecours, and G. Delisle. "Estimation of Gilbert's and Fritchman's models parameters using the gradient method for digital mobile radio channels." *IEEE Transactions on Vehicular Technology*, vol. 37, no. 3, pp. 158–166, 1988.

[18] A. D. Familua and L. Cheng. "Modeling of in-house CENELEC A-band PLC channel using Fritchman model and Baum-Welch algorithm." In *IEEE International Symposium on Power Line Communications and Its Applications*, pp. 173–178. 2013.

[19] A. Familua, K. Ogunyanda, T. Swart, H. Ferreira, R. Van Olst, and L. Cheng. "Narrowband PLC Channel Modeling using USRP and PSK Modulations." In *IEEE International Symposium on Power Line Communications and Its Applications*, pp. 156–161. 2014.

[20] L. E. Baum, T. Petrie, G. Soules, and N. Weiss. "A maximization technique occurring in the statistical analysis of probabilistic functions of Markov chains." *The annals of mathematical statistics*, vol. 41, no. 1, pp. 164–171, 1970.

[21] W. Tranter, K. Shanmugan, T. Rappaport, and K. Kosbar. *Principles of communication systems simulation with wireless applications*. Prentice Hall Press, first ed., 2003.

[22] L. Berger, A. Schwager, P. Pagani, and D. Schneider. *MIMO Power Line Communications: Narrow and Broadband Standards, EMC, and Advanced Processing*. CRC Press, 2014.

[23] M. Babic, M. Hagenau, K. Dostert, and J. Bausch. "Theoretical postulation of PLC channel model." *IST Integrated Project Deliverable D4v2. 0, The OPERA Consortium*, 2005.

[24] E. Biglieri. "Coding and modulation for a horrible channel." *IEEE Communications Magazine*, vol. 41, no. 5, pp. 92–98, 2003.

[25] S. Galli, A. Scaglione, and Z. Wang. "For the grid and through the grid: The role of power line communications in the smart grid." *Proceedings of the IEEE*, vol. 99, no. 6, pp. 998–1027, 2011.

[26] K. Iniewski. *Convergence of mobile and stationary next-generation networks*. John Wiley & Sons, 2011.

[27] K. Dostert. *Powerline Communications*. Prentice Hall P T R, New York, 2001.

[28] R. Pighi and R. Raheli. "On multicarrier signal transmission for high-voltage power lines." In *International Symposium on Power Line Communications and Its Applications, 2005.*, pp. 32–36. IEEE, 2005.

[29] D. Hyun and Y. Lee. "A study on the compound communication network over the high voltage power line for distribution automation system." In *Information Security and Assurance, 2008. ISA 2008. International Conference on*, pp. 410–414. IEEE, 2008.

[30] R. Aquilue, I. Gutierrez, J. L. Pijoan, and G. Sanchez. "High-voltage multicarrier spread-spectrum system field test." *IEEE Transactions on Power Delivery*, vol. 24, no. 3, pp. 1112–1121, 2009.

[31] P. A. Wouters, P. C. van der Wielen, J. Veen, P. Wagenaars, and E. F. Steennis. "Effect of cable load impedance on coupling schemes for MV power line communication." *IEEE Transactions on Power Delivery*, vol. 20, no. 2, pp. 638–645, 2005.

[32] R. Benato and R. Caldon. "Application of PLC for the control and the protection of future distribution networks." In *2007 IEEE International Symposium on Power Line Communications and Its Applications*, pp. 499–504. IEEE, 2007.

[33] A. Cataliotti, A. Daidone, and G. Tinè. "Power line communication in medium voltage systems: characterization of MV cables." *IEEE Transactions on Power Delivery*, vol. 23, no. 4, pp. 1896–1902, 2008.

[34] N. Pine and S. Choe. "Modified multipath model for broadband MIMO power line communications." In *Power Line Communications and Its Applications (ISPLC), 2012 16th IEEE International Symposium on*, pp. 292–297. IEEE, 2012.

[35] A. Rubinstein, F. Rachidi, M. Rubinstein, A. Vukicevic, K. Sheshyekani, W. Bschelin, and C. Rodrguez-Morcillo. "EMC guidelines, The OPERA Consortium, IST Integrated Project Deliverable D9v1.1.", October 2008.

[36] A. Vukicevic. *Electromagnetic compatibility of power line communication systems*. Ph.D. thesis, ÉCOLE POLYTECHNIQUE FÉDÉRALE DE LAUSANNE, 2008.

[37] N. Gonzez-Prelcic, C. Mosquera, N. Degara, and A. Currais. "A channel model for the Galician low voltage mains network." In *Power Line Communications and Its Applications (ISPLC), 2001 IEEE International Symposium on*, pp. 365–370. IEEE, 2001.

[38] M. Zimmermann and K. Dostert. "A multipath model for the powerline channel." *IEEE Transactions on Communications*, vol. 50, no. 4, pp. 553–559, 2002.

[39] H. Liu, J. Song, B. Zhao, and X. Li. "Channel study for medium-voltage power network." In *2006 IEEE International Symposium on Power Line Communications and Its Applications*, pp. 245–250. IEEE, 2006.

[40] H. Philipps. "Performance measurements of powerline channels at high frequencies." In *Proceedings of the International Symposium on Power Line Communications and its Applications (ISPLC)*, vol. 229–237. 1998.

[41] D. Liu, E. Flint, B. Gaucher, and Y. Kwark. "Wide band AC power line characterization." *IEEE Transactions on Consumer Electronics*, vol. 45, no. 4, pp. 1087–1097, 1999.

[42] T. Esmailian, F. Kschischang, and G. Glenn. "In-building power lines as high-speed communication channels: channel characterization and a test channel ensemble." *International Journal of Communication Systems*, vol. 16, no. 5, pp. 381–400, 2003.

[43] A. Schwager, L. Stadelmeier, and M. Zumkeller. "Potential of broadband power line home networking." In *Second IEEE Consumer Communications and Networking Conference*, pp. 359–363. IEEE, 2005.

[44] A. Cataliotti, V. Cosentino, D. D. Cara, P. Russotto, and G. Tin. "On the use of narrow band power line as communication technology for medium and low voltage smart grids." In *Instrumentation and Measurement Technology (I2 MTC), 2012 IEEE International Conference on*, pp. 619–623. IEEE, 2012.

[45] N. I. of Standards and P. A. P. . P. Technology (NIST). "Harmonize Power Line Carrier Standards for Appliance Communications in the Home, Coexistence

of narrow band power line communication technologies in the unlicensed FCC band.", 2010. URL http://collaborate.nist.gov/twiki-sggrid/pub/SmartGrid/PAP15PLCForLowBitRates/NB_PLC_coexistence_paper_rev3.doc.

[46] I. T. U. I. . T. S. S. S. G. 15. "Narrowband orthogonal frequency division multiplexing power line communication transceivers for G.hnem networks.", October 2012. Recommendation ITU-T G.9902.

[47] I. T. U. I. . T. S. S. S. G. 15. "Narrowband orthogonal frequency division multiplexing power line communication transceivers for G3-PLC networks.", October 2012. Recommendation ITU-T G.9903.

[48] I. T. U. I. . T. S. S. S. G. 15. "Narrowband orthogonal frequency division multiplexing power line communication transceivers for PRIME networks.", October 2012. Recommendation ITU-T G.9904.

[49] M. Sigle, M. Bauer, W. Liu, and K. Dostert. "Transmission channel properties of the low voltage grid for narrowband power line communication." In *Power Line Communications and Its Applications (ISPLC), 2011 IEEE International Symposium on*, pp. 289–294. IEEE, 2011.

[50] B. Varadarajan, I. H. Kim, A. Dabak, D. Rieken, and G. Gregg. "Empirical measurements of the low-frequency power-line communications channel in rural North America." In *Power Line Communications and Its Applications (ISPLC), 2011 IEEE International Symposium on*, pp. 463–467. IEEE, 2011.

[51] M. Sigle and W. Liu. "On the impedance of the low-voltage distribution grid at frequencies up to 500 kHz." In *Power Line Communications and Its Applications (ISPLC), 2012 16th IEEE International Symposium on*, pp. 30–34. IEEE, 2012.

[52] O. Hooijen. "A channel model for the residential power circuit used as a digital communications medium." *IEEE Transactions on Electromagnetic Compatibility*, vol. 40, no. 4, pp. 331–336, 1998.

[53] L. T. Berger and G. Moreno-Rodrguez. "Power Line Communication Channel Modelling through Concatenated IIR-Filter Elements." *Journal of Communications*, vol. 4, no. 1, pp. 41–51, 2009.

[54] S. Galli. "A simplified model for the indoor power line channel." In *IEEE International Symposium on Power Line Communications and Its Applications*, pp. 13–19. 2009.

[55] F. C. Corripio, L. D. del Río, and J. E. Muňoz. "A time variant model for indoor power-line channels." In *Proceedings of the International Symposium on Power Line Communications (ISPLC'01)*, pp. 85–90. 2001.

[56] A. Schwager. *Powerline communications: Significant technologies to become ready for integration*. Ph.D. thesis, Universität Duisburg-Essen, Faculty of Engineering, School of Electrical Engineering and Information Technology, 2010.

[57] F. J. Canete, L. Diez, J. A. Cortes, and J. T. Entrambasaguas. "Broadband modelling of indoor power-line channels." *IEEE Transactions on Consumer Electronics*, vol. 48, no. 1, pp. 175–183, 2002.

[58] M. Babic, M. Hagenau, K. Dostert, and J. Bausch. "Theoretical postulation of PLC channel model, The OPERA Consortium.", March 2005. IST Integrated Project Deliverable D4v2.0.

[59] T. Banwell and S. Galli. "A novel approach to the modeling of the indoor power line channel part I: circuit analysis and companion model." *IEEE Transactions on power delivery*, vol. 20, no. 2, pp. 655–663, 2005.

[60] T. Esmailian, F. Kschischang, and P. Gulak. "An in-building power line channel simulator." In *International Symposium on Power Line Communications and Its Applications (ISPLC)*, pp. 27–29. 2002.

[61] F. J. Canete, J. A. Cortes, L. Diez, and J. T. Entrambasaguas. "Modeling and evaluation of the indoor power line transmission medium." *IEEE Communications Magazine*, vol. 41, no. 4, pp. 41–47, 2003.

[62] S. Galli and T. Banwell. "A novel approach to the modeling of the indoor power line channel-Part II: transfer function and its properties." *IEEE Transactions on Power Delivery*, vol. 20, no. 3, pp. 1869–1878, 2005.

[63] T. Sartenaer and P. Delogne. "Deterministic modeling of the (shielded) outdoor power line channel based on the multiconductor transmission line equations." *IEEE Journal on Selected Areas in Communications*, vol. 24, no. 7, pp. 1277–1291, 2006.

[64] H. Philipps. "Development of a statistical model for powerline communications channels." In *Proceedings of the 4th International Symposium on Power-Line Communications and its Applications (ISPLC)*, pp. 5–7. 2000.

[65] S.-C. Kim, G.-W. Lee, H.-S. Lee, J.-h. Park, and J.-h. Lee. "Measurement, modeling and simulation of power line channel for indoor high-speed data communications." pp. 143–148.

[66] S. Barmada, A. Musolino, and M. Raugi. "Innovative model for time-varying power line communication channel response evaluation." *IEEE Journal on Selected Areas in Communications*, vol. 24, no. 7, pp. 1317–1326, 2006.

[67] D. M. Pozar. "Microwave Engineering 3e.", 2006.

[68] S. Galli and T. Banwell. "A deterministic frequency-domain model for the indoor power line transfer function." *IEEE Journal on Selected Areas in Communications*, vol. 24, no. 7, pp. 1304–1316, 2006.

[69] J. Anatory, N. Theethayi, and R. Thottappillil. "Power-line communication channel model for interconnected networksPart I: Two-conductor system." *IEEE Transactions on Power Delivery*, vol. 24, no. 1, pp. 118–123, 2009.

[70] J. Anatory, N. Theethayi, and R. Thottappillil. "Power-line communication channel model for interconnected networksPart II: Multiconductor system." *IEEE Transactions on Power Delivery*, vol. 24, no. 1, pp. 124–128, 2009.

[71] G. Moreno-Rodriguez and L. T. Berger. "An IIR-filter approach to time variant PLC-channel modelling." In *Power Line Communications and Its Applications, 2008. ISPLC 2008. IEEE International Symposium on*, pp. 87–92. IEEE, 2008.

[72] A. M. Tonello and F. Versolatto. "Bottom-up statistical PLC channel modelingpart II: inferring the statistics." *IEEE Transactions on Power Delivery*, vol. 25, no. 4, pp. 2356–2363, 2010.

[73] A. M. Tonello and F. Versolatto. "Bottom-up statistical PLC channel modelingPart I: Random topology model and efficient transfer function computation." *IEEE Transactions on Power Delivery*, vol. 26, no. 2, pp. 891–898, 2011.

[74] H. Philipps. "Development of a statistical model for powerline communication channels." In *IEEE International Symposium on Powerline Communications and its Applications*, pp. 5–7. 2000.

[75] M. Zimmermann and K. Dostert. "A multi-path signal propagation model for the power line channel in the high frequency range." In *Proceedings of the 3rd International Symposium on Power-Line Communications, Lancaster, UK*, vol. 30. 1999.

[76] M. Tlich, A. Zeddam, F. Moulin, and F. Gauthier. "Indoor power-line communications channel characterization up to 100 MHzpart I: one-parameter deterministic model." *IEEE Transactions on Power Delivery*, vol. 23, no. 3, pp. 1392–1401, 2008.

[77] M. Tlich, A. Zeddam, F. Moulin, and F. Gauthier. "Indoor power-line communications channel characterization up to 100 MHzpart II: time-frequency analysis." *IEEE transactions on power delivery*, vol. 23, no. 3, pp. 1402–1409, 2008.

[78] J.-P. Kermoal, L. Schumacher, K. I. Pedersen, P. E. Mogensen, and F. Frederiksen. "A stochastic MIMO radio channel model with experimental validation." *IEEE Journal on selected areas in Communications*, vol. 20, no. 6, pp. 1211–1226, 2002.

[79] M. Zimmermann and K. Dostert. "Analysis and modeling of impulsive noise in broadband powerline communications." *IEEE Transactions on Electromagnetic Compatibility*, vol. 44, no. 1, pp. 249–258, 2002.

[80] V. Degardin, M. Lienard, A. Zeddam, F. Gauthier, and P. Degauquel. "Classification and characterization of impulsive noise on indoor powerline used for data communications." *IEEE Transactions on Consumer Electronics*, vol. 48, no. 4, pp. 913–918, Nov 2002.

[81] Y.-t. Ma, K.-h. Liu, Z.-j. Zhang, J.-x. Yu, and X.-l. Gong. "Modeling the colored background noise of power line communication channel based on artificial neural network." In *The 19th Annual Wireless and Optical Communications Conference (WOCC 2010)*, pp. 1–4. IEEE, 2010.

[82] J. A. Cortés, L. Diez, F. J. Canete, and J. J. Sanchez-Martinez. "Analysis of the indoor broadband power-line noise scenario." *IEEE Transactions on electromagnetic compatibility*, vol. 52, no. 4, pp. 849–858, 2010.

[83] R. Vines, H. Trissell, L. Gale, and J. B. O'neal. "Noise on residential power distribution circuits." *IEEE Transactions on Electromagnetic Compatibility*, , no. 4, pp. 161–168, 1984.

[84] W. Sado and J. Kunicki. "Personal communication on residential power lines-assessment of channel parameters." In *Fourth IEEE International Conference on Universal Personal Communications*, pp. 532–537. 1995.

[85] J. Misurec. "Interference in data communication over narrow-band PLC." *International Journal of Computer Science and Network Security*, vol. 8, no. 11, p. 281, 2008.

[86] L. Cheng and H. C. Ferreira. "Time-diversity permutation coding scheme for narrow-band power-line channels." In *Power Line Communications and Its Applications (ISPLC), 2012 16th IEEE International Symposium on*, pp. 120–125. IEEE, 2012.

[87] N. Pavlidou, A. H. Vinck, J. Yazdani, and B. Honary. "Power line communications: state of the art and future trends." *IEEE Communications Magazine*, vol. 41, no. 4, pp. 34–40, 2003.

[88] J. Lin, M. Nassar, and B. L. Evans. "Impulsive noise mitigation in powerline communications using sparse Bayesian learning." *IEEE Journal on Selected Areas in Communications*, vol. 31, no. 7, pp. 1172–1183, 2013.

[89] K. F. Nieman, J. Lin, M. Nassar, K. Waheed, and B. L. Evans. "Cyclic spectral analysis of power line noise in the 3–200 kHz band." In *Power Line Communications and Its Applications (ISPLC), 2013 17th IEEE International Symposium on*, pp. 315–320. IEEE, 2013.

[90] H. Ferreira, H. Grové, O. Hooijen, and A. H. Vinck. "Power line communication." *Wiley Encyclopedia of Electrical and Electronics Engineering*, 1999.

[91] M. Zimmermann and K. Dostert. "An analysis of the broadband noise scenario in powerline networks." In *IEEE International Symposium on Powerline Communications and its Applications*, pp. 5–7. 2000.

[92] M. Nassar, J. Lin, Y. Mortazavi, A. Dabak, I. H. Kim, and B. L. Evans. "Local utility power line communications in the 3–500 kHz band: channel impairments, noise, and standards." *IEEE signal processing magazine*, vol. 29, no. 5, pp. 116–127, 2012.

[93] M. Katayama, T. Yamazato, and H. Okada. "A mathematical model of noise in narrowband power line communication systems." *IEEE Journal on Selected Areas in Communications*, vol. 24, no. 7, pp. 1267–1276, 2006.

[94] M. Nassar, A. Dabak, I. H. Kim, T. Pande, and B. L. Evans. "Cyclostationary noise modeling in narrowband powerline communication for smart grid applications." In *2012 IEEE International Conference on Acoustics, Speech and Signal Processing (ICASSP)*, pp. 3089–3092. IEEE, 2012.

[95] J. Lin and B. L. Evans. "Non-parametric mitigation of periodic impulsive noise in narrowband powerline communications." In *2013 IEEE Global Communications Conference (GLOBECOM)*, pp. 2981–2986. IEEE, 2013.

[96] P. van Rensburg and H. Ferreira. "Practical aspects of component selection and circuit layout for modem and coupling circuitry." In *IEEE 7th International Symposium on Power-Line Communications and its Applications*, pp. 197–203. 2003.

[97] P. V. Rensburg and H. Ferreira. "Step-by-step design of a coupling circuit with bi-directional transmission capabilities." *IEEE International Symposium on Powerline Communications and Its Applications*, pp. 238–243, 2004.

[98] P. Janse van Rensburg. *Effective coupling for power-line communications*. Ph.D. thesis, 2009.

[99] A. Gumaste and T. Antony. *First Mile Access Networks and Enabling Technologies*. Cisco press, 2004.

[100] J. Meng. "Noise analysis of power-line communications using spread-spectrum modulation." *IEEE transactions on power delivery*, vol. 22, no. 3, pp. 1470–1476, 2007.

[101] S. S. Haykin. *Digital Communication Systems*. Wiley & Sons, New York, 2013. URL https://books.google.co.za/books?id=YGZXAAAACAAJ.

[102] V. N. Papilaya, T. Shongwe, A. H. Vinck, and H. C. Ferreira. "Selected subcarriers QPSK-OFDM transmission schemes to combat frequency disturbances." In *Power Line Communications and Its Applications (ISPLC), 2012 16th IEEE International Symposium on*, pp. 200–205. IEEE, 2012.

[103] R. W. Chang. "High-Speed Multichannel Data Transmission with Bandlimited Orthogonal Signals." *Bell Sys. Tech. J*, vol. 45, pp. 1775–96, Feb 1966.

[104] B. Saltzberg. "Performance of an Efficient Parallel Data Transmission System." *Communication Technology, IEEE Transactions on*, vol. 15, no. 6, pp. 805–811, December 1967.

[105] S. Weinstein and P. Ebert. "Data Transmission by Frequency-Division Multiplexing Using the Discrete Fourier Transform." *Communication Technology, IEEE Transactions on*, vol. 19, no. 5, pp. 628–634, October 1971.

[106] A. Peled and A. Ruiz. "Frequency domain data transmission using reduced computational complexity algorithms." In *Acoustics, Speech, and Signal Processing, IEEE International Conference on ICASSP '80.*, vol. 5, pp. 964–967. Apr 1980.

[107] L. Cimini. "Analysis and Simulation of a Digital Mobile Channel Using Orthogonal Frequency Division Multiplexing." *Communications, IEEE Transactions on*, vol. 33, no. 7, pp. 665–675, Jul 1985.

[108] T. Zemen. *OFDM Multi-User Communication Over Time-Variant Channels*. Ph.D. thesis, Telecommunications research center Vienna, Vienna University of Technology, July 2004.

[109] J. G. Proakis and M. Salehi. *Digital Communications*. McGraw-Hilll Higher Education, 5 ed., Nov 2007.

[110] M. B. Balogun. *Frequency Synchronization in Multiuser OFDM-IDMA Systems*. Master's thesis, University of KwaZulu-Natal, Durban, South Africa, Oct 2013.

[111] S. H. Han, J. Cioffi, and J. H. Lee. "On the Use of Hexagonal Constellation for Peak-to-Average Power Ratio Reduction of an ODFM Signal." *Wireless Communications, IEEE Transactions on*, vol. 7, no. 3, pp. 781–786, March 2008.

[112] M. S. K. Sanjay Singh and H. Mruthyunjaya. "Effect of Peak-to-Average Power Ratio Reduction on the Multicarrier Communication System Performance Parameters." *International Journal of Electrical and Computer Engineering*, vol. 4, Dec 2009.

[113] M. Sandell, J.-J. V. D. Beek, and P. O. Brjesson. "Timing and Frequency Synchronization in OFDM Systems Using the Cyclic Prefix." In *Proceedings of International Symmposium on Synchronization, Essen, Germany*, pp. 16–19. Dec 1995.

[114] H. Zhou, A. Malipatil, and Y.-F. Huang. "Synchronization Issues in OFDM Systems." In *Circuits and Systems, 2006. APCCAS 2006. IEEE Asia Pacific Conference on*, pp. 988–991. Dec 2006.

[115] H. Elgala, R. Mesleh, H. Haas, and B. Pricope. "OFDM visible light wireless communication based on white LEDs." In *Vehicular Technology Conference, 2007. VTC2007-Spring. IEEE 65th*, pp. 2185–2189. IEEE, 2007.

[116] J. M. Kahn, J. R. Barry, M. D. Audeh, J. B. Carruthers, W. J. Krause, and G. W. Marsh. "Non-directed infrared links for high-capacity wireless LANs." *Personal Communications, IEEE*, vol. 1, no. 2, p. 12, 1994.

[117] H. Park and J. R. Barry. "Modulation analysis for wireless infrared communications." In *Communications, 1995. ICC'95 Seattle,'Gateway to Globalization', 1995 IEEE International Conference on*, vol. 2, pp. 1182–1186. IEEE, 1995.

[118] A. J. Moreira, A. M. Tavares, R. J. Valadas, and A. de Oliveira Duarte. "Modulation methods for wireless infrared transmission systems: performance under ambient light noise and interference." In *Photonics East'95*, pp. 226–237. International Society for Optics and Photonics, 1995.

[119] J. B. Carruthers and J. M. Kahn. "Multiple-subcarrier modulation for nondirected wireless infrared communication." *Selected Areas in Communications, IEEE Journal on*, vol. 14, no. 3, pp. 538–546, 1996.

[120] J. M. Kahn and J. R. Barry. "Wireless infrared communications." *Proceedings of the IEEE*, vol. 85, no. 2, pp. 265–298, 1997.

[121] S. Nakamura. "Present performance of InGaN-based blue/green/yellow LEDs." In *Photonics West'97*, pp. 26–35. International Society for Optics and Photonics, 1997.

[122] I. Niki, Y. Narukawa, D. Morita, S.-y. Sonobe, T. Mitani, H. Tamaki, Y. Murazaki, M. Yamada, and T. Mukai. "White LEDs for solid state lighting." In *Optical Science and Technology, SPIE's 48th Annual Meeting*, pp. 1–9. International Society for Optics and Photonics, 2004.

[123] T. Komine and M. Nakagawa. "Fundamental analysis for visible-light communication system using LED lights." *Consumer Electronics, IEEE Transactions on*, vol. 50, no. 1, pp. 100–107, 2004.

[124] K. Lee, H. Park, and J. R. Barry. "Indoor channel characteristics for visible light communications." *Communications Letters, IEEE*, vol. 15, no. 2, pp. 217–219, 2011.

[125] S. Goldfisher and S. Tanabe. "IEEE 1901 access system: An overview of its uniqueness and motivation." *Communications Magazine, IEEE*, vol. 48, no. 10, pp. 150–157, 2010.

[126] S. Rajagopal, R. D. Roberts, and S.-K. Lim. "IEEE 802.15. 7 visible light communication: modulation schemes and dimming support." *Communications Magazine, IEEE*, vol. 50, no. 3, pp. 72–82, 2012.

[127] H. Ma, L. Lampe, and S. Hranilovic. "Integration of indoor visible light and power line communication systems." In *Power Line Communications and Its Applications (ISPLC), 2013 17th IEEE International Symposium on*, pp. 291–296. IEEE, 2013.

[128] Y. Tanaka, S. Haruyama, and M. Nakagawa. "Wireless optical transmissions with white colored LED for wireless home links." In *Personal, Indoor and Mobile Radio Communications, 2000. PIMRC 2000. The 11th IEEE International Symposium on*, vol. 2, pp. 1325–1329. IEEE, 2000.

[129] G. Casella and R. L. Berger. *Statistical inference*, vol. 70. Duxbury Press Belmont, CA, 1990.

[130] E.-J. Wagenmakers, M. Lee, T. Lodewyckx, and G. J. Iverson. "Bayesian versus frequentist inference." In *Bayesian evaluation of informative hypotheses*, pp. 181–207. Springer, 2008.

[131] D. Gamerman. *Markov chain Monte Carlo*. Chapman and Hall, 1997.

[132] D. Gamerman and H. F. Lopes. *Markov chain Monte Carlo: stochastic simulation for Bayesian inference*. CRC Press, 2006.

[133] C. L. Atwood et al. *Handbook of parameter estimation for probabilistic risk assessment*. Division of Risk Analysis and Applications, Office of Nuclear Regulatory Research, US Nuclear Regulatory Commission, 2003.

[134] L. N. Kanal and A. Sastry. "Models for channels with memory and their applications to error control." *Proceedings of the IEEE*, vol. 66, no. 7, pp. 724–744, 1978.

[135] B. Zhen, M. Kim, J.-I. Takada, and R. Kohno. "Finite-state Markov model for on-body channels with human movements." In *Communications (ICC), 2010 IEEE International Conference on*, pp. 1–5. IEEE, 2010.

[136] S. Lin, Y. Li, Y. Li, B. Ai, and Z. Zhong. "Finite-state Markov channel modeling for vehicle-to-infrastructure communications." In *Wireless Vehicular Communications (WiVeC), 2014 IEEE 6th International Symposium on*, pp. 1–5. IEEE, 2014.

[137] Y. Luo, R. Zhang, L. Cai, and S. Xiang. "Finite-state Markov modelling for wireless." *IET Networks*, vol. 3, no. 2, pp. 119–128, 2014.

[138] H. Wang, F. R. Yu, L. Zhu, T. Tang, and B. Ning. "Finite-state Markov modeling for wireless channels in tunnel communication-based train control systems." *IEEE Transactions on Intelligent Transportation Systems*, vol. 15, no. 3, pp. 1083–1090, 2014.

[139] O. S. Salih, C.-X. Wang, B. Ai, and R. Mesleh. "Adaptive Generative Models for Digital Wireless Channels." *IEEE Transactions on Wireless Communications*, vol. 13, no. 9, pp. 5173–5182, 2014.

[140] A. Bildea, O. Alphand, F. Rousseau, and A. Duda. "Link quality estimation with the Gilbert-Elliot model for wireless sensor networks." In *Personal, Indoor, and Mobile Radio Communications (PIMRC), 2015 IEEE 26th Annual International Symposium on*, pp. 2049–2054. IEEE, 2015.

[141] R. Ranjan and D. Mitra. "HMM modeling for OFDM–BER performance." *AEU-International Journal of Electronics and Communications*, vol. 69, no. 1, pp. 18–25, 2015.

[142] X. Zhang and X. Zhang. "Error characterization of underwater acoustic channels based on the simple Fritchman model." In *Signal Processing, Communications and Computing (ICSPCC), 2016 IEEE International Conference on*, pp. 1–5. IEEE, 2016.

[143] P. Dymarski. *Hidden Markov Models, Theory and Applications*. INTECH, Croatia, 2011.

[144] L. Rabiner and B. Juang. "An introduction to hidden Markov models." *IEEE ASSP Magazine*, vol. 3, no. 1, pp. 4–16, 1986.

[145] L. Rabiner. "A tutorial on hidden Markov models and selected applications in speech recognition." *Proceedings of the IEEE*, vol. 77, no. 2, pp. 257–286, 1989.

[146] L. Tang, P. So, E. Gunawan, Y. Guan, S. Chen, and T. Lie. "Characterization and modeling of in-building power lines for high-speed data transmission." *IEEE Transactions on Power Delivery*, vol. 18, no. 1, pp. 69–77, 2003.

[147] H. Balzter. "Markov chain models for vegetation dynamics." *Ecological Modelling*, vol. 126, no. 2, pp. 139–154, 2000.

[148] I. J. Myung. "Tutorial on maximum likelihood estimation." *Journal of mathematical Psychology*, vol. 47, no. 1, pp. 90–100, 2003.

[149] A. D. Familua. "Noise modeling for standard CENELEC A-band power line communication channel.", 2013.

[150] J.-F. Mari and R. Schott. *Probabilistic and Statistical Methods in Computer Science*. Springer Science & Business Media, 2013.

[151] N. Metropolis, A. W. Rosenbluth, M. N. Rosenbluth, A. H. Teller, and E. Teller. "Equation of state calculations by fast computing machines." *The journal of chemical physics*, vol. 21, no. 6, pp. 1087–1092, 1953.

[152] W. K. Hastings. "Monte Carlo sampling methods using Markov chains and their applications." *Biometrika*, vol. 57, no. 1, pp. 97–109, 1970.

[153] A. Barker. "Monte Carlo Calculations of the Radial Distribution Functions for a Proton? Electron Plasma." *Australian Journal of Physics*, vol. 18, no. 2, pp. 119–134, 1965.

[154] P. H. Peskun. "Optimum monte-carlo sampling using markov chains." *Biometrika*, vol. 60, no. 3, pp. 607–612, 1973.

[155] C. Alasseur, L. Husson, and F. Pérez-Fontán. "Modelling of the Markovian behaviour of mobile satellite channels with MCMC methods." In *Communications, 2004 IEEE International Conference on*, vol. 6, pp. 3326–3330. IEEE, 2004.

[156] Y.-Z. Jiang, X.-l. Hu, X. Kai, and Z. Qi. "Bayesian estimation of class a noise parameters with hidden channel states." In *Power Line Communications and Its Applications, 2007. ISPLC'07. IEEE International Symposium on*, pp. 2–4. IEEE, 2007.

[157] R.-R. Chen, R. Peng, and B. Farhang-Boroujeny. "Markov Chain Monte Carlo: Applications to MIMO detection and channel equalization." In *Information Theory and Applications Workshop, 2009*, pp. 44–49. IEEE, 2009.

[158] H. Wan, R.-R. Chen, J. W. Choi, A. C. Singer, J. C. Preisig, and B. Farhang-Boroujeny. "Markov chain Monte Carlo detection for frequency-selective channels using list channel estimates." *Selected Topics in Signal Processing, IEEE Journal of*, vol. 5, no. 8, pp. 1537–1547, 2011.

[159] P. M. Djuric, S. J. Godsill, W. J. Fitzgerald, and P. J. Rayner. "Detection and estimation of signals by reversible jump Markov chain Monte Carlo computations." In *Acoustics, Speech and Signal Processing, 1998. Proceedings of the 1998 IEEE International Conference on*, vol. 4, pp. 2269–2272. IEEE, 1998.

[160] F. Hamza. "*The USRP under 1.5 x magnifying lens!*", 2008. http://gnuradio.org/redmine/attachments/129/USRP_Documentation.pdf [Accessed: 2016-08-31].

[161] M. Lülf. *Evaluation of Synchronization Algorithms with USRP*. Ph.D. thesis, Technische Universität München, 2012.

[162] D. A. Clendenen. *A software defined radio testbed for research in dynamic spectrum access*. Ph.D. thesis, Purdue University Fort Wayne, 2012.

[163] Ettus. "*USRP Hardware Driver and USRP Manual: Daughterboards.*" http://files.ettus.com/manual/page_dboards.html [Online]: Accessed: 2016-09-01.

[164] Ettus. "*LFTX/LFRX Daughterboard Specifications.*" https://kb.ettus.com/LFTX/LFRX#Daughterboard_Specifications [Online]: Accessed: 2016-09-01.

[165] S. Souissi, O. Benrhouma, and C. Rebai. "Design of coupling interface for narrowband Power Line Communication channel characterization." *IMEKO TC4*, pp. 483–488, 2014.

[166] N. Instruments. "*How to Update Firmware and FPGA Images for the USRP2.*" http://digital.ni.com/public.nsf/allkb/90378D6DB970B826862579DC006A0BFC [Online]: Accessed: 2016-09-01.

[167] R. K. Kodali, L. Bopppana, and S. R. Kondapalli. "DDC and DUC filters in SDR platforms." In *Advanced Computing Technologies (ICACT), 2013 15th International Conference on*, pp. 1–6. IEEE, 2013.

[168] C.-X. Wang and M. Patzold. "A novel generative model for burst error characterization in Rayleigh fading channels." In *Personal, Indoor and Mobile Radio Communications, 2003. PIMRC 2003. 14th IEEE Proceedings on*, vol. 1, pp. 960–964. IEEE, 2003.

[169] M. Chan and R. Donaldson. "Amplitude, width, and interarrival distributions for noise impulses on intrabuilding power line communication networks." *Electromagnetic Compatibility, IEEE Transactions on*, vol. 31, no. 3, pp. 320 –323, aug 1989.

[170] R. Vines, H. Trissell, L. Gale, and J. Ben O'neal. "Noise on Residential Power Distribution Circuits." *Electromagnetic Compatibility, IEEE Transactions on*, vol. EMC-26, no. 4, pp. 161 –168, nov. 1984.

[171] A. J. H. Vinck. "Coded modulation for powerline communications." *Int. J. Elec. Commun.*, vol. 54, no. 1, pp. 45–49, 2000.

[172] S. Haykin. "Communication systems." *IET, New York*, 2001.

[173] A. M. Wyglinski and D. Pu. *Digital Communication Systems Engineering with Software-Defined Radio*.

[174] E. Gilbert et al. "Capacity of a burst-noise channel." *Bell System Technical Journal*, vol. 39, no. 9, pp. 1253–1265, 1960.

[175] E. Elliott. "Estimates of error rates for codes on burst-noise channels." *Bell System Technical Journal*, vol. 42, no. 9, pp. 1977–1997, 1963.

[176] L. E. Vogler. "Comparisons of the two-state Markov and Fritchman models as applied to bit error statistics in communication channels." *NASA STI/Recon Technical Report N*, vol. 87, p. 11935, 1986.

[177] W. H. Tranter and O. H. Lee. "Wireless personal communications." chap. On the use of signal-to-noise ratio estimation for establishing hidden Markov models, pp. 159–170. Norwell, MA, USA: Kluwer Academic Publishers, 1996. URL http://dl.acm.org/citation.cfm?id=251300.251345.

[178] L. Cheng, T. G. Swart, and H. C. Ferreira. "Adaptive rateless permutation coding scheme for OFDM-based PLC." In *Power Line Communications and Its Applications (ISPLC), 2013 17th IEEE International Symposium on*, pp. 242–246. IEEE, 2013.

[179] "Using the UHD USRP2 Block in Simulink.", Nov. 2013. URL http://www.scribd.com/doc/133955483/uhd-usrp-simulink-doc-pdf.

[180] V. Papilaya, T. Shongwe, A. Vinck, and H. Ferreira. "Selected subcarriers QPSK-OFDM transmission schemes to combat frequency disturbances." In *Power Line Communications and Its Applications (ISPLC), 2012 16th IEEE International Symposium on*, pp. 200–205. March 2012.

[181] K. Lee and H. Park. "Modulations for visible light communications with dimming control." *IEEE photonics technology letters*, vol. 23, no. 16, pp. 1136–1138, 2011.

[182] E. Monteiro and S. Hranilovic. "Design and implementation of color-shift keying for visible light communications." *Journal of Lightwave Technology*, vol. 32, no. 10, pp. 2053–2060, 2014.

[183] A. Ndjiongue, H. Ferreira, K. Ouahada, and A. Vinckz. "Low-complexity SOCPBFSK-OOK interface between PLC and VLC channels for low data rate transmission applications." In *Power Line Communications and its Applications (ISPLC), 2014 18th IEEE International Symposium on*, pp. 226–231. IEEE, 2014.

[184] C. Xiang, W. Runze, and C. Min. "Research of OFDM power line carrier communication based on AMI." In *Wireless Mobile and Computing (CCWMC 2011), IET International Communication Conference on*, pp. 278–281. IET, 2011.

[185] Y.-H. Kim and J.-H. Lee. "Comparison of passband and baseband transmission schemes for power-line communication OFDM systems." *IEEE Transactions on Power Delivery*, vol. 26, no. 4, pp. 2466–2475, 2011.

[186] N. Nefedov. "Generative Markov models for discrete channel modelling." In *Personal, Indoor and Mobile Radio Communications, 1997. Waves of the Year 2000. PIMRC'97., The 8th IEEE International Symposium on*, vol. 1, pp. 7–11. IEEE, 1997.

[187] K. Rabie, E. Alsusa, A. Familua, and L. Cheng. "Constant envelope OFDM transmission over impulsive noise power-line communication channels." In *Power Line Communications and its Applications (ISPLC), IEEE International Symposium on*, pp. 13–18. 2015.

[188] K. Ogunyanda, A. Familua, T. Swart, H. Ferreira, and L. Cheng. "Adaptive permutation coded differential OFDM system for power line communications." In *2014 IEEE 6th International Conference on Adaptive Science & Technology (ICAST)*, pp. 1–7. IEEE, 2014.